2D materials : exfoliation in liquid-phase and electronics applications

Matilde Eredia

UNIVERSITÉ DE STRASBOURG

ÉCOLE DOCTORALE DES SCIENCES CHIMIQUES

UMR 7006 – Institut de Science et d'Ingénierie Supramoléculaires (I.S.I.S)

THÈSE

présentée par :

Matilde EREDIA

soutenue le : **24 Mai 2019**

pour obtenir le grade de : **Docteur de l'université de Strasbourg**

Discipline/ Spécialité : Chimie / Chimie physique

2D materials: exfoliation in liquid-phase and electronics applications

THÈSE dirigée par :

M. SAMORì Paolo	Professeur, Université de Strasbourg

RAPPORTEURS :

STEFANKIEWICZ Artur R.	Professeur, Adam Mickiewicz University in Poznań
MATEO-ALONSO Aurelio	Professeur, University of the Basque Country

---

AUTRES MEMBRES DU JURY :

RUBEN Mario	Professeur, Université de Strasbourg

To my family and my beloved friends.

RÉSUMÉ

Le développement à grande échelle de dispositifs électroniques plus performants, plus légers, pliables conduira à une nouvelle génération de technologies pour smartphone, ordinateur portable et de technologies sans fil. De tels outils sont essentiels pour de nombreuses autres applications technologiques, par exemple dans le domaine de la médecine, et plus généralement pour améliorer la qualité de nos vies.[1] Pour relever ces défis, il est important de développer des matériaux de pointe dont les propriétés sont ajustées en fonction de leur application.

Récemment, des matériaux bidimensionnels (2D) tels que le graphène, les chalcogénures de métaux de transition (TMDC) et le h-BN ont montré un grand potentiel comme matériaux actifs dans les transistors à couche mince[2-3], les photodétecteurs,[4] les capteurs,[5-6] les super condensateurs[7] et les cellules solaires.[8-9] Il s'agit de matériaux de seulement un ou de quelques atomes d'épaisseur et possèdent des propriétés physicochimiques uniques (par exemple, une conductivité électrique et thermique exceptionnelle) qui n'existent pas dans leurs équivalents 3D. De plus, ils sont transparents et peuvent supporter de grandes quantités de contraintes sans dégradation, ce qui en fait des candidats parfaits pour les technologies flexibles de nouvelle génération.[10]

Les propriétés exceptionnelles du graphène découvertes en 2004 par Geim et Novoselov[11] ont rendu ce matériau intéressant pour une grande variété d'applications technologiques potentielles.[12] Cependant, la production à grande échelle de matériaux 2D de haute qualité représente un problème majeur limitant l'émergence de nombreuses applications. L'approche la plus populaire jusqu'à présent pour produire des couches minces intactes et de haute qualité consiste en la méthode basée sur le «scotch-tape»,[11] qui a été exploitée pour isoler le graphène en 2004. Ce procédé repose sur le clivage répétitif d'un cristal stratifié avec un ruban adhésif. Bien que cette approche soit appropriée pour la réalisation d'études fondamentales visant à dévoiler les propriétés physiques et chimiques des matériaux 2D, cette méthode n'est guère applicable à grande échelle, ce qui empêche toute application technologique. Une méthode de production alternative qui peut être mise en œuvre pour croître un matériau 2D à l'échelle d'un wafer est le dépôt chimique en phase vapeur (CVD), qui peut être classé comme une approche «bottom-up». La principale faiblesse de ce processus de fabrication réside dans la nature même du procédé qui est très chronophage et énergivore. De plus, la qualité limitée du matériau obtenu par rapport aux couches minces vierges exfoliées mécaniquement est à considérer. D'autres améliorations de l'approche CVD sont nécessaires pour répondre à la demande de fabrication

industrielle, en termes de qualité, reproductibilité et coût.[13] Ainsi, il est clair que le principal obstacle à l'apparition de matériaux 2D dans notre utilisation quotidienne réside dans l'absence de méthodes fiables et évolutives pour leur synthèse.

L'approche la plus prometteuse pour la production en série de matériaux 2D consiste en l'exfoliation en phase liquide (LPE) de cristaux.[14] Les techniques associées à cette approche sont généralement très faciles, peu coûteuses et peuvent être écologiques. Des matériaux 2D exfoliés en phase liquide peuvent exister sous la forme d'encres pouvant être déposées sur n'importe quel substrat. Récemment, la communauté a constaté le développement de nouvelles méthodes de LPE, notamment l'exfoliation en phase liquide induite par ultrasons (UILPE),[14-15] éventuellement assistée par des molécules ad-hoc,[16] l'exfoliation électrochimique (EE) réalisée dans divers électrolytes, l'exfoliation par cisaillement[17] et par micro-fluidisation,[18] le broyage à billes[19] dans différents environnements, etc.

Cette thèse est consacrée à la production de matériaux 2D en phase liquide, en utilisant des approches pouvant permettre la production en masse de graphène et de matériaux apparentés. Notre objectif est de surmonter certains problèmes critiques pour le traitement et l'utilisation pratique des encres de matériaux 2D, tels que la tendance des nanofeuilles à se réagréger, leur capacité de traitement limitée.

Notre but est également d'obtenir une profonde comprehension des relations entre structure et propriété dans de tels matériaux, étant une étape obligatoire pour leurs futures applications. Ce travail couvre le passage de l'exfoliation en phase liquide par ultrasons à celle assistée par des molécules jusqu'au développement du processus d'exfoliation électrochimique. Plus précisément, nous nous sommes concentrés sur l'UILPE et l'exfoliation électrochimique du graphène et du disulfure de molybdène (MoS_2), qui ont été choisis comme matériaux prototypiques 2D. Les approches synthétiques sont combinées à une caractérisation physico-chimique des matériaux produits, à l'aide de techniques telles que l'AFM, la microscopie électronique, la spectroscopie XPS et Raman, couplées à des mesures électriques.

Le manuscrit est divisé en trois parties expérimentales principales ; la première est centrée sur la production et les études fondamentales des propriétés physiques et chimiques des matériaux produits, et les deux suivants sur l'utilisation possible des matériaux 2D en électronique :

- Exfoliation électrochimiques du graphène et de MoS_2 : propriétés structurales et électroniques
- LPE de MoS_2 induite par ultrasons pour des applications de détecteurs

- LPE de graphite induite en présence de polymères semiconducteurs pour l'amélioration de l'homogénéité et des performances électriques du film

Les processus d'exfoliation en phase liquide utilisent des forces physiques externes, telles que des ondes ultrasonores, des forces de cisaillement ou des forces motrices électrochimiques, pour surmonter les interactions de van der Waals entre des feuilles adjacentes dans des matériaux stratifiés immergés dans un solvant approprié. Celui-ci, à son tour, doit interagir avec le matériau 2D en équilibrant les forces attractives entre les feuilles pour maintenir le matériau en suspension. Les approches LPE sont des processus peu coûteux qui peuvent facilement aboutir à des dispersions pouvant être traitées par des méthodes bien établies, telles que le revêtement à la tournette, le dépôt par goutte et l'impression à jet d'encre.[20]

Investiguer la structure et les propriétés des matériaux 2D produits par des approches LPE et obtenir un contrôle précis de leurs propriétés sont des aspects essentiels pour révéler leur potentiel et permettre leur intégration dans de nouveaux dispositifs multifonctionnels.

Dans ce travail de thèse, nous avons exploité deux méthodes pour la production de matériaux 2D en milieu liquide, à savoir EE et UILPE. La première est une approche récemment développée pour la production à grande échelle et rapide de graphène, alors que la seconde approche est plus en adéquation avec l'exfoliation en milieu liquide de divers matériaux assemblés en couches.

La première partie expérimentale de la thèse est consacrée à l'exfoliation électrochimique du graphite en graphène. Contrairement aux autres procédés d'exfoliation en milieu liquide, l'EE sur feuille de graphite présente l'avantage unique de permettre la production de grandes quantités de graphène en peu de temps, dépassant également 20 g / heure.[21] Cependant, une compréhension approfondie de la relation entre structure-propriétés de ce matériau fait toujours défaut.

Nous avons mené une caractérisation physicochimique du graphène électrochimiquement exfolié (EEG) combinée à une étude des propriétés électroniques de ce matériau réalisée à la fois au niveau des feuillets de graphène et sur les films (Figure 1). De plus, nous avons utilisé pour la première fois l'irradiation par micro-ondes pour réduire la quantité de fonctionnalités d'oxygène dans l'EEG, démontrant ainsi qu'elles ne constituaient pas le goulot d'étranglement du transport de charges dans l'EEG, ce qui est plutôt gêné par la présence de défauts de structure dans le plan de base.

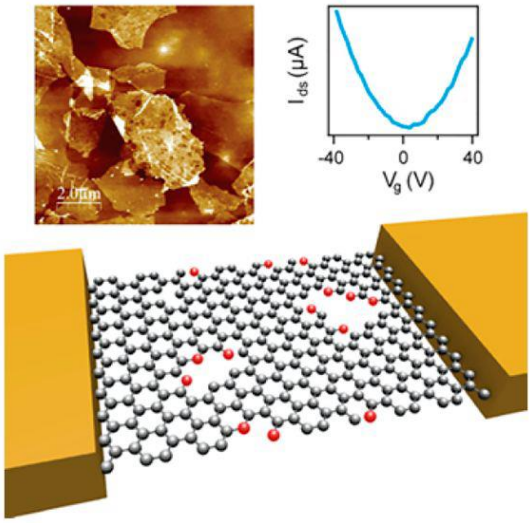

Figure 1 : Caractérisation morphologique et électronique de l'EEG montrant la présence de défauts de structure.

Une étude similaire a été réalisée après l'exfoliation de MoS_2 par intercalation électrochimique d'ions lithium. Comparée à la littérature antérieure,[22] cette approche permet d'obtenir plus de 60% de MoS_2 en phase 2H. Cependant, les analyses Raman et XPS montrent un matériau défectueux. Enfin, une forte amélioration des performances électriques des FET à base de feuillets de MoS_2 isolés, après traitement à la vapeur de butanethiol, montre que les lacunes en soufre constituent une part abondante des défauts dans un tel matériau. Ces travaux ont inspiré la deuxième partie expérimentale présentée dans cette thèse. Les défauts créés lors des processus d'exfoliation peuvent agir en tant que sites réactifs pour des interactions covalentes et non covalentes. La première peut être utilisée dans le but d'une modification ultérieure via une fonctionnalisation chimique, tandis que la nature réversible et sélective des interactions non covalentes est idéale pour la détection.

La détection chimique est un domaine scientifique d'actualité car elle apportera une contribution essentielle à l'amélioration de la qualité de la vie des personnes en proposant des solutions concrètes en matière de surveillance de la sécurité sanitaire des aliments, de l'environnement et de la santé (diagnostic précoce et surveillance continue des maladies), etc. Des études récentes ont révélé que le MoS_2 recèle un grand potentiel en tant que matériau actif pour la détection de gaz, en tirant parti du rapport surface / volume le plus élevé associé à des caractéristiques électriques semi-conductrices et à une composition chimique contrôlée. Grâce à ses propriétés chimiques et physiques uniques, le MoS_2 peut interagir avec le gaz adsorbé à sa surface (O_2, H_2O, NO_2, CO, NH_3, etc.), ce qui entraîne une modification de la conductivité du matériau, qui peut être mesurée en tant que variation de courant dans les appareils à deux et trois terminaux.[23] Cependant, à ce jour, les dispositifs basés sur des matériaux 2D ne peuvent pas concurrencer les capteurs disponibles dans le commerce en raison de leur faible sensibilité. Un autre inconvénient, qui empêche encore l'apparition sur le marché

d'appareils à base de matériaux 2D, est encore l'absence de méthode de production efficace et peu coûteuse à grande échelle de couches minces.

Nous avons exploité l'approche LPE pour préparer des nanofeuilles à base de MoS_2 à faible coût, dans le but de fabriquer des détecteurs de gaz ayant une grande surface spécifique. La méthode LPE induite par ultrasons a été conçue de manière à favoriser la formation de défauts sur les bords des feuilles, pouvant alors être bénéfiques pour les propriétés de détection de gaz. Grâce à une méthode de traitement simple et efficace, l'encre à base de MoS_2 a été déposée sous forme de films homogènes pour la fabrication de dispositifs chimiorésistif. Les couches minces de MoS_2 ont montré une sensibilité remarquable à l'humidité, avec une haute sélectivité vis-à-vis de diverses petites molécules, prouvant que l'approche LPE de MoS_2 peut être un bon choix pour l'élaboration de la prochaine génération de détecteurs de gaz, car elle peut permettre la fabrication de dispositifs flexibles de grande surface, légers et très performants.

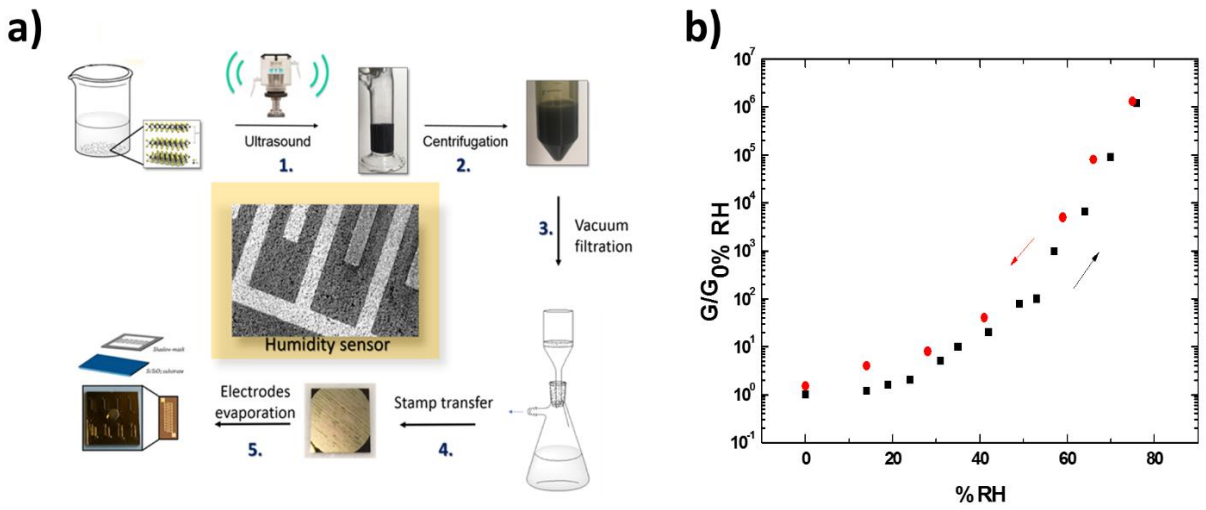

Figure 2. Schéma de la procédure de fabrication des détecteurs de gas à base de MoS_2-thiol (a) et performances des films de MoS_2 en tant que capteurs d'humidité à différentes humidités relatives (b). Le graphique indique le rapport G / $G_{0\%\ RH}$ par rapport à l'humidité relative (%RH), G étant la valeur de conductance en présence d'humidité et $G_{0\%\ HR}$, la valeur de conductance à 0% HR.

Enfin, dans la troisième partie expérimentale de la thèse, nous présentons une nouvelle stratégie pour moduler les propriétés des matériaux 2D en exploitant la méthode LPE. Ce projet implique l'utilisation de systèmes moléculaires tels que des semi-conducteurs organiques (OSC) en combinaison avec les matériaux 2D.

Bien que les matériaux pour l'(opto)électronique classique tels que les semi-conducteurs organiques (OSC), soient largement étudiés et peuvent présenter de nombreux avantages tels que la modulation

de leurs propriétés physiques via une fonctionnalisation chimique, pouvant être déposés de manière optimale, et présentant une aptitude aux processus évolutifs, même sur des supports flexibles, leurs performances restent modestes. Pour résoudre ce problème, plusieurs tentatives de combinaison d'OSC avec des matériaux 2D ont été rapportées dans la littérature antérieure.[24]

Dans la dernière partie de la thèse, nous proposons une nouvelle approche basée sur le mélange simultané d'OSC, tels que P3HT et PCDTPT, avec du graphène lors de l'exfoliation de poudre de graphite en nano-feuillets de graphène, les OSC jouant le rôle d'agents stabilisants de dispersion, en empêchant la réagrégation des feuillets de graphène exfoliés, permettant finalement la production de dispersions homogènes à deux composants. La caractérisation électrique des films hybrides résultants a révélé une forte amélioration des performances électriques dans le cas des films hybrides FLG / PCDTPT par rapport à ses composants d'origine (Figure 3).

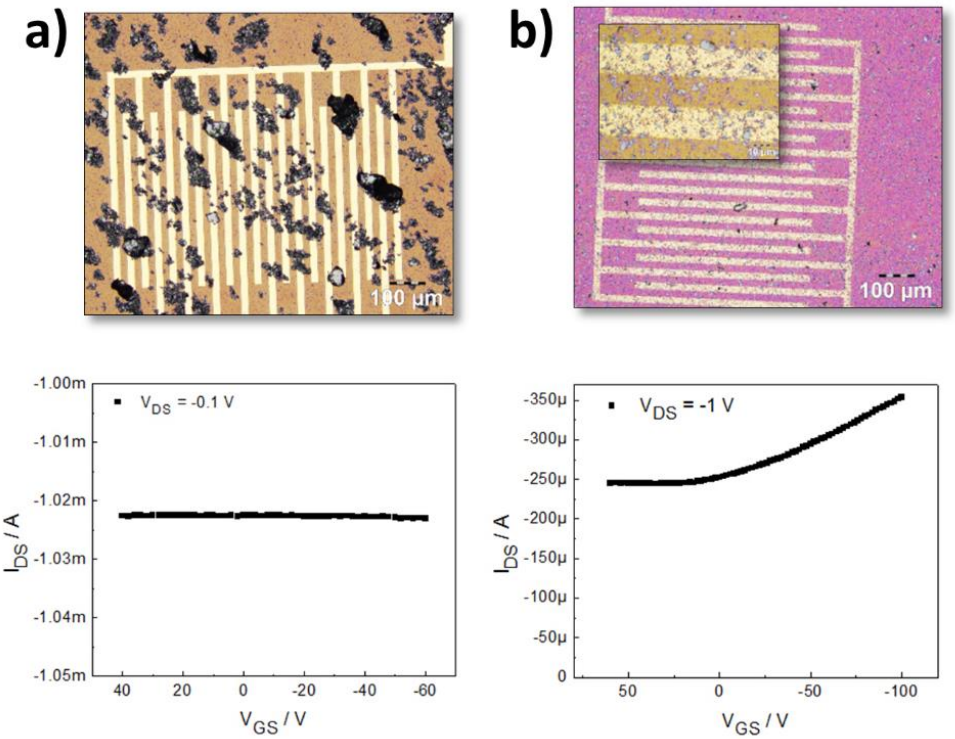

Figure 3 : Caractérisation optique et électrique du graphène exfolié en absence (a) et en présence (b) de PCDTPT.

Ces travaux pourraient ouvrir la voie à l'utilisation de méthodes LPE pour l'optimisation des propriétés des matériaux 2D en vue de leur utilisation en tant que composants actifs dans de nouveaux dispositifs multifonctionnels.

En conclusion, nous avons développé de nouvelles approches pour la production en milieu liquide de matériaux 2D ouvrant la voie à leur exploitation en tant que matériaux actifs pour des applications en électronique et en détection. En particulier, l'approche électrochimique a été largement étudiée, jetant ainsi les bases de l'amélioration du processus, vers la production en série de matériaux 2D pouvant être utilisés de manière pratique dans des dispositifs (opto) électroniques flexibles et à faible coût.

ABSTRACT

The tremendous pace towards the fabrication of more performing, lighter, foldable and wearable electronic components will lead to a new generation of smartphone, portable computer and wireless technologies. Such tools will be key for many other technological applications, e.g. in the field of medicine and healthcare, and more generally to improve the quality of our lives.[1] To afford these challenges, it is important to develop advanced materials whose properties are tuned in view of their final application.

Recently, two-dimensional materials (2DMs) like graphene, transition metal dichalcogenides (TMDs) and hexagonal boron nitride (h-BN), have shown great potential as components in thin film transistors,[2-3] photodetectors,[4] sensors,[5-6] supercapacitors[7] and solar cells.[8-9] They are just one or few atoms thick materials and hold unique physicochemical properties (e.g. exceptional electrical and thermal conductivity) that do not exist in their bulk counterparts. In addition, they are transparent and can bear large amounts of strain without degradation being, therefore, they are perfect candidates for next-generation flexible technologies.[10]

The discovery of graphene's exceptional properties in 2004 by Geim and Novoselov[11] has made graphene and related materials of great interest for a wide variety of potential technological applications.[12] Yet, the large-scale production of high quality 2DMs represents a greatest problem limiting the emergence of numerous daily life applications. Hitherto the most popular approach to produce high-quality pristine thin layers consists in the "top-down" "scotch-tape"[11] based method, which was exploited to isolate graphene for the first time. This method relies in the repetitive cleavage of a layered crystal by the use of an adhesive tape.[11] While it is appropriate for performing fundamental studies aimed at unveiling the physical and chemical properties of 2DMs, this method is hardly up-scalable, thereby hampering any technological application. An alternative production method which can be executed to the growth in wafer-scale is chemical vapour deposition (CVD), which can be classified as a "bottom-up" approach. The major weakness of such approach is the high energy- and time-consuming nature of the process, and the limited quality of the obtained material compared to pristine mechanically exfoliated (ME) thin layers. Further improvements of CVD approach are needed to meet the demand of industrial manufacture, e.g. high quality, reproducibility and low cost.[13] Thus, it is clear that the key bottleneck in the emergence of 2DMs in our daily use is in the absence of reliable and scalable methods for their synthesis.

Approaches that are proving being very promising for the mass production of 2DMs, consist in the liquid-phase exfoliation (LPE) of layered crystals.[14] These techniques are usually very easy, low-cost and can be environmentally-friendly. Liquid-phase exfoliated 2DMs can exist in the form of inks which can be deposited on any arbitrary substrate. Recently, the community has perceived an outbreak of new methods of LPE including ultrasound-induced liquid-phase exfoliation (UILPE)[14, 25] of layered crystals – eventually assisted by *ad-hoc* molecules[16] – , electrochemical exfoliation (EE) – carried out in a variety of electrolytes[26] – , shear exfoliation[17] and ball milling[19] in different environments, and so forth.

This thesis is devoted to the production in liquid-phase of 2DMs, by using approaches that may enable mass production of graphene and related materials. We aim to overcome some issues that are critical for the processing and practical use of 2DMs-inks like the tendency of nanosheets to undergo aggregation and their limited processability. Our purpose is also gaining a deep understanding of the structure-properties relationship in such materials being a mandatory step toward their future applications. This manuscript outlines the evolution of LPE approaches, from the liquid-phase exfoliation by means of ultrasounds to the one assisted by molecules, until the discovery and development of the electrochemical exfoliation process. More specifically, we focussed on ultrasound-induced LPE and electrochemical exfoliation of graphene and molybdenum disulfide (MoS_2), which have been chosen as prototypical 2DMs. The synthetic approaches were combined with a multiscale physico-chemical characterization of the produced materials by means of techniques such as atomic force microscopy (AFM), electron microscopies, X-ray photoelectron spectroscopy (XPS) and Raman spectroscopy, coupled with electrical measurements.

The manuscript is divided in three main experimental parts, with the first one more focussed on the production and fundamental studies on the physical and chemical properties of produced materials, and the latter two on the possible uses of the 2DMs in electronics:

- Electrochemical exfoliation of graphene and MoS_2: structural and electrical properties
- Ultrasound-induced LPE of MoS_2 for sensing applications
- Ultrasound-induced LPE of graphite in the presence of semiconducting polymers for improved film homogeneity and electrical performances

LPE processes use external physical forces, like ultrasound waves, shear forces or electrochemical driving forces, to overcome the van der Waals interactions between adjacent sheets in layered materials immersed in a proper solvent. This latest, in turn, needs to interact with exfoliated flakes

balancing the inter-sheet attractive forces to keep the material in suspension. LPE approaches are inexpensive processes that can be easily up-scaled to obtain dispersions processable by well-established methods, like spin coating, drop casting and ink-jet printing.[20]

Investigating on the structure and properties of the 2DMs produced with LPE approaches and achieving fine control over their properties are key aspects to unveil their potential and to allow their integration in novel multifunctional devices. In this thesis work, we have exploited two methods for the production of 2DMs in liquid-media, i.e. EE and ultrasound-induced LPE. The former is a recently developed approach for the large scale and fast production of graphene,[27-28] whereas the latter is a more established approach for the exfoliation in liquid-medium of various layered materials.[29]

The first experimental part is dedicated to the electrochemical exfoliation of graphite into graphene. Unlike the other exfoliation processes in liquid media, EE of graphite foil holds the unique advantage of allowing the production of large quantities of graphene – exceeding 20 g hours^{-1} – in a short time.[21] However, an in-depth understanding of the structure–properties relationship of this material is still lacking.

We conducted a physicochemical characterization of electrochemically exfoliated graphene (EEG) combined with an investigation of the electronic properties of this material carried out both at the single flake level and on the films. Additionally, we used for the first time microwave irradiation to reduce the amount of oxygen functionalities in EEG, demonstrating that they are not the bottleneck for charge transport, which is rather hindered by the presence of structural defects within the basal plane of the electrochemically exfoliated material (Figure 1).

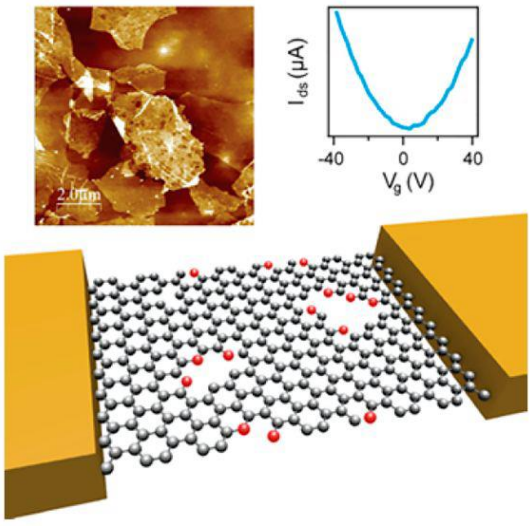

Figure 1. Morphological and electronic characterization of EEG showing the presence of structural defects.

The electrochemical approach was then extended to the exfoliation of other 2DMs, e.g. MoS_2, developing a novel method of exfoliation based on electrochemical lithium-ion intercalation. Compared to past literature,[22] this approach allows to obtain more than 60% of 2H-phase MoS_2. Raman and XPS analysis show that the material is rather defective, throwing light on its electrical characteristics. The electrical performances of FETs based on single MoS_2 flakes were greatly improved through butanethiol vapour treatment, proving that sulfur vacancies are an abundant part of defects in such a material. This work inspired the second experimental part presented in this thesis. Defects created during the exfoliation processes can act as reactive sites for covalent and non-covalent interactions. The first can be exploited for post modification *via* chemical functionalization, while the reversible and selective nature of non-covalent interactions is ideal for sensing.

Chemical sensing is a topical field of science as it will provide a key contribution to the improvement of people's quality of life by offering concrete solutions towards food safety, environmental and biohealth monitoring (as early diagnostics and continuous monitoring of diseases), etc. Recent studies have revealed that MoS_2 holds a great potential as an active material for gas sensing, by taking advantage of the highest surface-to-volume ratio combined with the semiconducting electrical characteristics and controlled chemical composition. Thanks to its unique chemical and physical properties, MoS_2 can interact with the gas adsorbed on its surface (O_2, H_2O, NO_2, CO, NH_3, etc.) yielding a consequent change in the conductivity of the material, which can be measured as a variation in current in two- and three-terminal devices.[23]

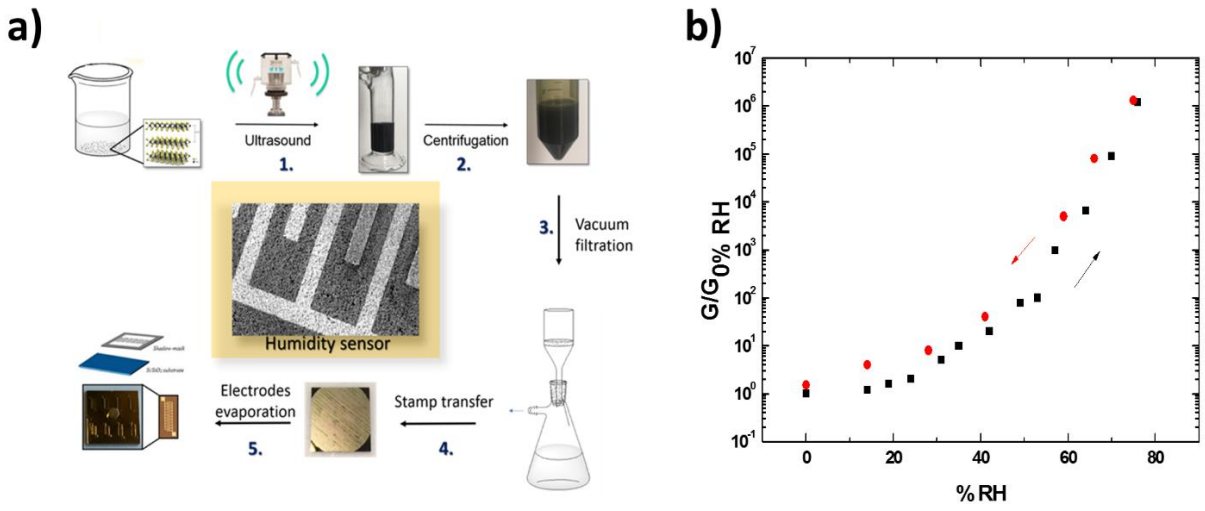

Figure 2. Sketch of the procedure for fabricating MoS_2-thiol sensors (a) and characteristic performance of MoS_2 films as humidity sensors at different relative humidity (b). The graph reports the ratio $G/G_{0\%\ RH}$ versus the relative humidity (%RH), where G is the conductance value in the presence of humidity and $G_{0\%\ RH}$ is the conductance value at 0% RH.

However, to date, 2D material-based devices cannot compete with commercially available sensors because of their low sensitivity. Another drawback, which is still hindering the appearance of 2D material-based devices on the market, is again the lack of an efficient and cost-effective method of production on a large scale of 2DMs with competitive sensing properties.

We exploited the LPE approach to prepare MoS_2 nanosheets at low cost for fabricating large-area gas sensors (Figure 2). The ultrasound-induced LPE method was tailored in order to promote the formation of edge defects which might be beneficial to MoS_2 gas sensing properties. Through a simple and effective processing method, MoS_2 ink was deposited in the form of homogeneous films for the fabrication of chemiresistor devices. MoS_2 thin films showed remarkable sensitivity toward humidity and selectivity to various small molecules, proving that LPE MoS_2 can be a good candidate for next generation of gas sensors as it can allow the fabrication of large-area, light and highly performant flexible devices.

Finally, in the third experimental part of the thesis, we present a new strategy for modulating the properties of 2DMs by exploiting the LPE methods. This project involves the use of molecular systems, e.g. organic semiconductors (OSCs) in combination with 2DMs.

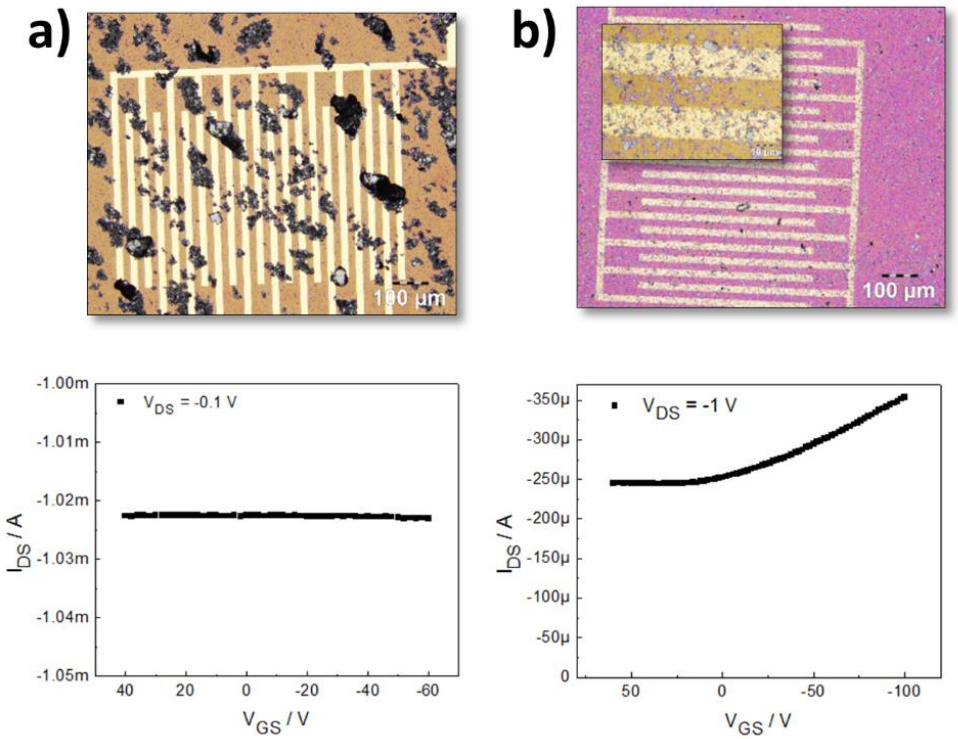

Figure 3. Optical microscopy images (top) and electrical characterization (bottom) of graphene exfoliated in the absence (a) and in the presence (b) of the polymer PCDTPT.

While conventional (opto)-electronic materials like organic semiconductors (OSCs) are well established and can display numerous advantages including the tunability of their physical properties *via* chemical functionalization, excellent processability, and suitability for up-scalable processes even on flexible supports, their electrical performances are modest. To solve this problem, several attempts of combining OSCs with 2D materials have been reported in the past literature.[24] Herein, we propose a new approach based on the simultaneous blending of OSCs, such as poly(3-hexylthiophene) (P3HT) and poly[4-(4,4-dihexadecyl-4H-cyclopenta[1,2-b:5,4-b']dithiophen-2-yl)-alt-[1,2,5]thiadiazolo-[3,4-c]pyridine] (PCDTPT), with graphene during the exfoliation of graphite powder into few-layer graphene (FLG) nanosheets, with OSCs acting as a dispersion stabilizing agents (DSAs) and preventing the re-aggregation of the exfoliated graphene flakes, ultimately enabling the production of homogeneous bi-component dispersions (Figure 3). The electrical characterization of the resulting hybrid films revealed a strong improvement of electrical performances in the case of hybrid FLG/PCDTPT films compared to its pristine components. This work might open the doors to the use of LPE methods for the tuning of 2DMs properties in view of their introduction as active components in novel multifunctional devices.

In conclusion, we developed new approaches for the production in liquid media of 2D materials paving the way to their exploitation as active materials for applications in electronics and sensing. In particular, the electrochemical approach has been extensively investigated, casting the basis for the process improvement towards the mass production of 2D materials which can be conveniently employed in low-cost flexible (opto)-electronic devices.

TABLE OF CONTENTS

CHAPTER

CHAPTER 1.

INTRODUCTION

Graphene, owing to its exceptional properties including the high thermal conductivity[30] and optical transparency,[31] outstanding mechanical strength and flexibility,[32] has revolutionized the field of material science and nanotechnology. It has reawakened and catalysed the research on other layered crystals beyond graphite – most of which already well-known like molybdenum disulfide (MoS_2) and hexagonal boron nitride (h-BN) – permitting the discovery of outstanding properties never revealed before. Unexpected characteristics show up when these materials are reduced to one or a few atomically thick sheets. The rise of graphene has hence led to the rapid development of a new class of nanomaterials, known as two-dimensional materials (2DMs). Among them, there are transition metal dichalcogenides (TMDs) most of which are semiconductors displaying a sizeable direct bandgap (1-3 eV) in their single layer form, extremely high I_{on}/I_{off} ratios reaching $\approx 10^8$ and field-effect mobilities within the range of 10-100 $cm^2V^{-1}s^{-1}$.[33] Black phosphorus (BP) stands out for its high carrier mobility (up to 1000 $cm^2V^{-1}s^{-1}$),[34] while there are also insulating 2DMs like h-BN which exhibits bandgap of ≈ 6eV.[35] Many other atomically flat materials are part of these growing family, each one holding their own distinctive properties. Such a wide range of diverse properties makes the 2DMs attracting components for numerous technological applications in opto-electronics, energy storage and generation and sensing to name a few.

Once demonstrated their existence and properties, one of the first objectives in this field has been to prepare such atomic-thin materials. Many strategies for the production of 2DMs have been proposed and classified in *bottom-up* and *top-down* methods.[20] *Bottom-up* techniques, such as chemical vapor deposition (CVD)[36-37] and epitaxial growth,[20, 38-39] makes it possible to produce high-quality materials which resulted good candidates for application in nanoelectronics. Nevertheless, these approaches are expensive and limited to the wafer scale production. Conversely, *top-down* methods are generally simple and low-cost, as they are based on the mechanical cleavage of layered crystals using exfoliation techniques such as Scotch tape method and liquid phase exfoliation (LPE).

Methods such as Scotch tape-based exfoliation, chemical vapor deposition and epitaxial grown have been essential for the isolation and the study of 2DMs fundamental properties, as well as, for the development of the first prototypes of flexible electronics, wearable sensors, batteries, membranes *etc*. Soon, however, it has become urgent the necessity of having low-cost and up-scalable methods to realize such applications on a real scale.

The methods of liquid-phase exfoliation represent the most viable way toward the large-scale production of 2DMs. Their success is due to the possibility to produce 2DMs in form of inks which can be deposited on different substrates enabling the formation of large area 2DMs. Moreover, the LPEs are cost-effective approaches and do not require specific production conditions such as high vacuum or high temperature. On the contrary, the exfoliation usually occurs in mild conditions. Presently, the approaches which operate in liquid media are numerous, e.g. ultrasound-induced LPE (UILPE),[16, 40] shear exfoliation (SE),[41] electrochemical exfoliation (EE),[26] ball milling,[42] *etc*. and can be carried out in a large variety of conditions e.g. various liquid media and operating parameters. As a result, LPEs yield rather different materials in terms of thickness, lateral size and quality. Although

that has aroused suspicious and notable confusion on the processes themselves and on the characterization and applicability of the produced materials, on the other hand, the possibility to produce materials with distinct and modulable characteristics makes LPE approaches very appealing for different applications. Yet, much greater attention on the structure and properties of the 2DMs produced with LPE approaches is necessary to unveil their potential and achieve fine control over their properties, as a prerequisite towards their integration in novel multifunctional devices.

Often, the characteristics of the 2DMs inks have been presented by indicating the performances of a chosen single flake devices. Considered the large inhomogeneity in terms of sizes of the nanosheets which form an LPE ink, it is clear that such findings are not representative of the overall ink's properties. On the contrary, they, often, overestimate the performances of the material with respect to its practical use as ink. As the use of LPE 2DMs is meant for large scale applications, and not as a single flake, approaches of deposition which permit of generating large continuous films from 2D inks are highly desirable. The deposition of these inks for electronics application should avoid the use of surfactants or polymers that cannot be easily removed. On the contrary, the development of methods of exfoliation and deposition from pure solvents or, alternatively, as embedded in a functional matrix which can be beneficial for the final product, would be the key for application in electronics. Once overcome these challenges, the properties of 2DMs can be investigated in form of films disclosing the practical potential of such materials. In addition, the comparison with single flake devices performances would allow understanding whether 2DMs films properties are affected by the deposition approach – which can be eventually improved – or reflect the intrinsic properties of the material.

The main goal of research in this field has been for a long time the one of achieving high-quality 2DMs flakes featuring large lateral sizes and nanometre thicknesses, aiming at similar performances to Scotch tape or CVD 2DMs but with the advantage of processing these materials into large-area thin films. That remains still an open challenge as it is now possible to obtain large amount of mictrometre-size thin flakes but at the cost of more defective materials. Nevertheless, many applications, for example in the fields of sensors, composites, energy *etc*., don't require such characteristics. Conversely, the use of inks constituted by nanometre-size flakes can be more convenient in certain respects.

By providing insight into the multiscale analysis of the chemical and physical properties of LPE materials and their relative films, with or without additional functionalities, this thesis aims to achieve a profound understanding of the fundamental properties of such materials in view of their future applications in electronics. To this purpose, we investigated different approaches of liquid-phase exfoliation (e.g. electrochemical exfoliation and liquid-phase exfoliation) and developed methods of deposition in order to explore the properties of the materials not only at single flake level, but on films as well, and to reach a deep comprehension of the relationship between their structure and properties. These fundamental studies have been supported by the development of new strategies to overcome some of the challenges in the introduction of LPE materials in working devices. In particular, this thesis intends to explore the use of LPE methods to modify 2DMs materials in order to achieve a control over their properties that is necessary for the integration of these materials in multifunctional devices.

This thesis has been divided in the following parts:

The next two chapters revise the state of the art on 2DMs production and related properties. Chapter 2 gives an overview of 2DMs and their properties, with a focus on the materials which have been investigated in this work, which are graphene and MoS_2. Particular attention is given to the methods for their production *via* liquid-phase exfoliation, providing the reader with a detailed literature review

on the latest advancements on ultrasound-induced liquid-phase exfoliation and electrochemical exfoliation approaches. Finally, some of the attractive applications of LPE materials are discussed. Chapter 3 introduces the techniques employed in this work for the characterization of the produced materials (optical microscopy (OM), atomic force microscopy (AFM), X-ray photoelectron spectroscopy (XPS) and Raman spectroscopy). Together with the fundamental principles of the technique, each chapter reviews the main achievements in the characterization of graphene and MoS_2.

These first two chapters are followed by three experimental chapters which are organized in a similar way: they include an introduction to the project, a part of materials and methods where the details regarding samples preparation and characterization are reported, a section that covers the results of the research and, finally, the conclusions of the project are summarized at the end of the chapter.

Chapter 4 is the first experimental chapter which deals with the method of electrochemical exfoliation. This chapter offers a detailed understanding over the chemical and structural properties of electrochemically exfoliated graphene (EEG) on different scales, combined with a focus on its electronic characteristics both at single flake level and on film. This approach has been extended to the exfoliation of MoS_2. The produced material has been characterized in detail demonstrating the applicability of electrochemical approach for the exfoliation of other 2DMs and unveiling the intrinsic characteristics of this material.

Chapter 5 explores one of the possible applications of LPE 2DMs in the field of sensors and show that MoS_2 produced by UILPE offers great potential as humidity sensor.

In chapter 6 the world of 2DMs is merged with molecular systems *via* LPE methods. This work shows that graphene can be advantageously combined with semiconducting polymers through ultrasound-induced LPE toward the generation of novel multifunctional devices.

In the last chapter 7, the main results of this research work are summarized. The work ends with conclusions and suggestion for future research, discussing the challenges which need to be faced for the integration of LPE 2DMs in electronics devices.

CHAPTER 2.

TWO-DIMENSIONAL CRYSTALS: A NEW GENERATION OF MATERIALS

2.1 2D materials' families and their properties

The discovery of the astounding properties that layered solids exhibit when layered down, or exfoliated, to monolayers like graphene has paved the route to a new branch of material science which is spreading like wildfire: two-dimensional materials. This topic became of interest for scientists in many classical disciplines including physics, chemistry, materials, engineering, biology, and also in the interdisciplinary fields of materials and nanoscience's.

Two-dimensional materials including graphene, transition metal dichalcogenides, hexagonal boron nitride *etc*. are a novel class of materials which can be thick just a few atoms, in the form of monolayers. Graphene can be even thinner, being just one carbon atom-thick. They belong to the family of nanomaterials and own unique physical and chemical properties compared to the bulk counterpart. They are transparent and flexible, with exceptional thermal and electrical properties. Therefore, there are great expectation that such materials will be soon part and parcel of our future technologies based on ultrathin and flexible devices towards a lighter and comfortable life style.

The breakthrough on the detected extraordinary properties of graphene isolated by "Scotch-tape method" in 2004 has led to a renewed interest in these materials, although the exfoliation of layered materials, like MoS_2 and graphite, dates back to the '60s.[43,44-45] Today, while graphene continues to play a dominant role in various fields, and research based on discovering its potentials is far from having reached the peak, they are approaching some limits. The "Scotch-tape approach", that is still the only effective method for the production of pristine graphene, cannot clearly be employed on an industrial level, while methods like CVD suffer from expensive production. Moreover, the use of graphene as active component in electronic-switching devices is not feasible due to its zero bandgap. As a consequence of such apparent drawbacks, researchers attention is being directed again to other materials such as 2D semiconductors. Indeed, there are plenty of other layered materials which have revealed peculiar properties when thinned to monolayers as a consequence of quantum confinement and they can either supplement or replace graphene in electronic devices. Moreover, their development is even more rapidly leveraging the understanding gained for graphene. Most of the elements of periodic table are involved in these materials (see **Figure 2. 1**). Consequently, these compounds exhibit a wide variety of electronic properties including metallic, insulating and semiconducting ones.

Besides graphene, that will be discussed more in detail in section 2.1.1, a carbon-based dimensional material that has gain lots of interest similarly to graphene, if not even more due to its higher versatility, is graphene oxide (GO).

GO is the oxidized form of graphene, that is mainly synthetized by Hummers' method, namely immersing graphite in concentrated acids in the presence of oxidizing agents, in particular in a mixture of sodium nitrate, potassium permanganate and concentrated sulfuric acid. GO can be readily dispersed in water. The negatively charged surface of GO flakes allows stable water dispersions

containing more than 90% of monolayers with concentrations up to 4 mg ml^{-1}. GO has given, therefore, the opportunity to explore the chemistry in solution of this material, although its final properties largely differ from graphene due to the extensive presence of oxygen functionalities and defects. To reach similar properties to graphene, GO needs to be reduced (electro)chemically, thermally or with other methods, giving rise to the, so called, reduced graphene oxide (rGO).

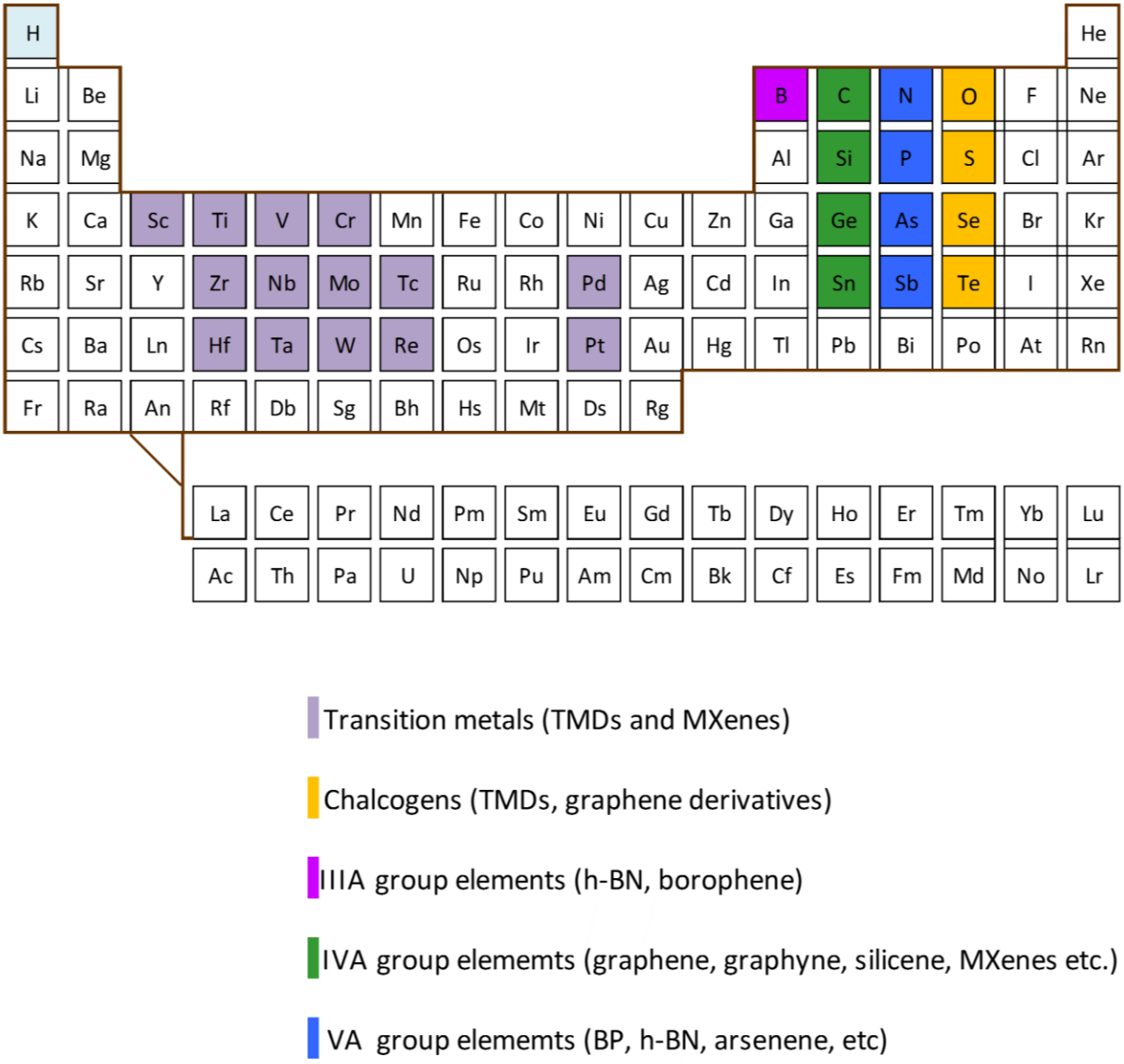

Figure 2. 1. Some of the elements across the periodic table involved in 2D materials (2DMs). The element families are color grouped and the 2DMs which contain the indicated elements are reported in brackets in the legend. (TMDs = transition metal dichalcogenides; h-BN = hexagonal boron nitride)

A big fraction of the other 2D materials are compounds made of two or more elements. Their bulk counterparts are generally layered crystals, featuring strong in-plane covalent bonds and out-of-plane van der Waals (vdW) forces, which hold the different planes together in a vertical layered structure. Therefore, these layered compounds are generally classified as vdW ls solids. Due to this structure, layered vdW materials are extremely anisotropic both mechanically and electrically. For example, in

bulk MoS_2 the conductivity along the planes is higher by a factor of at least 10^2 compared to the one perpendicular to the planes. Moreover, owing to their layered structure, characterized by weak forces between layers, these materials can be exfoliated making possible the formation of bi-dimensional materials.

Following the era of graphene and graphene oxide, an escalation of other layered compounds has been proposed. The list opens with MoS_2 and the other transition metal dichalcogenides (TMDs) like WS_2, $MoSe_2$ and WSe_2 and goes on with hexagonal boron nitride (h-BN), black phosphorous (BP), Mxenes, *etc*. When produced in form of mono- or few-layer, their atomic-scale thicknesses allow to have a good control of the properties. Furthermore, new properties have been discovered as a result of quantum confinement.

The class of 2DMs more studied after graphene is undoubtedly the one of TMDs. Unlike graphene which consists of only one carbon atom thick layer, TMDs follow a MX_2 structure where M is a transition metal (e.g. Mo, W, Nb, Ta, Re) and X is chalcogen element (S, Se and Te), being therefore more chemically versatile.[46] This family of materials results intriguing for the wide range of properties (electronic, optical, chemical and thermal ones) that they can cover.[47] They present a wide spectrum of electronic properties. For example, MoS_2 and WS_2 are semiconductors, NbS_2 and VSe_2 are metals, HfS_2 behave as insulator. Many TMDs are difficult to be produced by *bottom-up* approaches because of the high melting point of the precursors.[48] Nevertheless, they are relatively easy to exfoliate. A more detailed description of this class of materials is reported in section 2.1.2 where a particular attention is given to MoS_2, whose production by electrochemical exfoliation and ultrasonication, and its potential as gas sensor are the subject of this research work.

Relevant was also the discovery of the "white graphene", namely hexagonal boron nitride (h-BN), for its exceptional properties of insulator (bandgap of 5.97 eV). Similarly, to graphene, boron and nitrogen atoms are covalently bond in a planar h-BN layer. h-BN can be obtained either *via* LPE or CVD process, the latter being the preferred method for the good controllability of crystal size and quality. However, the CVD growth of h-BN is currently feasible only on some specific substrates, reaching the largest grain area of 7500 μm^2 on Cu-Ni alloy;[49] while the fabrication of large-area on other non-metal substrates still needs to be developed. h-BN could be practically used as gate dielectric layers or oxidation-resistant coatings.

Besides 2D compounds, there are also the elemental 2DMs, headed from graphene, which include elements from III-V A groups. Also these materials exhibit exotic electronic, magnetic and catalytic properties compared to their bulk counterparts. For instance, graphyne and its derivatives are new 2D allotropes of carbon, developed as alternative to graphene. They consist of sp- and sp^2-hybridized carbon atoms. In particular, one or more acetylenic units bonds two carbon atoms in different ways rising up to graphyne, graphdiyne, graphtriyne and so on. Unlike graphene, graphynes allotropes are semiconductors with a small bandgap (~1.2 eV for graphynes and ~0.46 eV for graphdiynes). However, despite the high carrier mobilities and suitable bandgaps, graphyne family finds difficulties to advance as alternative to graphene due to the efforts in synthesis of high quality large-area films.

Following carbon, in IV A group also silicon, germanium and tin exist as 2D structures, which analogously to graphene are called with the suffix –ene to distinguish the monolayer from the bulk: silicene, germanene and stanine. They have high carrier mobilities and are semiconductors with a direct bandgap. However, silicene and germanene are considered nonlayered materials as they are sp^3-hybridized and their synthesis is rather challenging. Their properties are mainly theoretically predicted. 2D materials from V A group are black phosphorus (PB), arsenene, antimonene and bismuthene. Among them, the one is receiving unquestionable attention for its high electron mobility

and non-zero band gap is BP. In BP each phosphorus atom is covalently bonded with three adjacent phosphorus atoms in a single layer honeycomb structure. Unlike few-layers TMDs having an indirect bandgap, BP is a direct band semiconductor with a tuneable electronic bandgap that increases from 0.3 to 1.5 eV when the thickness decreases going from bulk to monolayer. Moreover, few-layer BP presents a higher carrier mobility, as high as 1000 $cm^2V^{-1}s^{-1}$,[34] compared to TMDs (mobility of few $cm^2V^{-1}s^{-1}$) , even if with a smaller I_{on}/I_{off}, and an ambipolar behaviour, being therefore in between graphene and TMDs. Similarly, to graphene, BP single crystals are composed by vertically stacked layers held together by vdW interactions. Therefore, it can be easily produced by mechanical exfoliation or in liquid phase. Despite such positive characteristics, the main weakness of BP is related to its environmental instability. Finally, in 2018, a new 2D allotrope of phosphorus has been proposed and named blue phosphorus. In blue phosphorus atoms are arranged in a honeycomb structure similar to graphene, although not completely flat but regularly "buckled". Recently, it has been predicted its stability and its bandgap of 2 eV that bodes well for optoelectronic applications.[50] Antimonene is another semiconductor with a bandgap up to 2.28 eV and having the peculiarity of being transformed from indirect to direct bandgap semiconductor just applying a small strain to the monolayer. Similarly, the structure of bismuthene is compressed when the 3D crystal is thinned down to single-layer flake, leading to its transformation from semimetal to semiconductor which promote its introduction in optoelectronics. For III A group, the only elemental 2DMs is the borophene, whose structure and properties are predicted by theory. Most of the elements of transition group exist also as 2DMs, but the low yield of synthesis hinders their applicability.

Finally, recently a new group of 2D compounds named MXenes has joint the list of 2DMs that is growing fast. MXenes are transition metal carbides (TMCs), namely, crystals where the interstitial sites of early transition metals (group III–VI B, 3d elements and 4d/5d elements) are filled with carbon atoms. In particular, MXenes are layered TMCs and are the more recently studied of this family. The general formula of MXenes is $M_{n+1}AX_n$ where n= 1, 2, or 3, M is an early transition metal, A is an element from the main group (generally, group III A and IV A) and X is carbon. The strong M-X bond has mixed covalent/metallic/ionic character, whereas the M-A bond is metallic. Therefore, in contrast to other layered materials, such as graphite and TMDs, where weak vdW interactions hold the structure together, the bonds between the layers in the MAX phases are too strong to be broken directly by means of shear forces, cavitation and similar mechanical stimuli, but usually a preliminary etching process is necessary before the exfoliation. Immersing them in HF solutions results in the Al being selectively etched away. In this process Al atoms are replaced by O, OH and/or F atoms. In other words, the metallic bond M-A are replaced by hydrogen bonds using aqueous HF as etching agents. That dramatically weakens the interaction between the layers making possible the exfoliation of the material. These new materials were labelled as MXenes to emphasize the loss of the A element from the MAX parent and highlight their 2D nature, similarly to graphene. They have attracted interest because they combine the metallic conductivity of transition metal carbides with the hydrophilic nature of their hydroxyl or oxygen terminated surfaces in one material only. In other words, they behave as “conductive clay”.[51] MXenes can be extensively used in battery electrode materials, as electrons can move fast across their microstructures.

This list of 2DMs could probably be longer since always new materials are added, thereby inspiring numerous studies and challenges. However, it can be already seen as a rich library where finding materials with specific properties for any kind of application. Importantly, to enable the use of these materials for practical applications, it is necessary to overcome one of the main challenges in this field, that is the production of 2DMs at large scale.

In this thesis we explore new methods of exfoliation in liquid media towards the large production of these materials. To this aim, we have focussed our effort to two prototypical 2DMs, that are graphene and MoS_2. Some of the aspects of their structure and proprieties, that can be relevant for this work, are reported in section 2.1.1 and 2.1.2.1.

2.1.1 Graphene

Graphene is a single layer of carbon atoms arranged in a hexagonal lattice. Actually, it can be seen as a single atomic layer of graphite that is its bulk counterpart. In a graphite crystal, graphene layers are stacked on top of each other with an interlayer distance of 0.335 nm and held together by vdW interactions.

Graphene is the thinnest and lightest known material. Furthermore, it holds exceptional properties. It displays extremely high electrical and thermal conductivities, transparency, flexibility, strength and impermeability to molecules. It exhibits an extremely i) high mobility of 200,000 $cm^2V^{-1}s^{-1}$ in comparison with 1,400 $cm^2V^{-1}s^{-1}$ for silicon, ii) high thermal conductivity [52] > 4000 WmK^{-1} that is 10 times larger than copper and aluminium, iii) high theoretical surface area of 2600 $m^2\ g^{-1}$,[53] and iv) high optical transparency of 97.7%, to name a few. Such extraordinary characteristics result from its structure. Graphene is a planar carbon allotrope where carbon atoms are sp^2 hybridized. The superposition of 2s orbital with $2p_x$ and $2p_y$ ones generates stable and localized σ -bonds with the three neighbouring carbon atoms. Being strongly covalent bonds, they are responsible for stability and flexibility of graphene. The remaining $2p_z$ orbitals are perpendicular respect to the plane connecting carbon atoms. Their overlap form delocalized π bond that are responsible of the exceptional thermal and electronic properties. Since only the π bond contributes to the electronic properties, the electronic band structure of graphene can be described by an orthogonal nearest-neighbour tight-binding approximation, that consider graphene as a set of atoms with a single p_z orbital per site. The band structure of graphene yields conduction and valence bands which are symmetric with respect to the Fermi energy, also called *Dirac point* or *Charge neutrality point*, which is set at 0 eV. Graphene valence and conduction bands are degenerated in 6 points, located at the corner of the Brillouin zone, called Dirac points (**Figure 2. 2**).[54]

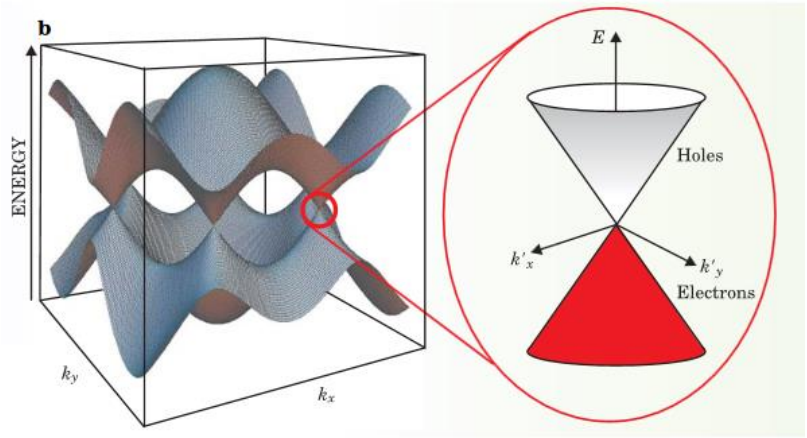

Figure 2. 2. Representation of graphene band structure, the inset shows the valence and conduction bands that touch at the k points in the Brillouin zone. Adapted from ref. 54.

Because of this characteristic, graphene is called gapless semiconductor or semi-metal. In neutral graphene the Fermi level is located at these points. Such peculiar band structure explains the

characteristic ambipolar electric field-effect in graphene (**Figure 2. 3**). Charge carriers can be tuned continuously between electrons and holes in concentrations n as high as n =10^{13}cm^{-2} and their mobilities can exceed 15,000 cm^2 V^{-1} s^{-1}, even under ambient conditions.[55] The gate voltage induces a surface charge density and accordingly the Fermi level shifts. The surface charge density is expressed as $n = \varepsilon_0 \varepsilon V_g/te$, where ε_0 is the permittivity of free space and ε the one of SiO_2, *e* is the electron charge and t is the thickness of SiO_2 layer. The doping induced by the electric field transforms the shallow-overlap semimetal into either completely electron or completely hole conductor through a mixed state containing both electrons and holes. For the regions with only electrons or holes, the Hall coefficient decreases with increasing carrier concentration as 1/n*e*. The resistivity also follows the standard dependence $\rho^{-1} = \sigma = ne\mu$, where σ is carrier mobility. In the mixed state, σ changes little with V_g, indicating the substitution of one type of carrier with another, while the Hall coefficient is proportional to the difference between electron and hole concentration. Without electric field doping i.e. at zero V_g, FLG was found to be a hole metal, showing a shift of the peak to large positive V_g. However, this shift is attributed to doping of the films by absorbed water. In fact, by annealing the devices in vacuum a shift of the peak close to zero voltage is observed. The mobility of FLG was determined as $\mu = \sigma(V_g)/en(V_g)$.[11]

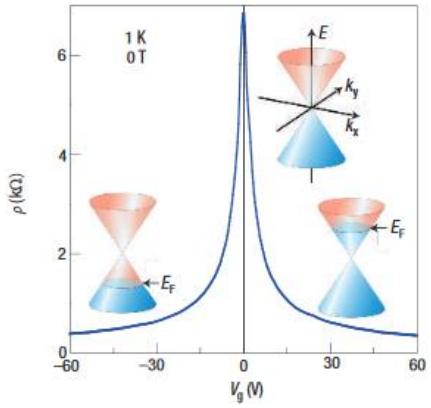

Figure 2. 3. Ambipolar electric field effect in graphene monolayer. The insets show the conical low energy spectrum E(k) that show the changes in the position of Fermi level with the gate voltage Vg. Positive voltage induce electrons, vice versa a negative voltage induces holes. Reproduced from ref. 55.

A similar study is challenging in the case of graphene produced by ultrasound-induced LPE due to the nanometre size of the flakes. On the contrary, benefitting of the micrometre sizes of electrochemically exfoliated graphene (EEG) flakes, it is possible to investigate on the electrical properties of such material at single flake level shedding light on its potential.

2.1.2 Transition metal dichalcogenides (MS_2, MSe_2 *etc*.)

Transition metal dichalcogenides (TMDs) consist of a hexagonally packed layer of transition metal atoms (e.g. Mo, W, Nb, Ta, Re) sandwiched between two layers of chalcogen atoms (S, Se and Te). While in-plane M-X bonds are usually covalent, intralayer interactions are governed by vdW forces.

TMDs cover a wild spectrum of electronic properties by virtue of their different structure. For example, MoS_2 and WS_2 are semiconductors, NbS_2 and VSe_2 are metals, HfS_2 behaves as an insulator. The electronic structure of TMDs strongly depends on the coordination environment of the transition metal and its d-electrons. Referring, for the sake of simplicity, to monolayers, in both 1H and 1T phases

(a description of such polymorphs is displayed for the representative case of MoS_2 in section 2.1.2.1), d-orbitals in the non-bonding *d* bands are located within the gap between the bonding (σ) and antibonding (σ*) bands of M-X bonds. According to ligand field theory, octahedrally coordinated transition metal centres (D_{3d}) of TMDs form degenerate dz^2, x^2-y^2 (e_g) and $d_{yz,xz,xy}$ (t_{2g}) orbitals that can together accommodate the TMDs' d electrons (a maximum of 6, for group 10 TMDs). On the other hand, the d orbitals of transition metals with trigonal prismatic coordination (D_{3h}) split into three groups, d_z^2 (a_1), $d_{x^2-y^2,xy}$ (e), and $d_{xz,yz}$ (e′), with a sizeable gap (~1 eV) between the first two groups of orbitals (**Figure 2. 4**).

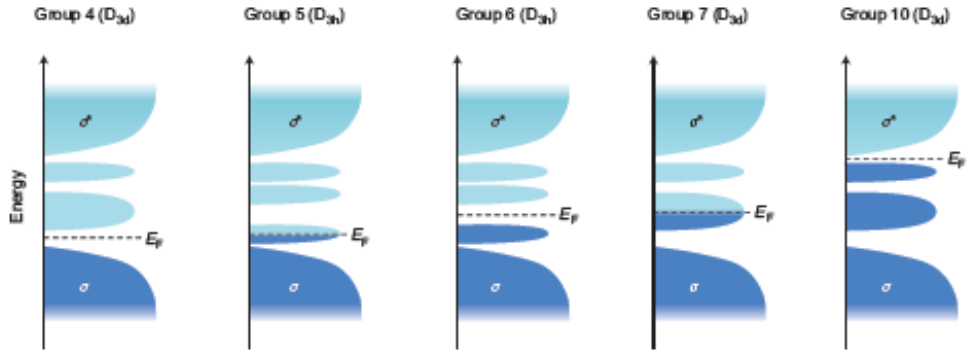

Figure 2. 4. Qualitative sketch that describes the progressive filling of d orbitals located within the bandgap between the bonding (σ) and antibonding (σ*) bands in TMDs. D3d and D3h refer to trigonal prismatic and octahedral coordination of transition metals. Reproduced from ref. 46.

The diverse electronic properties of TMDs (metals, semiconducting, *etc*.) arise from the progressive filling of the non-bonding *d* bands from group 4 to group 10 species.[46] When the orbitals are partially filled, as in the case of 2H-$NbSe_2$ and 1T-ReS_2, the Fermi level (EF) is within the band and TMDs exhibit metallic character. When the orbitals are fully occupied, such as in 1T-HfS_2, 2H-MoS_2 and 1T-PtS_2, the Fermi level is in the energy gap and the materials are semiconductors. The effect of chalcogen atoms on the electronic structure is minor compared with that of the metal atoms, but a trend can still be observed: the broadening of the *d* bands and corresponding decrease in bandgap with increasing atomic number of the chalcogen. For example, the bandgap of 2H-MoS_2, 2H-$MoSe_2$ and 2H-$MoTe_2$ decreases gradually from 1.2 to 1.0 eV.

Table 2. 1. Properties of layered TMDs. The values of energy bandgap are reported for the semiconducting materials in form of bulk and monolayer (1L). Adapted from ref. 56.

MX_2	$-S_2$	$-Se_2$	$-Te_2$
Mo	**Semiconducting** 1L: 1.8 eV Bulk: 1.2 eV	**Semiconducting** 1L: 1.5 eV Bulk: 1.1 eV	**Semiconducting** 1L: 1.1 eV Bulk: 1.0 eV
W	**Semiconducting** 1L: 1.9 eV Bulk: 1.4 eV	**Semiconducting** 1L: 1.7 eV Bulk: 1.2 eV	**Semiconducting** 1L: 1.1 eV
Nb	**Metal** **Superconducting**	**Metal** **Superconducting**	**Metal**

These models assume ideal coordination but, when a structural distortion occurs, as often seen in group 7, the electronic structure can change. Destabilization of the original phase may be attributed to the effective change in the *d*-electron count. For example, when 2H-MoS_2 is intercalated with lithium, the transfer of an electron from the valence *s* orbital of the alkali metal to the *d* orbital of the transition metal centre can cause the transformation of 2H phase in 1T phase.[46, 57] The opposite transition from 1T to 2H has also been observed in TaS_2 after Li intercalation.[58] Bulk semiconducting 2H-phase TMDs, such as MoS_2, WS_2, WSe_2 and $MoSe_2$ have an indirect bandgap but when thinned down to monolayer they exhibit direct bandgaps, resulting in an enhanced PL intensity (See section 2.1.2.1 dedicated to the representative example of MoS_2). With an intrinsic bandgap typically in the range of 1-2 eV, 2D TMDs can be used instead of graphene for switching applications, having on/off current ratio that is 8 orders of magnitude higher than graphene. Moreover, in function of the application, one can chose the proper TMDs based on their different properties, which has been summarized in **Table 2. 1**.

2.1.2.1 Molybdenum disulfide (MoS_2)

Among all the TMDs, the best known is certainly MoS_2, which is commonly used as dry lubricant in racing car engines and ultrahigh-vacuum technology.[59] Similarly to graphite, MoS_2 is a vdW solid. Both materials have a similar bulk structure formed by stacking of atomic layers weakly interacting among each other, while the atoms within each plane are covalently bond. Consequently, even MoS_2 can be exfoliated into mono and few-layer flakes like graphene. However, while graphene is the thinnest material possible, being only one atom thick, MoS_2 monolayer consist of three atomic layers, i.e. a plane of Mo atoms sandwiched between two planes of S (S-Mo-S) in a trigonal prismatic coordination. Such chemical structure is responsible for the differences in chemistry and properties between graphene - only composed by carbon atoms- and MoS_2. For example, while graphene is a semimetal with a zero bandgap, MoS_2 monolayer is a semiconductor. Therefore, MoS_2 can be used, instead of graphene, in digital electronic switches. Moreover, MoS_2 is offering more opportunities for its functionalization, mainly through coordination chemistry,[60] besides *via* non-covalent interactions (e.g. vdW or electrostatic interactions).

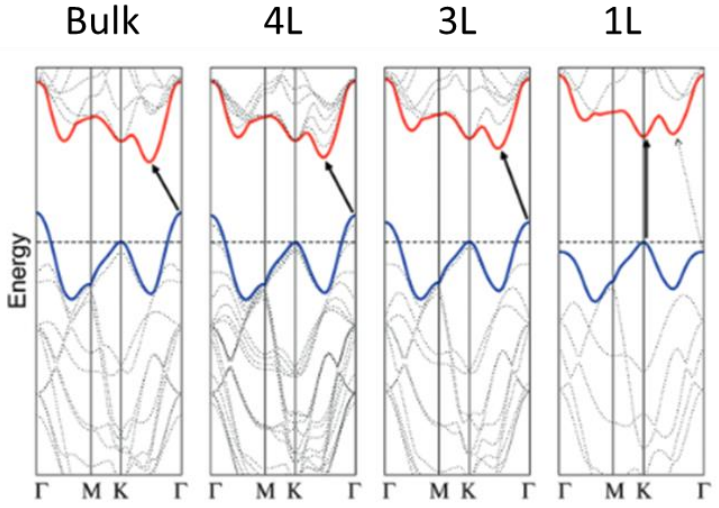

Figure 2. 5. Band structure of MoS_2 bulk crystal, four-layer (4L), tri-layer (3L) and monolayer (1L). In blue is highlighted the highest VB and in red the lowest CB. Adapted from ref. 61.

MoS_2 is an indirect bandgap semiconductor ($E_g \sim 1.2$ eV), where the valence band (VB) maximum lies at the high-symmetry point Γ and the conduction band (CB) minimum at a low-symmetry point between K and Γ. As the thickness is reduced from bulk to monolayer, the indirect gap increases while the direct gap at the K point remains almost unaffected. In monolayer (1L in **Figure 2. 5**) the indirect gap is larger than the direct gap and both CB minimum and VB maximum shift to the K point. Therefore, monolayer MoS_2 can be considered a direct bandgap semiconductor. The occurrence of an indirect-to-direct bandgap transition is demonstrated through a much stronger photoemission in monolayers than in few layers where the photoluminescence can be quenched.[61-62] Although studies on optical and electronic properties of MoS_2 date back to the 60s, the interest toward this material exploded in the era of graphene and in particular in 2011 when the first single-layer MoS_2 transistors displayed remarkably high on/off current ratio ($I_{on}/I_{off} \approx 10^8$).[33] The possibility to have a semiconductor at atomic-scale thickness has raised enormous interest towards MoS_2 and similar materials, demonstrating the viability of these materials in electronics.

The crystal structure of MoS_2 was reported in 1923 by Dickinson and Pauling, who revealed the hexagonal lattice and the structural parameters of MoS_2 by X-ray diffraction.[63] Bulk MoS_2 displays three polymorphs that are usually indicated as 2H, 3R and 1T (**Figure 2. 6**). The polymorphs 2H and 3R share the same structure where each Mo atom is covalently bonded to 6 atoms of S with trigonal prismatic coordination (D_{3h}). The difference between the two polymorphs is in the stacking of the layers. 2H has two layers per unit cell stacked in hexagonal symmetry, whereas 3R has three layers per unit cell stacked in rhombohedral symmetry. In 1T polymorph, Mo and S atoms are arranged in octahedral coordination (O_h) with only one layer per unit cell (tetragonal symmetry).

In single-layer MoS_2 only 1T and 2H can exist. Among them, the most stable is the 2H polymorph that is an intrinsic semiconductor, whereas 1T is metastable and it is the metallic phase of MoS_2. A powerful tool for identifying the presence of 2H and/or 1T phase is high resolution transmission electron microscopy (HRTEM).

In the next section, we report on the methods for producing 2DMs. In particular, we will focus on the methods of exfoliation in liquid-phase since they allow the easy and low-cost production of thin layers in large quantities, giving the opportunity to exploit their properties also on large scale. A particular attention will be paid to the approaches of exfoliation in liquid media that were explored in this research work, that are ultrasound-induced LPE (UILPE) and electrochemical exfoliation (EE).

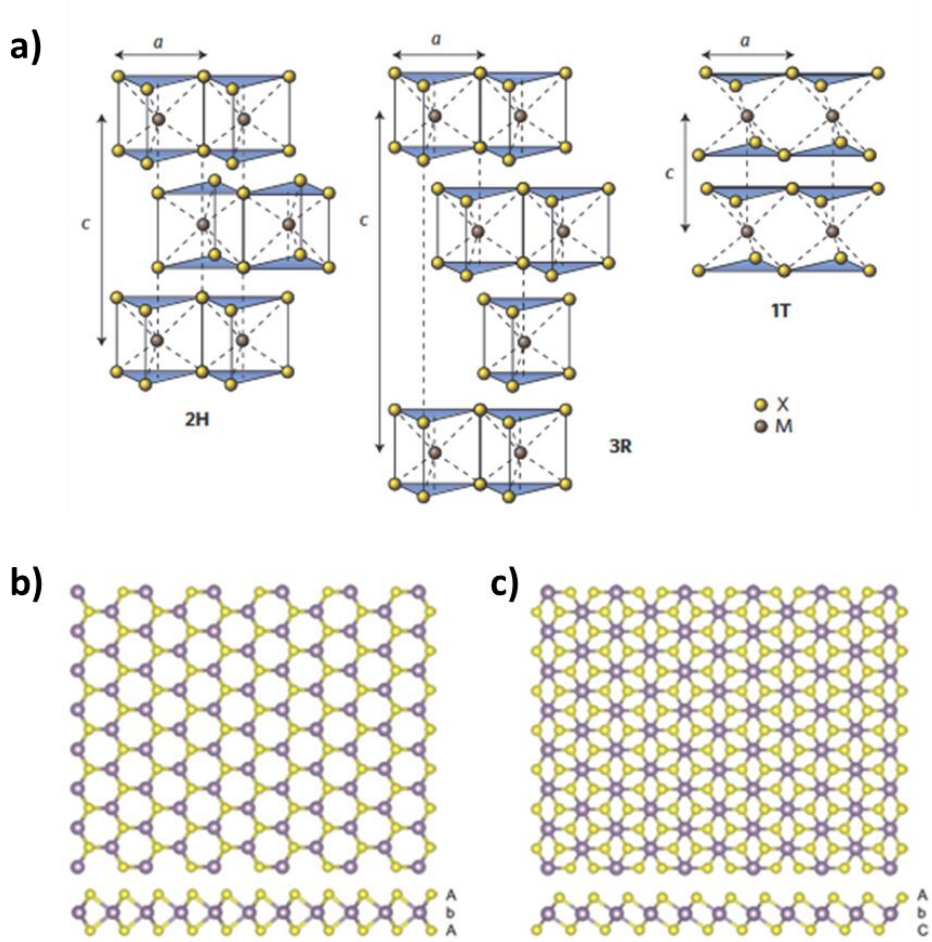

Figure 2. 6. a) Schematic representation of MoS_2 polymorphs: 2H, 3R and 1T; Top view of monolayer MoS_2 crystalline structure with b) trigonal prismatic and c) octahedral coordination. Reproduced from ref. 56.

2.2 2D materials *via* liquid-phase exfoliation of layered crystals: the approaches

Likewise graphene, 2DMs can be produced either by following the *bottom-up* or *top-down* strategies. *Bottom-up* approaches generally exploit the chemical reaction of small molecular building blocks to form 2D networks.[64-65] The chemical synthetic approaches produce generally limited quantities of material. On the other hand, other *bottom-up* technologies like CVD and epitaxial growth have advanced in the last years because they can lead to large area, high quality 2DMs. Nevertheless, they are rather complex methods that generally require high temperatures and high vacuum, resulting expensive. They lack versatility because in some cases, the precursors are not easily accessible, or they are expensive. Moreover, additional transfer step are always needed to exploit the properties of 2DMs on different target substrates.

In parallel, a great effort has been devoted to the development of new strategies for the large-scale production of 2DMs by employing low cost methods, so that the potential of such extraordinary materials can be finally exploit for industrial applications. LPE methods are proving very promising towards the large-scale production of 2DMs because, by means of easy and chip processes, allow to

obtain the largest number of thin layers possible. LPE methods share the same basic principle. These methods take advantage of the common structure of some layered materials that are characterized by weak interlayer forces and exploit different phenomena to lower and/or overcome such interactions between adjacent layers, allowing the separation of the individual sheets, or exfoliation. The benefit of producing 2DMs by LPEs is that the methods employed are very simple and require basic laboratory equipment. Moreover, exfoliated 2DMs can be solution-processable, facilitating their applications.

Originally, the term liquid-phase exfoliation (LPE) was referred to the process of exfoliation of graphite into graphene by ultrasonication in a proper liquid.[66] Now that the number of proposed methods is increased, it has become commonplace using this term in a general extent when referring to all the approaches of exfoliation occurring in liquid phase such as shear mixing, ball milling, the more recent microfluidization, electrochemical exfoliation, *etc*.

As it will be shown throughout this thesis, LPE methods are attractive approaches, being extremely versatile and applicable to various experimental conditions. 2DMs dispersed in liquid media can be modified by exploiting the solution chemistry, can form composites by solution mixing, produce films or coating by means of well-established techniques like spin-coating,[67-68] dip-coating or spray coating[9, 69-70], and more recent ones like inkjet printing.[71-72] These systems can be used for many applications like battery electrodes, barrier composites, photodetectors or energy storage systems and there can be wide space even for new other applications.

In the next subchapters, we discuss the two methods of exfoliation in liquid phase that were employed in this work, namely the ultrasound-induced liquid phase exfoliation and the electrochemical exfoliation. We point out the mechanisms of exfoliation that have been proposed and recent advances in the production of mono- and thin-layer sheets by LPE methods.

2.2.1 Ultrasound-induced liquid-phase exfoliation (UILPE)

The ultrasound-induced LPE, or UILPE, has been introduced in 2005 by McEuen[73] who partially exfoliate graphite in dichlorobenzene, while the first observation of graphene monolayers was reported by Coleman in 2008.[15] So far, this is the method that has demonstrated the highest versatility, enabling the exfoliation of many others 2DMs beyond graphene like h-BN,[74] TMDs,[14, 75] phosphorene, $Ni(OH)_2$,[76] MXenes,[77] *etc*.

Generally, this process consists of three steps: i. the sonication process in a liquid media, that provide the energy necessary to overcome the interlayer interactions allowing the actual exfoliation, ii. the stabilization of the exfoliated material in dispersion, iii. the size selection of exfoliated sheets. The primary phenomenon behind the process of sonication is the cavitation. The cavitation is the growth and collapse of micrometre-sized bubbles or voids in liquids due to pressure fluctuation. During ultrasonication, tensile and shear stress, together with cavitation, act on the bulk material inducing both exfoliation and fragmentation (**Figure 2. 7**).[78] It has been demonstrated that collapse of these micro-bubbles unavoidably lead to defects in the material, that are mainly localized on the edges for short sonication while they occur also on the basal plane of the flakes for sonication longer than 2 hours, appearing as 'hole-like' defects.[79] The same group suggest that it is not about sp^3 defects or vacancies, but rather topological defects.

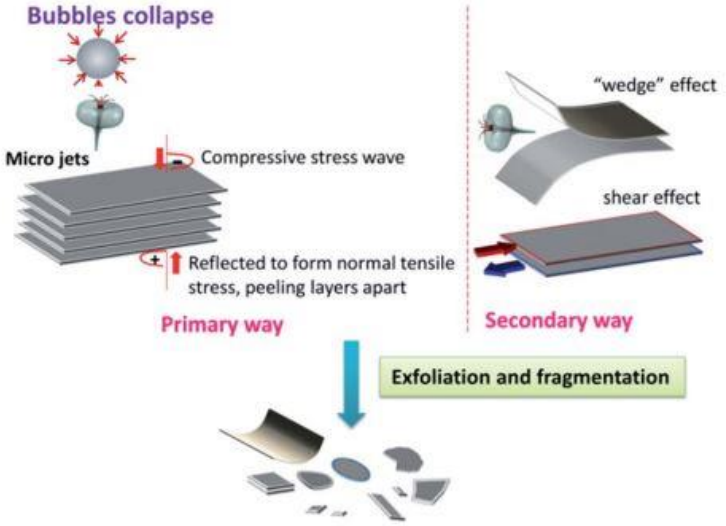

Figure 2. 7. Sketch of the mechanism of exfoliation *via* ultrasound-induced liquid-phase exfoliation. Reproduced from Ref. 18.

Interestingly, it was found that the intensity of the ultrasounds is strictly dependent on the dimension and shape of the vessel. That would explain large discrepancies and poor reproducibility of the experiments from one lab to the other, due to the lack of such kind of details in the previously published studies. Nevertheless, too many other parameters can affect this process such as sonication power, amplitude, frequency, volume, *etc*. Therefore, the process of exfoliation *via* UILPE is still not totally understood.[80] In addition, beside the common laboratory equipment originally used for such studies, like the sonication bath, other kind of ultrasounds sources have been recently introduced e.g. tip sonicator, cup-horn sonicator, *etc*. While in the bath sonication the ultrasonic waves propagate through both the tank and the vessel, resulting in a non-uniform and low intense ultrasounds exposure, the tip sonicator allow high power sonication but only localized beneath the tip. A good compromise can be represented by the cup-horn system which allow a more homogeneous sonication, and compared to the conventional sonication bath, it allows to operate at different frequencies in function of the target system.

Concerning the step of dispersion of exfoliated material, it generally occurs in the same liquid medium where the exfoliation is performed, except some examples that require the post exfoliation solvent exchange generally to aid the processing of the material for example using low boiling point solvents or mixture.[81-82]

UILPE process can be divided in two major classes that is molecule-free and molecule-assisted UILPE, as depicted in **Figure 2. 8** for the particular case of graphene.[83] In the first case, the exfoliation is performed in solvents, organic or aqueous; while in the second one, different molecular systems, e.g. small molecules or polymers, are introduced during the exfoliation process. Following the classical solution thermodynamics, an efficient stabilization occurs when the net energetic cost of mixing a solute in a solvent is minimized, that is when the solubility parameters of solvent and solute match. It appears clear that, due to the different dimensionality, 2DMs cannot be treated as small molecules. Therefore, classical models have been modified to be extended to these new systems. Solubility parameters that well describe the exfoliation and stabilization of these new systems are solvent surface tension, Hildebrandt or Hansen parameters.[14-15, 84-85] Typical solvents that are known to give stable dispersions include N-methyl-2-pyrrolidone (NMP), dimethlyformamide (DMF), dimethyl sulfoxide

(DMSO) and isopropyl alcohol (IPA).[66] The exfoliation in such solvents can be controlled in order to maximize the concentration of exfoliated material. However, that become possible only by increasing the sonication time up to hundreds of hours (e.g. 200 h). That determine the reduction of the flakes lateral sizes as a consequence of the fragmentation during the sonication process, beside be a very long process.[86] Alternatively, it has widely demonstrated that the use of organic molecules can enhance the exfoliation of 2D crystals leading to higher concentrations of thin layers in dispersion. That occurs when the chosen molecules have a high energy of adsorption on the basal plane of the material, so that they can act as dispersion stabilizing agents (DSAs). Usually, the stabilization is dominated by non-covalent interactions, for example through physisorption of hydrophobic chains in the case of classical amphiphiles, while hydrophilic heads are usually responsible for the stabilization in dispersion.[87] In most of the cases, molecule-assisted UILPE is employed to produce 2D crystals in water solution, where usually the dispersion and exfoliation are not favoured, or in general to avoid the stabilization in hazardous, toxic and high-boiling point solvents. Moreover, molecules prevent re-aggregation of exfoliated nanosheets by electrostatic and/or steric repulsion.[88] While the large conjugated surface of graphite give rise to many examples of non-covalent interactions with aromatic molecular systems, TMDs have attracted interest towards their covalent functionalization at the sulphur vacancies or non-covalent functionalizzation with organic molecules that are believed to adsorb to the nanosheets predominantly *via* vdW and dipole-dipole interactions.[16, 89]

For the molecule-assisted UILPE of graphite, several molecular systems like polycyclic aromatic hydrocarbons (PAHs) with different substituents, naphthalene diimide (NDI)- and perylene diimide (PDI)- based derivatives have been used, since the π-π interactions with graphene basal plane allow their adsorption.

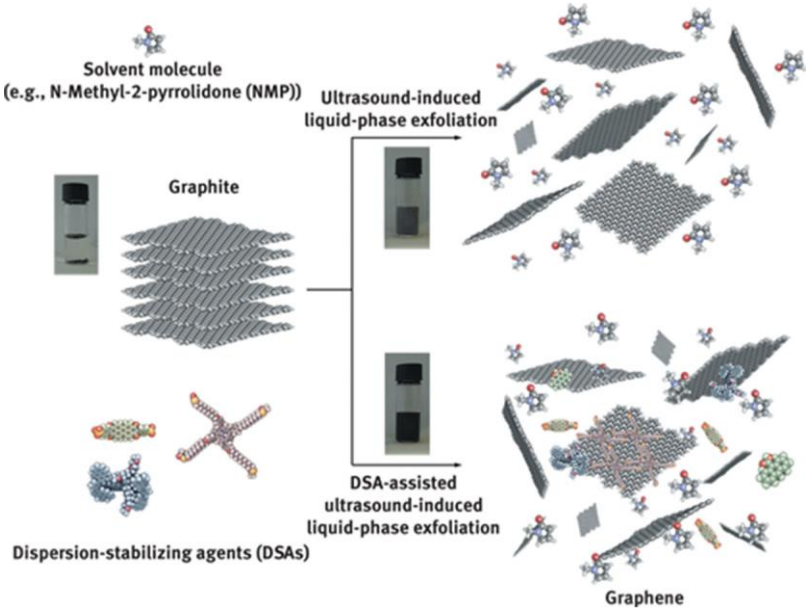

Figure 2. 8. Schematic representation of ultrasound-induced liquid-phase exfoliation in presence of absence of molecules that act as stabilizing-agents. Reproduced from Ref. 8.

On the other hand, more recently, the exfoliation of graphene and other layered crystals is being performed by using simpler and easily available surfactants like sodium cholate (SC), sodium dodecyl benzyl sulfonate (SDBS), sodium dodecyl sulfate (SDS) as anionic surfactants, cetyltrimethylammonium bromide (CTAB) as cationic surfactant or Triton X100 or Brij as nonionic representatives, because they are easier to be in large part removed. Finally, the use of many polymers, including proteins as well, has been investigated to assist the exfoliation of 2DMs. Despite the great

versatility of the exfoliation in the presence of polymers which can stabilize the material both in aqueous and organic environment, this field was not widely studied. This is may be due to the lower quality of exfoliation – as shown and discussed in chapter 6, compared to the use of small molecules, or because the polymer cannot be removed after exfoliation due to the strong interaction with the material.

Finally, the third aspect of UILPE process is the size selection. UILPE samples are always highly polydisperse in terms of sizes and thicknesses of the flakes. Consequently, very often the dispersion cannot be used as prepared, but further step of size selection are essential. That is requested especially for electronic applications where it is important to have dispersion that are homogeneous in size and thicknesses or for those applications which exploit the potential of monolayers sheets and thin layer. During the years, several approaches of size selection have been proposed. One of the most recent developed and improved to efficiently separate the flakes in term of sizes is called liquid cascade centrifugation (LCC), and it is based on multiple centrifugation steps at centrifugation rates that increase from one step to the following. Finally, each sample obtained following such procedure, reported in detail in ref, [66] contains nanosheets in a given size ranges. This appears, at the moment, the most efficient approach of size selection for materials produced by UILPE. However, many factors should be taken into account. Despite the ease of the process, it is certainly time-consuming if considered that for having good separation supernatant/sediment long centrifugation are needed (>2h for 20 mL of dispersion). Dispersions of thin flakes, that are in general the most requested, are usually the final outcome of multiple steps that can last many hours in total. Moreover, this process discriminate the flakes in function of their mass, therefore it is difficult to select at the same time thin and large flakes. Finally, depending on the density of the material, of the solvent, *etc*. this process must be tailored each time for the production of different 2DMs in different conditions. These all are important issues that need to be addressed for the progress of ultrasound-induced LPE. By and large, although in some cases, such issues can be avoided by using alternative new exfoliation approaches, UILPE continues to stand out for its high versatility.

2.2.2 Electrochemical exfoliation (EE)

Recently electrochemistry has been considered an alternative route to produce 2DMs in liquid media. The EE of layered materials occurs in a electrolytic cell where a fixed potential is applied between the layered crystal and a counter electrode both immersed in a electrolyte which ensure the intercalation of ionic species between the layers. The ionic intercalation weakens the interlayer forces in the bulk crystal, while Coulomb repulsion between charged layers and formation of gas molecules lead to the exfoliation of the material.

Electrochemical exfoliation has earned a great success because, unlike other LPE approaches, enable the production of gram quantities of graphene per hour that can be collected in form of powder or processed as ink. The produced material is remarkably rich in monolayers and bilayers with lateral sizes on the order of micrometer. Besides, the production is extremely fast, lasting from minutes to hours, in function of the amount of material one want to obtain. Finally, it requires mild conditions and very basic equipment. The exfoliation can indeed occur in water solution without using harmful reactants and harsh reaction conditions. The key point of the electrochemical exfoliation is thus its high efficiency.

The set-up that is generally used for the electrochemical exfoliation is a very simple electrolytic cell, composed by two electrodes, an electrolyte and a power supply. The working electrode is the material

that you want to exfoliate, and the counter electrode is usually a platinum wire or a graphite electrode as cheapest option. The electrochemical exfoliation can occur either in anodic or cathodic conditions according to electrolyte and potential applied. This means that the working electrode can be either positively or negatively charged, allowing the intercalation of anion or cation respectively.

This chapter, that describes the electrochemical approach used for producing 2DMs, has been divided in two sections relative to the two operating modes generally used, namely anodic and cathodic one. The two paragraphs report the historical background and more recent advances in the EE of graphene and other related materials. Moreover, some conclusions regarding the influencing factors of this process are reported, though the electrochemical method is still in its infancy and not totally understood.

2.2.2.1 Anodic intercalation of anions

Anodic exfoliation occurs by applying a positive voltage to the working electrode, thereby driving intercalation of negative ions present in solution within the layered crystal. Usually anodic exfoliation is carried out in aqueous solution. This aspect makes the process extremely appealing for industrial application, being safer and environmentally friendly. Furthermore, it has been observed that the electrochemical exfoliation in water is particularly efficient.

However, to observe the direct and effective exfoliation of the material, the electrolyte must be conveniently chosen. First attempts of EE of graphite have been demonstrated by Wang et al. who applied a bias of 5 V for 4 hours to a graphite rod immersed in poly(sodium-4-styrenesulfonate) (PSS),[90] and Li. who used sodium dodecyl benzene sulfonate (SDBS) to act both as intercalant and stabilizer, for a 48 hours electrolysis at 30 V.[91] These approaches produced good quality graphene, but PSS molecules remain adsorbed on the sheets. Moreover, the efficiency of the process is clearly not so high, as proved by electrolysis processes that span from 4 to 48 hours.

One of the earliest works that has shown a very fast and efficient exfoliation of a graphite electrode consists in the exfoliation in dilute H_2SO_4 by applying a positive potential of 10 V. In this study, many other electrolytes were tested, including HBr, HCl and HNO_3, but an ideal exfoliation efficiency was observed only in the case of H_2SO_4 based electrolyte. However, this process produces highly oxidized material, rich of structural defects.[28] In similar conditions, or rather applying a potential of +10 V and using the same electrolyte (H_2SO_4), Parvez et al. demonstrated the production of graphene with low defects and oxygen content.[92] A lower content of oxygen has been reported by adding glycine, thus forming a glycine-bisulfate ionic complex, but the exfoliation was interrupted in this case after 5 minutes of electrolysis.[93] Later, many different electrolytes including inorganic salts, such as ammonium sulfate, ammonium chloride, sodium sulfate, sodium nitrate, potassium sulfate, sodium chlorate,[27] perchlorates, phosphates,[94] *etc*. have been examined in the same conditions (applied voltage +10 V) in the attempt of exfoliating the material in milder conditions improving the quality of the resulting material. While chlorides have not shown any potential to exfoliate graphite, perchlorate ions lead to an extensive oxygen content.[26, 95] Other electrolytes display instead different efficiencies of exfoliation, difficult to interpret.

According to the procedure used by Su[28] and by Parvez[27], many of the methods proposed later were based on similar operative conditions.[21, 96-101]After many screening studies, indeed, it has been established that the most efficient anionic intercalant is sulfate[102] and the optimal potential applied to observe graphite exfoliation is +10 V. Such unconventional electrochemical conditions at which the

exfoliation takes place[103] justify the use of a two-electrode cell, without the reference electrode. Only few works have used a three-electrode set up to achieve a better understanding of the mechanism and the conditions at which the exfoliation occurs.[104] On the contrary, most of the following studies, especially regarding the applications of electrochemically exfoliated graphene (EEG), were performed employing the aforementioned standard parameters.

Lower potentials (+1-3V) have been used but in different electrolytes, e.g. in a mixture of NaOH, H_2O_2 and water, impressive yields have been obtained owing to the crucial role exploited by H_2O_2. On the other hand, this method led to thicker graphene sheets (3-6 layers) compared to the standard methods that use sulphate ions and a standard bias of 10 V.[98, 105] The effect of the potential has been investigated also in a study where a saccharin aqueous solution was used as electrolyte and has shown that the potential has an effect on yield and quality of the exfoliated material. In particular, by raising the applied potential the yield of graphene would increase together with the defect density, whereas the thickness of the exfoliated flakes would decrease.[106] Otherwise, very little is reported on the effect of the applied potential on efficiency and quality of exfoliated material. A possible explanation is that when changing the potential, for example higher than 10 V, one could have higher efficiency of exfoliation in terms of yield and thinner layers (as reported in ref. 105) but lower quality, e.g. higher degree of oxidation or structural defects, that however could be balanced by modifying the electrolysis time.

The pH of the electrolyte can have also a role on the quality of the exfoliated material, as it was demonstrated by comparing the material produced in H_2SO_4 and Na_2SO_4, or by adding NaOH in perchlorate solution which aide the reduction of defects and oxidation.[107] In parallel the effect of NaOH addition has been investigated during the exfoliation in sulfonated poly(ether-ether-ketone) (SPEEK) and it was proved the reduction of oxygen functionalities on graphene surface.[108] Regarding the electrolyte concentration, it was observed, for instance, that when the concentration of H_2SO_4, HNO_3 or $HClO_4$ is increased, a more efficient exfoliation occurs,[97] but rise also the degree of oxidation of the material.[109-111]

In general, the electrochemical processes are evaluated in terms of efficiency, considering time of exfoliation and yield of exfoliated material, as well as in terms of quality expresses as C/O ratio and density of defects, generally determined by X-ray photoelectron spectroscopy and Raman spectroscopy respectively. Although the significant higher yields of thin layers (1-3 layers) obtained by EE in contrast with other LPE approaches, the process by its nature leads to a polydisperse material. Therefore, judge on the quality of the material in terms of thickness or defects must be done with caution, as strictly dependent on how the material is processed and analysed. The same procedure of purification of the material, and sample preparation for a standard characterization, should be used to enable the comparison from one work to the others. However, such standardization of the procedures is not developed yet for new systems like 2DMs produced by electrochemical exfoliation. While the efficiency of the process is generally not quantified, Yang et al.[21] performed an attempt of upscaling their process of exfoliation in a aqueous solution of tetra-n-butylammonium bisulfate (TBA·HSO4) at neutral pH by applying an alternating current to exfoliate both electrodes. They report a value of graphene production rate that exceed 20 gh^{-1} in laboratory scale. Clearly, this result must be interpreted with caution bearing in mind that, keeping constant electrolyte and its concentration, the amount of produced material strictly depends on the size of both working and counter electrode and their reciprocal distance, volume of the electrolytic cell, time during which the electrolysis is performed on the same working electrode, number of electrodes changed in one hour, *etc*. All these details are often in part missing, making difficult the reproducibility of the experiments. More importantly, many works, as well as our findings reported in chapter 4, prove that by varying these

parameters the quality of the material changes with consequent effects on the efficiency. Therefore, most of the time, it is necessary reaching a trade-off between amount of produced material and its quality in function of the applications. However, by reporting the amount of graphene produced per hour (20 gh^{-1}) during laboratory tests, Yang gives an idea of the great potential of this process for large-scale production of graphene, predicting further improvement by optimizing of the operative conditions and engineering the set-up. Moreover, it is important to note that the total yield of exfoliation that they report, being up to 80%, probably is referred to the fact that the electrode is not completely exfoliated. This value, as well as the mass of exfoliated material, are related to the total material produced, that includes un-exfoliated particles as well. Therefore, such results cannot be directly related to the goodness of the exfoliation process in terms of thin sheets. Nevertheless, combining such findings with the yield of mono- and few-layer sheets, determined analysing the material in dispersion, one can conclude that the yields of electrochemical exfoliation process are significantly higher compared to other LPE methods, as discussed in more detail in chapter 4.

It is undoubtedly recognised that the anodic process, especially when performed in aqueous solution, is way more efficient than cathodic process. This difference can be attributed to the different mechanisms behind anodic and cathodic EE exfoliation. Interestingly, though countless methods that operate in anodic conditions have been developed, the mechanism used for explaining these processes is always the same;[101] while a more detailed understanding of the mechanism has not been suggested yet. As reported by Parvez, the anodic EE of a graphite electrode in an aqueous electrolyte containing an inorganic sulphate salt is the result of a multiple step process (see **Figure 2. 9**).

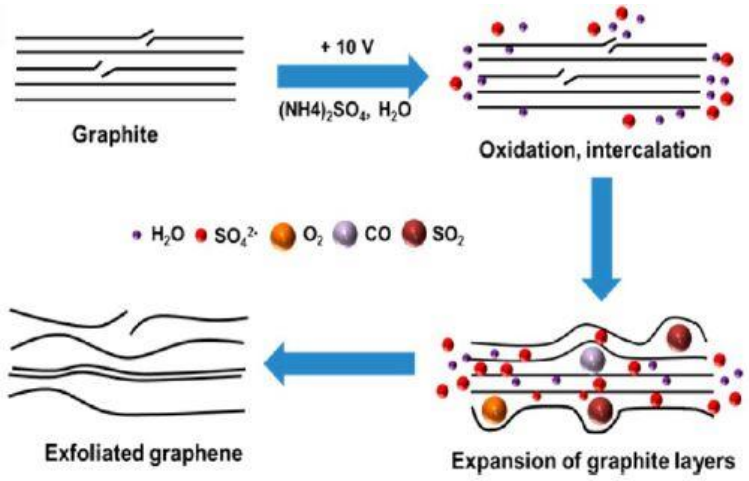

Figure 2. 9. Sketch displaying the mechanism of electrochemical exfoliation of graphite in anodic conditions using ammonium sulphate, $(NH_4)_2SO_4$, as electrolyte. Reproduced from ref. 27.

The exfoliation is enabled by the nucleophilic attack at edges sites and grain boundaries of graphite by hydroxyl ions (OH^-) generated from the reduction of water at the cathode (reaction 1). The oxidation of the electrode leads to the expansion of graphite layers, thereby facilitating the intercalation of negative ions, together with water molecules, into the interstitial spaces between the graphitic layers. There, the oxidation of water (reaction 2) and the reduction of SO_4^{2-} (reaction 3) produces gaseous species, including SO_2 and O_2, that exert large forces which are sufficient to overcome the weak interactions between graphitic layers, thereby causing the effective exfoliation of graphite electrode. This mechanism has been also used to explain the process of exfoliation of other 2DMs (see **Figure 2. 10**).[102]

At the cathode: $2H_2O + 2e^- \rightarrow 2OH^- + H_2$ (1)

At the anode: $2H_2O \rightarrow O_2 \uparrow + 4H^+ + 4e^-$ (2)

$SO_4^{-2} + 4H^+ + 4e^- \rightarrow SO_2 \uparrow + 3H_2O$ (3)

Only recently, Pumera et al. suggested a slightly different interpretation of the mechanism. Unlike the previous proposed mechanism, this considers the formation of active radicals from water electrolysis. The attack at graphite edge sites and grain boundaries is carried out by active radical species OH· and O·, which are generated from the oxidation of water when a positive voltage is applied. This attack by radicals is thought to produce oxygen functional groups which increase the graphite interlayer distance. The expansion of the material is favoured by the intercalation of other radicals as well as ions present in solution. Finally, the anodic oxidation of the radicals and anions that takes place inside the material produces gaseous species (O_2, SO_2, CO_2 *etc.*) that completely separate the layers.

Despite the lack of a more detailed mechanism, the experimental findings achieved so far show that the exfoliation is enabled by the intercalation of species that release gas molecules inside the material, as a consequence of electrochemical reactions occurring at the anode. The energy developed by a vigorous gas evolution, that occur when working at high potentials, is most likely the key of an effective exfoliation.

However, when the electrochemical exfoliation is performed in water, the produced material always suffers from unavoidable oxidation. Many attempts have been made in order to avoid or minimize this oxidation, for example, using sacrificial agents, that are more readily and preferably oxidized than the 2D material, such as sodium benzene 1,3-disulphonate or sodium naphthalene 1,5 disulfonate in aqueous solution.[112] An alternative is using some reducing agents like (2,2,6,6-tetramethylpiperidin-1-yl)oxyl (TEMPO)[113] which are expected to preferentially react with OH radicals to protect graphene from the extensive oxidation. By adding TEMPO to $(NH_4)_2SO_4$ electrolyte, an improvement on the quality of the material has been expressed as a higher C/O ratio (= 25.3) determined by XPS. Similarly, melamine, that is supposed to adsorb on graphitic basal planes, has been used to protect graphene from the extensive oxidation caused by the exfoliation in sulfuric acid, achieving similar results (C/O = 26.17).[114] Recently, also sodium halides (NaCl, NaBr and NaI) have been used as electrolyte for the exfoliation of graphite producing graphene sheets with C/O ratio of 16.7.[115] Nevertheless, structural degradation, caused by the use of a large positive voltage and consequent vigorous gas development, remains a general issue for anodic exfoliated graphene as discussed in detail in chapter 4.

The electrochemical approach in anodic conditions has been extended to other 2DMs as well. Similarly to graphene, MoS_2 has been exfoliated in a two-electrode cell by applying a positive bias of 10 V between a Pt cathode and a crystal of MoS_2 as anode, in a H_2SO_4 based electrolyte. [116] Later, MoS_2 has been also exfoliated in sulphate ions and, employing similar anodic conditions, larger flakes and lower degree of oxidation have been observed.[96]

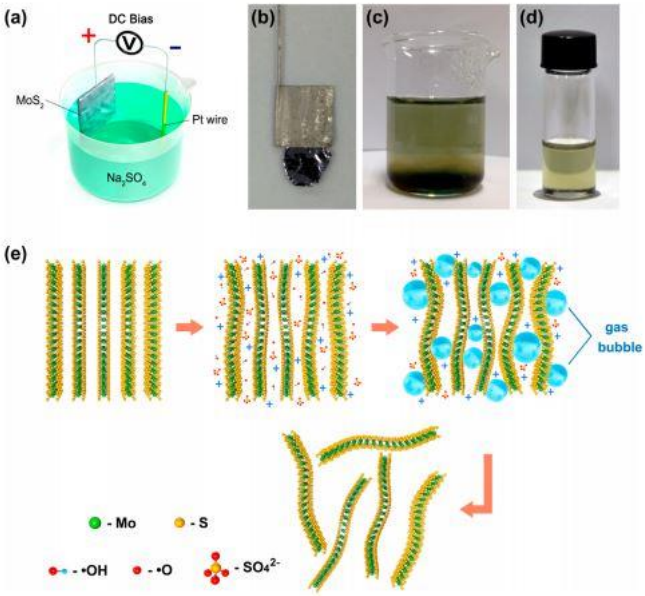

Figure 2. 10. Schematic illustration of the set-up (a) used for anodic electrochemical exfoliation of a MoS_2 crystal (b) in Na_2SO_4 aqueous solution; product of the exfoliation process before (c) and after (d) purification and dispersion in NMP; (e) sketch of the mechanism of exfoliation. Reproduced from ref. 96.

Using a similar set up also Bi_2Se_3 and Bi_2Te_2 have been exfoliated,[117] while the anodic exfoliation of black phosphorous has been also observed in dilute sulfuric acid applying a voltage of +3 V for few hours, but no information about yield and thicknesses of the flakes are given.

In conclusion, by exploring different operative conditions, it has been observed that the anodic electrochemical approach can be exceptionally effective in the exfoliation of graphene and other related materials. Although the production is a trade-off between yield and quality, the anodic exfoliation method ranks first in the large-scale production of high-quality graphene.

2.2.2.2 Cathodic intercalation of cations

By applying a negative voltage, it is possible to drive the intercalation of positive ions in solution within a layered crystal used as cathode in an electrolytic cell. The exfoliation in cathodic conditions is performed in organic solvents. Some of the solvents generally used are dimethyl sulfoxide (DMSO), acetonitrile, propylene carbonate (PC) and N-Methyl-2-pyrrolidone (NMP).

Inspired by Li-intercalated compounds used in batteries since 1970, one of the first cation chosen for the intercalation of a graphite cathode has been lithium. Cathodic exfoliation in a 1 M LiCl-DMSO electrolyte produces graphene with flake sizes ranging from 1 to 20 μm and thickness lower than 5 nm.[118] $LiClO_4$ in PC was used to exfoliate graphite applying -15±5 V but a post treatment by ultrasounds was necessary to achieve the exfoliation.

In general, indeed, the cathodic process doesn't lead to the effective exfoliation of the material, that can be achieved only in the presence of a further external stimulus e.g. given by ultra-sonication or chemical reactions. For example, by using lithium metal as anode and source of lithium ions in a 0.1 M $LiPF_6$ electrolyte, once Li^+ is intercalated, the exfoliation is observed upon sonication in water where the formation of H_2 releases enough energy to guarantee the separation of graphitic layers (**Figure 2. 11**).[119] This method has been extended to other 2DMs like MoS_2, WS_2, TiS_2, TaS_2, ZrS_2.[120] Other cation

species have been tested as well. It was observed, for example, that intercalation of tetra-alkyl-ammonium cations with various alkyl chains yields few-layer graphene (2–5 layers) with good quality and low content of oxygen.

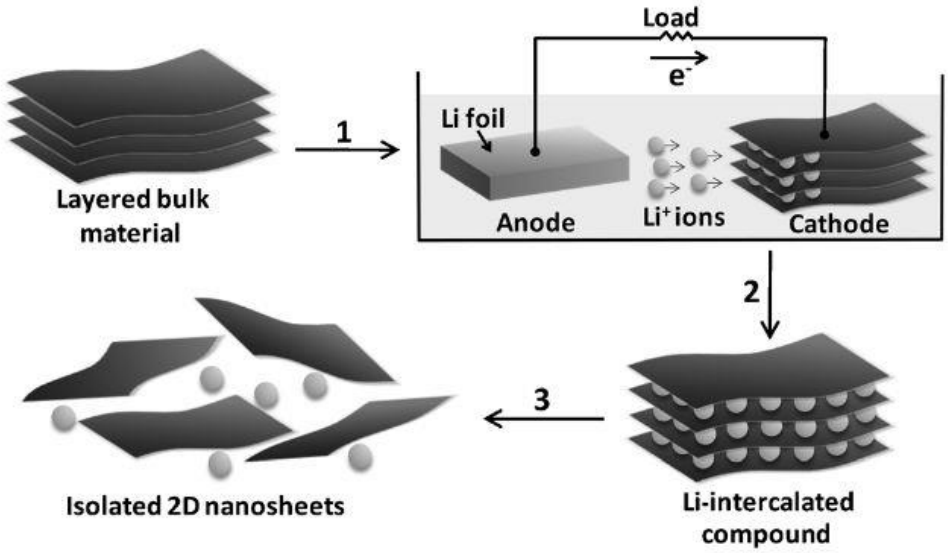

Figure 2. 11. Mechanism of exfoliation driven by electrochemical intercalation of lithium ions. Reproduced from ref. 120.

Generally, exfoliation in organic solvents preserves the structural quality of graphene. However, an additional sonication step is necessary to reach thorough exfoliation, with consequent fragmentation and higher thicknesses of the flakes.[104] Therefore, for the production of graphene, the anodic approach has been for a long time preferred to the cathodic one because higher amount of graphene sheets can be produced in only one step, and their lateral sizes and thicknesses are not affected by the sonication. To overcome this problem, recently new strategies involving the multistep intercalation before with Li^+ and then successively with TBA^+ have been explored to maximize the cathode expansion, weakening even more the interaction between layers and favouring the following step of exfoliation induced by ultrasounds.

Other solvents with low-boiling points, such as acetonitrile, have become popular alternatives. By electrochemical co-insertion of perchlorate anions and acetonitrile molecules, graphite was intercalated and partially expanded at a voltage of +5 V for 30 minutes. Then microwave irradiation was applied to complete the exfoliation process. Notably, 69% of the graphene flakes were bilayers and 28% of them were single layers with mean lateral dimensions of 1–2 μm.[121]

On the other hand, the cathodic approach was preferred to the anodic one for the production of other 2DMs beyond graphene, to avoid their extensive oxidation that has been widely demonstrated for graphene obtained in anodic conditions. However, it has been discovered that when Li^+ intercalation is used for the production of MoS_2, it compromises the structure of MoS_2 that results rich in 1T phase.[120, 122-123] A large number of intercalated Li^+ ions lead to electron injection into the crystal that, when exceed a certain threshold, induces a phase transition from the semiconducting 2H phase to the metallic 1T phase, that is not desired in certain applications. To overcome such a limitation, the most recent discovery shows that replacing the small Li^+ ions with larger quaternary ammonium ions limits the number of molecules that intercalate and thus the electron injections as well. [124] In this study MoS_2

has been expanded by THA^+ intercalation in acetonitrile in a two-electrode electrochemical cell and then sonicated in a mixture PVP/ DMF with PVP acting as stabilizer agent (**Figure 2. 12**).

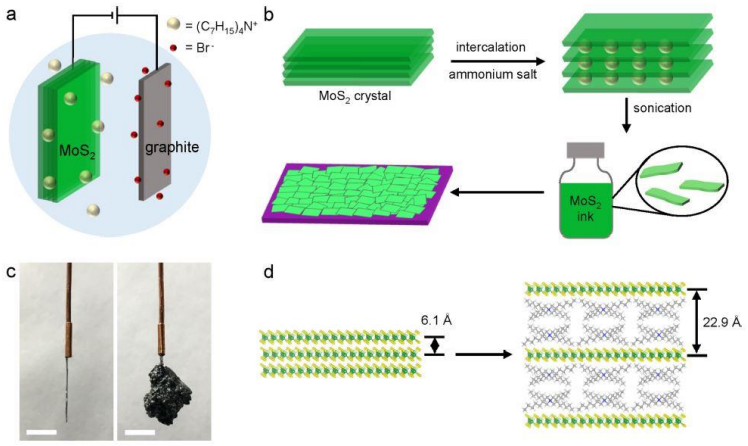

Figure 2. 12. a) Schematic representation of electrochemical intercalation mechanism of MoS_2 with THAB; b) sketch of ink preparation and processing in large area film; c) photograph of MoS_2 crystal before and after intercalation; d) schematic representation of the interlayer spacing expansion due to the intercalation process. Reported from ref. 124.

In summary, layered structures can be exfoliated by means of the electrochemical approach when placed as anode or cathode of an electrolytic cell. The anodic exfoliation allows the highly efficient, one-step, production of thin layer sheets with a certain degree of oxidation. Contrarily, working in cathodic conditions would prevent the exfoliated material from the oxidation, leading to higher quality materials. However, the cathodic intercalation appears a less efficient process, that occurs mainly in organic solvents, being therefore less appealing for industrial application. There is, therefore, still need for improved conditions, including finding new electrolytes that can promote a more efficient exfoliation. Nevertheless, new strategies to overcome some of the initial limitations of this process are being developed. For example, the EE was believed being limited to the production of conductive materials. That is in part the reason why the exfoliation of semi conductive materials, like MoS_2, is less efficient compared to graphite EE. However, recently it has been demonstrated that through the inclusion of a conducting additive, it is possible to exfoliate layered materials regardless their conductivity.[125]

Despite some limitations, EE is a cost-effective strategy for the large-scale production of 2DMs that can find application in various fields, such as energy storage, catalysis, sensing *etc*.

Finally, in the next section we report some of the practical applications of these materials, specifically referring to the possible uses of 2DMs produced by exfoliation in liquid media.

2.3 Attractive applications of liquid-phase exfoliated 2D materials

Owing to their exceptional properties, 2DMs can find application in many fields including composites, sensors, electronics, energy and biomedicine, to name a few.

Graphene that is the most studied among the 2DMs is an appealing material for the industries which produce composites, because of its conductivity, strength, light weight, thermal properties and surface area. Its strong and flexible nature combined with large surface area and high conductivity are ideal characteristics for sensing and for energy storage devices. For example, graphene, but recently other 2DMs as well, demonstrated to be good candidates for gas sensing, pressure sensing and biological sensing. They might contribute thus to enhance our life quality, for example, allowing the fabrication of smart packaging that monitor the quality of our food. Moreover, sensing ability, combined with flexibility, could also be used in the next generation of wearable electronics to monitor our health e.g. glucose and cholesterol sensors. Strength and flexibility could also make possible the fabrication of flexible displays and bendable batteries.

Having said that, developing methods to produce graphene and other 2DMs on large scale is urgently needed as the possibility of realizing the above-mentioned applications on real scale strictly depend on that.

Methods like LPE, although need to be still improved to let access to the superlative properties of 2DMs, give the concrete chance of introducing such materials in our daily life. Benefitting of their nanoscopic sizes, as well as mechanical and electrical properties, they allow the miniaturization and improvement of currently used devices making them lighter, flexible and stronger. Some practical examples involve the use of graphene in composites for aerospace applications, supercapacitors, or products like tennis rackets, ski, training shoes which are already commercially available; or as coatings, for example, to dissipate heat and ensure long-lasting performance to motorcycle helmets. LPE approaches are also extremely versatile since they allow to produce a wide variety of 2DMs holding many different properties. On this view, in function of a given final application, one can chose the more convenient 2D material that possess the properties needed to satisfy the technological request, and the proper LPE method that allow to achieve such characteristics.

In this chapter we report on some of the numerous potential applications of 2DMs which can be made possible using 2D crystals exfoliated in liquid phase, and therefore can be considered potentially up-scalable. Nowadays, for example, a still open challenge is the one to replace indium tin oxide (ITO) – that is the most used material as transparent electrode – with a cheaper, less brittle and stable material. In general, the electrodes are used to inject or extract charge carriers in electronic devices. Therefore, the requirements for good electrodes are high conductivity and low barrier height at the interface. The two figures of merit used for evaluating a material as transparent electrode are sheet resistance, expressed in Ω/square, and transmittance at 550 nm, expressed in percentage. ITO is the most used transparent electrode because of its high conductivity, around 10 Ω/square, and transmittance of 90%.[126-128] Graphene can be an alternative, since it is a thin and transparent conductor, chemically inert, environmentally stable and holds much better mechanical properties than ITO. Indeed, it has been demonstrated that CVD graphene possesses the right combination of high transmittance (90%) and high conductivity (30 Ω square^{-1}) to be considered a good alternative to ITO. However, producing graphene by CVD can be costly and complex from the industrial point of view, hindering its practical application. On the contrary, the ability to process LPE graphene either on rigid and flexible substrates, in a costless way, makes it an interesting material for such application. Nevertheless, the deposition of LPE graphene in homogeneous and uniform large area thin films is a critical point

towards its use as transparent electrode. In the past years, many techniques such as spin-coating, spray-coating, dip-coating, ink-jet printing, *etc*. have been employed for the deposition of LPE materials, but many factors hinder the formation of thin and homogeneous films. Especially in the case of graphene produced by ultrasound-induced LPE, the use of high boiling point solvents doesn't fit with the techniques mentioned above, including spin-coating or dip-coating. Moreover, the material produced is inhomogeneous in terms of thickness and size, that generally doesn't exceed few hundreds of nanometers. These two last factors, in particular, force to perform multiple depositions to reach complete covering of the substrate, resulting in inhomogeneous and thick films that, although are conductive, don't meet the criteria of transparency. On the contrary, EEG stands out for the capacity to form thin and large homogeneous films by vacuum filtration[129], spray-coating[130] or deposition at the interface with water (as proved in chapter 4). That may be ascribed to the higher content in thinner sheets (1-3 layers) and larger sizes of the sheets, that are usually on the order of micrometers, rather than to the used solvent, that is generally dimethylformamide (DMF, bp: 153 °C). Recently, EEG films have been produced by spray-coating with a transparency of 70% and 520 Ω square^{-1} resistance.[131] Considering that most applications of transparent electrodes, e.g. smart windows, do not require very high conductivity, but a few hundreds of Ω square^{-1} are sufficient, EE and, more in general, LPE graphene can be considered a cheaper option of transparent electrode for such low-tech applications,[80] while still being far from conductivity and transmittance necessary for photovoltaic devices or liquid crystals devices.

Other applications that require high surface area and electrical conductivity can benefit of the use of 2DMs. Graphene and other 2DMs can be used, for example, as conducting additive in battery electrodes to replace the conventionally used carbon black or carbon nanotubes. The high surface area to volume ratio, allow in fact to improve not only the electron transport but also the ion diffusion within the electrode of the electrochemical storage system. Moreover, the reduced dimensions can allow the use of mobile energy storage devices. In particular, EE, that lead to mass-production of thinner flakes, allows to produce potential materials for applications in energy-related fields (batteries, supercapacitors, fuel cells, solar cells *etc*.). Small amount of EEG has been added to carbon-coated $LiFePO_4$ used as the cathode in Li-ion batteries leading to beneficial effects in terms of capacity enhancement and retention.[132] Alternatively, EEG has been employed as electrodes for all-solid-state thin film supercapacitors or for producing aerogels for the same application. [133]

EEG has been used also as ultrathin transparent film with a high strain sensing capability for use as artificial electronic skin or in health monitoring,[134] and as transparent and conductive continuous graphene circuits.[135]

The ability to process 2DMs as uniform and large area thin films enable the scalable fabrication of thin-film transistors that can be included in more complex devices, such as logic gates and integrated circuits. Owing to the development of deposition methods like inkjet printing, for example, it is possible to prepare large area films based on 2DMs inks and that made possible the production of the first devices all made by 2DMs. For instance, a photodetector with graphene interdigitate electrodes and MoS_2 channel has shown improved conductance compared to the dark conditions,[136] and similar achievement are obtained for WS_2, demonstrating that these systems are applicable as low cost photodetector.

2DMs have shown applicability in the field of sensing, as gas sensors or bio sensors. While for ultrahigh sensitive sensors, to detect small signals, pristine 2D crystals are necessary (e.g. CVD), less demanding applications, like detection of analytes for food and environmental monitoring can exploit the

properties of LPE 2DMs.[80] Sensing capacity towards different gases has been demonstrated for films prepared from rGO and MoS_2 inks.[137]

For electronic applications, whereas graphene is not suitable due to its zero bandgap, e.g. for making switching devices, other 2DMs that show semiconducting properties, such as TMDs, BP *etc*. can be used. Single and multilayers MoS_2 transistors produced by ME or CVD exhibit outstanding performance such as high I_{on}/I_{off} (10^7) and mobility of around 100 cm^2. However, the integration of complex logic circuits necessitates the scalable fabrication of high performance thin-film transistors. That is challenging due to the low performance materials produced by LPE which have limited carrier mobility, low I_{on}/I_{off} and poor film quality. An inkjet-printed MoS_2 films have, for example, I_{on}/I_{off} of 2 and $\sigma = 10^{-5}$ S m^{-1}.[72]

On the other hand, an improvement of such qualities would allow the successful creation of integrated circuits beyond the use of single or few transistors based on mechanically exfoliated and CVD produced materials.

CHAPTER 3.

CHARACTERIZATION TECHNIQUES

3.1 Optical microscopy (OM)

Optical microscopy (OM) is a reliable technique that is commonly used in the field of 2DMs materials for estimate thickness and size of 2D flakes on large scale. When deposited on silicon oxide substrates, atomically thin layers, such as graphene or TMDs, can be rapidly identified by OM.[138-139] This is made possible due to the optical contrast between a 2D nanosheet and the substrate.

The contrast difference between the 2D nanosheet and the substrate can be simply obtained from the brightness profile of their colour images. By creating a calibration curve, where the values of contrast difference are reported for different layers numbers, it is possible determining the number of layers of a given flake, e.g. graphene, MoS_2, WS_2 and TeS_2, with a certain accuracy.[140] To this purpose, it is important to know that the contrast value depends on different parameters such as the thickness of SiO_2, the intensity of illumination, exposure time and the wavelength of light.[139]

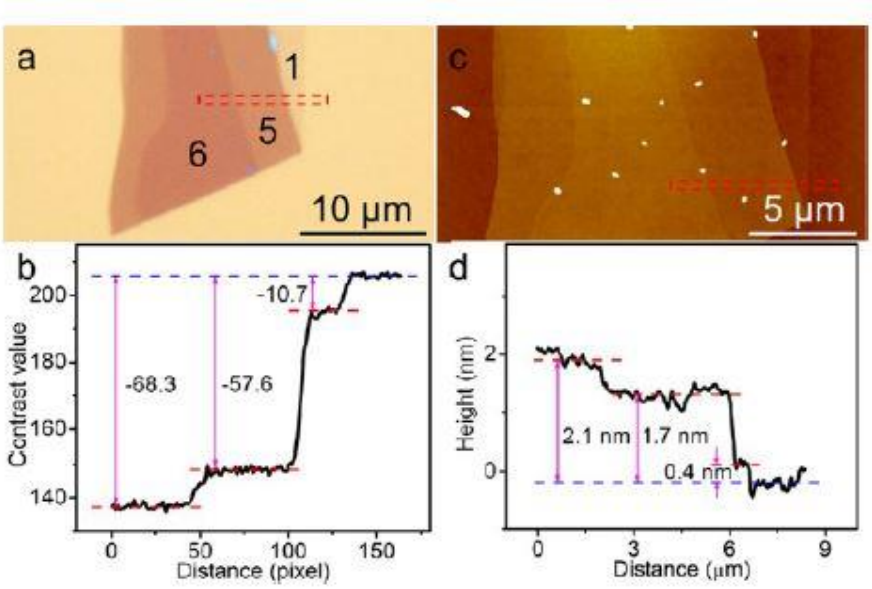

Figure 3. 1. Optical microscopy (a) and AFM (c) images of mechanically exfoliated graphene few-layer flake. According to the calibration curve of this system, the values of contrast difference reported in (b) correspond to 1 layer, 5-layer and 6-layer graphene sheets. They are, therefore, correlated with AFM height profiles (d). Reported from ref. 140.

During this thesis OM was used to follow the experiments of exfoliation. Based on the different optical contrast between thinner and thicker flakes, it has been possible to qualitatively evaluate the degree of exfoliation. In alternative, this technique was used for controlling the quality of inks deposition on Si/SiO_2 substrates. OM was chosen, indeed, for a having a rapid and preliminary insight into the samples on large scale, while avoiding time-consuming techniques like atomic force microscopy (AFM) for such screening tests. AFM was employed in a second step for the quantitative characterization of optimized samples.

3.2 Atomic force microscopy (AFM)

The atomic force microscopy, which belongs to the family of scanning probe microscopies (SPM), was developed by G. Binnig et al, in 1986.

This technique allows to investigate the surface topography of a sample and other physico-chemical properties, such as viscoelasticity. This information derives by the detections of the interacting forces between a sharp tip (radius < 10 nm), mounted at the end of a flexible cantilever, and the surface of the sample. These forces lead to the deflection of the cantilever during scanning the sample so that they can be recorded, providing a map of the surface's sample and its properties. The advantage of AFM over the scanning tunneling microscopy (STM) is that it is not limited to the characterization of conductive samples but allow the study of semi-conducting or non-conducting samples as well.

When the AFM tip approaches into proximity of the surface's sample depending on the tip-sample distance both attractive and repulsive forces between the tip and the sample are generated. The deflection of the cantilever can be, in first approximation, attributed to a combination of vdW attractive forces and repulsive forces. The formers are more long range than the latter and scale with r^{-6}. Contrary to the attractive forces, the repulsive forces are short distance forces (< 3 Å). This is the main reason why AFM can image the topography of a surface with a resolution below the nanometer in a non-invasive way. In particular, AFM provides lateral resolution ≤ 1 nm and vertical resolution ≤ 0.1 nm. The dependence of such forces to the sample distance is described by using the Lennard-Jones potential (V_{LJ}):

$$V_{LJ}(r) = 4\,\varepsilon\,[\,\left[\left(\frac{\sigma}{r}\right)^{12} - \left(\frac{\sigma}{r}\right)^{6}\right]$$

where the first term of the equation describes the short-distance repulsion, the latter takes into account the long-range attractions caused by a dipole-dipole interaction (**Figure 3. 2**). In this equation ε is the minimum potential energy, r is the distance between atoms and σ is their equilibrium distance at which the potential value is minimal.

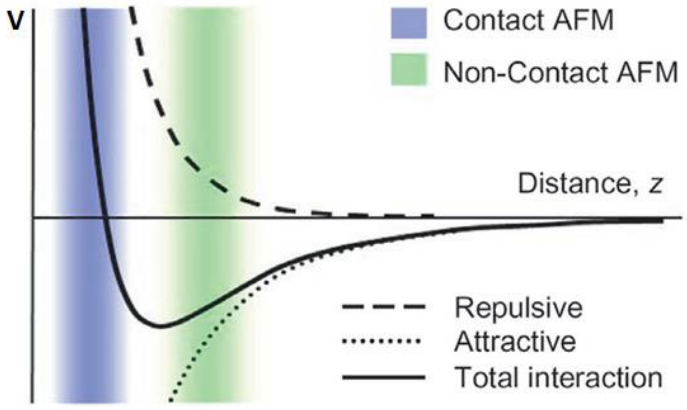

Figure 3. 2. Lennard-Jones potential model (solid line) is the sum of the attractive and repulsive potential (indicated with dotted and dashed lines, respectively). The regions for the different type of AFM measurements are indicated by different colors.

While scanning, the tip will interact with the sample with forces down to 10^{-9} N-10^{-12} N which cause the deflection of the cantilever. Therefore, the tip will follow precisely the topography of the surface and the cantilever will respond to changes in the sample such as roughness of a film or presence of nanoscopic features on the substrate. The movement of the cantilever is read through a laser beam

that is focused by an optical system onto the reflective back side of the cantilever. Its reflection is detected at a four-section photodetector which allows to distinguish between the bending of the cantilever, due to attracting and repulsing forces, and the torsion, caused by lateral forces. For an accurate scan of the sample's surfaces, AFM uses a scanner which controls the position of the tip in all the directions. The scanner is made of piezioelectric materials which have the properties of changing their sizes when exposed to an external electric field. The scanning systems consist of 3 scanning elements which control the tip movement in each three directions (x,yz).

AFM can be operated in three different modes: contact mode, non-contact mode and intermittent contact mode. In contact mode the tip is in contact with the sample. The measure can be obtained operating in constant height or constant force mode. In constant height mode, the piezoelectric crystal is frozen along the z-axis, therefore while scanning the interaction force between the tip and the sample surface represents the dataset. In constant force mode, a feedback loop controls the tip-sample distance in order to keep their interaction force constant. In order to do not damage soft samples, AFM can be used in non-contact mode, where the tip oscillates at a distance of 10-100 Å from the sample. This approach is less used due to the low lateral resolution. A good compromise is represented by the tapping mode. In this modality, a short and stiff cantilever is connected to an additional piezoelectric component that let it vibrate near its resonant frequency (typically 100-400 kHz). The tip approaches perpendicular toward the sample till it barely touches the surface. During the vibration the tip will experience both contact and non-contact regimes. Amplitude and frequency of the oscillation will vary with the interaction of the tip with the sample, defining the topographic image of the sample. Usually tapping mode is operated in constant frequency mode as the best performance are obtained at a frequency 5% below the resonance frequency of the tip. To this purpose, a feedback loop is used to move the tip when the frequency change as a result of the interaction tip-sample and to restore the fixed one. Imaging in tapping mode requires lower scan rate compared to contact mode and provide high spatial resolution, allowing to imaging features having thicknesses up to few μm. In tapping mode, it is possible recording the phase image simultaneously with the topographic one. The phase image is given by the shift of the phase of the cantilever's oscillation caused by the attracting and repulsive forces between the tip and the sample when this latest is formed by two or more components of different nature. The phase image gives hence information on the viscoelastic properties and changes in chemical composition. Resolution and response are the same of the topographic image, but phase imaging can provide more detail in fine structures which are not clear when the topography is too rough.

In this thesis AFM was employed for the characterization of graphene and MoS_2 flakes produced by LPE approaches and deposited on flat substrates (chapters 4 and 5). AFM was used to quantitatively determine the dimensions of the flakes (thickness and lateral size) and to assess detailed information on the topography of flake's surface. Moreover, AFM served to characterize graphene films in chapter 4 and evaluate, although qualitatively, the degree of exfoliation in the presence of polymers and the quality of the deposition of polymer/graphene composites in chapter 6.

3.3 X-ray photoelectron spectroscopy (XPS)

The X-ray photoelectron spectroscopy (XPS) is a technique commonly used to determine the elemental composition of a sample, as well as to obtain information on the chemical binding.

XPS technique is based on the photoelectric effect. An incoming photon with energy hν, higher than the work function and up to 10 KeV, interacts with the core levels electrons, mainly through photon absorption process, and transfer them their energy. This energy transfer determines the consequent emission of photoelectrons from the core levels of the material (**Figure 3. 3**). The kinetic energy of the resultant photoelectrons, which are experimentally detected, is:

$$(KE) = h\nu - BE - \phi$$

where hν is the photon energy (generally the AlKα = 1486.6 eV is the most common used X-ray source), BE is the binding energy of the electron in the atom and ϕ is the spectrometer work function. The binding energy of electron depends on the element from which the electron is emitted, more in particular from the orbital, and from the chemical environment of the atom as well. By measuring the kinetic energy E_{kin} of the collected electrons which reach the detector, it is possible to calculate the binding energy of the electrons and in this way to identify the different elements at the surface's sample and their chemical state. As a result, a survey of the surface composition of the probed area will be obtained (as the one reported in Figure 4.6).

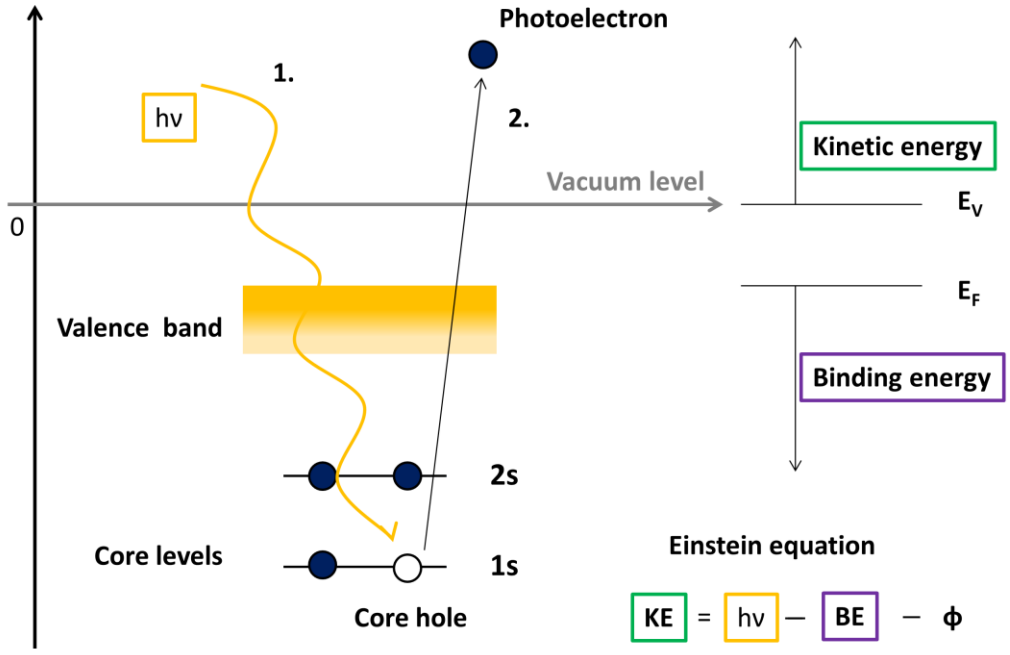

Figure 3. 3. The fundamental principle of XPS: photoelectric effect and the Einstein law.

Besides giving information on the type of atoms which form a determined molecular system, the study of ionization energy of inner electrons allows to obtain information on the charge density of an atom and on the oxidation state of the atom. More in general, XPS allows determining the structure and molecular binding through the determination of chemical shifts.

The binding energy for an electron in a given atom is sensitive to chemical environment of the atom. Any changes in the chemical environment of an atom determines indeed a spatial redistribution of the valence electrons. For instance, when an atom is bonded with another one having a different electronegativity, the electrons will be partially attracted by the more electronegative atom. This redistribution of the electrons results in a change in binding energy, as these electrons will leave the surface with a different energy. For example, if carbon is covalently bonded to oxygen as it was observed for EEG in chapter 4, its core electrons will be attracted by the oxygen atoms, exhibiting consequently a slightly shift to higher binding energy, compared for instance to the CIs of alkyl chains. Based on simple Coulomb consideration, the chemical shift can be correlated to the charge density of the considered atom as follows:

$$\Delta E = k\, q_a + \sum_b q_b / R_{ab} + l$$

where K and l are parameters which depend on the atom (carbon, nitrogen, *etc*.) and on the type of considered orbital (ls, 2p, 3d *etc*.), while q_a is the charge density of the considered atom, q_b the charge density of the neighboring atoms and R_{ab} is the distance between the atom a and the vicinal atoms b. Consequently, XPS don't allow only an elemental analysis but provides also information on the chemical groups which are present in the studied system. An example is reported in **Figure 4. 7** where XPS has been used to identify the different oxygen functional groups present in the electrochemically exfoliated materials.

This aspect is even more surprising if one thinks that this information comes from the surface of our material. XPS is indeed a surface sensitive technique due to the short mean free path of the photoelectrons in the material. The generated electrons can undergo inelastic scattering events which determine loss in their energy, while part of the electrons don't have energy sufficient to leave the material due to the collision with other atoms of the solid. The mean free path of an electron before inelastic scattering changes with the kinetic energy of the electron following a parabolic trend as reported in **Figure 3. 4**. Therefore, despite X-ray can penetrate several hundreds of nanometers through the material, the emitted photoelectron only originates in the first few nanometers of the material. This features perfectly fit with the analysis of nanometer thick materials, such as 2DMs.

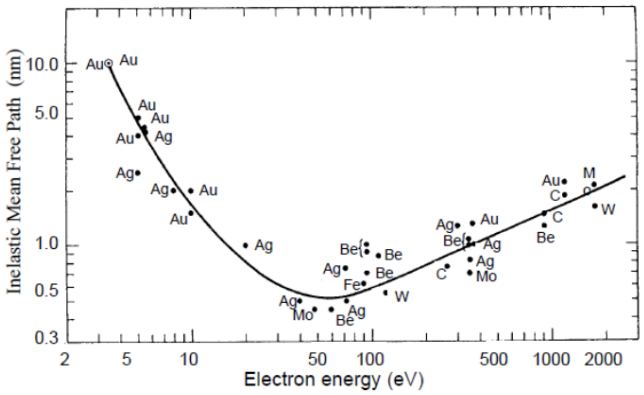

Figure 3. 4. Universal curve of electron inelastic mean free path, λ, in function of KE (eV).

The total angular momentum of an electron is given by the vector sum of orbital and spin angular momentums. An electron is therefore characterized by a quantum number $J = |l \pm s|$ where l and s are respectively orbital and spin angular momentum number. For l = 0 (s orbitals) levels are singlets. For l>0, p, d, and f levels give rise to doublets, because the unpaired electron left in an orbital can have its

spin and orbital angular momentum either parallel or antiparallel. Examples of singlets are reported in this thesis in **Figure 4. 7** for Cls high resolution spectra of electrochemically exfoliated graphene, while doublets are displayed in **Figure 4. 24** and **Figure 5. 10** in Mo3d and S2p spectra.

For some materials, such as the conjugated ones, including graphite and graphene, intrinsic energy loss process generates further bands in the XPS spectra such as the shake-up satellites. Shake-up peaks appear when photoelectron interacts with a valence electron and excite it (shake it up) to a higher-energy level. The energy of the core electron is reduced, thereby the emitted photoelectron is shifted at higher binding energy than the core level position and gives a broad and low intense peak. In **Figure 4. 7** shake-up peaks in Cls spectra of graphite and EEG are indicated.

During XPS analysis a local lack of electrons is created on the surface of the sample. When insulating samples are analyzed, they are not able to compensate this deficiency of electrons, leading to the so-called charge effect. As a consequence, the whole spectrum is shifted toward higher binding energy. To overcome this problem, the analysis of insulating samples is performed with the flood gun active to generate a low energy unfocused electron beam that is necessary to compensate the charging of the sample. In addition, the spectra are calibrated, generally respect to the binding energy of the adventitious carbon.

When photoelectrons leave the sample, they can scatter on the atoms. Electrons from deeper below the surface loose energy and are emitted with reduced KE (increased apparent BE). Electrons very deep in surface lose all energy and cannot escape. These inelastic collisions are responsible of the characteristic XPS background where the intensity of the background toward higher BE is always greater than at lower BE ("stepped" background). Therefore, the XPS background must always be subtracted from the spectra before their analysis.

The main components of an XPS spectrometer are the X-ray source and an electron energy analyzer. Usually in XPS systems the X-rays are obtained by the bombardment with high energy electrons (tens KeV) of an Al or Mg anticathode which generate the correspondent Kα of 1487 eV and 1284 eV, respectively. The X-ray beam is focused on the sample from which photoelectrons are emitted. These photoelectrons are then collected by a system of lens and focused on the analyzer, where they are separated according to their kinetic energy. Finally, they are registered in the detector. For a precise measurement of the kinetic energies of extracted electrons, they need to reach the energy analyzer without energy loss by the collision with air or other gaseous species. For such reason, the XPS measurements are performed under ultra-high vacuum (~10^{-9} mBar in the main chamber). In the instrument available in Nanochemistry laboratory that was used for the XPS analysis reported in this thesis, the high vacuum is ensured by turbomolecular pumps which allow a gradual decrease of the pressure between two independent chambers: the antechamber, where the sample is inserted and parked till an optimal pressure of ~ 10^{-7} mBar is reached, and the the analysis chamber, where the sample is afterward moved for the analysis that is carried out at a pressure of 10^{-9} mBar.

While this technique is generally employed for the analysis of metals, molecular systems and polymers, in the last years XPS has been extensively used for the analysis of 2DMs as well. Nevertheless, the difficulties encountered in the attempt of extending this technique to 2DMs, which differ from traditional molecular systems, are not few. The major challenges regard the quantitative analysis of these systems by XPS, as discussed below.

In this thesis XPS was used as a powerful tool for evaluating the quality of the materials produced by exfoliation in liquid media, that are graphene and MoS_2.

Ideally, XPS spectrum of graphite and graphene present only one peak at a binding energy around 284 eV that is related to sp^2 carbon atoms. However, based on the method of preparation, XPS spectra have shown additional peaks. In particular, when exfoliated in liquid media, XPS spectra of graphene can exhibit, in the region of CIs, extra peaks at higher binding energies related either to the presence of solvent traces[141] or oxygen functionalities formed during the process of exfoliation, i.e. hydroxyl and epoxide groups at about 285-286 eV, as well as carbonyl at 288.5 eV and carboxyl 289 eV moieties.[27] Therefore, XPS can be a necessary tool for evaluating the possible reactions occurring during the exfoliation process and the quality of the resulting material.

By integrating the area of CIs and OIs peaks, the ratio between carbon and oxygen content in the sample can be determined. This could be a method to quantify the number of oxygen functionalities which are chemically bonded to the carbon and to determine, in this way, the chemical structure of the material produced. This is usually done in a very simple way, that is calculating the ratio between carbon and oxygen peaks from Survey spectrum (**Figure 4. 6**). However, this method doesn't give a precise measure of the degree of functionalization of graphene. Indeed, the values of C/O extracted from the Survey spectrum give an indication of the total content of oxygen and carbon in the analysed samples. In this regard, it is worth to note that carbon is always present in XPS spectra, even when analysing samples don't contain carbon as element. In these cases, the detected carbon is adventitious carbon. Similarly, the oxygen detected in the sample can be due to contaminations or solvent traces, as the material is produced in liquid media. Therefore, the analysis of high-resolution carbon spectra is more appropriate as it gives information on the oxygen, or other atoms, directly bond with carbon *via* chemical bonding. In this way, the contribute of species which are simply physiosorbed on the material are not taken into account in the quantification.

To quantify the functionalities present in graphene samples from the high resolution CIs spectrum, or equivalently from OIs spectrum, these peaks must be deconvoluted in their relative components. As XPS technique has been only recently applied to these 2DMs, the literature present on this topic is rather scarce. Due to its complexity, the deconvolution of the XPS peaks is often avoided and high resolution XPS spectra are generally used only qualitatively. Indeed, in absence of a standard metrics for the deconvolution and the quantitative analysis for graphene-based systems, it become quite worthless to provide C/O ratios which cannot be compared with those reported in other works due to different fitting procedure. For these reasons, in this thesis, the C/O ratios are determined by Survey spectra, in agreement with related publications. However, the XPS spectra reported in this work were accurately deconvoluted, and the C/O ratios values calculated by deconvoluted spectra were in good accordance with C/O determined from XPS Survey, proving the absence of contaminations in the samples analysed.

XPS technique has demonstrated to providing useful information on MoS_2 as well. XPS permits indeed to determine and quantify the eventual oxidation of the material, through the appearance of additional peaks related to higher oxidation states. Furthermore, it allows to reveal the presence of other defects in the material such as vacancies,[142] edges,[143] *etc*. and to discriminate among the different MoS_2 polymorphs.[144-145]

For example, XPS technique allowed to determine the presence of sulfur vacancies in mechanically exfoliated FL MoS_2.[142] As reported in **Figure 3. 5**a, XPS Mo3d spectra exhibit different components which have been attributed to the intrinsic MoS_2, indicated as i-MoS_2 (doublet located at 232.3 and 229.1 eV), and sulfur vacancies indicated as v-MoS_2 (peaks at 231.8 and 228.8 eV). Moreover, the presence of peaks at higher binding energy indicate the presence of oxidized material (MoO_3). In this work, the area of the components associated with v-MoS_2 increases after a thermal annealing process

(T>200 C) demonstrating the presence of sulfur vacancies, further confirmed by calculating the ratio S/Mo from XPS spectra.

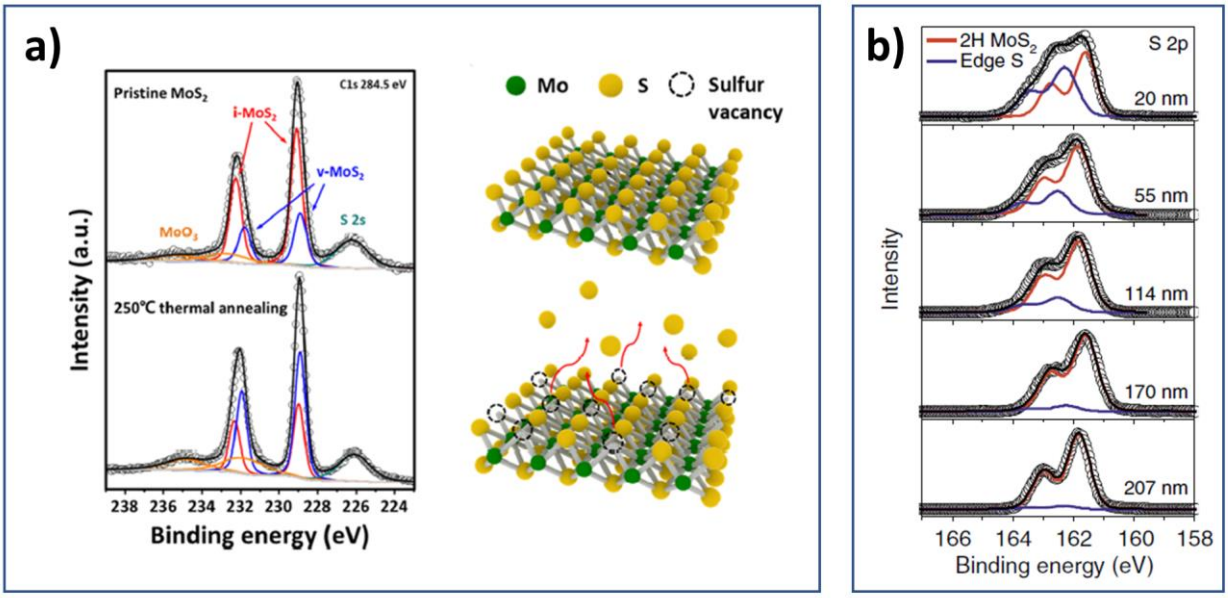

Figure 3. 5. a) XPS Mo3d spectra of mechanically exfoliated MoS_2 showing an additional doublet at lower binding energy (in blue) attributed to the presence of vacancies (v-MoS_2). The intensity of this additional doublet increases after thermal annealing (spectrum below) indicating the formation of further sulfur vacancies; b) fitted XPS S2p spectra of MoS_2 nanosheets collected by filtration of dispersions with different mean flake lengths. While the doublet in red is the characteristic XPS signal of MoS_2, the additional doublet at higher binding energy (in blue) is attributed to edge S. Reproduced from refs 142-143.

In the case of LPE MoS_2, XPS can allow to quantify the edges of the nanosheets. **Figure 3. 5**b shows the appearance of an additional doublet in the sulfur spectra which increases in intensity with decreasing of the lateral sizes of the flakes, demonstrating thus to be related with the edge's density.

An example of XPS quantification of 2H and 1T phases in MoS_2 is shown in this thesis, in chapter 4.

3.4 Raman spectroscopy

In this paragraph, there will be discussed some information useful to reading the following chapters (chapters 4 and 5) regarding the analysis of graphene and MoS_2 by means of Raman spectroscopy.

Raman spectroscopy is another indispensable technique for the characterization of graphene and related materials. Indeed, it is widely employed to assess the quality and structural integrity of the exfoliated materials, as well as the number of layers of the nanosheets. Additionally, it can give many other information regarding the effects of doping, strain, temperature, perturbations such as electric and magnetic fields, *etc.*[146] Moreover, the great advantage of Raman technique is that this information is obtained through a fast and non-destructive analysis, although its interpretation is often not so simple.

Raman spectroscopy is a technique based on interaction of the light with the chemical bonds of a material and on the analysis of the inelastically scattered light from the medium. Usually, in a Raman experiment the shift in energy between the incident and inelastically scattered light is measured. This technique is normally used for the analysis of molecules but since 2006, when it was reported the first Raman characterization of graphene from Ferrari et al[147], it has been extended to the analysis of 2DMs as well. Every peak in a Raman spectrum corresponds to the vibrational frequency of a bond of the analyzed system. Raman spectroscopy is, hence, a very sensitive technique, even to small differences in structure. For this reason, by Raman spectroscopy it is also possible to discriminate the different allotropes of carbon, e.g. diamond, graphite and graphene, which differ only in the orientation of the C-C bonds. Indeed, while diamond is characterized by only one peak, graphite and graphene Raman spectra exhibit two main peaks at 1580 cm^{-1} and 2680 cm^{-1} which are commonly indicated as G and 2D peaks. G peak is associated to the relative motions of sp^2 carbon atoms, therefore is a characteristic peak of both graphene and graphite. This peak was observed for the first time for the analysis of graphitic materials and for that reason it takes this name. The G mode of graphite has E_{2g} symmetry and involves in-plane bond-stretching vibration of pairs of Csp^2 atoms.[148] D peak is also called "defect band" because correlated to the presence of defects in the material. In fact, this peak corresponds to a breathing mode of the sp^2 carbon rings which symmetry is forbidden for Raman selection rules in pristine graphite and graphene, while only becomes active in the presence of disorder (**Figure 3. 6**). This band is present only if the sp^2 conjugation is interrupted by interstitial defects, vacancies, including flake edges. Finally, the 2D band is the second order of the D band. However, it derives from a vibrational process which involves two phonons and it doesn't need to be activated as the D band. Therefore, it is always present also in the absence of the D band.

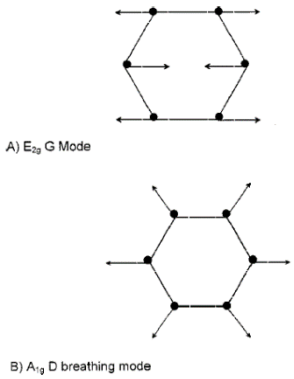

Figure 3. 6. Vibration modes associated with G and 2D peaks of graphene: a) E_{2g} G mode of sp^2 rings, b) A_{1g} D breathing mode in rings. Reproduced from 148.

The G peak can give an information on the thickness of the material as its position changes from bulk to mono and bilayers.[149] However the position of the peak can be also affected by other factors, such as doping or strain, therefore must be carefully interpreted. In graphite and pristine graphene Raman spectra the D band is very weak. **Figure 3. 7** shows the D band at the edge of graphite and single-layer graphene. While D peak in pristine graphene is a single sharp peak, the D band in graphite consist of two peaks, named D_1 and D_2.

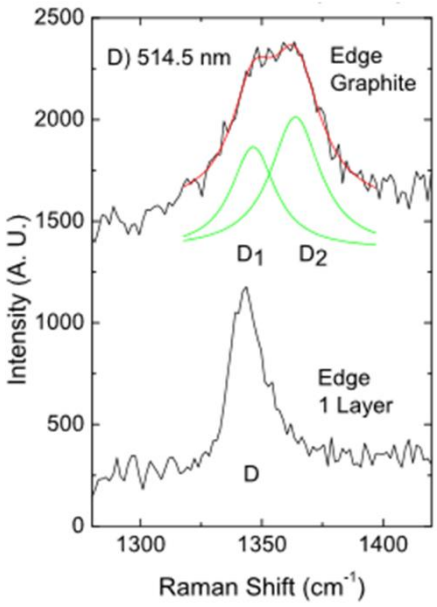

Figure 3. 7. D peak at the edge of graphite and single layer graphene. While the graphene D peak is a single sharp peak, the one of graphite is a band which consist of two peaks, named D_1 and D_2.

When D band is intense, it indicates that there are many defects in the material. For that reason, the ratio of the intensities I_D/I_G can be used to characterize the level of disorder in graphene. This ratio follows two different behavior in function of the amount of disorder. In the regime of low defect density, I_D/I_G ratio increases with the defects because a higher density of defects generates a more elastic scattering. However, once I_D/I_G ratio reaches a certain value, that correspond to the beginning of the regime of high defect density, this ratio will begin to decrease. This behavior is described in the plot in

Figure **3. 8**a, from which it is also possible to extract the distance of defects (L_a) known the ratio I_D/I_G, following the Tuinstra and Koenig equation:[148]

$$I(D)/I(G) = C(\lambda)/L_a$$

Where C (515.5 nm) ~ 44 Å.

In the same work, Ferrari et al. report a three-stage model for the interpretation of Raman spectra of disordered carbon systems which defines the amorphization trajectory from graphite to a ~100% sp^3 system. This model can be useful to evaluate the quality of the graphene produced by exfoliation and the eventual presence of amorphous carbon. The three stages involve the transition from graphite to nanocrystalline graphite (stage 1), from nanocrystalline graphite to amorphous carbon (stage 2) and from amorphous carbon, containing rather small content of C-C sp^3, to 100% sp^3 systems. The evolution of G peak and I_D/I_G ratio among the three phases is reported in

Figure 3. 8b. In particular, in stage 1, or passing from graphite to nanocrystalline graphite, the G peak moves from 1581 to 1600 cm^{-1}, and the I(D)/I(G) increase following the Tuinstra and Koenig equation. The shift of the G peak occurs concomitantly with the appearance of D' peak, which is thus indications of presence of defects. Graphene is considered being in the stage of nanoscrystalline graphite, indicated in **Figure 3. 8**b.

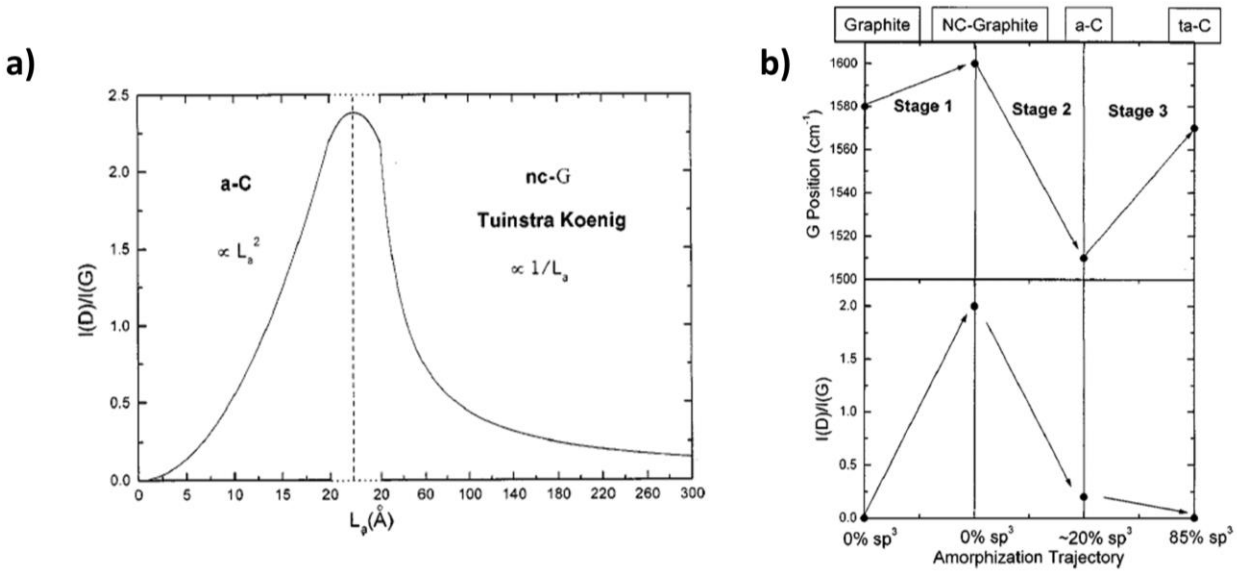

Figure 3. 8. a) Transition between the two regimes of low and high defect density and relation between I_D/I_G and defect distance (L_a), as reported in ref. 148 b) Variation of G position and amorphization along the amorphization trajectory.

In 2006 Ferrari et al. reported also the evolution in the shape of the 2D band with the thickness, indicating that 2D band can give precious indications on the thickness of the flakes. It was shown that while graphite has an asymmetric 2D peak which can be fitted with two components $2D_1$ and $2D_2$, in graphene this band can be fitted with only one sharp peak.[150] In few layers graphene, because of the interactions between layers, the spectrum change compared with monolayer graphene, and in particular the 2D band that is a sharp single intense peak in monolayer graphene, start to split in an increased number of vibrational modes. **Figure 3. 9**a shows the 2D band of a bilayer which can be deconvoluted in 4 Laurentian components corresponding to the four vibrational modes of a bilayer: $2D_{1B}$, $2D_{1A}$, $2D_{2A}$, $2D_{2B}$. The deconvolution of 2D peak can thus give information on the number of layers and, in principle, being considered as a measure of the degree of exfoliation as the ratio of intensities I_{2D}/ I_G is.[147] An increase of the number of layers determine indeed a significant decrease of the peak at lower frequency, $2D_{1B}$, but for more than 5 layers, the 2D shape become indistinguishable from bulk graphite one (**Figure 3. 9**b). Therefore, Raman spectroscopy can clearly distinguish a single layer from a few-layer graphene flakes that feature a maximum of 5 layers.[150] However, it is important to mention that such quantitative measurements have been carried out only on mechanically exfoliated single nanosheets. In the case of graphene exfoliated in liquid media, typically the Raman spectrum is only qualitatively interpreted, while flake thickness (i.e. mean number of layers) is not extracted from the spectrum.[151] This is reasonable if thinking to the high polydispersity of the material produced and its relatively bulky nature.

Generally, indeed, the thickness distributions ofLPE graphene or MoS_2 flakes are centred at higher values than 5 layers. Therefore, they appear overall as bulk materials to the Raman analysis. Additionally, the small sizes (few nanometers) of the thinner flakes make challenging reproducing the above reported experiments which were performed on micrometer-size mechanically exfoliated single and few-graphene. Furthermore, due to the small size, LPE nanosheets generally appear rather defective.

Only recently, some reports have shown that it is possible to assess to the average number of flakes in LPE graphene. The method reported by Sarro et al.[152] is still a more qualitative approach that allow to distinguish FLG sheets from bulky graphite in function of the 2D peak shape. They report indeed that, differently from ME graphene, the 2D band in LPE graphene can be never fit with a single Lorentzian but is generally composed of two Lorentzian components $I2D_1$ and $I2D_2$. When $I2D_1 > I2D_2$ the film can be considered composed by FLG sheets and not by bulky material.

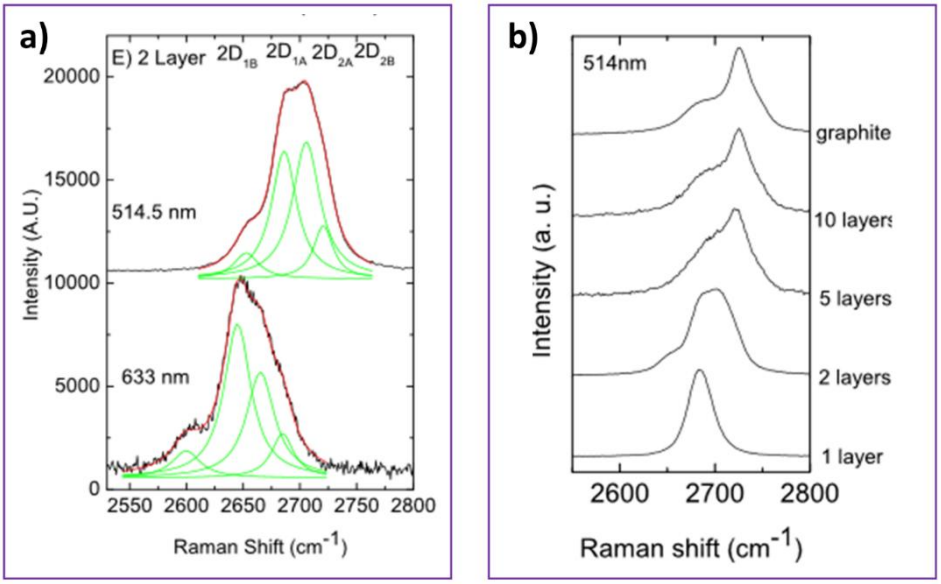

Figure 3. 9. a) 2D band in a bi-layer graphene deconvoluted in its four components at 514 and 633 nm. Reproduced from 150; b) variation in the 2D band shape with the number of layers for 514 nm excitation.

A new metric[151] has been instead developed recently for materials exfoliated in liquid media and allow to estimate the exact average number of layers from the ratio I_{2D}/I_G. The authors report that correctly fit the 2D band of LPE graphene can be challenging because the samples are composed by nanosheets with different thickness distribution. Therefore, they assess that the simplest method is probably considering the intensity of 2D peak. They propose a metric for the determination of number of layers which consider the ratio of intensities between 2D band and G band:

$$\langle N \rangle = 1.04 M_1^{-2.32}$$

t valid for N < 10 layers, with $M_1 = I_{2D}/I_G$.

In conclusion, the quantification of the number of layers by Raman spectroscopy for what regard the materials exfoliated in liquid media is still objected of study. The adaptability of the proposed models to materials exfoliated with other approaches, that differs from the UILPE, still need to be proved. Consequently, in this thesis we simply qualitatively interpreted Raman spectra although some considerations were done regarding the presence of defects in EEG, based on the above.

Raman spectrum of single-layer MoS_2 is characterized by two peaks which are the first-order Raman modes associated with in-plane E^1_{2g} (385 cm^{-1}) and out of plane A^1_g (405 cm^{-1}) vibrations.[153] In bulk MoS_2 these modes are located at 382 and 407 cm^{-1} respectively, and also their full widths at half maximum are smaller than in monolayer, where the phonon confinement in ultra-thin structure determine broader peaks.[119] When the thickness of MoS_2 decreases respect to the bulk the frequency

of E_{2g} up-shifts while the A_{1g} downshifts till the difference between the two bands is 19 cm^{-1} for monolayer MoS_2; while from monolayer and bilayer there is a difference in frequency of 3 cm^{-1}. Consequently, the difference between the frequency of E_{2g} and A_{1g} modes can be used to determine the number of layers in a thin MoS_2 sheet. As it was said for graphene, the position of these peaks can be influenced by many factors. Therefore, this measure is not always accurate and need to be supported by other complementary techniques. Moreover, in MoS_2, intensity and width do not depend on the number of layers.[154]

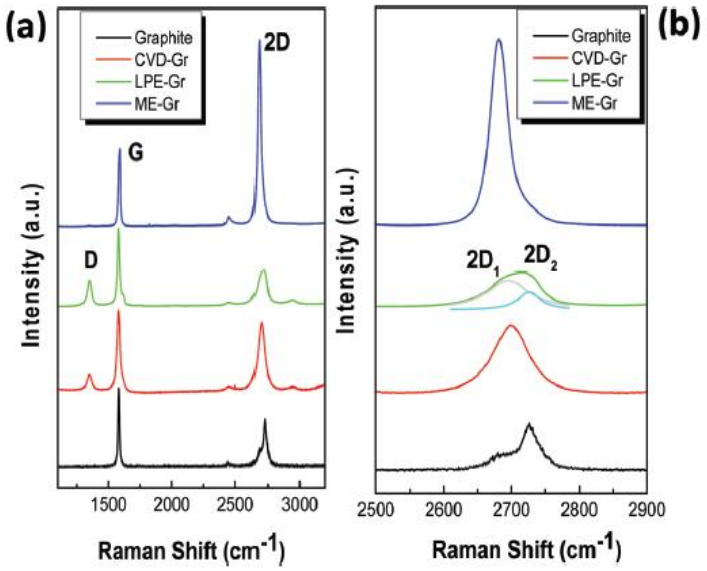

Figure 3. 10. a) Comparison among Raman spectra of graphite and graphene materials produced with different methods: chemical vapor deposition (CVD), liquid-phase exfoliation (LPE) and mechanically exfoliated graphene (ME), each spectra is determined as the average of 100 spectra captured on areas of 100 × 100 μm2; b) magnification on the 2D band which show the difference in the 2D band of graphite and few-layer graphene produced by LPE, whose 2D peak can be fitted by 2 components: $2D_1$ and $2D_2$, with $2D_1$>$2D_2$. Reported from ref. 151.

Hence, similarly to the case of graphene, Raman spectroscopy can be used as fast and non-destructive method for discriminating among mono- and few-layer MoS_2 nanosheets. **Figure 3. 11** shows the dependence of the frequencies of these two bands on the number of layers.

Recently, Raman spectroscopy has been considered a reliable technique to quantify defects in single-layer MoS_2. Many strategies have been indeed developed for introduce defects on monolayer MoS_2, since they can be beneficial for tailoring MoS_2 properties, e.g. introducing doping, enhancing the photoluminescence, improving its reactivity *etc*. Mignuzzi, for instance, demonstrated that the controlled introduction of structural defects by ion bombardament determines the appearance of characteristic features in the Raman spectrum of single layer MoS_2, demonstrating viability of Raman spectroscopy in the determination of structural disorder. In particular, upon increasing of defect density a broadening of the two main components, E' and A_1' (as indicated for monolayer MoS_2) is observed and is accompanied by a shift in the position of the two peaks. In particular, when the distance between defects decrease the E' peak downshifts while A_1' upshift and the FWHM of both bands increase. By DFT calculation, this evolution has been attributed to phonon confinement. Moreover, the introduction of disorder activates new Raman scattering peaks in the region between

140 and 420 cm^{-1}. These modes involve phonons at the edge of the Brillouin zone, which may be activated in the presence of defects satisfying the Raman selection rule. In close proximity of the first-order peaks, for instance, appear a defect-induced peak at ~357 cm^{-1} that was assigned to the TO branch at the M point.

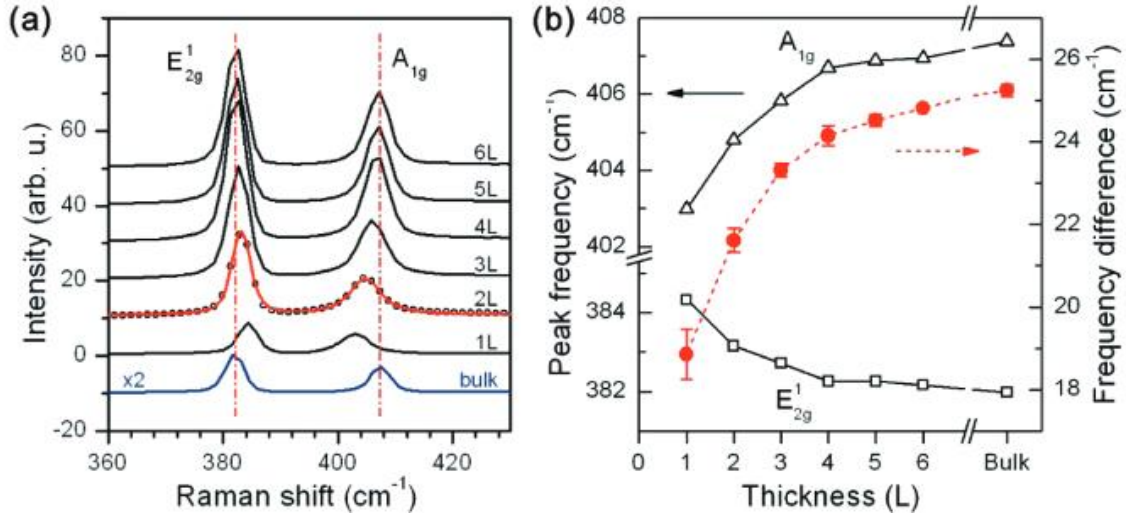

Figure 3. 11. a) Raman spectra of MoS_2 bulk and nanosheets with different number of layers (L); b) frequency of the two modes E_{2g} and A_{1g} and their frequency difference as a function of the number of layers. Reproduced from ref. 155.

Finally, Raman spectroscopy allows also to distinguish between the MoS_2 polymorphs, 1T and 2H. As reported by Calandra, the 1T phase is dynamically unstable and undergoes a phase transition towards the most stable 1T' structure composed of separated zig-zag chains. The Raman spectra of 1T' phase display a more complex Raman spectrum. It is richer in active peaks than the 2H phase due to its reduced symmetry. While the 2H MoS_2 spectra show only the two modes E_{2g} and A_{1g}, the Raman spectra of 1T phase miss the E_{2g} peak, but shows five additional peaks. The principal of these components are J_1, J_2 and J_3 which were already detected in 1986, but interpreted more recently by Calandra.[156] The broadest, generally at 227 cm^{-1}, is so called J_2 peak. This mode is related to the contraction of the distance between the two zig-zag chains to recover the 1H structure. At 156 cm^{-1} appears the so called J_1 peak which is related to an antiphase out-of-plane shift of each line of Mo atoms inside the zig-zag chain and an in-plane shearing mode of one stripe of an atom with respect to the other inside a chain. The J_3 mode at 333 cm^{-1} tends to break each zig-zag chain in two stripes with an out-of-plane component. The mode at 412 cm^{-1} is the same A_{1g} mode that appears is 1H polytype. This work also points out the key role of adsorbates or vacancies which can stabilize the 1T metallic structure.

According to these and other studies, Raman spectroscopy can be a considered a reliable technique to determine the content of defects in MoS_2, similarly to graphene. Therefore, in this thesis Raman spectroscopy has been used to assess the quality of the materials produced by exfoliation in liquid media.

CHAPTER 4.

PRODUCTION OF 2D MATERIALS IN LIQUID MEDIA: FROM ULTRASOUND-ASSISTED TO ELECTROCHEMICAL EXFOLIATION[1]

The main focus on this chapter is to cast light onto structure and electrical properties of electrochemically exfoliated graphene (EEG) and molybdenum (IV) disulfide (MoS_2). The chapter begins by outlining the most recent discoveries which had tremendous impact on the development of electrochemical exfoliation (EE) approach for the production of 2D materials. Later, the focus is given on the anodic EE of graphite, that is one of the most promising methods for the mass production of graphene. EE holds in fact the unique advantage compared to other liquid-phase exfoliation (LPE) methods of producing large quantities of high-quality graphene in a short time.

Recent works suggest that EEG possesses properties that are markedly different from graphene and graphene oxide (both in its pristine and reduced forms). However, an in-depth understanding on the structure-properties relationship of this material is still lacking. While initial efforts in this field have been dedicated to finding better conditions (e.g. combination of electrolyte and applied voltage, electrodes working distance, *etc*.) to control the EE of graphite,[27, 102, 113] this chapter aims at providing insights into the modulation of the structure and properties of this material. Such a control can be instrumental when tailoring the properties of the material for its specific future applications. By pursuing this challenge, a control over the process and obtained material can be achieved only by unravelling the mechanism that underpin electrochemical exfoliation. Ultimately, this will lead to an improvement of the process towards the production of high-quality graphene.

In this work, a graphite foil is electrochemically exfoliated in an aqueous electrolyte. We report a comprehensive physico-chemical characterization of EEG, combined with an investigation on the electronic properties of this material carried out both at the single flake level and on the EEG based films. Additionally, we employed for the first time microwave irradiation to reduce the oxygen content in EEG and demonstrate that the oxygen functionalities are not the bottleneck for charge transport in EEG, which is rather hindered by the presence of structural defects within the basal plane. Finally, the electrochemical method has been extended to MoS_2, that has been exfoliated as consequence of the electrochemical intercalation of DMSO-solvated lithium-ions. Similarly, the structural ad electrical characterization of the as produced material has been exploited in order to investigate its quality.

[1] Large part of the work displayed within this chapter have been published: a) Eredia, M.; Bertolazzi, S.; Leydecher, T; El Garah, M.; Janica, I.; Melinte, G.; Ersen, O; Ciesielski, A.; Samorì, P. Morphology and Electronic Properties of Electrochemically Exfoliated Graphene. J. Phys Chem Lett 2017, 8, 3347-3355; b) El Garah, M.; Bertolazzi, S.; Ippolito, S.; Eredia, M. Janica, I; Melinte, G. Ersen, O.; Marletta, G.; Ciesielski. A. Samorì, P. MoS_2 nanosheets via electrochemical lithium-ion intercalation under ambient conditions. FlatChem 2018, 9, 33–39.

4.1 Introduction

In the recent years, 2D materials (2DMs) have gathered a great interest because of their unique physical and chemical properties which may render them key components in disruptive technologies. Different *bottom-up* and *top-down* procedures have been developed and optimized in order to generate monolayer thick sheets with different chemical composition and structure. Interestingly, it has been noticed that the physicochemical properties of 2DMs closely depend on the method employed for their production and processing.

The most outstanding properties that are generally reported for graphene and other 2DMs have been discovered mainly by investigating mechanically exfoliated nanosheets e.g. produced by Scotch-tape exfoliation. Scotch-tape method is the approach used by K. Novoselov and A. Geim to exfoliate graphite.[11] Through this approach, which relies on the use of simple adhesive tape, a layered crystal can be surprisingly exfoliated into pristine monolayers in a relatively small number of cleaving attempts - despite the fact that, for example, a typical crystal of graphite contains about 10^6 layers of carbon atoms.[157] Due to its simplicity, this method is still preferred when the exfoliation is done from bulk naturally occurring crystals as in the cases of graphite, MoS_2, *etc*. Moreover, it is the only method that allows isolation of defect free 2DMs' nanosheets. Clearly, the ease with which monolayers rather than few-layers sheets are obtained by mechanical exfoliation (ME) depends on the strength of interlayer interactions. In some cases, as for example for $PtSe_2$, producing single layers is much more complicated than in the case of graphite.[158] However, even in the case of graphite exfoliation, the probability to obtain monolayers is rather low and uncontrollable. Therefore, this approach cannot be employed to produce 2DMs at large scale. Yet, it remains appropriate for fundamental studies aimed at unveiling the physical and chemical properties of new 2DMs.

In the last years, many efforts have been devoted to the development of new strategies that maximize the yield and the quality of 2D nanosheets, reducing costs and processing times. As a result, an outbreak of synthetic approaches has been proposed in the last decade. Only 4 years after the demonstration of the Scotch-tape approach, Coleman and colleagues reported a ground-breaking method for the production of 2DMs in a liquid media. The liquid phase exfoliation (LPE), contrary to other approaches e.g. Scotch-tape method and chemical *bottom-up* synthesis, is potentially enabling the transition from theoretical and laboratory experiments to real application of 2DMs, because of its potential up-scalability. Such a breakthrough enabled graphene not being any longer "only a single flake on a silicon chip", but also an ink that can be brought out from the laboratories and tested in innovative applications to address societal needs.

LPE exploits ultrasonic energy to fragment layered crystals both in their lengths and thickness. Therefore, the exfoliation into thin layers is always accompanied by the reduction of the particles' lateral dimensions as well. The exfoliation occurs in a solvent properly chosen to interact with the material and balance the inter-sheet attractive forces. In this way, the material is kept in suspension. In particular, it has been demonstrated that ideal solvents to exfoliate 2DMs are those having a similar surface energy to the one of the exfoliated 2DMs' sheets.[159] This implies that the exfoliation occurs only in a limited number of solvents, most of which exhibit high boiling point and are toxic, e.g. NMP and DMF, that are commonly used for exfoliating graphite. The use of surfactants or stabilizing agents which help to match the surface tensions of exfoliated particles to those of the liquid medium, thereby stabilizing the dispersion, has partially solved this problem allowing the use of greener solvents like water or ethanol.[88] Such approach is also known as molecule-assisted LPE. Organic molecules are properly selected for interacting non-covalently with the material, resulting in a clear enhancement of the exfoliation efficiency and a better stability of 2DMs in dispersions with increased concentration.[16]

Despite these expedients, the yield of exfoliation is moderately low, compared to the expectations of mass production. Moreover, extensive sonication times, coupled with time-consuming procedures of purification and flakes size selection, are necessary to obtain the desired dispersions of mono- and few- layers nanosheets.[66] The concentration of final dispersions following post-exfoliation treatments is clearly even lower; without considering that get rid of stabilizers is challenging, if not impossible, and causes the re-aggregation of the flakes.

Until recently, liquid phase exfoliation (LPE) was synonymous of sonication-based exfoliation. Today, the number of synthetic approaches has enormously grown, and this acronym has been extended to all the approaches which operate in liquid media including ultra-sonication,[14, 25] shear-mixing[17, 160] and micro-fluidization.[18] Shear exfoliation (SE) is carried out in rotor stator mixers, or even in household kitchen blenders, where rotating blades generate turbulent shear throughout the liquid.[160] Consequently, while the exfoliation induced by ultrasounds primarily exploits the phenomenon of cavitation (see Chapter 2), SE is a shear-force dominated method. This method benefits thus of less fragmentation, respect to ultrasound-induced LPE (UILPE), being mainly limited to milling by the rotor. Though, shear exfoliation requires longer processing times to yield the same concentration obtained by UILPE. If one considers that the UILPE is already a process that last hours, shear mixing process can need also 24h to reach the same concentration. On the other hand, SE allows the processing of larger volumes that make it a scalable process.[66] In both shear mixing and ultrasonication based processes, the exfoliation is mainly localized around the probe or in the gap between rotor and stator, respectively, implying an efficient exfoliation only in that region.[161] This limit is overcome with microfluidization technique where the high shear rate (10^{-6} s^{-1}) is applied to the whole fluid, that is forced to pass through a microchannel, undergoing to high pressure (> 200 MPa). Moreover, microfluidization can be performed in continuous, resulting therefore highly scalable.[18] Although this continuous process determines a yield by weight of few layer graphene that is almost 100%, only 4% of these layers are <4nm.[18] All the above-mentioned techniques have thus their own pros and cons and, more interestingly, it has been observed that their performances strictly depend on the material. For instance, while UILPE and SE methods result relatively comparable for what regard the exfoliation of graphite, when SE is used to produce thin layer transition metal dichalcogenides (TMDs) its performance are way lower than UILPE as it leads to rather low concentrations (μg l^{-1} in <24h).[66]

In view of the LPE's limitation for 2DMs production, a major step forward consisted in the use of EE to produce graphene from graphite bulk precursors.[28] EE can occur either under anodic or cathodic conditions (see section 2.2.2).[26] In anodic conditions, an applied voltage drives the anionic intercalation into graphite electrode. Intercalation together with the formation of gas species lead to the expansion and exfoliation of the material. This method allows the production of large quantities of graphene in a short time. In particular, while UILPE makes it possible to produce dispersions with the maximum concentration of 1 mg ml^{-1},[162] it requires long (up to 1000 hours) sonication processes and multi-step post treatments, the EE allows to generate 1-10 mg ml^{-1} dispersions in the time scale spanning from minutes to a few hours. Even more surprisingly, our experiments prove that the exfoliation already happen in the first few seconds of the process. However, differently from UILPE, EE performed in anodic conditions generally may result in oxidized graphene flakes. For that reason, many research groups have proposed the EE method as an alternative to classical Hummers and Staudenmaier' to produce graphene oxide (GO). In other words, EEG has been often labelled as a GO-like material.[163-168] On the other hand, contradicting reports have appeared in the last few years[17]. These works consider the electrochemical process as a new route to the mass production of defect-free graphene.

In fact, the oxidation of graphene sheets is unavoidable during the anodic EE, and it depends on many factors, such as exfoliation time, electrolyte, electrodes distance, *etc*. Although EE in non-aqueous electrolytes prevents the extensive oxidation of graphitic material which occurs in anodic conditions, cathodic EE of graphite is not as efficient as the anodic process. Generally, cathodic EE is a two-step process where positive ions are electrochemically intercalated into graphite electrode, while the effective exfoliation occurs upon sonication. In this case, the intercalation process causes the expansion of the material only, being therefore limited compared to the combined effect of intercalation and gas development that characterize the anodic process and leads the complete exfoliation of the material. Time-consuming further steps of ultrasonication are necessary to promote the effective exfoliation of the graphite cathode into graphene. Consequently, materials exfoliated in cathodic conditions have the same characteristics of materials exfoliated by ultrasounds, i.e. limited lateral sizes of the flakes (in the range of hundreds of nm)[169] and lower yields in thin layers in respect to the anodic approach. Because of this reason, current research endeavours are focused on the anodic exfoliation of graphite, which, on the contrary, allows the one-step production of single- and few-layered graphene sheets in high quantities.

While the production of high quantity of defect-free graphene sheets *via* wet methods attracts the attention of both industrial and academic sectors,[170] alongside the degree of oxidation, little is known about the physico-chemical properties of EEG sheets, such as the nature of the defects and electronic properties of the material. It has been shown recently that devices based on the thin EEG film possess a maximum hole mobility of ca. 100 $cm^2V^{-1}s^{-1}$, whereas single-layer (SL) EEG gives a hole mobility of ca. 300 $cm^2V^{-1}s^{-1}$ and a sheet resistance of 2 $k\Omega\ sq^{-1}$,[171] being comparable to that of undoped CVD-grown graphene (1 $k\Omega\ sq^{-1}$).[172] Such low mobility (if compared to pristine graphene)[11, 173] has been attributed to the inter-flakes boundaries, which are bottlenecks for charge transport, and to the presence of the oxygen functionalities in the structure of the flakes, the latter acting as electronic traps.

Here we show that the EE of graphite foil under the most commonly employed anodic conditions,[28, 92, 100, 112, 163-164, 171, 174-175] i.e. using ammonium sulfate as electrolyte, not only causes the oxidation of the graphitic material, but also results in the structural degradation of the sheets. Structural and compositional characterization of the produced material corroborated with the investigation on the electronic properties of both SL flakes and films provide unambiguous evidence that the electrical characteristics of EEG are not hindered by the amount of oxygen functionalities, which can be nearly completely removed upon microwave (MW) irradiation but are rather limited by the presence of structural defects.

We also investigated the electrochemical production of other 2DMs, e.g. MoS_2. In this case, to avoid the oxidation of the material and the formation of extensive structural defects, as demonstrated in the previous work, we developed an electrochemical approach in cathodic conditions for the exfoliation of MoS_2 *via* lithium-ion intercalation in dimethyl sulfoxide (DMSO). Unlike the conventional intercalation methods based on dangerous organolithium compounds, our approach leads to the possibility to obtain mono-, bi- and tri-layer thick MoS_2 nanosheets with a large fraction of the semiconducting 2H phase (~60%), as estimated by X-ray photoelectron spectroscopy (XPS). We further show that the electrical characteristics of field-effect transistors (FETs) based on this material can be significantly improved through a combination of thermal annealing (150 °C) under vacuum conditions (5×10^{-8} mbar) and upon exposure to vapor of short-chain alkanethiols, suggesting that a good deal of defects in our electrochemically exfoliated MoS_2 ($EEMoS_2$) consists in sulphur vacancies.

The following sections of this chapter are dedicated to the experimental work.

Section 4.2.1 describe setup and conditions used for the EE of a graphite foil and a MoS_2 crystal. Moreover, it reports the procedure to obtain large area EEG film. The other sections provide a description of samples preparation and operative conditions for morphological, chemical (section 4.2.2) and electrical (section 4.2.3) characterization of the exfoliated materials. Finally, section 4.3 presents and discusses the findings of this research.

4.2 Materials and methods

4.2.1 Electrochemical exfoliation and film preparation

In this subchapter, the production of EEG under anodic conditions by using a simple electrolytic cell, as depicted in **Figure 4. 1**, is described. The electrolytic cell was built by employing a few basic components such as a platinum wire as cathode and a graphite foil as anode immersed in an electrolytic solution. In this work we used $(NH_4)_2SO_4$ as electrolyte that was solubilized in water at a concentration of 0.1 M.

The exfoliation of graphite foil (cathode) occurs as immediate consequence of the applied voltage between the two electrodes placed at a distance of around 2 cm. By means of ISO-TECH IPS-603 DC power supply, we applied a voltage of +15 V which generate a starting current of ca. 0.4 A. The produced powder was collected by vacuum filtration on PTFE membranes (pore's diameter of 5 µm) and, after several rinsing steps needed to remove salt residuals, it was dispersed in dimethylformamide (DMF) by mild sonication for 20 minutes. Such dispersion was kept decanting for 48 h to promote the sedimentation of un-exfoliated material.

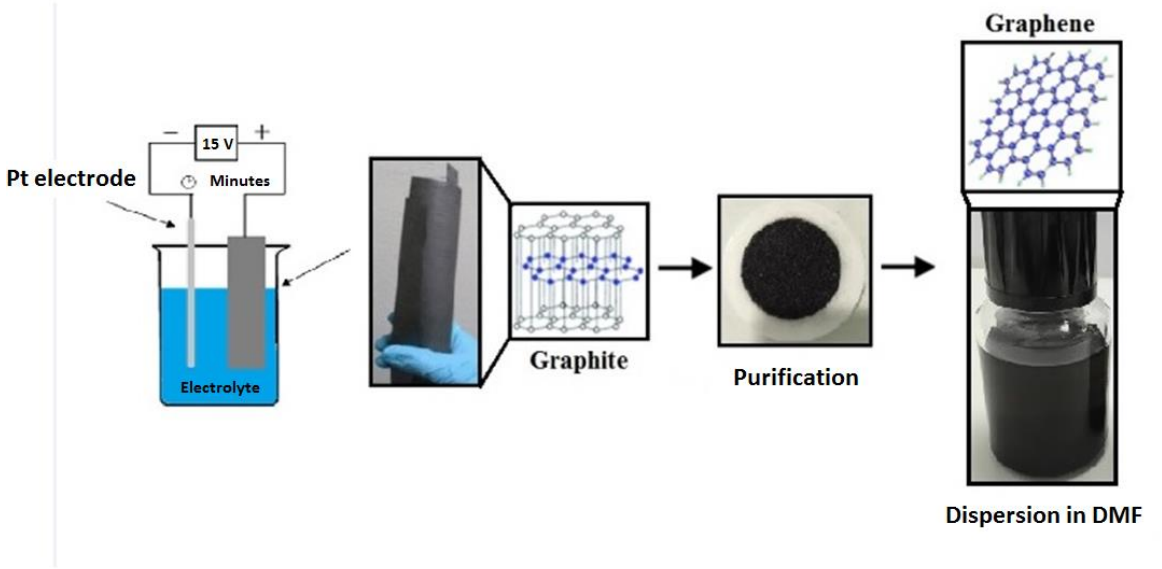

Figure 4. 1. Schematic representation of the procedure to prepare a stable dispersion of graphene though electrochemical exfoliation of a graphite foil, followed by purification step and dispersion of graphene flakes in dimethylformamide (DMF).

EEG films were prepared by starting from a pristine and stable dispersion of EEG in DMF. The preparation of thin and uniform films is extremely challenging. While techniques like spin-coating, even after subsequent depositions or varying the concentration of EEG dispersion, typically lead to inhomogeneous coverage of the substrate; drop-casting or dip-coating do not allow controlling the

thickness and uniformity of the film. On the contrary, continuous films were obtained by employing the following protocol. Few drops of EEG dispersion were gently spread on water surface. Once re-organized at the interface, thin flakes form a uniform greyish film floating onto the sub-phase. The transfer was done by dipping a SiO_2 substrate at 45 degrees in order to withdraw the film formed at the liquid-air interface. This process can be easily up-scaled enlarging the dimensions of water bath and consequently increasing the amount of loaded dispersion. Additionally, the process is not substrate dependant and can be extended to any kind of substrates (rigid or flexible), with any shape.

For MoS_2 exfoliation, a crystal of MoS_2 (7 × 4 mm, 1 mm thick) and a Pt wire were used as working and counter electrodes, respectively. Some works on the lithium-ion electrochemical methods reports optimal potential around 4—5 V in DMSO, mixtures of dimethyl carbonate and ethylene carbonate or other electrolytes.[176-177] Here, by using a two electrodes cell and applying a potential of -5 V, the expansion and intercalation process of MoS_2 bulk crystal occurred in about 45 minutes using a 1 M solution of LiCl in DMSO as electrolyte and source of Li-ions. Then, the intercalated material was washed several times with acetone, filtrated and finally sonicated for 25 minutes in a mixture DI H_2O /ethanol (70:30%). The dispersion was centrifuged at 4500 rpm for 30 minutes, in order to separate the thick unexfoliated materials, and then the supernatant was collected and used for the preparation of the samples.

4.2.2 Physico-chemical characterization

The physico-chemical characterization of EEG and EEMoS_2 has been performed by means of various microscopic and spectroscopic techniques. Samples for the characterization of EEG by means of optical microscopy (OM), Raman spectroscopy and atomic force microscopy (AFM) were prepared by spin-coating a graphene dispersion at a concentration of 1 mg ml^{-1} in DMF onto SiO_2 substrates. For these analyses indeed the presence of isolated flakes is preferred to overlapped ones or aggregates. However, in some cases, it is also necessary having a considerable number of flakes which are only few nanometres far apart, and still not overlapped, especially in the case of AFM for the purpose of a statistical study. Therefore, the deposition method was optimized varying the parameters of spin-coating, while verifying from time to time the quality of the deposition by OM. All the substrates were cleaned by subsequent ultrasonication in acetone and isopropyl alcohol (30 minutes each), in order to wash off the protective photoresist layer, and then dried under nitrogen flow. Afterward, the substrates were treated by UV-O_3 for 5 minutes followed by 25 minutes of exhaust.

A fast and preliminary investigation of the quality of the exfoliation was attained by OM, which allows quick determination of the presence of single- and few-layer thick graphene flakes deposited on the SiO_2 substrate, as a result of optical contrast with respect to empty substrate.[139] OM images were recorded with an Olympus BX51 set-up. Subsequently, an in-depth morphological characterization of the exfoliated material has been performed by AFM, which was the technique offering the best lateral resolution available during my experimental work. AFM imaging was carried out using a Veeco Dimension 3100 atomic force microscope operating on a Nanoscope IV control unit under ambient condition, the only one accessible when I performed these experiments. Yet, better resolution could be obtained by multimode AFM which with a small scanner allows to reach scan sizes even smaller than 1 μm x 1 μm. Topography and phase images were acquired simultaneously operating in tapping mode, by using antimony (n) doped silicon cantilever.

AFM was used to perform statistical studies of flake size and thickness. In these cases, AFM images were generally acquired at scan sizes of 15 μm x 15 μm. While, to determine thickness and surface

coverage of the EEG films, 30 μm x 30 μm or 50 μm x 50 μm AFM images were analysed. In particular, for evaluating the thickness of the film, it was measured the average height step between film and bare substrate at the edges of the film. The procedure used for the film preparation, indeed, leaves a small part of substrate uncovered by EEG flakes, that is the area where the substrate is supported by the tweezers during the transfer (see **Figure 4. 17**). This part of the sample is exploited for the determination of film thickness, similarly to the common procedure of scratching a polymer film to determine its thickness. The surface coverage was determined by image processing, creating a mask, using Gwyddion software, that is adjusted in order to mark all the flakes excluding the substrate, and vice versa, using a threshold grain detection algorithm. The ratio between the two selected areas gives an idea of the film surface coverage. To perform these analyses, the image was necessarily treated, with the main objective to level the flat base.

The number of layers per sheet was also determined with a high precision by using high-resolution transmission electron microscopy (HR-TEM), in the framework of a collaboration with Professor Ovidiu Ersen at the Institute of Physics and Chemistry of Materials in Strasbourg (IPCMS). Samples for HR-TEM analysis were prepared by drop-casting on a lacey carbon-coated copper grid, followed by solvent evaporation. HR-TEM micrographs were taken on a FEI Tecnai F20 TEM equipped with a Schottky emitter and operated at 120-200 keV. The number of graphene layers was estimated from the number of (0,0,2) diffraction fringes at the edge of folded graphene sheets.

XPS was employed to determine the quality of EEG in terms of oxidation degree. To quantitatively compare samples prepared in different conditions and, more in general, EEG with graphitic starting material, the ratio between carbon and oxygen content was calculated from XPS survey. Then, a particular attention was paid to the high-resolution spectra of C1s that give an information on the amount of oxygen directly bond to carbon in our carbon-based material. In this regard, to avoid the presence of components related to solvent when C1s high-resolution spectra are analysed, the material was characterized in form of powder, after drying it for 48 hours in desiccator. Film deposited on native silicon wafers were analysed by XPS as well.

All XPS spectra for MoS_2 analysis have been referenced to C1s adventitious carbon at 284.8 eV, and the peak fitting was performed with constraints on the full width half maximum (FWHM) and the peak-area ratio of the spin-orbit components.

XPS analysis were carried out with a Thermo Scientific K-Alpha X-ray photoelectron spectrometer equipped with an aluminium X-ray source (energy 1.4866 keV) and working at pressure of 10^{-8}-10^{-9} mbar in the main chamber. X-ray spot size was settled at 400 μm. Survey spectra were recorded as result of 10 scans with a pass energy of 200.00 eV and a step size of 1 eV; high-resolution spectra are average of 10 scans with a pass energy of 50.00 eV and a step size of 0.1 eV.

Raman spectra were acquired at room temperature by a Renishaw microscope equipped with a 532 nm laser, using a 100x objective (numerical aperture NA = 0.85) that provide a beam spot size of ~700 nm; laser power of 1%. The silicon peak at 520.3 cm^{-1} was took as reference for wavenumber calibration.

MoS_2 dispersion was transferred in a 10 mm path length quartz cuvette and analyzed by means of UV-vis-IR absorption spectroscopy using a Jasco V670.

4.2.3 Electrical characterization

Devices fabrication and electrical characterization of EEG material, both on film and at single flake level, have been carried out in close collaboration with two coleagues of Nanochemistry laboratory, Dr. T. Leydecker and Dr. S. Bertolazzi, respectively. In the two cases, FETs devices have been fabricated using two different configurations. Top-contact bottom gate FETs based on EEG film were fabricated depositing EEG film on silicon substrates with a 90 (or 230) nm silicon oxide layer and evaporating gold electrodes (70 nm thick) on top of graphene film by shadow mask method; while multiterminal back-gated FETs based on single flake were fabricated using standard e-beam lithography, metal deposition (3/40 nm of Ti/Au) and lift-off. In the latter case, indeed, the use of e-beam lithography is necessary to build the device on the single micrometer-size flake. When shadow mask was used, devices with different channel length (120, 100, 80, 60 μm) between source and drain electrodes and W=10,000 μm (oxide thickness = 90 nm) were tested. Four-probe measurements were possible in the case of multiterminal devices, in order to remove the contribution of the contact resistance and access to graphene sheet conductivity.

FETs transistors and electrical properties of MoS_2 single-sheet have been investigated by Dr. S. Bertolazzi. In this case, back-gated FETs were fabricated on thermally-oxidized heavily n-doped silicon substrates ($\rho Si \approx 0.001\ \Omega$ cm, $t_{ox} \approx 290$ nm) by means of e-beam nanolithography, thermal evaporation of Au (90 nm) and lift-off. All the electrical measurements were carried out under inert atmosphere (N_2-filled glovebox).

4.3 Results

The application of a positive voltage > 10 V (see operative conditions in section 4.2.1), causes a dramatic expansion of the graphitic working electrode that is accompanied by the fast detachment of the material (**Figure 4. 2**).

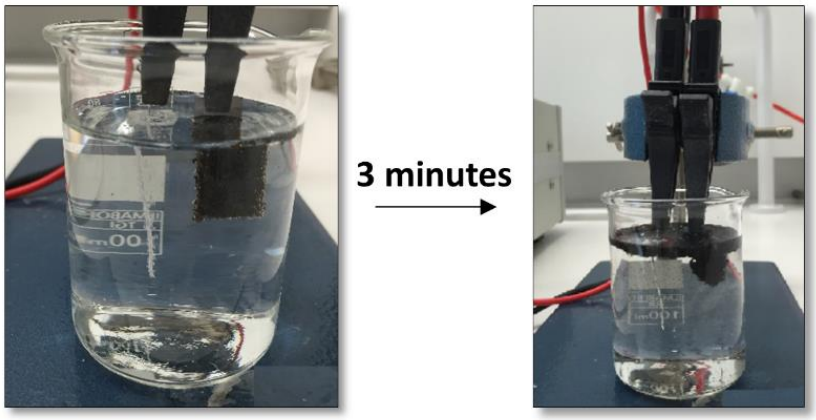

Figure 4. 2. Setup used for the electrochemical exfoliation of a graphite foil in $(NH_4)_2SO_4$ aqueous electrolyte. The photographs show the vigorous development of gases bubbles at the electrodes after few seconds from the application of a positive voltage (left) and the detachment of exfoliated material after three minutes of electrolysis (right).

During the electrolysis, the area of the graphite electrode, is being reduced determining a variation of the current intensity passing between the electrodes. Noteworthy, a prolonged electrolysis in aqueous

solution affects the oxidation degree of the produced material as observed by following the C/O ratio determined by XPS as a function of the electrolysis duration (**Figure 4. 3**). In particular, an electrolysis process lasting 1 and 60 min results in a C/O ratio of 8 and 4, respectively. These preliminary studies have driven the choice of focusing the following work on EEG sample with the highest C/O ratio (C/O = 8), i.e. the material collected after 1 minute of electrolysis.

A multiscale characterization of the produced EE graphene has been carried out using a set of complementary techniques. AFM and HR-TEM, for example, have been used to evaluate the efficiency of the exfoliation expressed in terms of thin layers. AFM allows to quantify the thickness of the flakes and indirectly dating back to the number of layers, being known the thickness of a single layer. AFM images show large single-layer graphene (SLG) and few-layer graphene (FLG) sheets (**Figure 4. 4**). Moreover, in a number of cases, folded or wrinkled sheets are also monitored, being commonly observed in solution processed samples. AFM and HR-TEM analyses (**Figure 4. 4** and **Figure 4. 5**) have revealed a considerable fraction of folded SLG sheets with lateral sizes > 1 μm, as typically observed for graphene produced *via* EE.[28, 92, 171]

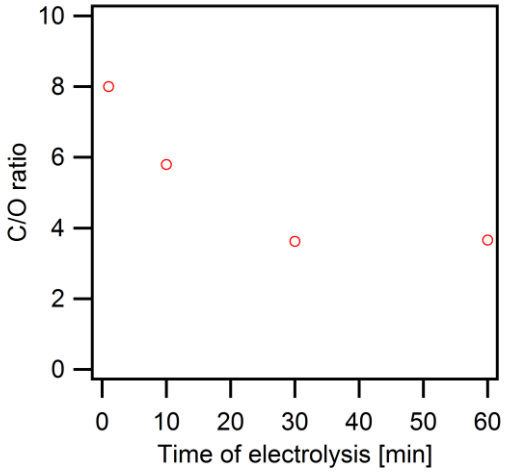

Figure 4. 3.XPS analysis: plot of C/O ratio in function of time of electrolysis.

The thickness distribution (see **Figure 4. 4**b), as quantified by AFM and HRTEM, reveals a discrepancy which is a consequence of the intrinsic nature of the measurements. While in the case of HR-TEM the number of layers (*N*) is counted by analysing the folded edges,[43] AFM enables the estimation of *N* by measuring the height of the deposited flakes from topographical profiles and dividing it by the graphite interlayer distance. Moreover, it is worth noting that the estimation of the height of a SLG *via* AFM depends on the substrate and on the experimental conditions such as relative humidity, presence of adsorbed solvent and magnitude of the force applied by the tip to the sample. For example, on SiO_2, a SLG can show an apparent height of ca. 1 nm,[178] while on mica it amounts ca. 0.4 nm.[179] Here, the *N* is estimated by assuming that the apparent thickness of the thinnest graphene sheet observed on our AFM images is amounting to 0.8 nm. Interestingly, all the flakes analysed with AFM are less than 3.2 nm thick; therefore, the thickest flakes are considered to be four-layer thick. Both analyses, i.e. AFM and HR-TEM, show that EEG is mostly composed by SLG and bi-layer graphene sheets. As shown by AFM in **Figure 4. 4**a,c and by TEM in **Figure 4. 5**a,b, EEG samples are composed by micrometer sized flakes. Remarkably, among the LPE methods, EE stands out for the significant larger lateral dimensions of the flakes compared to UILPE or SE graphene whose sizes are typically in the order of few hundreds of nanometers.[15, 18, 180] On the contrary, EEG flakes approach the micrometer lateral dimension of Scotch-tape graphene, with average lateral sizes generally of few microns that can also sporadically

reach several tens of micrometres as have been reported.[27] However, differently from Scotch tape method, EE approach allow to produce large quantities of graphene in only one step, that can even last 1 minute only. The micrometer sizes of EEG thin flakes, combined with their high concentration, may offer positive implications on the production of large-area thin film, as discussed later in this chapter. The yield of thin sheets which are produced by EE is higher than UILPE and easier accessible. Stable EE dispersions of thin layers have usually concentrations that span between 1 to 10 g L^{-1} in suitable solvents like DMF, and without the use of surfactants or stabilizers. Contrarily, pristine graphene obtained from prolonged UILPE or shear mixer in NMP or DMF usually has low concentration (< 1 mg ml^{-1}), while higher concentrations can be achieved only in the presence of stabilizers.[18, 143, 151] However, if one consider dispersions of SLG, the concentrations are even lower (about 0.01 g l^{-1})[181], while dispersions of FLG can reach concentration of 0.1 g l^{-1} in NMP or 0.2 g l^{-1} in water, in the presence of surfactants.[71, 182]

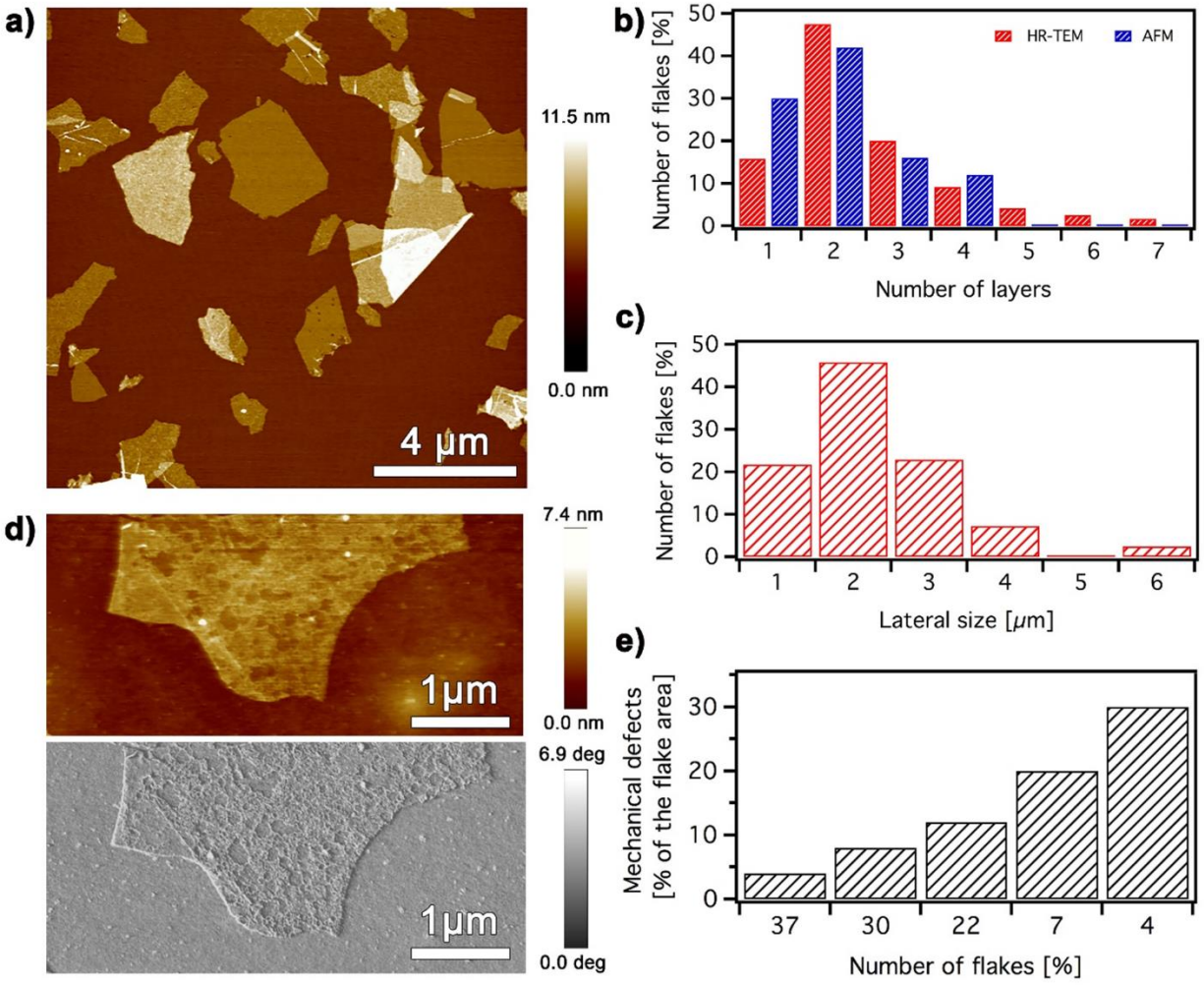

Figure 4. 4. Statistical thickness and flake size analysis for electrochemically exfoliated graphene, together with a statistical study of structural defects caused by the electrochemical process. (a) Topographical AFM image of flakes produced by electrochemical exfoliation of graphite and deposited on SiO_2 substrates by spin-coating from DMF dispersions; (b) distribution of the number of layers per sheet determined by AFM cross-sectional analysis (in blue) and HR-TEM (in red); (c) distribution of flakes lateral size determined by AFM; (d) AFM topographic and phase-contrast images showing structural defects on a representative SLG flake; (e) density of the structural defects plotted in function of the number of defective flakes.

In addition, EE inks can be produced easily and in short time. The exfoliation itself occurs already in the first seconds after the voltage is applied, as proved by a predominance of mono- and bilayers in the sample obtained after 60 seconds of electrolysis (**Figure 4. 4**). In our procedure, after the exfoliation, only 20 minutes of sonication in a standard lab sonicator are enough to disperse the material in its solvent. Finally, the decantation of the solution is sufficient to promote the precipitation of un-exfoliated material and thick flakes, without needs of time-consuming subsequent cycles of centrifugation. A final dispersion is, thus, prepared in less than 1 hour and it will be stable for several weeks.

In this work, AFM was also employed to gain in-depth insight into the surface morphology of EEG flakes. High magnification imaging revealed that the surface of the flakes is damaged and nanoscopic holes are observed (**Figure 4. 4**d). The density of those defects was estimated by automatic pixel counting. Such analysis shows that the defective area of the flakes ranges from 4 to 30% (**Figure 4. 4**e), yet, it does not exceed 10% for the majority of the flakes (67%). Several attempts to visualize such structural defects by HR-TEM were done, yet the imaging is hindered by a contamination with physisorbed carbonaceous material, which after exposure to TEM electron beam converts into amorphous carbon.

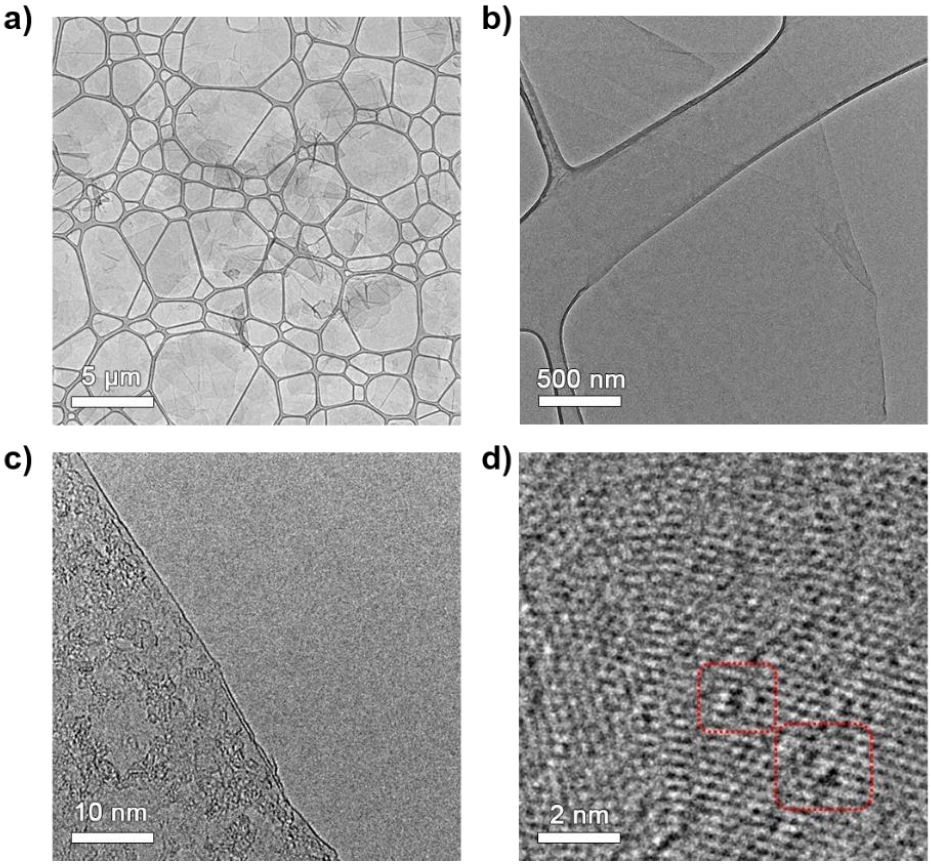

Figure 4. 5. High-resolution transmission spectroscopy of electrochemically exfoliated graphene flakes. (a) low-magnification TEM image of EEG thin flakes, (b, c) high-magnification TEM images of EEG flake edges showing the presence of monolayers; (d) example of punctual defects shown by HR-TEM image.

According with AFM imaging, in fact, most of the EEG flakes appear damaged and characterized by rough surfaces. That can be interpreted as the result of a non-uniform disintegration of the outer sheets due to the complicated interplay of water electrolysis, anionic intercalation, and gas evolution

that can induce cracks and nanoscopic defects on the material. Therefore, we believe that the main source of carbon contamination is represented by the remaining shreds of the external graphene layer of an EEG sheet, which are transformed in amorphous carbon under the influence of the electron beam. On the other hand, besides the nanoscopic defects observed by AFM, the HR-TEM analysis highlights the presence of point defects (**Figure 4. 5**d). The mechanical pressure caused by gas bubbling (O_2 and SO_2) in between graphite layers during the electrolysis is considered being the most important factor leading simultaneously to the fragmentation and exfoliation of the material. At the unusual electrochemical conditions employed, the development of gas is so violent that causes also the spreading of the graphitic material from the anode, even before the complete exfoliation, which in fact is well reflected in the heterogeneity over the thickness and sizes of the produced material (**Figure 4. 4**b,c).

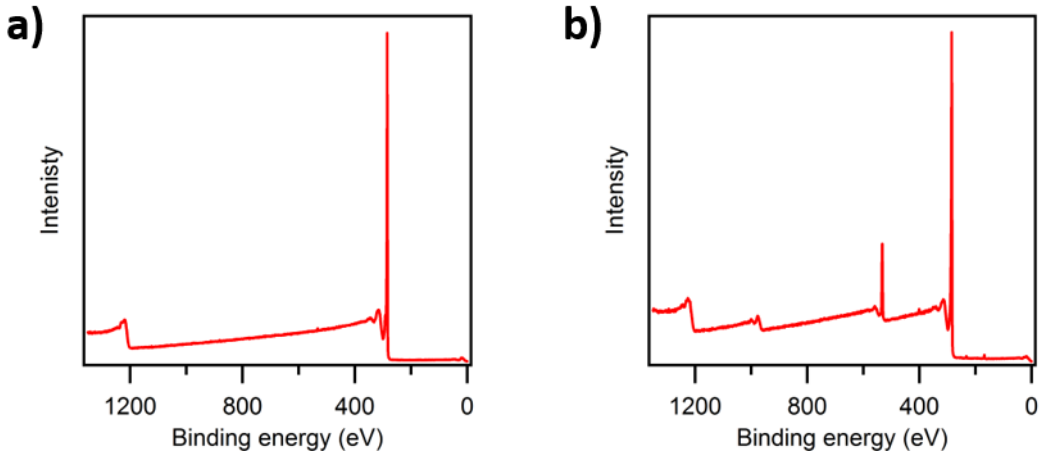

Figure 4. 6. XPS survey spectrum of a) pristine graphite foil and b) EEG with C/O = 8.

Compositional characterization of the material was carried out by X-ray photoelectron spectroscopy (XPS). Firstly, the starting material, i.e. the graphite foil, was analyzed, and considered as standard, aiming to follow how the chemical composition of the material evolves during electrochemical exfoliation. Survey spectra show the rise in intensity of the oxygen peak already after 60 seconds of electrolysis (**Figure 4. 6**). To know if this amount of oxygen interests the produced material, XPS high-resolution spectra have been considered. **Figure 4. 7**a displays a comparison between CIs spectra of the starting material and EEG. As previously reported,[183] the high-resolution CIs spectrum of the starting material (**Figure 4. 7**b), displays an asymmetric peak centered at 284.48 eV and a broad "shake-up" peak related to the π to π* transition, at ca. 290.9 eV. No components related to the oxidation of the starting material are observed, as confirmed by the low atomic percentage of oxygen (0.58 %) given from the survey spectra (**Figure 4. 6**a). After the exfoliation, the CIs spectrum of EEG powder (**Figure 4. 7**c) reveals, besides the main peak centered at 284.45 eV, a second component at higher binding energy, which indicates the oxidation of the material during the EE. Its deconvolution allows identification of four additional components typically attributed to oxygen-containing groups, i.e. hydroxyl (285.47 eV) and epoxide (286.68 eV) groups, as well as carbonyl (288.22 eV) and carboxyl (289.08 eV) moieties.[184-185] To fit the sp^2 component, the same parameters (FWHM and asymmetry parameters) extrapolated from the fitting of pristine graphite have been used. This method is meant to take into account the asymmetry of CIs sp^2 peak, instead of employing the gaussian-based approaches conventionally used in fitting XPS spectra. In such a way, better accuracy in quantifying CIs contributions from graphitic carbons (sp^2), defects (sp^3 carbon) and functional groups can be achieved, as it was recently demonstrated using a similar approach.[186]

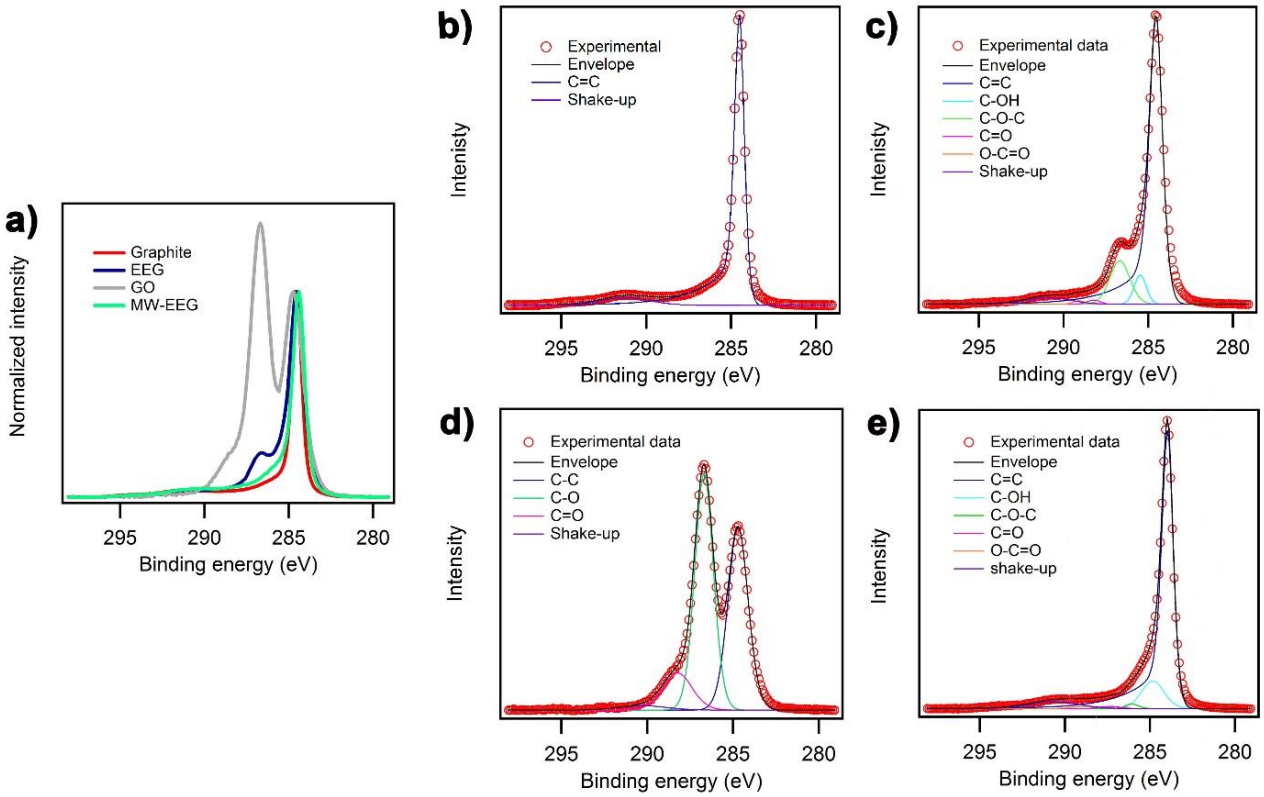

Figure 4. 7. XPS characterization of electrochemically exfoliated graphene (EEG) in comparison with pristine graphite, graphene oxide (GO) and EEG after microwave irradiation (MW-EEG): (a) overlapped high resolution carbon spectra; (b) CIs spectrum of graphite; (c-e) CIs curve fitting of EEG, GO and MW-EEG, respectively.

Even though the electrochemical process, under anodic conditions, unavoidably oxidizes the material, the level of oxidation is much lower if compared with the oxidation degree of GO. Here, for comparison, a water dispersion of GO, purchased from Graphenea, was dried in a vacuum oven at ca. 30 °C; the collected powder was characterized by XPS in the same conditions of EEG powder. (**Figure 4. 7**d). Moreover, the content of oxygen, and consequently the C/O ratio, determined by XPS for EEG, is comparable with the results of elemental microanalyses (see Table 4.1).

Table 4. 1 Microanalyses of EEG samples: nitrogen, carbon and hydrogen atomic percent.

	% N	% C	% H
EEG	0.20	82.38	1.08

XPS interpretation of EEG chemical composition was further supported by ATR-FTIR and thermogravimetric analysis (TGA) (**Figure 4. 8**a and **Figure 4. 8**b), which corroborates the presence of oxygen functional groups although to a lesser amount compared to graphene oxide (GO). In **Figure 4. 8**a, ATR-FTIR spectra of EEG and MW-EEG (introduced later in this chapter) were compared with GO. The bands associated to oxygen functional groups, which are clearly distinguishable in GO (in black), have a very low intensity and they are barely perceptible, or totally absent, in EEG samples (in red). In particular, the band at 1610 cm^{-1} related to the C=C stretching, skeletal vibrations from

unoxidized graphitic domains, is clearly evident in EEG, while almost undetected are the band at 3000-3500 cm^{-1} (O-H stretching vibrations from hydroxyl or carboxyl groups) and the commonly narrower bands at about 1720 cm^{-1} (C=O stretching vibrations from carbonyl and carboxyl groups); in the range of 1300–1450 cm^{-1} slightly appears a broad band related O-H bending vibrations from hydroxyl groups and C–OH stretching. The same occurs for the signals related to epoxy groups, at 1260 cm^{-1} (breathing vibrations from epoxy groups) and 1070 cm^{-1} (C–O stretching in ethers or epoxides).[100]

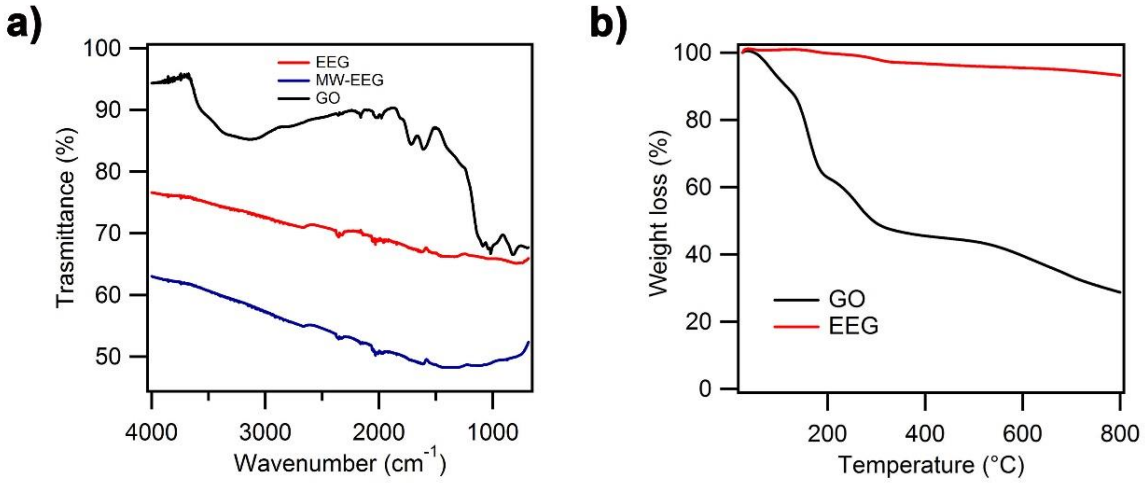

Figure 4. 8. ATR-FTIR and thermogravimetric analysis, a comparison between electrochemically exfoliated graphene and graphene oxide: (a) ATR-FTIR spectra of graphene oxide (GO), electrochemical exfoliated graphene (EEG) and EEG after treatment with microwave at 1000 W for 10 seconds (MW-EEG); (b) TGA spectra of EEG and GO.

Nearly the same spectrum was recorded after treatment with microwave at 1000 W for 10 seconds (in blue), proving that annealing treatment doesn't remove completely the oxygen functional groups but, as it is clearer by XPS (**Figure 4. 7**a), the amount of oxygen is markedly decreased. TGA was performed in the range from 25 and 900 °C, under nitrogen, in dynamic modality (heating rate of 10 °C/min). Once again, the thermogravimetric curve of EEG was compared with GO one (**Figure 4. 8**b). Both samples start to lose weight already below 100 °C due to the evaporation of loosely bound and absorbed water and gas molecules.[187] In GO samples, the weight loss (around 8%) at about 100 °C is attributed to the evaporation of residual water, while the major weight loss occurred at around 150 °C and it can be related to oxygen groups that easily are removed as CO_2 and CO. The EEG shows similar characteristics but with consistent lower total weight loss of 6% compared to GO (residue of 43.75% at 500 °C), which translates in a smaller amount of oxygen functional groups in good accordance with IR and XPS analysis.

Raman spectroscopy was used to characterize the quality of the EEG. The dispersions were spin-coated on SiO_2 substrates and the solvent was slowly evaporated at room temperature. Raman spectra (**Figure 4. 9**a) show a disordered material as indicated by the presence of a defective peak higher than the G-peak and a very low intense and broad 2D band, providing evidence for a reduction of the size of the in-plane sp^2 domains subsequently to the anodic process. In particular, I_D/I_G ratio of EEG (c.a. 1.5) lies in the transition region between stage 1 and 2 following the classification of disorder defined by Ferrari and Robertson (described in paragraph 3.4), in which a mean distance between two defects is being estimated as Ld ~ 2-4 nm and consist of a low sp^3 species content (<15%).[188]

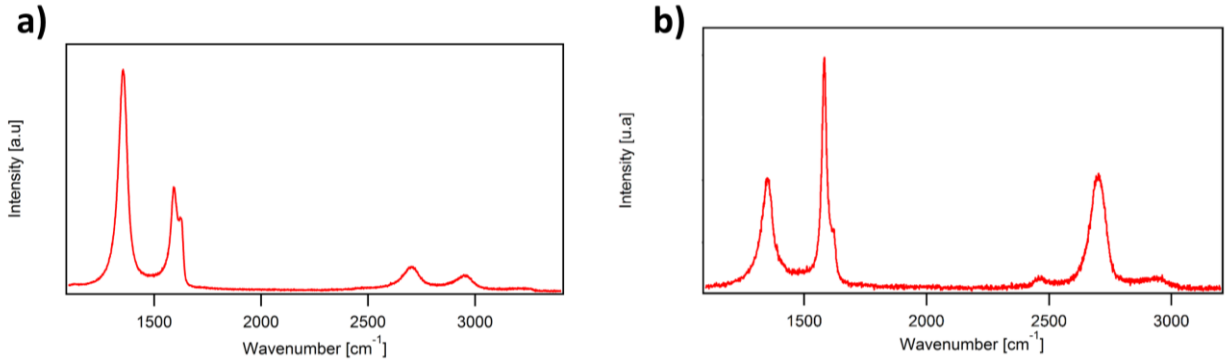

Figure 4. 9. Representative Raman spectra of EEG in the region between 1100 and 3200 cm^{-1}, including D, G and 2D bands. a) EEG flake with $I_D/I_G \sim 2$; b) EEG flake having $I_D/I_G \sim 0.5$.

The position of G peak at 1593 cm^{-1} further proves the defective nature of EEG, which, in agreement with previous reports,[188-189] can be defined as nanocristalline graphite. Moreover, an apparent shoulder of the G peak, known as D' peak, can be clearly distinguished, indicating a moderate defect concentration.[190] Nevertheless, besides the defective flakes, few high-quality FLG sheets, with I_D/I_G of 0.5, were also observed (**Figure 4. 9**b). **Figure 4. 10** shows that the ratio between I_D and I_G peaks do not change significantly within the same flake, as demonstrated analysing six point of the same flake, three in the inner part of the flake and other three on its edges. This experiment has allowed to conclude that degree of defects in EEG doesn't interest only the edges of the flake, but in plane defects are present as well.

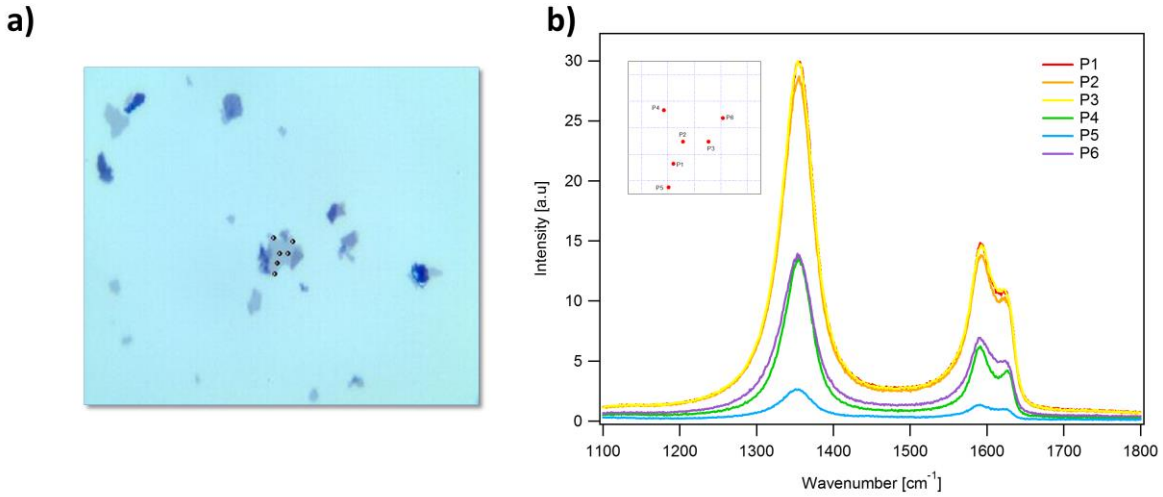

Figure 4. 10. Raman characterization of EEG in different points of the same flake: a) optical image of the analysed flake, few microns large. The red spots indicate the points were Raman laser was spotted. b) Raman spectra in the region between 1100 and 1800 cm^{-1}. P1, P2, P3 are three points on the EEG flake plane; P4, P5, P6 are points at the edges of the flake.

By exploiting the large size of EEG flakes, it was possible to investigate on the electrical characteristics at single-flake level, similarly to the studies performed on mechanically exfoliated 2DMs by adhesive tape. Conversely, this is not common for other LPE materials, where the nanometer sizes of the flakes and their polydispersity in terms of thickness don't promote these studies. In this case, EEG flakes were deposited on SiO_2 substrates ($\rho Si \approx 0.001$ L cm, tox = 290 nm) by spin-coating a 1 mg ml^{-1}

dispersion in DMF and were further characterized *via* a combination of OM and AFM (**Figure 4. 11**). SiO_2/Si substrates with well-defined thicknesses of the oxidized layer offers a high optical contrast for the visualization of 2D crystals, which greatly facilitates the evaluation of exfoliation's quality. In **Figure 4. 11**a, for example, is reported the optical micrograph of an EEG sample, deposited on 90 nm SiO_2/Si substrate, where it is possible to discriminate between thin layers that appear light violet, and that are barely distinguishable from the substrate when are monolayers, and thicker ones that are dark violet or blueish. Once an effective exfoliation and a proper sample preparation are demonstrated using an optical microscope, AFM is used to measure flake's thickness.

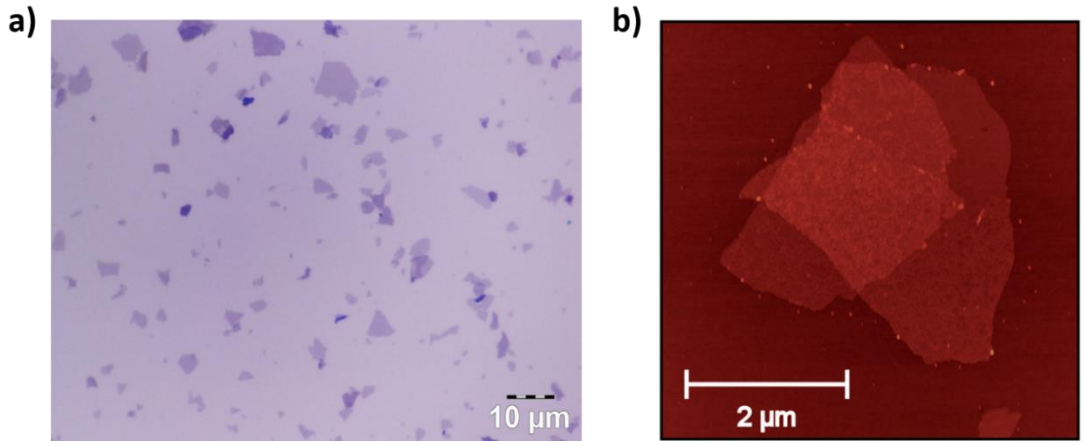

Figure 4. 11. Thin graphene flakes produced by electrochemical exfoliation. a) Optical micrograph of EEG flakes deposited on Si/SiO_2 (90 nm) substrate by spin-coating; b) Representative AFM image of two overlapped EEG flakes with a thickness of 1.2 nm each, and lateral sizes of 3.5 µm and 2.4 µm. AFM z-scale bar: 40 nm.

Once, individuate a thin isolated flake, multi-terminal back-gated field-effect transistors (FETs) were fabricated using e-beam lithography with polymethyl methacrylate (PMMA) resists, metal deposition (3/40 nm of Ti/Au) and lift off in acetone. The four-probe measurement configuration was employed to remove the contribution of the contact resistance and access the intrinsic sheet resistivity of EEG, which is found to span within the range 15-30 kΩ sq^{-1}.

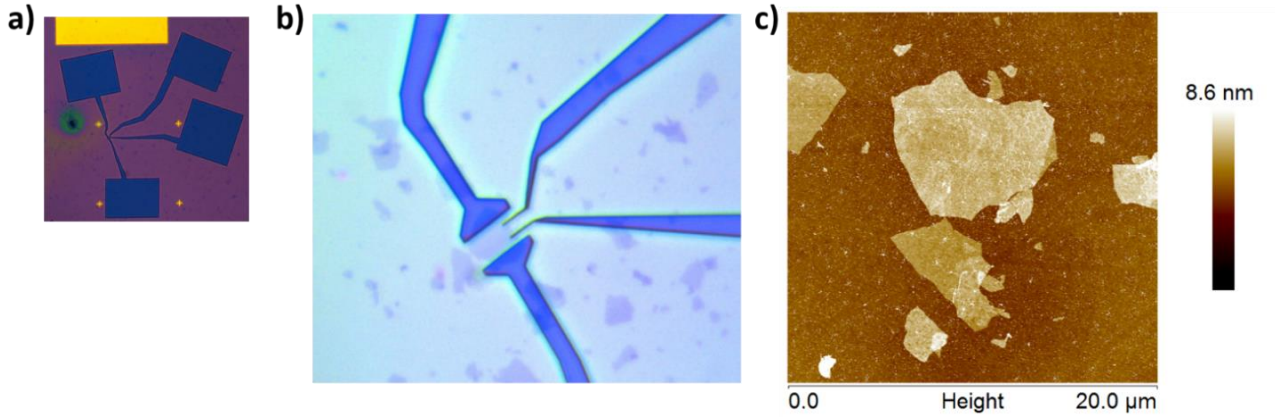

Figure 4. 12. Field-effect transistors based on EEG single sheet: (a-b) Example of FET fabricated on a EEG flake individuated by optical microscopy and characterized by AFM (b). The analyzed flake is a tri-layer, being thick 2.3 nm as measured by AFM.

To minimize the influence of environmental adsorbates, such as O_2 and H_2O, all the measurements are carried under inert atmosphere (N_2-filled glovebox). Moreover, a vacuum annealing step (p ~ $5x10^{-8}$ mbar, T ~60 °C) is performed to desorb solvent traces, as well as O_2 and H_2O, which are known to be detrimental electron-acceptor traps — and thus reduce the level of hole doping within the material. Upon annealing, the behaviour of the EEG FETs changes from unipolar (p-type) to ambipolar, as in the case of mechanically exfoliated or CVD-grown graphene devices. A well-defined charge-neutrality point can be identified in the transfer characteristics acquired after vacuum annealing (**Figure 4. 13**c, inset) at V_g values of ~ 4 V.

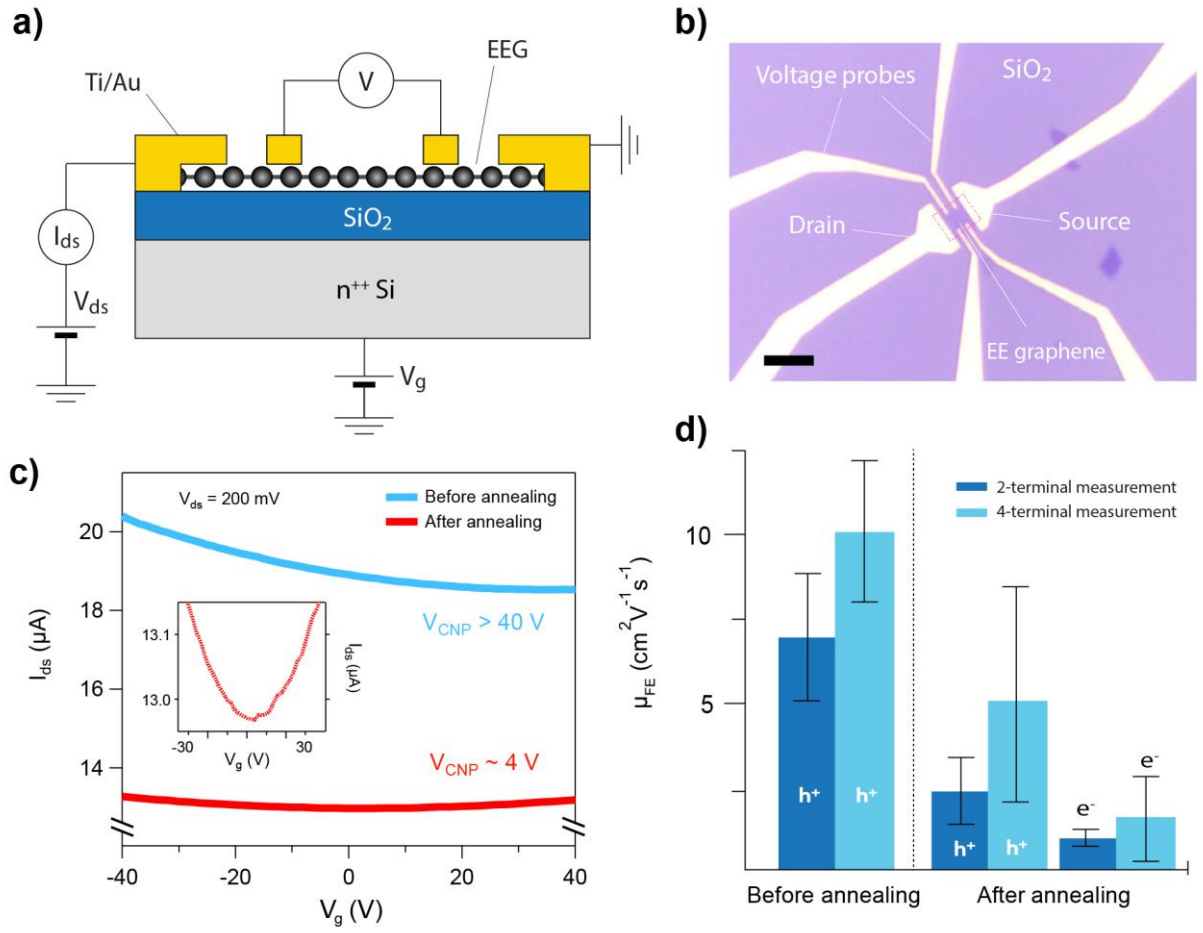

Figure 4. 13. Electrical transport measurements on individual EEG flakes. (a) Schematics and (b) optical micrograph of the multiterminal back-gated FETs used for electrical characterization. The scale bar in (b) amounts to 5 μm. (c) Drain-source current (I_{ds}) *vs*. gate voltage (Vg) transfer characteristics of an EEG FET acquired before (blue) and after (red) high-vacuum annealing at ~60 °C. The curve is plotted also in the inset (magnified y-scale) to show the occurrence of the charge neutrality point (VCNP) at ~4 V. (d) Histogram of the field-effect mobility for holes (h^+) and electrons (e^-), as measured in the two- and four-terminal measurement configuration.

To the best of our knowledge, this is the first observation of ambipolar transport in EEG nanosheets, which proves that the level of oxidation in our EEG is considerably lower than in the case of graphene oxide (GO). However, at this stage, the electron and hole mobilities (1-10 $cm^2V^{-1}s^{-1}$) appear to be dominated by a high degree of structural defects, as elucidated in the following of the manuscript. The field-effect mobilities – measured in both two- and four-terminal configuration – are reported in the histogram in **Figure 4. 13**d. On average, the two-terminal measurements provide mobility values 30-

40% lower than the four-terminal counterpart, indicating a non-negligible contribution of the contact resistance due to injection barriers at the metal/EEG interface. Upon annealing, the hole field-effect mobility drops by ~50%. We suggest two plausible mechanisms behind such charge-transport degradation, namely the thermally-activated expansion of structural defects[191] and the remarkable decrease in hole density. The effect of high-vacuum annealing process on single flakes of EEG has been investigated *via* a combination of AFM and Raman spectroscopy, as shown in **Figure 4. 14**. Though we could not identify significant changes (e.g. peeling or tearing) at the micrometre scale in the morphology of the flakes (**Figure 4. 14**, panel a and b), we observed a significant increase of structural disorder upon annealing by means of Raman spectroscopy (**Figure 4. 14**, panel c). The Raman spectra acquired before and after the annealing step — with the laser beam positioned onto the same region of the flake (red circle in **Figure 4. 14**) — are displayed in **Figure 4. 14**c, in blue and red respectively. They exhibit different I_D/I_G and $I_{D'}/I_G$ ratios. In particular, the I_D/I_G ratio is higher after thermal annealing, indicating an increase of disorder at the nanometre scale.

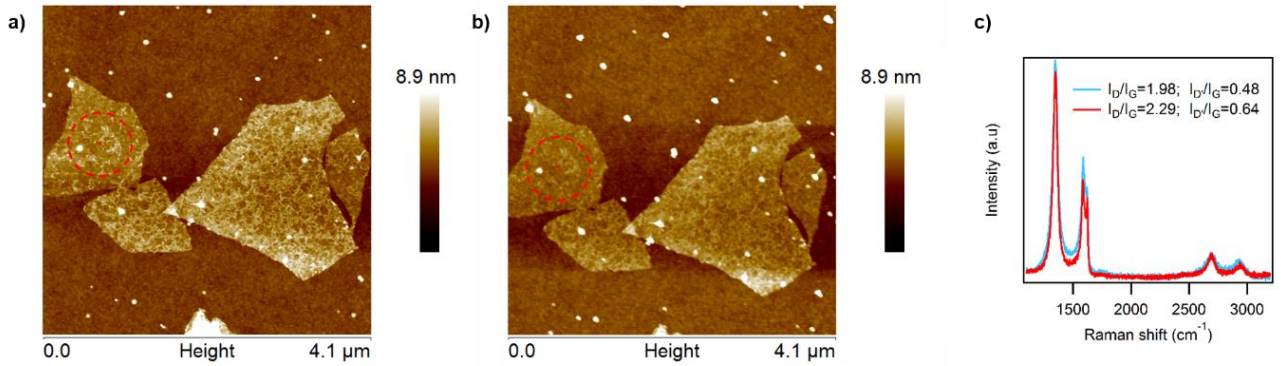

Figure 4. 14. Effect of thermal annealing on EEG single flake: AFM images of the flakes analysed by Raman before (a) and after (b) vacuum annealing; c) Raman spectra before (in blue) and after (in red) annealing treatment.

The drop in the hole field-effect mobility can be also ascribed to the remarkable decrease in hole density upon high-vacuum annealing. In the case of defective graphene sheets, the dependence of the mobility/conductivity on the charge-carrier density has been previously investigated.[192] The remarkable non-linearity observed in the transfer characteristics of our EEG-based FETs — see **Figure 4. 15**— can be ascribed to the presence of electronic defect states, which degrade the charge transport in the low charge-density regime.

It can be seen that the hole mobility — as obtained by the linear extrapolation of the I_{ds} *vs* V_g curve — increases significantly with the increasing effective gate voltage $|V_g - V_{ds}|$, or equivalently with increasing hole/electron density. In our experiments, graphene is heavily p-doped before annealing and the charge transport is evaluated in the high hole-density regime. On the other hand, after annealing the hole doping is considerably lower and the mobility is extracted at smaller values (low hole-density regime), where it is more severely affected by the defects.

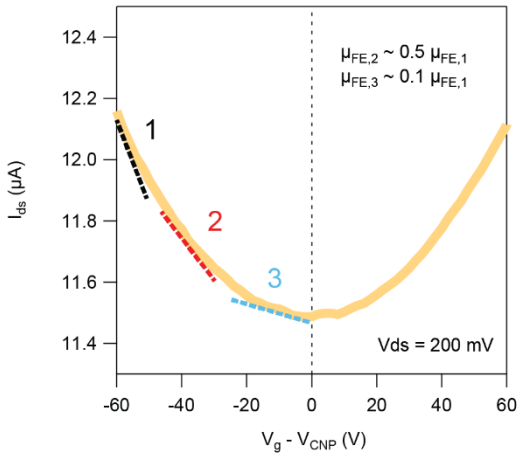

Figure 4. 15. Representative transfer characteristic of as-annealed EEG-based FETs at low drain-source voltage V_{ds}. The field-effect mobility μFE increases considerably with increasing effective gate voltage $|V_g - V_{ds}|$. For instance, the mobility extracted in region 1 can be up to ten times larger than the mobility extracted near the charge neutrality point V_{CNP} (region 3).

Turning now to EEG films, we briefly summarize their preparation, discussed in detail in section 4.2.1, and we report here the results of their characterization. Graphene films were prepared by depositing a few drops of EEG dispersion in DMF into a water-containing beaker. Once re-organized at the interface, EEG flakes form a uniform greyish film floating onto the sub-phase, which was transferred onto the solid substrate. This method makes it possible to avoid time consuming and laborious purification steps, as a consequence of the EEG tendency to form a film at the water/air interface, leaving heavier particles, i.e. unexfoliated graphitic material diffusing in the sub-phase together with DMF. In this way, extensive formation of aggregates typical for other deposition methods such as drop-casting, dip-coating, spin-coating is avoided. By this method atomic level thin flakes can uniformly adhere to other materials having any shape, as shown in **Figure 4. 16** which display EEG film deposited both on rigid silicon substrate and on flexible PET. Furthermore, the thickness of such films can be modulated as a function of the amount of loaded solution.

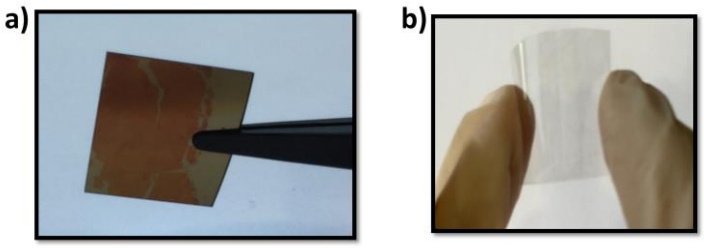

Figure 4. 16. Photographs of EEF film deposited on solid (SiO2/Si) and flexible (PET) substrates.

Morphology and homogeneity of the films on Si/SiO_2 were investigated by OM and AFM, as reported in section 4.2.1. Closely packed EEG sheets form large-area films having average thickness of about 3 nm and surface coverage above 80% (**Figure 4. 17**).

Gold source and drain electrodes were then evaporated on the top of the film. The I_{ds} current is plotted as a function of the applied gate potential V_g and the resulting transfer curves are fitted in order to extract the mobility values in the linear regime. Unlike what is observed in the case of single flake

measurements, the electrical performance of films recorded before and after thermal annealing result being almost identical, displaying mobilities of 3.4 $cm^2 V^{-1} s^{-1}$ and 4 $cm^2 V^{-1} s^{-1}$, respectively. Electrical characterization also reveals a large shift in threshold voltage: the Dirac point is now at very high positive gate bias, even after annealing. This strong *p*-doping of the EEG film can be ascribed to the effect of trapped adsorbates (oxygen and solvent) between overlapped flakes, which cannot be easily desorbed and hamper the emergence of ambipolar transport.

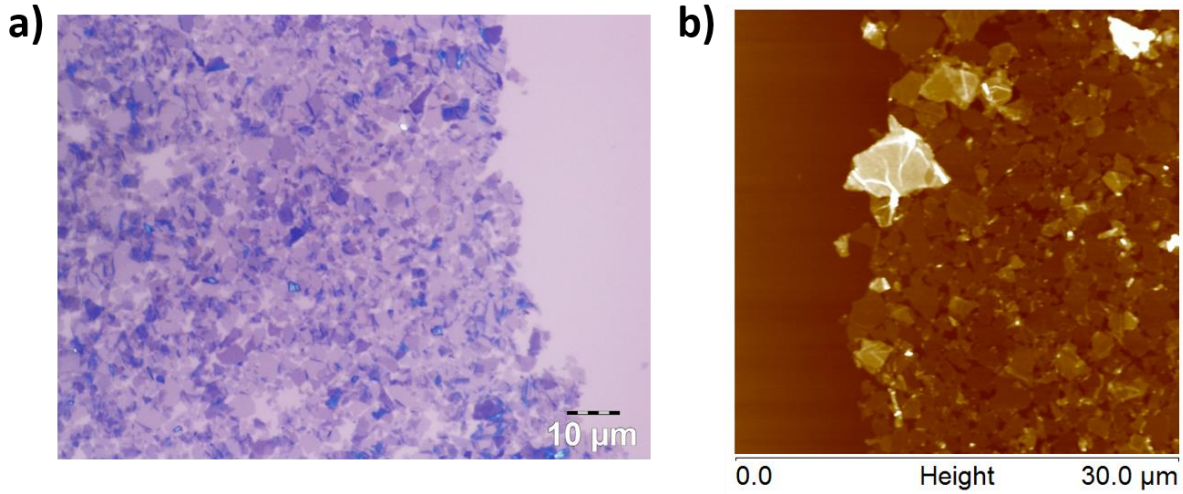

Figure 4. 17. Morphological characterization of EEG film: a) optical micrograph which show the formation of a homogeneous film made of few-layer EEG sheets with the presence of some thicker particles by optical contrast respect to the bare substrate on the right of the OM image; b) 30 µm x 30 µm AFM image of EEG film that allowed to determine an average film thickness of 3 nm by measuring the height step between film and bare substrate. AFM z-scale: 30 nm.

A percolation path for charges among adjacent flakes guarantees the conductivity of our film and proves the high-quality overlapping among sheets observed by microscopies. More importantly, EEG films show similar mobility values to those of the single flake. Therefore, albeit the observed mobilities remain below state of the art, our approach offers the exciting possibility of producing large-area graphene performing as an ideal large monolayer.

Recently, microwave (MW) irradiation has been introduced as powerful technique to reduce graphene oxide achieving high-quality graphene.[193] Typically, (electro)chemical and thermal reduction of GO results in a highly defective and still oxidized material,[194-197] known as reduced graphene oxide (rGO), due to the difficulty of removing stable epoxy and carbonyl groups.[198] On the contrary, microwave treatments, based on a rapid and localized heating of the sample, causes the desorption of oxygen functional groups as well as the reordering of the carbon atoms within the graphene basal plane, leading to defect- and oxygen-free graphene.[193] Consequently, electronic mobility values rise from 1 $cm^2V^{-1}s^{-1}$, reported for rGO,[199-200] to 1000 $cm^2V^{-1}s^{-1}$ after MW irradiation.[193] Here, for the first time, this approach was exploited to lower the degree of oxidation on EEG and studying the effect on its electronic properties. While a preliminary thermal annealing is necessary to increase the conductivity of GO, so that it can absorb microwaves, this step was unnecessary in the case of EEG powder, which is successfully reduced upon a few seconds of microwaves irradiation with a conventional microwave oven (**Figure 4. 7**a, green curve).

As evident from the XPS survey spectra, the overall percentage of oxygen decreases from 12% to 7%. In particular, the C1s spectrum of EEG powder (**Figure 4. 7**e) shows a nearly total reduction of epoxy and carbonyl groups to hydroxyl ones, as evidenced by the increase in –OH peak intensity. The shake-up satellite peak observed at 290.59 eV in MW-EEG spectrum indicates that the conjugation of the system is preserved and eventually restored as well. Moreover, the global shift of peak-maxima back to lower binding energy after MW irradiation points out the increment of the conducting nature of the material. We verified that the approach reported in literature[193] effectively reduces both EEG powder (**Figure 4. 7**e) and EEG films on silicon dioxide substrates (**Figure 4. 19**).

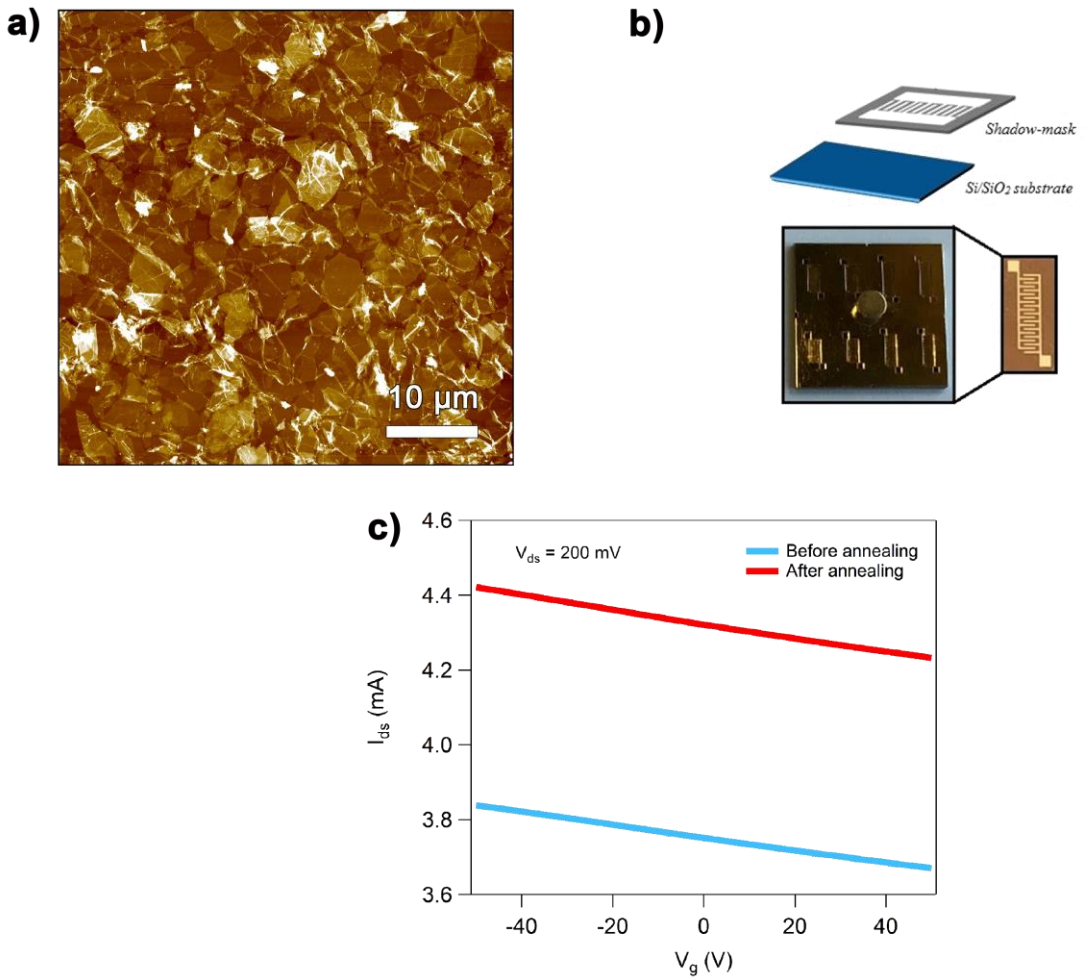

Figure 4. 18. Electrical characterization of FETs based on EEG films. (a) AFM image of an EEG film (scale bar: 45 nm); (b) sketch and photograph of the device fabrication on graphene films by gold evaporation using the shadow-mask approach; (c) representative transfer curves before and after annealing at 60 °C for 12 h in nitrogen atmosphere. (Vds = 200 mV)

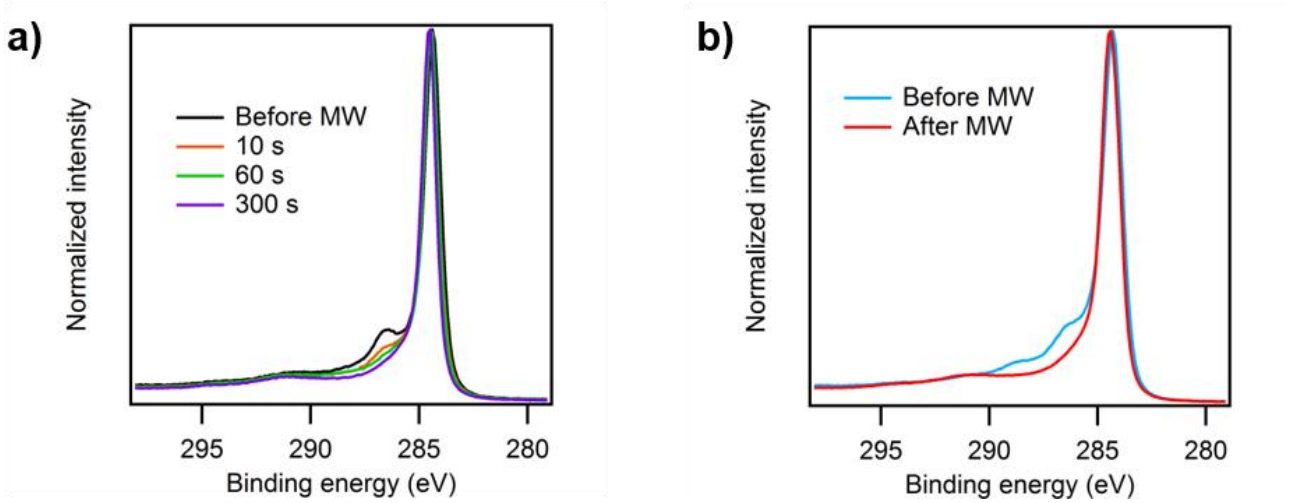

Figure 4. 19. Effect of MW irradiation on the XPS spectra of EEG powder and films. XPS high-resolution C1s spectra of (a) EEG powder before and after 10s, 60s and 300s of microwave irradiation at 1 kW; (b) EEG film before (blue) and after (red) MW treatment (P = 1 kW, t = 1 min). X-ray beam spot ≈ 400 μm.

Surprisingly, when MW treatment is performed on EEG films, no noticeable changes in electrical performances were observed (**Figure 4. 20**d and Table 4. 2). We point out here that due to technical limitations we could not perform the same type of investigation in the case of EEG single-flake FETs before and after MW irradiation. In fact, a device composed by metallic pads, leads and contacts to the 2D flake cannot be safely exposed to 1 kW MW radiation within a household oven. The large amount of heat developed during the MW exposure unavoidably damages the metallic lines — smallest features of ca. 200 nm (inner voltage probes) — and ultimately leads to the failure of the device.

While the results of electrical measurements can be well explained by the Raman spectra on the films of EEG before and after MW treatments, which appear very similar (**Figure 4. 20**c), the C1s region of the XPS spectra shows that the MW treatment is accompanied by a lowering of the peak at ca. 286 eV which is associated to oxygen-containing groups (**Figure 4. 20**b). Although the combination of thermal annealing and microwave irradiation of GO is known to be beneficial to the healing of point defects,[193] our nanometer sized structural defects cannot be recovered in the same way upon MW. As a result, MW-irradiation is not effective in improving the electronic properties of EEG, which are at this stage limited by the presence of structural defects.

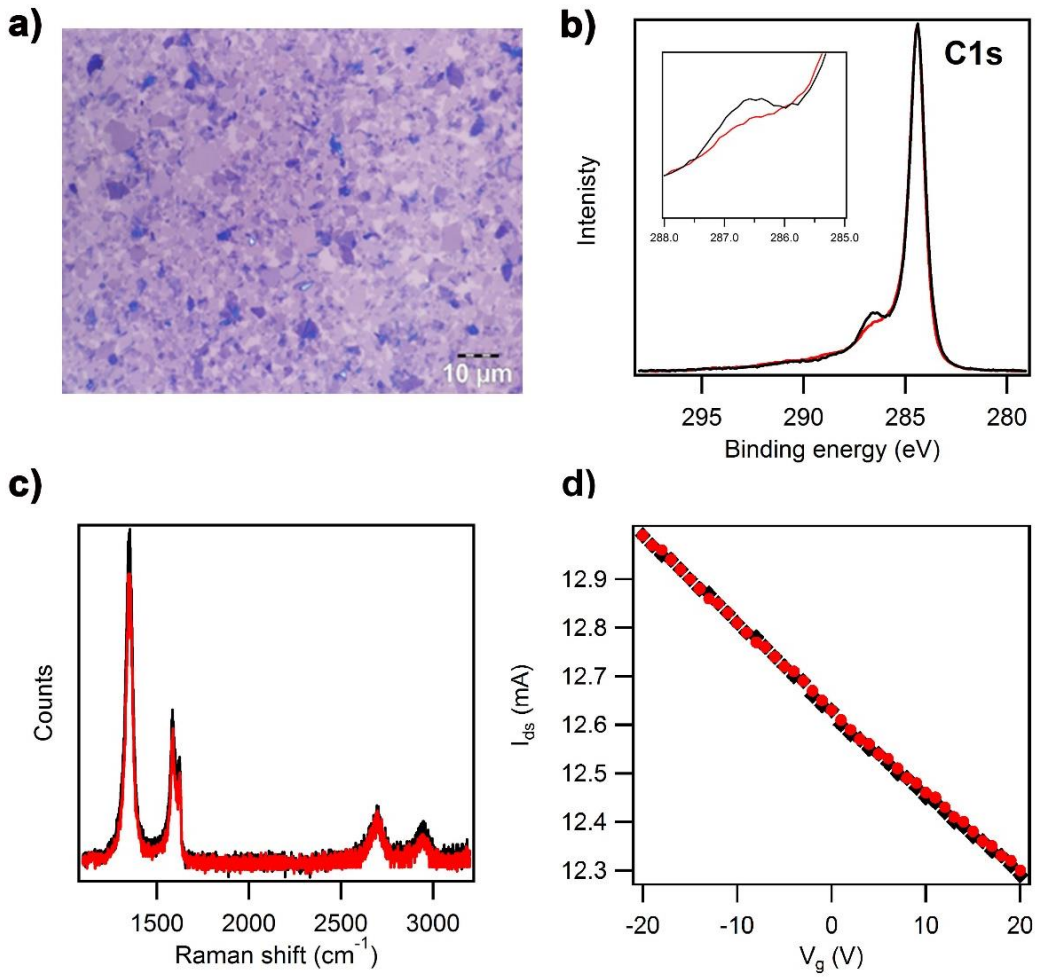

Figure 4. 20. Characterization of EEG films before (in black) and after (in red) microwave irradiation: (a) Representative optical microscopy image; (b) XPS CIs spectra with a zoom in the spectral region between 288 and 285 nm; (c) Raman and (d) transfer curves of EEG films before and after MW treatment.

Table 4. 2 Mobility values of EEG film before and after microwave treatment.

	Mobility / $cm^2V^{-1}s^{-1}$
Pristine film	2.83
After MW treatment	2.82

To conclude this part, we reported an overview of the electrical performances of FETs based on different neat graphene as active layer (Table 4. 3). Among the several methods for graphene production, the scotch-tape approach provides the best quality of graphene in terms of purity, defect densities, electronic and optical properties. The charge carrier mobility can be as high as 10^5 $cm^{-2}s^{-1}V^{-1}$ at room temperature. For this reason, such technique is still very popular for laboratory research, but it is clearly not suitable for practical applications. Techniques such as CVD and epitaxial growth on SiC allow for producing wafer-scale graphene, but the manufacturing process is expensive and requires complex procedures; however, devices based on such large-area materials do not offer the same high performances as the mechanically-exfoliated graphene. On the other hand, LPE is low-cost and up-scalable, and therefore is attracting a great deal of attention. The structural and electronic quality of

ultrasound-induced LPE graphene is significantly lower than that produced by epitaxy or CVD, and typical mobilities range between 0.1 and 1 $cm^{-2}s^{-1}V^{-1}$ in the case of devices based on graphene films obtained *via* UILPE and deposition by solution processing methods.

Table 4. 3 Comparison of the electrical performances of FETs based on different neat graphenes as active layer.

Graphene types		**Conduction type**	**FE mobility ($cm^2V^{-1}s^{-1}$)**	**Ref.**
Scotch tape	Single flake	*ambipolar*	10^4-10^5	11, 201
CVD	Film	*ambipolar*	10^3-10^5	202-205
Epitaxy	Film	*n-type ambipolar*	10^4	206
Liquid-phase exfoliated (LPE) *via* ultrasonication	Film	*p-type ambipolar*	0.1-1	191, 207
Electrochemically exfoliated (EE)	Single flake	*p-type*	10^2	21
	Film + single flake	*ambipolar*	1-10	This work

As compared to UILPE approaches, EE exfoliation enables the production of large quantities of graphene in relatively short time without further degrading the electrical properties. Previous reports on EEG showed promising results.[21] However, the exfoliated flakes and the films presented a high level of p-type doping and the charge neutrality point was not observed in the FETs' transfer characteristics. The EEG produced in this work has electrical characteristic superior to that of graphene sheets obtained *via* UILPE; in addition, it displays a clear ambipolar behaviour, which was not reported before in the literature. The unique properties of EEG and the high efficiency of the EE of a graphite foil into thin graphene layers have triggered our interest towards the exfoliation of other layered materials using a similar approach. TMDs, for example, similarly to graphene, are characterized by strong in-plane covalent bonds and weak vdW interactions between adjacent layers. The latest can be weakened by applying external stimuli allowing the exfoliation of the material. Moreover, single-layer nanosheets of TMDs possess different properties from those of their bulk counterparts. For these reasons, recently, many approaches are being explored to exfoliate TMDs into single- or few-layer thick sheets, such as mechanical exfoliation [208], sonication and dispersion in liquid media[209-213] and electrolysis[96, 214-215].

Herein, we extended the knowledge acquired from the EE of graphite to another prototypical 2D material, i.e. molybdenum disulfide (MoS_2). Among the TMDs, MoS_2 is the most investigated material due to its abundance in nature and its extensive use as a lubricant.[216-217] Being the most studied, after graphene, it was considered in this study a good choice for investigating a new process like the EE.

Moreover, being a semiconductor, 2D MoS_2 appears a very attractive material for electronics applications, as complementary to graphene, that on the contrary has a zero band-gap.

While for the exfoliation of graphite the anodic process in aqueous solutions is the most widely used due to the higher efficiency compared to the cathodic one, for the exfoliation of other layered materials, the most universally used methods are those based on Li intercalation in organic solvents.[102] Usually lithium is intercalated in the layered material forming the intercalated compounds (e.g. Li_xMoS_2). The latest are then sonicated in water or ethanol where lithium react generating H_2 gas, that promotes the exfoliation of the material in thin nanosheets. Intercalating lithium and, thus, working in cathodic conditions, we want to avoid the oxidation we observed in the anodic exfoliation of graphite.

The electrochemical exfoliation of a bulk MoS_2 crystal typically leads to the formation of flakes with two distinct crystal structures, i.e. the semiconducting (2H) and metallic (1T) phases. [218] More specifically, chemical exfoliation *via* lithium-ion intercalation leads to the formation of electron-rich sheets, characterized by a large fraction — between 60 and 70% — of 1T (or distorted 1T′) polytype. [219] In order to obtain single-phase semiconducting flakes the use of post-exfoliation processes, such as thermal annealing, [220] laser irradiation [212] and microwaves treatments[221] is required. Exploiting the electrochemical intercalation process, Ejigu and co-workers [176] recently reported the exfoliation of a MoS_2 pellet by using lithium perchlorate ($LiClO_4$) dissolved in a mixture of ethylene carbonate (EC) and dimethyl carbonate (DMC): the experiments were carried out under inert atmosphere (N_2), lasted for ca. 2 hours and resulted in a percentage of semiconducting 2H phase around 40%.

In our laboratory, we developed a fast (<1 hour) electrochemical exfoliation of MoS_2 *via* lithium-ion intercalation, by using a solution of lithium chloride (LiCl) in DMSO, where lithium salt is used as source of lithium ions. The use of DMSO leads to the formation of Li^+-DMSO adducts that can penetrate in between MoS_2 layers and increasing the interlayer spacing. Its effect is proven by the large expansion of MoS_2 crystal after the intercalation process (**Figure 4. 21**). Unlike the conventional intercalation methods based on dangerous organolithium compounds,[222-224] our approach leads to the possibility to obtain mono-, bi- and tri-layer thick MoS_2 nanosheets with a large fraction of the semiconducting 2H phase (~60%), as estimated by XPS.[225]

Figure 4. 22 displays scanning transmission electron microscopy (STEM) images of the exfoliated MoS_2 nanosheets. To give an estimation of the size and the thickness of resulted nanosheets, we performed STEM and HR-TEM statistical studies on 150 and 60 flakes produced by different batches, respectively. The analysis showed the presence of a large amount of mono-, bi- and tri-layer thick MoS_2 flakes with an average lateral size of ~0.8 μm. HR-TEM images (**Figure 4. 22** d-g) reveal the co-existence of two crystal phases within individual MoS_2 nanosheets, i.e. 1T (highlighted in yellow) and 2H (highlighted in blue), with characteristic diffraction patterns (**Figure 4. 22**f and h, respectively).

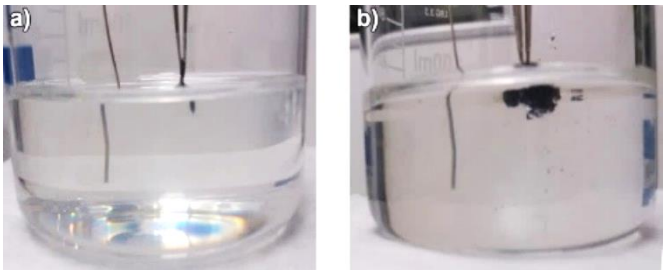

Figure 4. 21. Experimental setup used for the preparation of MoS_2 nanosheets *via* DMSO-solvated lithium-ions intercalation. The photographs were taken (a) before, and (b) after the intercalation process, which induces a significant expansion of the bulk MoS_2 crystal.

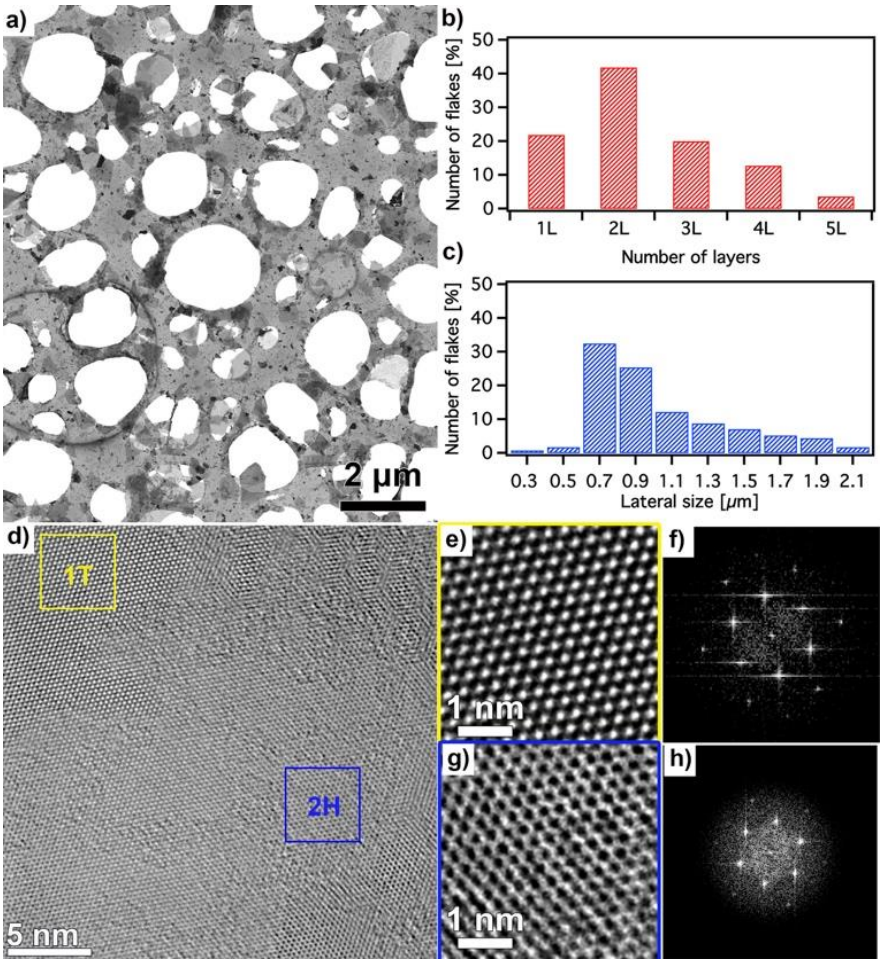

Figure 4. 22. (a) STEM image of MoS_2 nanosheets exfoliated *via* lithium-ion intercalation in DMSO and deposited onto a holey carbon grid. (b) Thickness distribution obtained from STEM measurements on 60 different nanoflakes. (c) Lateral-size distribution based on data from 150 different nanoflakes. (d) HR-TEM image showing the presence of two distinct crystalline phases. (e) Zoom-in image of the 1T region marked in yellow and (f) its corresponding diffraction pattern. (g) Zoom-in image of the 2H region marked in blue and (h) its corresponding diffraction pattern.

UV-Vis absorption spectroscopy (

Figure 4. 23) shows the presence of two peaks at λ ≈ 672 nm and ≈ 612 nm that can be attributed to the A and B excitons, respectively, corresponding to optical transitions occurring at the K point of the Brillouin zone[210].

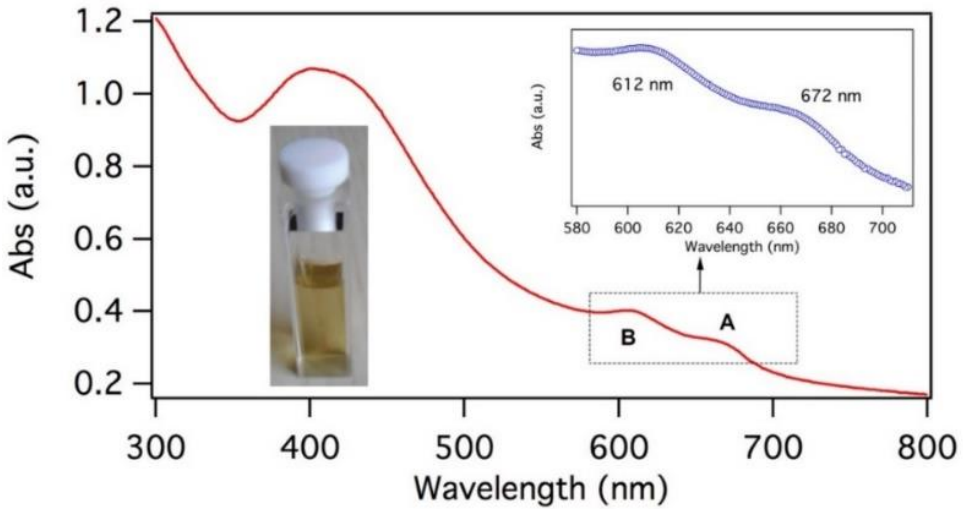

Figure 4. 23. UV-Vis absorption spectrum of MoS_2 nanosheets dispersed a mixture of H_2O (70%) and ethanol (30%). The inset shows a magnified view of the spectrum in the region of the A and B exciton peaks.

XPS measurements were performed on both pristine and exfoliated material. **Figure 4. 24** compares the Mo 3d and S2p high-resolution XPS spectra of the MoS_2 bulk crystal used as starting material with those of the exfoliated flakes. In the case of pristine MoS_2, the Mo 3d spectrum (**Figure 4. 24**a) shows the characteristic doublet of the semiconducting 2H phase at 229.4 eV and 232.5 eV, corresponding to Mo^{4+} $3d_{5/2}$ and Mo^{4+} $3d_{3/2}$ spin-orbit components. The S 2p spectrum is also splitted in the two components related to S $2p_{3/2}$ and S $2p_{1/2}$ spin orbits and appear at 162.2 eV and 163.4 eV, respectively (**Figure 4. 24**b). On the other hand, after exfoliation, the Mo 3d spectrum (**Figure 4. 24**c) displays an additional doublet — located at lower binding energies ($\Delta E_b \approx 1$ eV) — that can be assigned to the metallic 1T phase.[226-228] The S 2p spectrum (**Figure 4. 24**d) also presents broader peaks that can be fitted by to two pairs of doublets, i.e. those of the 2H phase at higher binding energy (green) and those relative to 1T phase at lower binding energy (light blue). By peak fitting of Mo 3d and S 2p high resolution spectra, we estimated the relative content of 1T and 2H phases, that is 40% and 60% respectively. We have estimated the S/Mo stoichiometric ratio through fitting and integration of high-resolution XPS spectra acquired in the regions of the Mo 3d and S 2p peaks. After background correction, the data were fitted with Gaussian-Lorentzian bell functions by making use of the Thermo Avantage software to obtain the area A of the peaks. The ratio between A(S 2p) and A(Mo 3d) was normalized to 2 in the case of the unexfoliated bulk material, where it was assumed for simplicity that the density of sulfur vacancies in the source is negligible. The same normalization factor was then used in the case of the MoS_2 nanosheets prepared *via* lithium intercalation in DMSO. Upon exfoliation, the stoichiometric ratio was found to decrease from 2 to ≈ 1.94, revealing a non-negligible generation of sulfur vacancies. By XPS quantification, we can conclude that our approach enables the preparation of nanosheets that are preferentially semiconducting, whereas previous works based on chemical or electrochemical exfoliation have shown the formation of metallic nanosheets with 1T content

exceeding 60%. The change from 2H to 1T upon intercalation is commonly associated to a strong electron transfer from the lithium atoms to MoS_2[229-230]. In our case, the presence of DMSO molecules coordinating the Li ions [231] could presumably mitigate the intercalation step and consequently such electron-transfer process, thereby limiting the conversion to the metallic 1T phase.

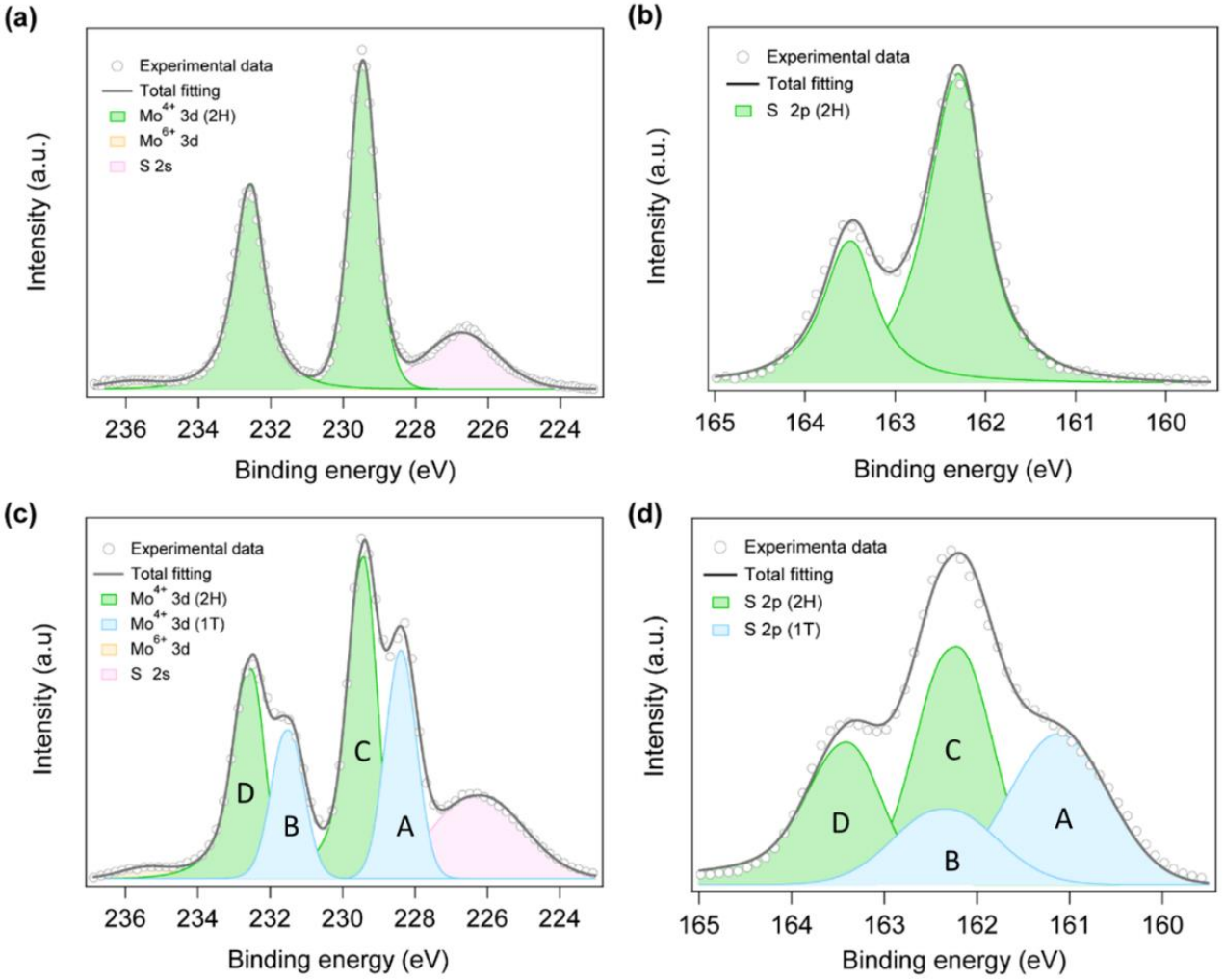

Figure 4. 24. (a, b) High-resolution XPS spectra of (a) Mo 3d and (b) S 2p regions acquired from unexfoliated MoS_2 crystals. The relatively small peak at 235.7 eV (Mo^{6+} state) reveals the presence of a low level of oxidation in the unexfoliated material. (c, d) High-resolution XPS spectra of the (c) Mo 3d and (d) S 2p regions acquired from MoS_2 nanosheets prepared *via* lithium-ion intercalation in DMSO. The deconvolution of the Mo 3d (c) and S 2p (d) displays the peaks related to 1T (light blue) and 2H (green) phases. The oxidation level is not modified by the intercalation/exfoliation process. All the peak positions were corrected according to the C 1s signal at 284.8 eV.

Table 4. 4 Areas under the curve of the 1T and 2H peaks obtained from the deconvolution of the high-resolution XPS spectra shown in **Figure 4. 24** c,d. The values reported in the table have been used to calculate the fraction of 1T and 2H phases in the exfoliated MoS_2 nanosheets.

Peak	Mo 3d		S 2p	
	1T	2H	1T	2H
A	57117.73	-	25374.73	
B	39373.77	-	13120.61	
C	-	82471.36	-	30889.76
D	-	57869.16	-	22190.02
1T% (A+B)/(A+B+C+D)	~40 (60% of 2H)		~42 (58% of 2H)	

MoS_2 nanosheets were further investigated by means of Raman spectroscopy. **Figure 4. 25** a portrays the Raman spectra of a MoS_2 flake obtained by DMSO-solvated lithium-ion intercalation process (blue) and by mechanically exfoliation (red). The former exhibits three additional peaks located at ~157 cm^{-1}, ~227 cm^{-1} and ~331 cm^{-1}, which can be ascribed to the J1, J2 and J3 modes of 1T′ crystal phase, respectively. The A_{1g} and E^1_{2g} modes maintain a similar frequency and relative intensity in the two spectra indicating that both polytypes coexist in our electrochemically exfoliated MoS_2 nanosheets within a lateral scale of ~0.7 μm (laser-beam diameter), in agreement with the results of TEM and XPS investigations. On the other hand, the peaks separation is estimated being ~21.8 cm^{-1} which confirms the formation of an average thickness about two-three monolayers. Noteworthy, the peak at ~227 cm^{-1} can be also ascribed to the longitudinal acoustic phonons (LA) at the M point in the Brillouin that are active only in the presence of defects, as discussed in detail by Mignuzzi and co-workers. The quality of the MoS_2 nanosheets can be assessed by calculating the ratio between the intensities of the LA(M) and A_{1g} modes [214]. If we assume for simplicity that the peak at ~227 cm^{-1} arises exclusively from LA(M) acoustic vibrations, we can extract $I(LA(M))/I(A_{1g})$ values within the range 0.1-0.3, which correspond to an average inter-defect distance L_D of 1-2 nm. The strong contribution of defects in the Raman spectra of electrochemically intercalated MoS_2 can be also evaluated by the line shapes of the A_{1g} and E^1_{2g} modes (**Figure 4. 25**b), which present shoulder peaks at ~378 cm^{-1} and ~410 cm^{-1}, corresponding to defect-activated LO(M) and ZO(M) phonon modes, respectively.[232]

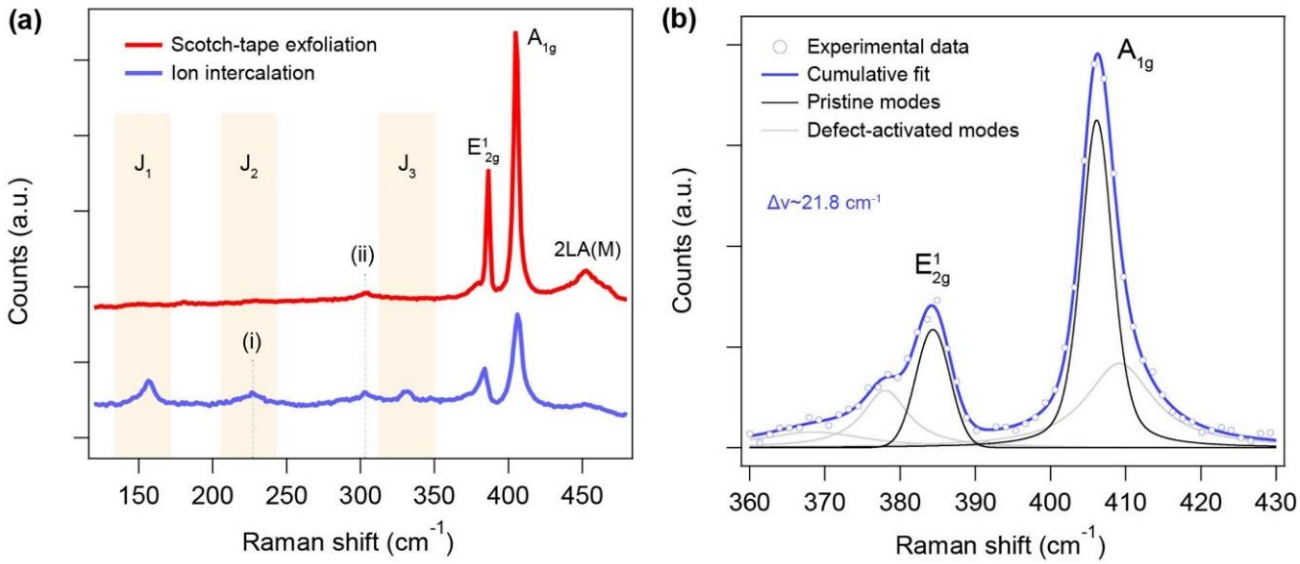

Figure 4. 25. (a) Raman spectra of MoS_2 nanosheets exfoliated by DMSO-solvated lithium-ion intercalation (blue, bilayer) and scotch-tape technique (red, monolayer). The peak (i) can be also attributed to the defect-activated LA(M) mode at ~227 cm^{-1}, whereas the peak (ii) — present in both spectra — corresponds to the 2TA(*X*) Raman mode of the SiO_2/Si substrate. (b) Raman spectrum of a bilayer MoS_2 flake obtained *via* DMSO-solvated lithium-ion intercalation in the spectral region of the E^1_{2g} and A_{1g} modes. The fitting was carried out with the method presented in ref. [233] for defective MoS_2 sheets.

Similarly to the previous work, the electrical properties of the exfoliated material were investigated through the fabrication and characterization of back-gated FETs based on individual MoS_2 nanoflakes (2-4 layers thick) by means of electron-beam nanolithography. As-fabricated devices displayed unipolar semiconducting behavior (*n*-type), similar to that of semiconducting MoS_2 nanosheets obtained by scotch-tape method. Field-effect mobility was estimated $\mu_{FE} \leq 10^{-3}$ $cm^2 V^{-1} s^{-1}$ with $I_{on}/I_{off} \leq 10$. EE MoS_2 performances appeared thus limited by the 1T/2H polymorphism and defects (e.g. sulfur vacancies) induced during the intercalation/exfoliation process. Interestingly, in this work Dr. S. Bertolazzi, demonstrated a significant enhancement of the electrical performances achieved through a combination of vacuum annealing (150 °C) and sulfur-vacancy healing with vapors of short-chain alkanethiols, a technique that has been recently developed in our laboratory for healing sulfur vacancies generated by low-energy ion irradiation.[234] Such approach allows the increasing of μ_{FE} up to 2×10^{-2} $cm^2 V^{-1} s^{-1}$ and enables I_{on}/I_{off} ratio ≈ 100, [225] suggesting that sulfur vacancies are an abundant type of defects in nanosheets exfoliated *via* DMSO-solvated lithium-ion intercalation.

Moreover, it is worth noting that the figures of merit of our devices are comparable with those reported in the literature for UILPE nanosheets and their network films.[214, 235-236] However, they remain still much lower than those of mechanically-exfoliated MoS_2 flakes,[237-241] indicating that other forms of disorder — as discussed above — are responsible for the degradation of the charge-transport properties in the nanosheets obtained *via* lithium-ion intercalation in DMSO. Similarly, to what observed for graphene obtained by electrochemical exfoliation, the large discrepancy between the aforementioned μ_{FE} and I_{on}/I_{off} values and those of state-of-the-art devices – based on high-quality MoS_2 nanosheets obtained by mechanical exfoliation *via* scotch tape peeling – highlights the presence of a more complex/detrimental disorder, which requires to be minimized towards practical (opto-)electronic applications. These results pave the way towards the fast preparation — under ambient conditions — of semiconducting MoS_2 nanosheets, suitable for application in low cost (opto)electronic devices.

Moreover, it casts the basis for more comprehensive studies of the effects of exfoliation-induced disorder on the charge-transport properties of ultrathin MoS_2 FETs.

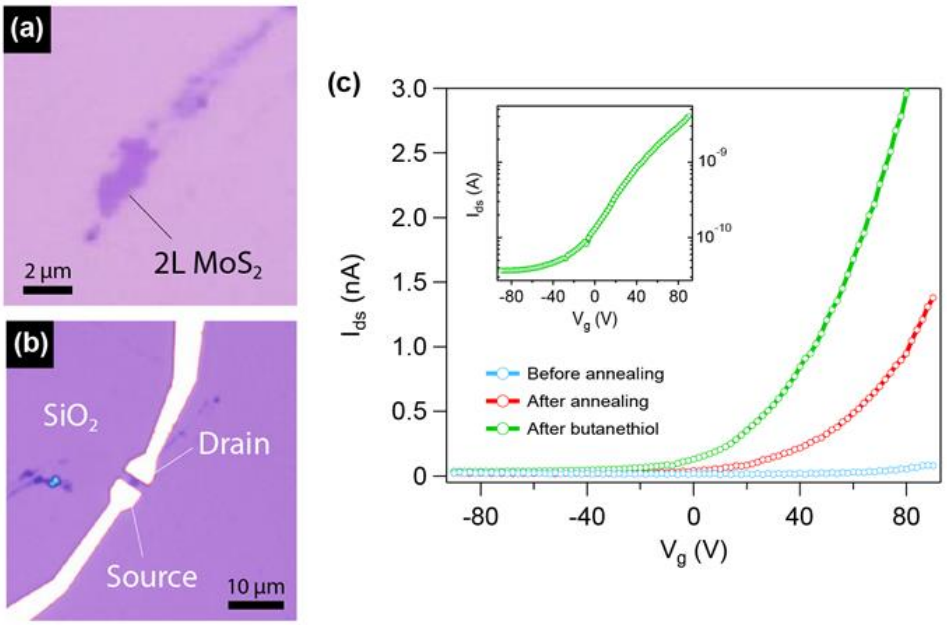

Figure 4. 26. Fabrication and characterization of FETs based on exfoliated MoS_2 nanosheets. (a,b) Optical micrographs of a bilayer MoS_2 flake deposited on a SiO_2/Si substrate before (a) and after (b) the fabrication of the source and drain contacts (Au, 90 nm). The heavily-doped silicon substrate is used as the back gate. (c) Transfer curves of the FET device shown in (b) acquired at different stages under inert atmosphere (N_2-filled glovebox). The drain-source bias voltage V_{ds} was set at 4 V. The curve obtained after butanethiol treatment (green) is reported in semi-log scale in the inset and displays I_{on}/I_{off} current ratio up to 10^2. Reproduced from ref. [225].

4.4 Conclusions

In summary, in this chapter we first investigated the correlation between structure and electrical characteristics in electrochemically-exfoliated graphene.

Stable dispersions of graphene were prepared by means of the electrochemical approach using ammonium sulphate as electrolyte. We demonstrated the versatility of EEG towards different uses, that is uncommon for other materials such as UILPE graphene or graphene oxide. In EE process it is possible to obtain a broad range of oxidation levels by simply tuning the parameters of the process, such as the time of electrolysis, as it was proved by XPS.

We have carried out a multiscale characterization of the physico-chemical properties of EEG, in order to cast light onto the factors that influence the charge-carrier transport in this material. Taking advantages of the micrometer size of graphene flakes, multi-terminal FETs based on single flakes were fabricated allowing measuring mobilities of 1-10 $cm^2V^{-1}s^{-1}$ at the single flake level. Such mobilities turned out to be very similar to those measured on continuous EEG films. EEG results thus an

attracting alternative material for transparent electrodes. In the past years, GO has been used for this purpose due to the relative ease with which uniform thin film can be deposited from solution. However, to obtain a conductive film, reduction and/or surface modification are necessary. On the contrary, EE combined with the method of deposition reported in paragraph 5.2, give rise to conductive film. This approach offer thus the possibility of avoiding harsh synthesis of graphene oxide followed by unavoidable reducing process, while giving a conductive material with similar properties than rGO film in one simple step. Moreover, in most cases GO reduction (chemical, thermal or microwave- induced) can be detrimental for the other components of a more complex system. This problem can be avoided using EEG that can be deposited on any other material without changing its properties.

Interestingly, we have reported for the first time the emergence of the *n*-conductivity in EEG upon thermal annealing, leading to an ambipolar transport, which may be of interest for the development of logic circuits. We have also showed that MW treatments can be successfully exploited on EEG in order to lower the oxygen content, enabling to demonstrate that charge transport within EEG is mostly hindered by structural defects rather than by oxygen containing defects. The presence of structural defects that is here shown for the first time, has to be reconducted to the unconventional electrochemical conditions generally used to achieve the exfoliation. The intensive oxygen and hydrogen evolution during the anodic process when a high voltage is applied, creates defects which unavoidably affects the properties of the material, and at the same time make difficult to control the process of EE. Providing new insight on the structure and properties of EEG, we aim to drive further studies towards the optimization of EE process, that is at present the most promising method for the production of large quantities of graphene. These studies should focus on improving the structural quality of the material, allowing thus better electrical characteristics. On the other hand, shedding light on the nanoscopic properties of the as produced material can open the route to other applications which exploit structured graphene surfaces and porous, as for example membranes, energy storage, catalysis, sensors *etc*.

Finally, we have presented a facile and low-cost approach to exfoliate MoS_2 crystals under ambient conditions *via* DMSO-solvated lithium-ion intercalation. Our method allows producing single-, bi- and tri-layer thick nanosheets of MoS_2 with an average lateral size of ~0.8 μm. HR-TEM, XPS and Raman spectroscopy revealed the presence of a large amount of semiconducting 2H phase (~60%). The electronic properties of single flakes were investigated through the fabrication and characterization of back-gated field-effect transistors (FETs), which displayed unipolar semiconducting behavior (n-type), in line with the observation of a predominant 2H phase within the exfoliated flakes. We succeeded in improving the electronic properties of our FETs through a combination of vacuum annealing and defect healing with short linear thiolated molecules, resulting in μFE values up to 2×10^{-2} $cm^2V^{-1}s^{-1}$ and $I_{on}/I_{off} \approx 100$. Such findings cast the basis for future investigations on the influence of exfoliation-induced disorder on the charge transport properties. The approach we developed paves the ways towards the fast preparation — under ambient conditions — of semiconducting MoS_2 nanosheets.

Overall, we discovered that many factors and limitation must be taken into account when the electrochemical process is extended to other 2DMs different from graphene, e.g. the structural deformation affecting MoS_2 when intercalated with Li-ions; the capacity of the material to support strong anodic or cathodic conditions without undergoing to decomposition; the stability of the material under ambient conditions; the nature of the electrode that need to be conductive, and so forth. These factors make the electrochemical process more challenging. Nevertheless,

electrochemical approach holds a great potential for the fast and low-cost preparation of 2DMs at large scale, that is encouraging further endeavours to overcome such challenges.

CHAPTER 5.

MoS_2 NANOSHEETS FOR CHEMICAL SENSING

In the previous chapter, the electrochemical exfoliation of graphene has been investigated with a particular focus on the relationship between structure and properties of the exfoliated material. Furthermore, the electrochemical method towards MoS_2 nanosheets fabrication has been introduced. These studies showed that the electrochemical exfoliation approach is a promising method to produce 2D materials (2DMs) with controlled sizes and defects including mechanical and chemical defects, e.g. oxygen functionalities and sulfur vacancies. Such defects act as reactive sites for interactions at the covalent and non-covalent level with molecules. The latter, due to their reversible nature and selectivity, are ideally suited for sensing. By relying on the reversibility and the strength of non-covalent interactions, a sensor can respond quickly to environmental changes and recover fast (e.g. real-time monitoring). Moreover, it can interact with the analyte multiple times, ensuring the repeatability of the process.

Previously, we have shown that electrochemically exfoliated MoS_2 features some structural defects, which compromise its electrical characteristics when compared to mechanically exfoliated MoS_2. Yet, the presence of defects is not necessarily detrimental for all applications. Our studies have indicated that a large part of these defects can be assign to the presence of sulfur vacancies, as proved by improved electrical performances through butanethiol vapors treatment. Recently, the presence of such kind of defects, e.g. vacancies in the basal planes and at the edges of MoS_2 nanosheets, has been considered beneficial as it allows improving the chemical sensitivity (e.g. towards NO_2 and EtOH molecules)[242] and chemical reactivity of the material (e.g. with thiol molecules),[243-245] compared to the pristine crystals that are considered being rather chemically inert.[246] Such findings have inspired the following work which relies on exploring the use of MoS_2 exfoliated in liquid media as active material for gas sensing.

5.1 Introduction

Chemical sensing is a topical field of science as it is expected to provide a key contribution to the improvement of people's quality of life by offering concrete solutions towards, environmental[247] and biohealth monitoring (as early diagnostics and continuous monitoring of diseases),[248] food safety,[249-250] *etc*. In particular, having a good control over the humidity in the environment is the key for ensuring a good quality of the air in living and working places, besides being essential for many industrial processes.

Recently, 2DMs have been considered potentially ideal materials for gas sensing due to the fact that almost all the atoms of the material are exposed to the environment and can interact with the analyte of choice. In other words, the potential of 2DMs as sensors is mainly due to their highest surface-to-volume ratio that allows to maximize the effective detection of the analyte such as, for instance, the detection of variations of humidity in the environment. Moreover, owing to flexibility and transparency of 2DMs, these sensors could be integrated on wearable or bendable devices, or simply their dimensions could be reduced, making the sensors minimal and invisible.

In order to use a material in gas sensors, besides the requirements of sensitivity to the selected analyte, fast response and reversibility of the process, the device based on it should give a certain output which allows read-out the occurred detection.

When pristine graphene is tested as humidity sensor, for example, the absorption of water molecules can generate a variation in its electrical resistance, *via* doping. However, this change in resistance is usually rather small due to the absence of a sufficient amount of active sites for the interaction with the analyte and its very high starting electrical conductivity, thereby hampering the use of graphene as humidity sensor because of the low sensitivity. On the contrary, graphene oxide and reduced graphene oxide exhibit higher performances due to their different chemical structure. Water molecules can indeed interact with functional groups present in GO determining a change in its conductivity, but they can also chemically adsorb on the material and limit the reversibility of the process that can take longer to recover the initial resistance. An alternative to these 2DMs can be represented by transition metal dichalcogenide (TMDs) due to their high surface-to-volume ratio, adjustable and direct bandgaps and availability of reactive sites for redox reactions.[137] Usually, the dominant mechanism behind the observed sensing characteristics is a charge-transfer mechanism. For example, when *n*-type MoS_2 monolayers are exposed to electron-acceptor gases like O_2, H_2O, NO, NO_2 and CO_2, electrons are transferred from MoS_2 to the gas molecules determining a decrease of the carrier density within MoS_2 and a consequent increase of the resistance. In the case of monolayers which features direct bandgap, changes in the photoluminescence are observed as well. These and other studies have been performed on mechanically exfoliated MoS_2 (ME MoS_2), which is unsuited to practical applications because cannot be produced on a large scale.

One possibility for the use of MoS_2 for gas sensing applications could rely on generation of sulphur vacancies by electrochemical exfoliation of MoS_2 – as demonstrated in chapter 4 – and investigating their effect on the sensitivity of this material towards humidity. However, from our previous studies, we learned that, although the electrochemical exfoliation in cathodic conditions makes it possible to produce MoS_2 without oxidizing the exfoliated material, this occurs at the cost of much lower efficiency of the process compared to anodic exfoliation. Furthermore, MoS_2 crystals employed as an electrode in the electrochemical approach are very expensive, and therefore formation of a material to be employed in sensing application *via* this approach would not be acceptable for economic reasons. In light of this, we have decided to produce the sensing material starting from MoS_2 powder, which is accessible at a low cost in large quantities.

In general, many different types of defects can be found on the edges and in the plane of exfoliated MoS_2 nanosheets. The most abundant are vacancies which include single sulfur vacancies, double sulfur vacancies, a vacancy of Mo atoms bonded with three sulfur atoms in one plane, molybdenum occupying a sulfur vacancies or a pair of S atoms occupying a Mo position. [251] Among them, single sulfur vacancies have the lowest energy of formation (~2eV).[252-253] Because sulfur atoms on the basal plane are strongly bonded, the formation of a vacancy is easier at the edges of a layer where the coordination is incomplete and the sulfur is chemically labile.[254] Due to the low energy of their formation, sulfur vacancies at the edges can be particularly favoured during the exfoliation processes as the material undergo mechanical stress and fragmentation.[143] The S and Mo atoms around the vacancies will consequently present dangling bonds, making the material richer in reactive sites at the edges.[255] The reactivity of defects has been extensively studied for hydrogen evolution reaction (HER). Experimental and theoretical studies proved that the active sites for HER lie along the edges of MoS_2 nanosheets, and in particular are associated with edge sulfurs,[256-257] that can absorb H_2, while the basal plane are catalytically inert. Moreover, it has been proved that in MoS_2 the edges are metallic and chemically active in contrast with the semiconducting and inert basal plane.[257-258] Therefore,

numerous studies have been based on the reduction of nanosheets sizes to increase the number of unsaturated sulfur edge sites and consequently the number of catalytically active sites.[259-263] More generally, it has been demonstrated that MoS_2 and other TMDs can interact *via* dipole-dipole, electrostatic and vdW interactions with (charged) molecules, enhancing the occurrence of adsorption events. Theoretical studies, for example, support the existence of weak vdW interactions between non-polar gas molecules (CO_2 and CH_4) and monolayer MoS_2 containing vacancies, that shows a response to these gases, contrarily to pristine MoS_2.[264] The introduction of defects can allow new and tuneable properties, opening the door to novel properties that cannot be found on pristine 2DMs, such as enhanced electron transfer rate and electrochemical activity as it was proved for graphene.[137] Therefore, defects might play a key role in gas sensing as well. Generating defects can improve the selectivity and overall performance of sensors as a result of the increase in the strength of the interactions. In particular, the presence of uncoordinated atoms at the edges of MoS_2 and the high density of electrons can enhance the interaction with the gas molecules. Indeed, through DFT calculation it can be seen that, in the presence of defects, the adsorption energy and the amount of charge transfer are larger. Consequently much more significant is the change in the electrical response caused by the strong interaction between orbitals of gas molecules and those of 2D systems.[265-266] The MoS_2 edges containing undercoordinated S or Mo atoms are therefore expected to interact strongly with adsorbates.

In this chapter, we take advantage of the liquid-phase exfoliation approaches of MoS_2 to produce a large amount of material at low cost that can be explored in gas sensing. The material produced as dispersion can be also processed on rigid and/or flexible substrates. In such a way, the properties of MoS_2 as gas sensor could be exploited on large-area flexible devices, allowing practical and innovative applications. Moreover, we show that the presence of edges defects formed during the processes of liquid-phase exfoliation can be the cause of an enhanced sensitivity of the material to gases.

Noteworthy, some studies performed on mechanically exfoliated (ME) MoS_2 flakes having different thickness (from 1 to 5 layers) have shown that 5-layers thick sheets exhibit higher and more stable response toward gases (e.g. NO,[23] NO_2 and NH_3[267]) than mono- and bi-layers, which on the contrary always give unstable signals. Based on these results, we evaluated that the material produced *via* ultrasound induced exfoliation in solution could result in good gases sensing performances since solution based processes usually allow formation of nanosheets with a mean thickness of about 10 layers.[66, 268] We took advantage from the versatility of the liquid-phase exfoliation, which offers to choose among various methods such as ultrasonication, electrochemical exfoliation, shear mixing, *etc.,* yielding 2DMs with different size and defect nature, which could be most suitable in view of the specific application. For our preliminary studies, we considered appropriate the use of the ultrasonication as it is a well-established approach and low-cost.

Indeed, for the applications in gas sensing, it is more important to reach the homogeneity of the active material on the large area, in order to bridge two electrodes and having an electrical read-out, rather than having a high content in monolayers or pristine 2DMs.

Noteworthy, although some works claim that ultrasound-induced LPE makes it posible to produce defect-free 2DMs, there are some works that highlight the formation of defects on the basal plane of 2D flakes as a result of cavitation process (see sub chapter 2.2.1). Moreover, the materials produced by ultrasonication features very small particles sizes due to the fragmentation process that occur concomitantly with the exfoliation (see Chapter 2). Smaller particles sizes imply a high content of edges, that are known for their high chemical reactivity and extensively studied for their catalytic

properties, as discussed above. For these reasons, ultrasound-induced LPE material can potentially be an ideal platform for sensing applications.

Some research groups have explored the possibility of using liquid-phase exfoliated MoS_2 as gas sensor. They used various techniques, with a deferent level of complexity, for the production of the sensing material, such as combination of grinding and sonication of the bulk material[269] or lithium intercalation.[270] Methods as drop casting or inkjet printing are used for the deposition of the material. These systems have been used as active materials to detect different gases, including NH_3, NO_2, H_2, humidity. However, the sensitivity of such devices is rather low. For such reasons, chemical functionalization of MoS_2 nanosheets with molecules that interact better with the analyte has been taken into account as a way for enhancing LPE MoS_2 sensitivity.[244]

In this work, we produced the sensing material by ultrasound-induced LPE of MoS_2 powder in isopropanol. The material has been characterized with different microscopic and spectroscopic techniques, and then deposited in form of thin film by a stamp-transfer approach on a silicon substrate. MoS_2 films were exploited for fabricating chemiresistors, that are commonly used as devices for gas-sensing bacuse of their ease of fabrication and operation, low cost and low power consumption. In a chemiresistor, the adsorption of molecules on the active material induce a change on its electrical resistance and by measuring this resistance the analyte can be detected. Herein, we reported thus the sensing behavior of MoS_2 films towards humidity for chemiresistor devices. We demonstrated that MoS_2 nanosheets produced by ultrasound-induced LPE can be processed in large area thin films which exhibit remarkable sensitivity towards humidity. We found that MoS_2 film sensors show different sensing behaviour towards various gases (small molecules). While the presence of humidity generates an increase of the current (positive response), the other molecules (O_2, CO_2, acetone, chloroform, ethanol and methanol) generate a decrease of the current (negative response) with a sensitivity that depends on the specific molecule. Such difference in the sensing behaviour toward different analytes might be indicative of the different nature of the interactions between MoS_2 and the analyte, as well as, of a different mechanism of sensing (e.g. sensing to humidity with respect with other molecules).

The following section describes the procedure used to prepare MoS_2-based sensors. All steps, from the preparation of MoS_2 thin sheets to the fabrication of the devices were performed in our laboratory and are summarized in **Figure 5. 1**. Section 5.3 discuss the main findings of this study and the main conclusions are summarized at the end of this chapter.

5.2 Materials and methods

5.2.1 Production of MoS_2 by UILPE

MoS_2 nanosheets were produced by ultrasound-induced liquid-phase exfoliation of MoS_2 powder (Sigma Aldrich, flake size > 6 μm) in 2-propanol, IPA (step 1 in **Figure 5. 1**).

MoS_2 dispersion (20 mg/mL) was sonicated for 5 hours using a cup horn sonicator. The sonication was operated at 60% amplitude and the system was pulsed 6 seconds on/ 2 seconds off to reduce overheating of the machine and samples.

An initial step of sonication (1 hour) was needed in order to remove impurities present in the MoS_2 powder, according with previous reports.[268] After a centrifugation step at 5000 rpm the supernatant was indeed thrown away. The precipitate was dispersed again in fresh solvent (IPA), the dispersion

was degassed (5-10 vacuum/nitrogen cycles) using a Schlenk line and then sonicated in the same conditions for other 4 hours. Finally, the dispersion was centrifuged at 1500 rpm for 60 minutes in order to precipitate the un-exfoliated material (step 2) and the supernatant dispersion was used, without further treatments, for characterization and devices preparation.

Exfoliation of MoS_2 powder in IPA, followed by centrifugation step, leads to a stable yellowish dispersion shown in **Figure 5. 3**a.

5.2.2 Morphological characterization by atomic force microscopy

The as prepared dispersion was deposited by spin-coating (acceleration: 1000 rpm s^{-1}; spin rate: 800 rpm for 60 seconds) on SiO_2/Si n++ for AFM characterization. Thickness and lateral size of the flakes were measured over 500 particles selected and marked by a mask created by Gwyddion software. Flakes thickness was then converted in number of layers. On this regard, generally the apparent thickness of a MoS_2 monolayer is determined through step height analysis and evaluated being in the range of 1.5-1.9 nm.[143, 271] However, other reports show also thickness of 0.9-1.3 nm for MoS_2 monolayer.[96] Here we want to avoid considering values reported in literature that can be affected by different operational conditions, different used solvents and/or use of surfactants, whose contribute is only roughly estimated. Therefore, we decided to determinate the number of layers considering the thickness of a monolayer MoS_2 as equal to 0.615 nm, being its theoretical thickness, although the obtained values for the number of layers will be overestimated. One should bear in mind, indeed, that the apparent thickness of liquid-exfoliated nanosheets measured by AFM is typically larger than the theoretical thickness of the nanosheets due to adsorbed/intercalated water or solvent molecules. Statistical analysis of the flake dimensions was performed by measuring the longest axis of the flake that was defined as the flake length and considered a measure of the flake lateral dimension, according with the literature of the field.[86] Here the length of the flake was named "Dmax" and expressed in nanometers. MoS_2 nanosheets were characterized by high-resolution transmission electron microscopy (HR-TEM) in the collaboration with the group of Prof. Ovidiu Ersen (University of Strasbourg). The samples were characterized by Raman spectroscopy using the Renishaw microscope available in Nanochemistry laboratory that is equipped with a 532 nm laser. The silicon peak at 520.3 cm^{-1} was took as reference for wavenumber calibration.

5.2.3 Chemical and structural composition

The samples for XPS characterization were prepared by collecting the material in form of thick films by vacuum filtration on a PTFE membrane. Once the sample was dried, it was analyzed directly on the filter. We found this approach way easier and faster than drop casting to produce thick and homogeneous films on silicon substrate. Moreover, it ensures the removal of the majority of solvent by vacuum filtration. The XPS analysis was carried out using the XPS machine available at the Nanochemistry lab and in the same condition as described in the previous works. After background subtraction, the Mo3d and S2p peaks were deconvoluted using constrains on the relative intensity ratio of the doublets and the full width half maximum (FWHM).

5.2.4 Fabrication of MoS_2 based thin film sensors and electrical characterization

Thin film chemiresistor sensors were prepared by vacuum filtration of 3 mL MoS_2 dispersion to form a film on the filtration membrane (step 3 in **Figure 5. 1**). This film was then transferred on a SiO_2/Si n++ substrate using a custom-made press to allow the filter-substrate stamping of the film (step 4 in **Figure 5. 1**). The thickness of the films was controlled by the volume of filtered dispersion and it measure about 1.5 µm as determined by profilometer.

To fabricate a chemiresistor based on this film, 50 nm of gold were thermally evaporated on the film (Plassys ME300B) through a shadow mask to form interdigitated gold electrodes (L = 80 µm, W = 1 cm).

Morphology of the films was investigated by Scanning Electron Microscopy (SEM) using a Quanta FEG 250 (FEI). Images were recorded on conductive samples prepared by filter-substrate stamping (see section 0) on SiO_2/Si n++ substrates. The microscope was operated in high vacuum using 3 nm electron spot size and 10 kV acceleration voltage.

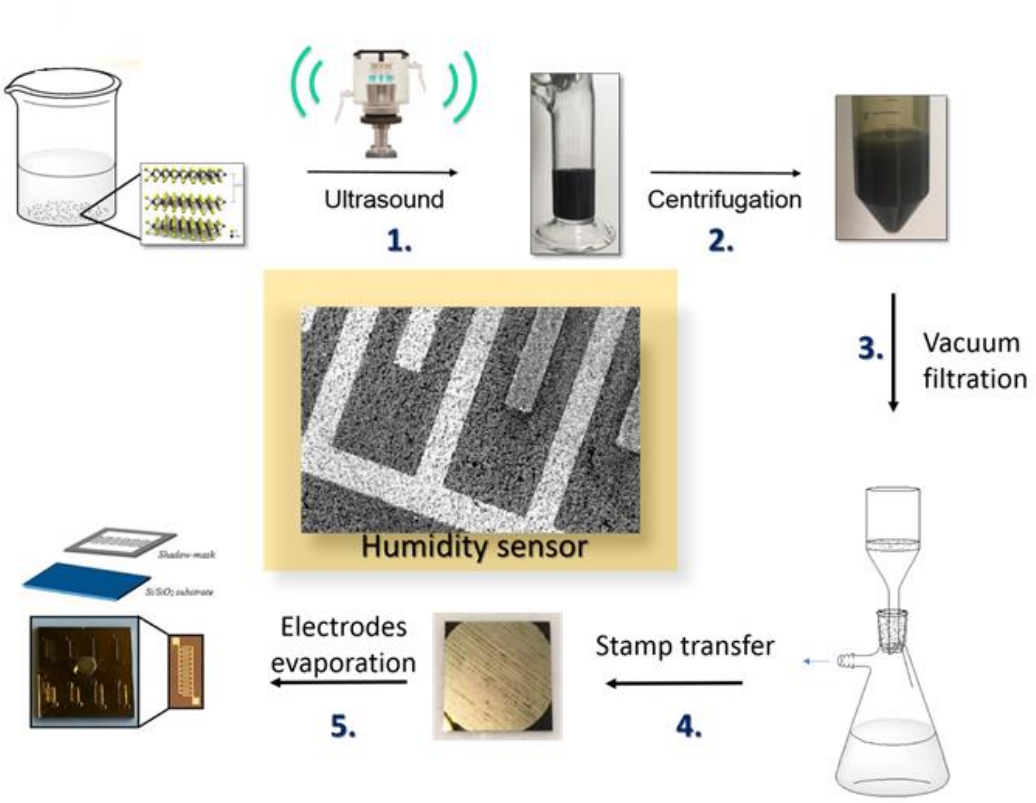

Figure 5. 1. Sketch describing the preparation of MoS_2-based gas sensors. Each step of the procedure is enumerated as following: 1. exfoliation of MoS_2 flakes by cup-horn sonicator; 2. purification by centrifuge to remove un-exfoliated particles; 3. filtration of PTFE membranes for film preparation; 4. film deposition onto Si++/SiO_2 chips by filter-substrate stamp transfer; 5. sensor fabrication by gold electrodes evaporation trough shadow mask approach.

The humidity was controlled with the help of aqueous solution saturated in lithium chloride or sodium chloride, allowing to reach around 14% and 75% of relative humidity (RH), respectively, in a sealed chamber containing a commercial humidity sensor (Sensirion SHT31 sensor). The devices were electrically connected to a Keithley 2636B sourcemeter with the help of copper and indium wires (E = 4 V cm^{-1}). The measurement in low level of humidity was done in a glovebox filled with nitrogen. Vapour of small organic molecules were produced by moderately heating a sealed beacker containing the solvent and connected to a nitrogen line in order to propel the vapour onto the sample.

The response of the sensor is plotted according to the ratio between the difference of resistance in the presence and absence of gas molecules and the original resistance value of the sensor, through calibration curves. The sensitivity is defined as the magnitude of current changes in presence of different concentrations of gas molecules.

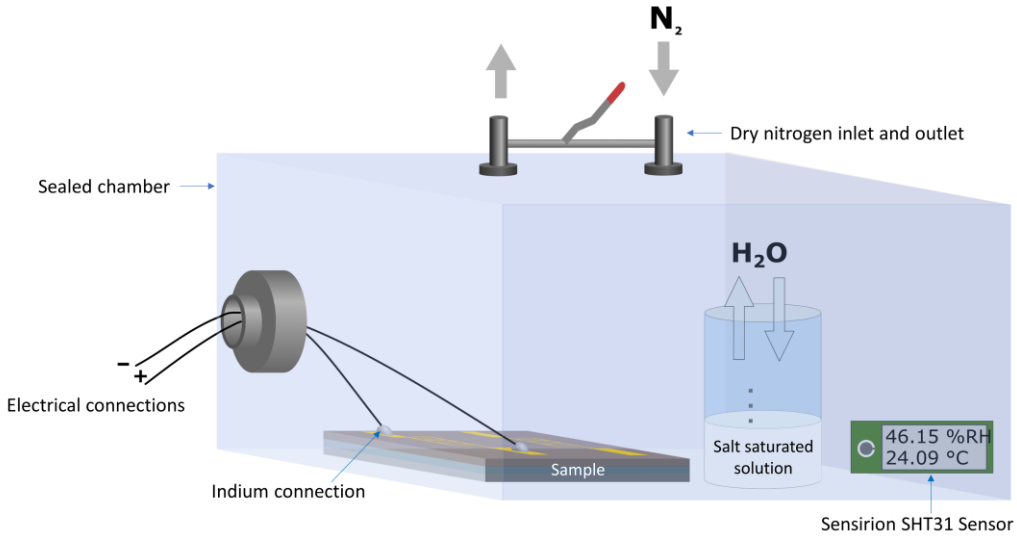

Figure 5. 2. Sketch of the sealed chamber in controlled atmosphere where the electrical measurements on MoS_2-based devices were performed at various levels of humidity generated by saturated salt solution.

5.3 Results

One of the parameters that can affect the sensitivity of MoS_2 based sensors is the number of reactive sites that are known to reside to the flake edges.[272]

As aforementioned, recent works showed that MoS_2 in the vicinity of the edges or grain boundaries exhibits distinct properties from the central regions.[143, 273] Moreover, it was reported that the edge sites of MoS_2 show much higher catalytic activity compared to the basal plane which is attributed to the different local stoichiometry. Consequently, also the gas adsorption behaviour of MoS_2 has been considered significantly affected by edge sites. A possible explanation has been attributed to the high d-orbitals electrons density at the edges that can enhance the interaction with the gas molecules, as demonstrated by a higher adsorption of gas molecules onto edge sites of vertically aligned MoS_2 compared to basal plane. DFT calculation confirm that the binding energies near the edges sites of MoS_2 are much stronger than those on the of the basal plane.[242] Reducing the sizes of MoS_2 particles could be a strategy for increasing the ratio between edge sites and basal planes, thereby increasing the number of active sites for the interaction with gas molecules.[274]

Among the methods of exfoliation in liquid media which have been discussed throughout this thesis, e.g. electrochemical exfoliation, shear mixing, ultrasonication, etc., this latest is known for yielding high fragmentation of the flakes together with the exfoliation of the material, as a result of cavitation phenomenon. Furthermore, the fragmentation can be, eventually, further promoted by modulating the parameters of exfoliation, e.g. increasing the number of hours of sonication.[14, 17]

For this reason, in order to produce an edges-rich material, in this work MoS_2 powder has been exfoliated by ultrasonication approach.

The choice of the medium of exfoliation is based on previous reports of MoS_2 liquid phase exfoliation. Among the liquid media which have been proposed such as NMP,[86] mixture ethanol/ water[275] or water with surfactants[143, 276] we have chosen to perform the exfoliation in isopropanol following a well-established procedure.[277] This choice has been primarily driven by the relatively low boiling point of the solvent that ensure its easy removal, being therefore ideal for devices preparation. On the contrary, it is difficult to remove surfactants from the nanosheets surface which can be potentially detrimental for the resulting properties of the system. On the other hand, the use of solvents like NMP, although probably it leads to a slightly higher degree of exfoliation, was avoided for its toxicity and because the high boiling point of this solvent would have required additional annealing processes.

To maximize the fragmentation of the flakes, the exfoliation has been carried out at a relatively high power (350 W) for 6 hours in a cup-horn sonicator that ensure a homogeneous ultrasounds exposure (see section 5.2.1). The final dispersion, after centrifugation, were very stable for at least few months. They appear tending to yellowish green colour (**Figure 5. 3**a) that suggests partial absorption in the visible range and is an indication of the semiconducting behaviour of the nanosheets (2H-MoS_2), in contrast with the black colour of 1T-MoS_2 which indicates complete and featureless absorption in the visible range and metallic nature of the nanosheets.[123, 268]

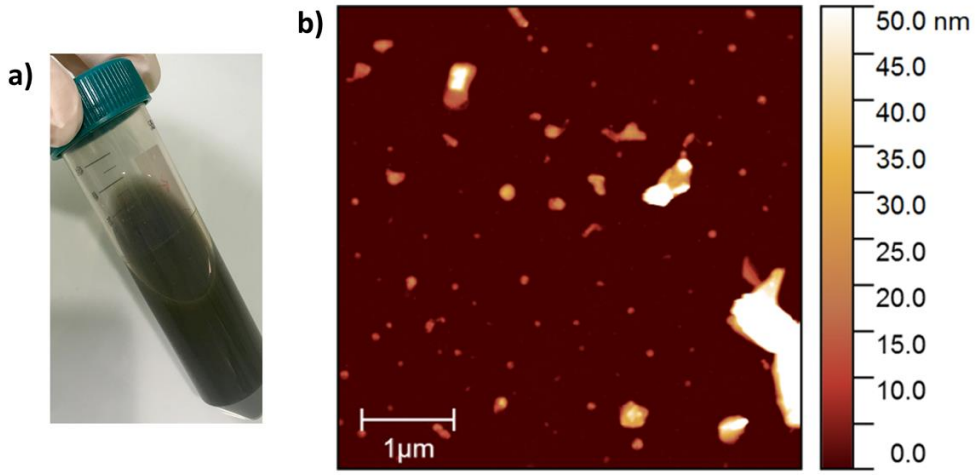

Figure 5. 3. a) Photograph of a typical dispersion of MoS_2 in isopropanol prepared by UILPE and purified by centrifugation to remove unexfoliated particles; b) representative AFM image of MoS_2 flakes produced by UILPE in IPA and deposited on Si/SiO_2 by spin-coating.

Figure 5. 3b shows the typical AFM image of exfoliated MoS_2 which displays nanosheets having various size and thickness, with a large number of tiny particles. The statistical analysis, performed on over 500 flakes, revealed the formation of MoS_2 flakes with lateral sizes on the order of hundreds of nanometers, including a high content of small particles with diameter below 50 nm (see inset in**Figure 5. 4**).

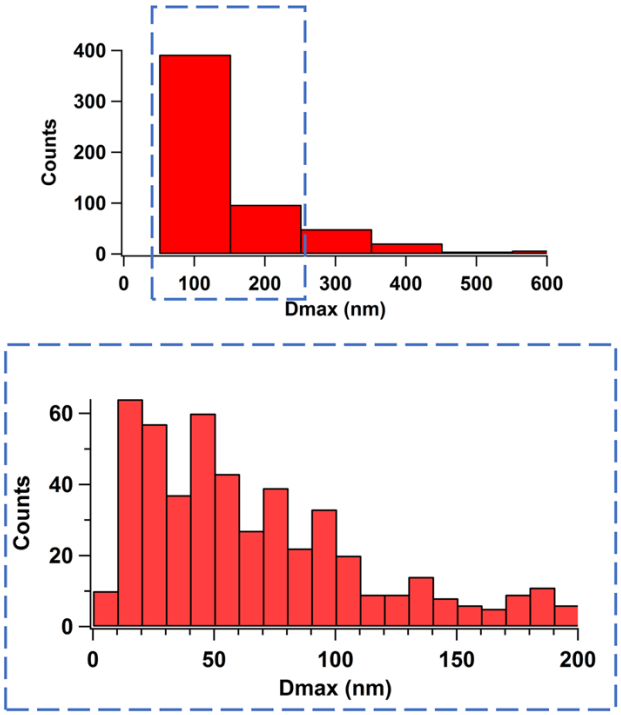

Figure 5. 4. Statistical distribution of flakes lateral sizes expressed as Dmax (=the maximum dimension of the grain in the horizontal plane). The inset (highlighted with a dashed blue line shows a detail of the distribution in the range between 10 and 200 nm.

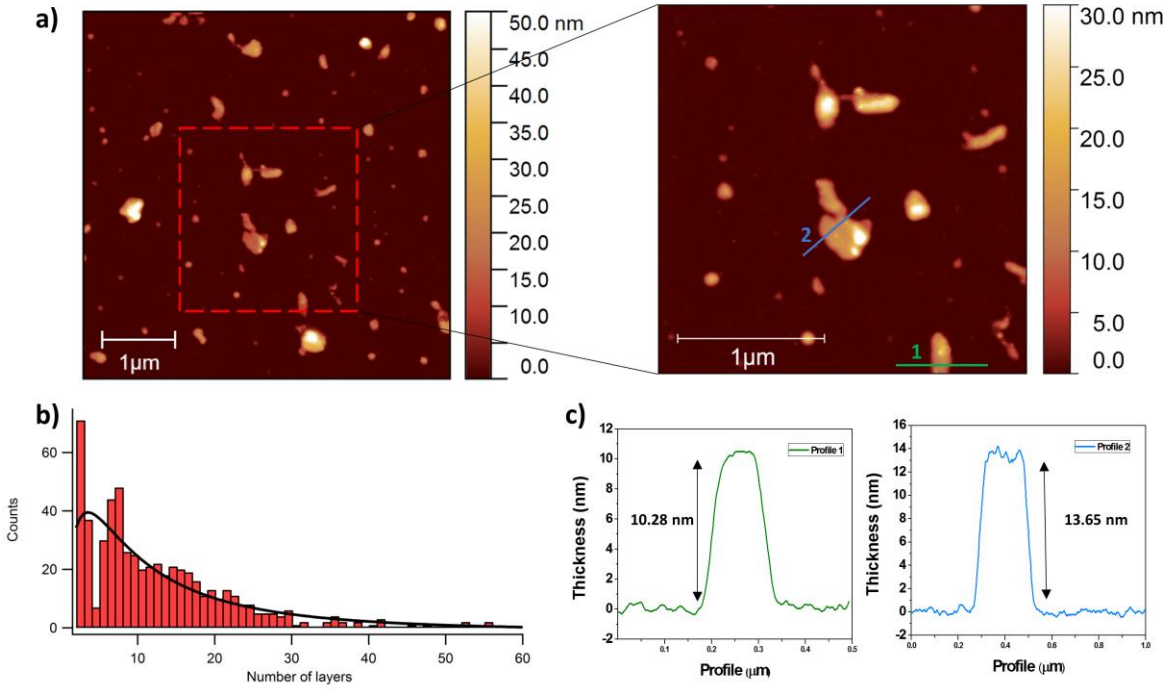

Figure 5. 5. a) (Left) Representative AFM image of MoS_2 exfoliated by UILPE in IPA and deposited on Si n++/SiO_2 by spin-coating. (Right) A zoomed-in AFM of the region indicated in red; b) statistical distribution of thickness after conversion of AFM height to number of layers, considering the monolayer thickness equal to 0.9 nm. c) height profiles of the nanosheets indicated in (b).

The distribution of flakes thickness is also rather broad as shown in AFM images reported in figures **Figure 5. 3**b and **Figure 5. 5**a. The statistical study on the flake thickness determined by AFM - here expressed as number of layers per sheet - indicated that a large part of the flake's population (~54%) has a thickness ranging from 3 to 10 layers per sheet, in agreement with previous reports (**Figure 5. 5**b). Some representative height profiles are reported in **Figure 5. 5**c to let visualize typical flake thicknesses (~10 and 14 nm).

The high polydispersity of the samples was confirmed by other characterization techniques, such as scanning transmission electron microscopy (STEM) and high-resolution transmission electron microscopy (HR-TEM).

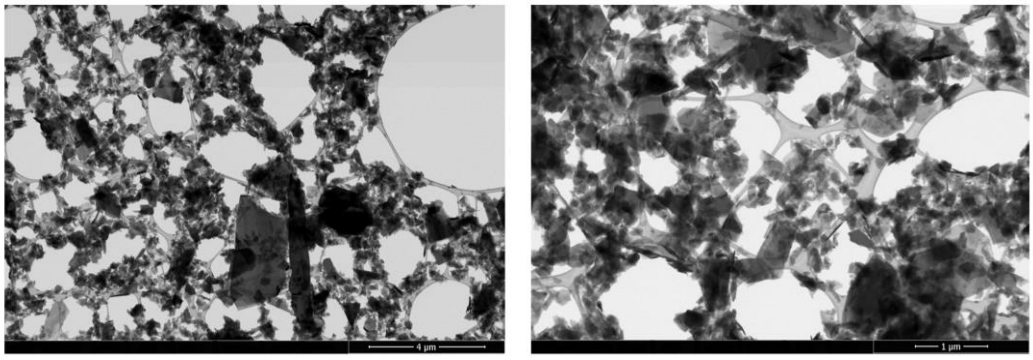

Figure 5. 6. STEM images of MoS_2 nanosheets deposited from a MoS_2 dispersion in IPA by drop-casting on a lacey carbon-coated copper grid.

STEM images (**Figure 5. 6**) show, indeed, a different contrast in the samples, with alternating dark defined areas, which can be qualitatively ascribed to thick MoS_2 sheets or overlapped/aggregated flakes, and lighter regions which indicate the presence of thinner nanosheets. Accordingly, HR-TEM allowed to visualize both thin sheets (**Figure 5. 7**a) and thicker ones, which are composed by more than five layers as it is possible counting from the edge of bended flakes (**Figure 5. 7**b). A study at higher magnification by means of HR-TEM has allowed also to observe the coexistence of 2H and 1T phases within the same flake, as reported in **Figure 5. 8**. Ultrasound-induced LPE is not known to generate the transition between 2H and 1T phase, that we instead observed in the case of the electrochemical exfoliation of MoS_2 *via* Li-ions intercalation (discussed in chapter 4). We indeed believe that the presence of 1T phase, proved by HR-TEM, can originate from the starting material. Such hypothesis was confirmed by the following characterization (e.g. XPS and Raman spectroscopy).

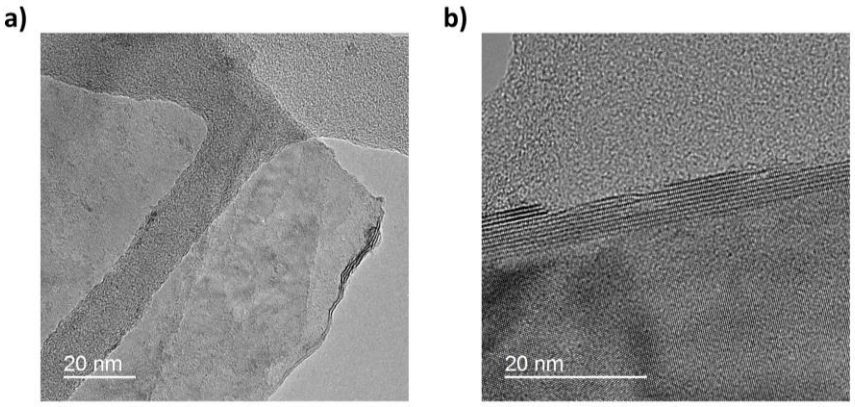

Figure 5. 7. Representative HR-TEM images of MoS_2 folded nanosheets representing a) thin layer flakes and b) thicker ones (number of layers > 5).

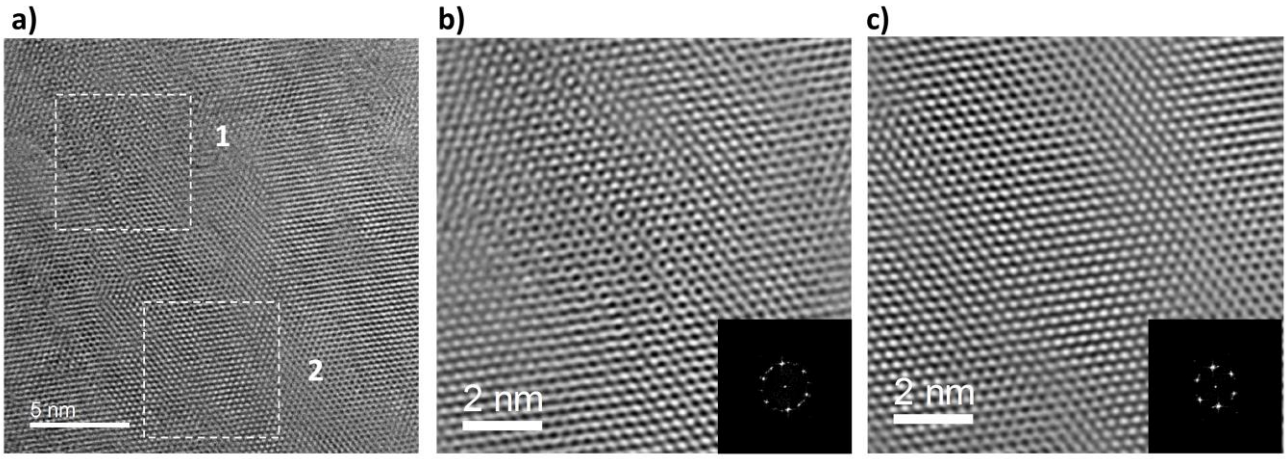

Figure 5. 8. Representative HR-TEM image (a) showing the coexistence of 2H- and 1T- phases within the same MoS_2 flake, which zoom-in are reported in (b) and (c) respectively together with the selected area electron diffraction of the two regions.

The exfoliated material has been further characterized by Raman spectroscopy and X-ray photoelectron spectroscopy. The representative Raman spectrum reported in **Figure 5. 7** shows the characteristic modes of 2H phase, A_{1g} and E^1_{2g}.

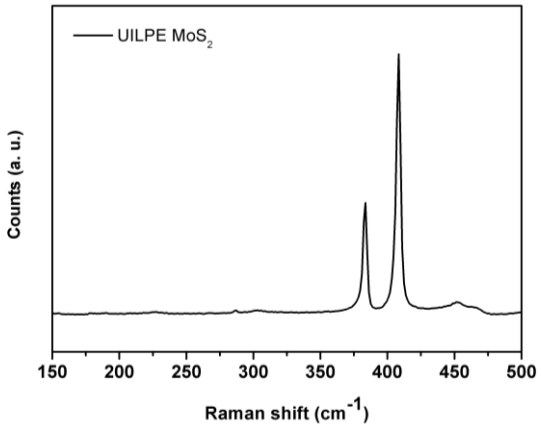

Figure 5. 9. Characteristic Raman spectrum of MoS_2 exfoliated by ultrasounds.

XPS analysis corroborates the semiconducting nature of the produced MoS_2, revealing the characteristic signals of the 2H phase. High resolution spectrum of Mo 3d shows a doublet peak relative to Mo^{4+} $3d_{5/2}$ and Mo^{4+} $3d_{3/2}$ at binding energy of 229.1 eV and 232.3 eV (**Figure 5. 10**a) and sulphur spectrum features the two components S $2p_{3/2}$ and S $2p_{1/2}$ at 161.9 eV and 163.2 eV (**Figure 5. 10**b).

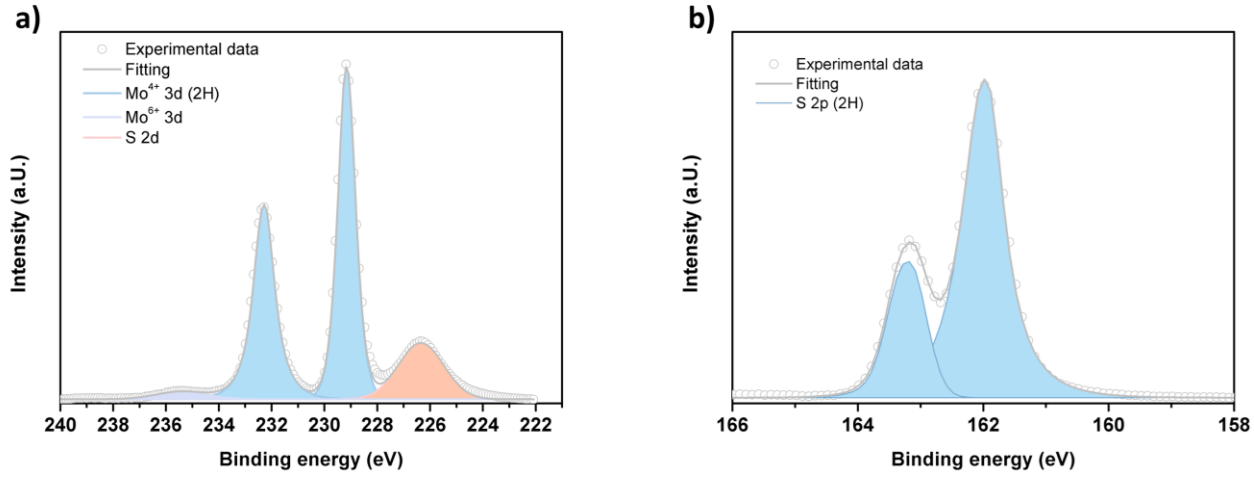

Figure 5. 10. High-resolution XPS Mo 3d (a) and S2p (b) spectra for MoS_2 exfoliated by ultrasound induced liquid phase exfoliation. The spectra were deconvoluted to display the components relative to 2H-MoS_2. Binding energies: 229.1 eV (Mo^{4+} $3d_{5/2}$) and 232.3 eV (Mo^{4+} $3d_{3/2}$),; 161.9 eV (S $2p_{3/2}$)and 163.2 eV (S $2p_{1/2}$)

Indeed, the XPS spectrum of exfoliated MoS_2 appears similar to the spectra obtained from the XPS analysis of bulk MoS_2 (**Figure 5. 11**), indicating that the exfoliation process doesn't affect the overall chemical structure of the material. Moreover, according to the literature and the deconvolution of XPS spectra of exfoliated MoS_2 (**Figure 5. 10**), the sonication approach doesn't generate significant formation of sulphur vacancies confirming that the dominant source of defects are the edges generated during the sonication process. In conclusion, both Raman and XPS analysis do not evidence the presence of significant amount of 1T phase, indicating that overall the material exhibits a semiconducting behaviour. Such findings indicate that the 1T-phase regions revealed by HR-TEM are most likely due to the starting material rather than being induced massively during the exfoliation process.

The as prepared MoS_2 nanosheets were tested as gas-sensing material. In order to fabricate a chemiresistor to detect changes in the nearby environment, e.g. changes in the relative humidity, the sensing material has to bridge the gap between the interdigitated electrodes, ensuring the electrical contact. Therefore, a certain uniformity of the material on large area needs to be reached. This is known to be a key issue for materials prepared by ultrasonication, whom deposition in form of thin film, ideally atomically thick, is rather challenging. Techniques which are commonly used for thin film preparation, like spin-coating, not allow the formation of large uniform films of LPE materials. Drop-casting, instead, lack of reproducibility and do not ensure the uniformity of the deposited material. We developed here a deposition technique which consists of the formation of a film by vacuum filtration of a nanosheets dispersion and consequent transfer of the film on a solid substrate by means of a press. The resulting films appear uniform both at macroscopic and nanoscopic scale, as observed from SEM imaging (**Figure 5. 12**a), even though, at this stage, film homogeneity was limited by the porosity of the filter membrane, which led to the formation of some stripe pattern.

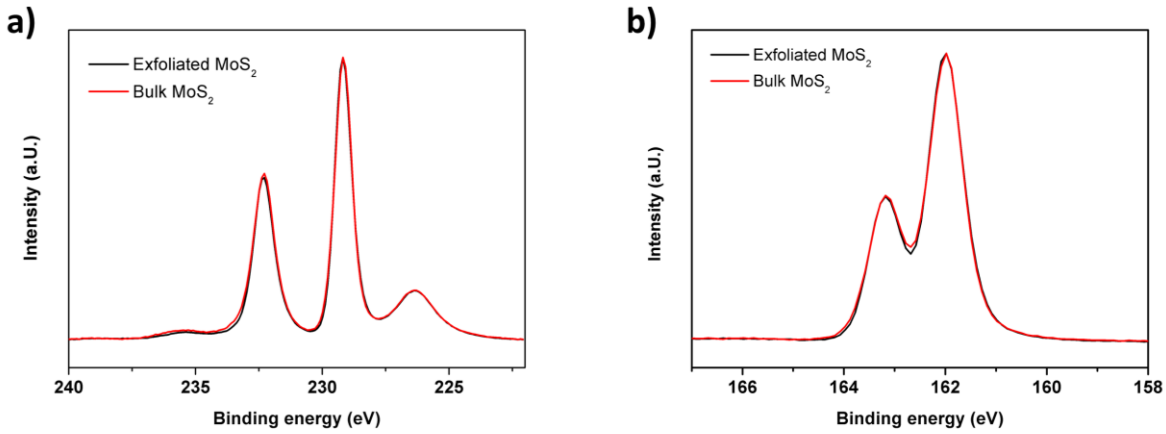

Figure 5. 11. XPS comparison between exfoliated MoS_2 and bulk MoS_2: high-resolution XPS a) Mo 3d and b) S 2p spectra.

Once evaporated gold electrodes on top of the film, the material was tested as humidity sensor. Pulses of humid air were sent on the sample and the electrical response of MoS_2 over time was recorded while applying a constant bias of 5V.

Figure 5. 12b shows the result of two typical pulses of humid air sent on the exfoliated material, in ambient conditions (around 45% RH). This simple experiment allowed to demonstrate that LPE MoS_2 exhibits unprecedented sensitivity to humidity, as evidenced by a significant change in current when short pulses of humid air are sent on the sample's surface. Moreover, the response time of the devices to humidity is extremely fast, taking place in ~ 100 ms, and the process is fully reversible, allowing the recovery of the initial current in about 600 ms (**Figure 5. 13**a).

The sensors were calibrated by recording the evolution of the current at different relative humidity. To this purpose, the electrical measurements were performed in a controlled atmosphere, at constant temperature, within a sealed chamber while increasing RH from 0% to 80% (as shown in **Figure 5. 2**). A commercially available humidity sensor was used as reference to control the relative humidity inside the chamber. The response of the sensor was indicated as ratio $G/G_{0\%\ RH}$ where G is the conductance value in the presence of humidity and $G_{0\%\ RH}$ is the conductance value at 0% RH. The calibration curve allowed to follow and quantify the dependence of the conductance on the relative humidity. When the environmental humidity changes from 0% RH to 80% RH a current variation of 7 orders of magnitude is measured, proving the exceptional sensitivity of the material produced in respect to the state of the art (**Figure 5. 13**b).

In a similar work in which MoS_2 powder is exfoliated at different sonication power and then tested as humidity sensor, Zhang et al., show that the maximum changes in resistance have been observed at RH value of about 60%, where the resistance values changed by a factor of 3. Similarly, a response of few units, at 80% RH, has been reported both before and after functionalization of MoS_2 obtained via Li-intercalation with butyl lithium.[270]

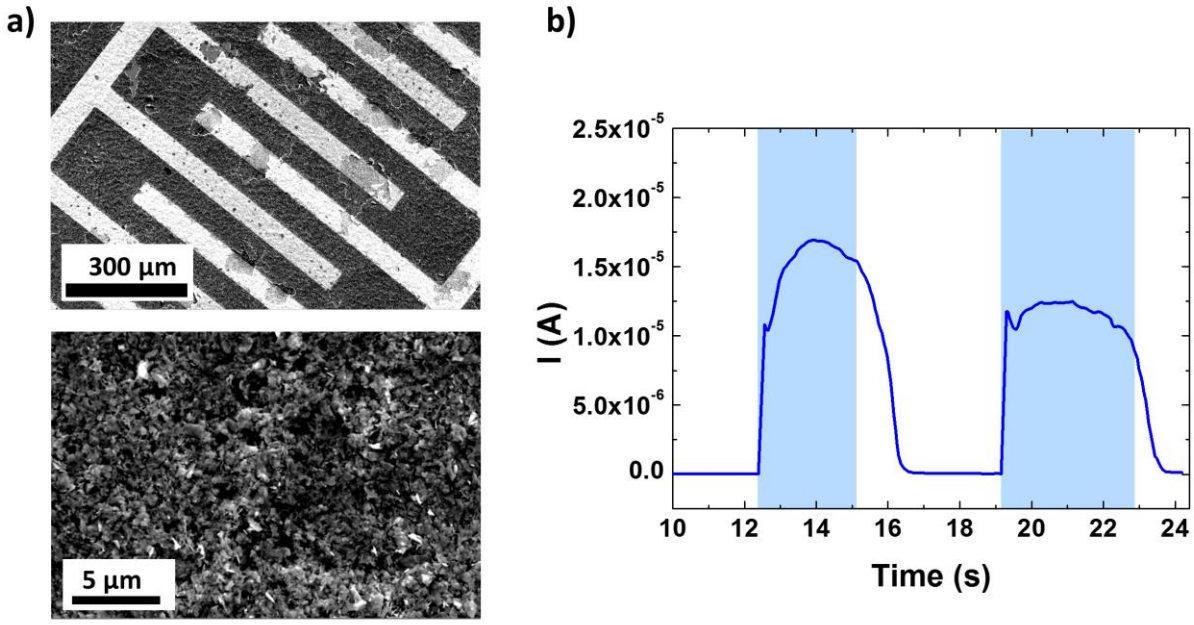

Figure 5. 12 a) SEM images of the gas-sensing chemiresistor based on LPE MoS_2 deposited on Si n++/SiO2 substrate and interdigitated gold electrodes deposited onto the film by shadow mask approach. SEM image show that the sensing material uniformly cover the whole centimetre-scale substrates; b) typical pulses of humid air sent on humidity sensors based on MoS_2 exfoliated by sonication at ~45 %RH.

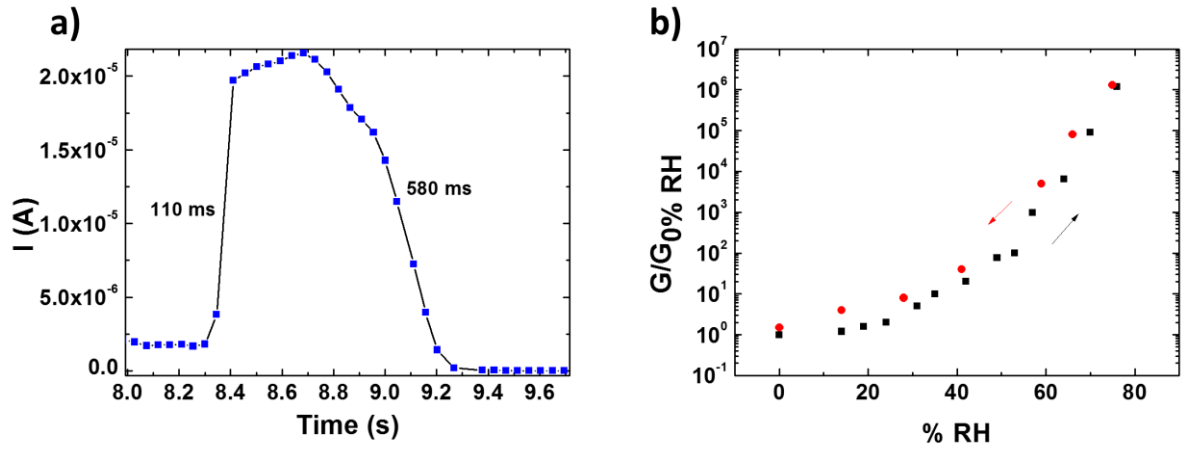

Figure 5. 13 a) Response time of the device for one humidity pulse; b) calibration curve of humidity sensor based on MoS_2 exfoliated by sonication.

Compared to previously reported LPE MoS_2-based sensors, our sensor devices exhibit hence remarkably higher sensitivity. In particular, as shown in the calibration curve (**Figure 5. 13**b), the response of our devices is on the order of 10^3 and 10^6 at 60% and 80% RH, respectively, demonstrating the potential of 2DMs as gas sensors.

This excellent sensitivity is attributed to the large surface area of the material when exfoliated and to the smaller sizes of the MoS_2 flakes, which implies a higher density of reactive edges sites and dangling bonds which can play a key role on the sensing of gas molecules. In their work, Zhang et el., indeed, demonstrated a correlation between the response of the sensors and the sizes of the nanosheets

obtained at different sonication power. In their optimized conditions, e.g. sonication at high ultrasonic power (550W), they reached an average size of the nanosheets of about 100 nm.

The distribution of MoS_2 nanosheets produced with our approach is instead centred below 50 nm and most of the particles have lateral sizes in the range of 20-30 nm (**Figure 5. 4**). The reduced sizes, although obtained working at a lower sonication power (350 W), are due to a prolonged sonication process which lasted 6 hours in or case. On the contrary, in the mentioned work, the material is exfoliated for 1-hour only. Moreover, many other parameters can play a role in such different findings, including different sonicator and medium of exfoliation. Besides increasing edge density, it has been demonstrated that introducing the metallic 1T phase enhance the catalytic properties of MoS_2.[278-279] Therefore, we believe that the presence of 1T phase detected by HR-TEM (**Figure 5. 8**c) in our ultrasound-induced LPE MoS_2 can be considered another factor determining the high sensitivity of the material toward water molecules. Another aspect that could play a key role in the different performances with respect to those reported in Zhang's work is the thickness of MoS_2 films. Recent studies demonstrate that the catalytic performances of MoS_2 electrodes can be optimized by maximizing the electrode thickness till a value of 5 μm, at which is reached the saturation.[280] Similarly, a homogeneous deposition of the sensing material in μm-thick film through stamp-transfer can result in a higher sensitivity to gases molecules than films produced by drop-casting, which performance are discussed above. Alongside the reduced dimensions of the as prepared MoS_2 nanosheets and the morphology of the films, another possible explanation of the high sensitivity of our MoS_2-sensors can be attributed to the employed conditions of exfoliation. The exfoliation of MoS_2 powder was carried out under controlled atmosphere in order to prevent the oxidation of the material. In particular we aimed to avoid the passivation of sulfur vacancies - thermodynamically favoured due to the oxygen isoelectronic nature[281] – during the prolonged exfoliation process. Consequently, a higher density of available (not oxidized) reactive sites could explain the high affinity of MoS_2 films for water molecules, determining a strong change in the electronic properties of the material. Control experiments in which the exfoliation of MoS_2 is performed in air might confirm such hypothesis and contribute to unveil the mechanism of sensing of these devices. The latter is indeed still unclear. The presence of humid air determines an increasing of the current, contrary to past works which show the increase of the resistance of the film when water molecules are absorbed on the surface's sample. This opposite response allows us to hypothesize the occurrence of alternative sensing mechanisms. According with theoretical study,[263] the interaction of small inorganic molecules such as H_2 and O_2 with MoS_2 defects can lead to molecular dissociation. In particular, the molecular dissociation of O_2 is originated from the interaction of the metallic dangling bonds of MoS_2 defects associated to Mo atoms and the electronegative oxygen atoms. These molecules are highly attracted to metallic defects (Mo atoms occupying S vacancies) leading an increase of the adsorption energy that suggest that the molecules will be trapped in the defects.

Such theoretical model was not successfully applicable to water molecules suggesting that a higher barrier need to be overcome to have the same dissociative effects. In our system water molecules can be similarly trapped due to the porosity of the edge-rich MoS_2 films and the application of an external electric field can provide the energy required for the efficient dissociation of water molecules which would explain the positive change in the current, and at the same time the fully reversible process of humidity sensing as shown in Figures 5.11b and 5.12a,b. Such hypothesis needs confirmation, which is beyond the scope of this thesis, but it was partially supported by studies on the selectivity to other small molecules.

The selectivity of MoS_2 based sensor devices was valuated in the presence of vapour of various small molecules such as oxygen, carbon dioxide, acetone, chloroform, ethanol and methanol. **Figure 5. 14**

shows the normalized sensor response (G/G_0) measured for different cycles absorption/desorption of the indicated gas molecules.

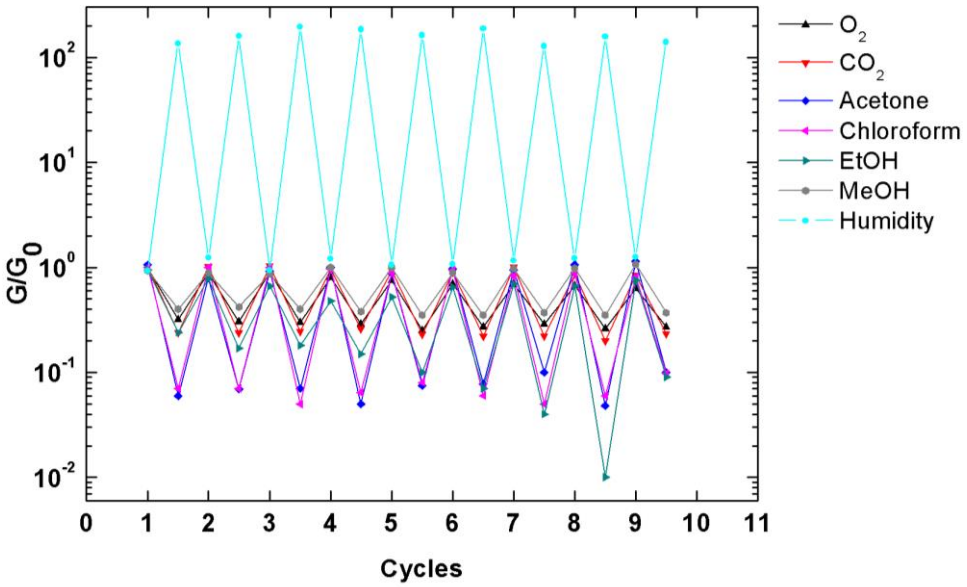

Figure 5. 14. Electrical response of LPE MoS2 based sensors exposed to short pulses of various gases. In this graph each cycle corresponds to an event of absorption and desorption of gas molecules.

Here G_0 and G represent the baseline resistance of the sensor and the change in resistance upon exposure to the different gas molecules. Since this measurement was done in ambient conditions, it is worth point out that while the G_0 of the small molecules were measured in absence of molecule, the G_0 for humidity is measured at approximately 45% RH. MoS_2 devices appear sensitive to all the tested gases (Figure 5.13). Yet, different changes in the conductance of the MoS_2 films were recorded upon exposure to different gases. Besides humidity which gives the most significant response, we can distinguish two different classes of molecules respect to which MoS_2 exhibits different sensitivity. In particular, our measurements reveal a higher sensitivity toward acetone, chloroform and ethanol than to CO_2, O_2 and methanol. This different behaviour may be indicative of different molecular interactions between MoS_2 and the analyte and, therefore, could be useful in the comprehension of the mechanism of sensing in our MoS_2 devices. However, these measurements have been done under ambient conditions, so with a certain humidity as said before. Consequently, we cannot exclude that by sending pulses of other gas and small organic molecules (the latter been propelled by nitrogen gas), we are changing (and most probably decreasing) the relative humidity close to the device. This would affect the electrical response of the sensor, leading to a reduction of the conductivity. In any cases, this suggest that our MoS_2-based sensor has a strong response to humidity. In essence, such experiments allowed us to conclude that our MoS_2 can be considered a good candidate for humidity sensor featuring a high and selective sensitivity towards humidity. Finally, interestingly, the device responds with a decrease of the conductance when vapours of small molecules approach the sample's surface, while only humidity lead to a positive response (increase of G). This result gives also a strong indication in view of propose a possible sensing mechanism, because it show that the origin of the sensing behaviour in our MoS_2 devices has to be attributed to different chemical interactions and possible reactions which occur in the presence of water rather that other molecules.

5.4 Conclusions

In summary, in this chapter we have shown that MoS_2 produced *via* exfoliation in liquid media can be conveniently introduced as active material in gas sensors. We have fabricated MoS_2 nanosheets using a simple method based on ultrasound-induced exfoliation approach which was tailored to obtain large quantities of nanometer sizes nanosheets, including particles with lateral sizes < 50 nm. Thin films were prepared from pure MoS_2 inks (without surfactants or additives) by a facile dry-transfer approach and used to develop large area chemiresistor sensors for gases detection. The MoS_2-based sensors exhibited a very high sensitivity (> 10^6 at 80%RH) towards humidity, high response speed (~100 ms) and fully reversibility.

The results obtained in this work exceed the state of the art of MoS_2 gas sensors measured in two-terminal configuration, whom practical use is mainly limited by the low sensitivity. Recently, a great deal of effort has been devoted to the functionalization of MoS_2 and other 2DMs with molecules which can interact better with the analyte determining an improvement of their sensitivity. From the best of our knowledge, our devices based on pure exfoliated MoS_2 have reached unprecedented sensitivity, even higher than functionalized MoS_2, where changes in resistance of few units are generally recorded. Here, MoS_2 nanosheets-based sensors have displayed a good sensitivity to other small molecules (O_2, acetone, chloroform and ethanol than to CO_2, O_2 and methanol) as well. The different response of the sensors has proved the selectivity of MoS_2 devices towards different gases.

Further investigations are needed to understand the mechanism of our MoS_2 based sensors which can differ from the generally reported sensing mechanisms. For instance, measuring the device in FET geometry would provide information on the doping of MoS_2 and allow to extract relevant parameter if measured in different humidity environment, such as changes in carrier density. A comparison with controlled dimensions flakes would allow demonstrating the edges effects on the gas sensing mechanism, which have been supposed the major cause of the high sensitivity of our devices. Finally, a natural progression of this work, as discussed at the beginning of this chapter, is to investigate on the sensing properties of electrochemically exfoliated MoS_2 where the significant presence of sulphur vacancies can further support our preliminary results.

In conclusion, in this chapter we have proved that MoS_2 prepared by solution processes can be successfully employed as highly sensitive material for the detection of humidity. The possibility of having the sensing material in form of a cost-effective ink paves the way to the fabrication of light and flexible sensing devices.

CHAPTER 6.

MERGING 2D MATERIALS WITH MACROMOLECULAR SYSTEMS: TOWARDS MULTIFUNCTIONAL DEVICES[2]

The great success of graphene and the others 2D materials (2DMs) is due primarily to their intrinsic properties including outstanding electrical, thermal and optical characteristics. Although exceptional, these properties cannot be modulated on demand, as it would be required for the integration of 2DMs in complex multifunctional devices. On the contrary, molecular systems stand out for their versatility. Their structure and properties can be modified and tuned by chemical functionalization, and that has determined their introduction in many technological fields, e.g. biomedicine and organic electronics. Merging these two worlds, i.e. the one of 2DMs with that of molecular materials, represents a promising approach for tuning the properties of 2DMs and/or improving their processability. Introducing new functionalities on 2D systems would allow the design of novel multifunctional systems. Moreover, both the constituents of a multicomponent system, 2D material/ molecular material, might take advantage of their mutual properties.

The ideal and simpler condition to mastering the chemical approach and take full advantage of the combination of 2DMs with functional molecular systems would be having both materials dispersed in a liquid medium. Furthermore, in order for this process to be viable for practical applications, large quantities of the starting materials must be available.

The approaches of exfoliation in liquid phase, that has been introduced in chapters 2 and 5, including ultrasound-induced liquid-phase exfoliation, electrochemical exfoliation, shear exfoliation and the more recent microfluidizzation, not only allow the large production of 2DMs, but they also offer the opportunity of exploit the solution chemistry. Among them, ultrasound-induced LPE is the most established and versatile because can be carried out under a variety of different environmental conditions.[78, 282] Yet, the material produced by ultrasonication features still several drawbacks that hinder most of the forecasted applications. As we have already discussed in chapter 5, the yield of exfoliation in the sonication process, in particular, the number of monolayers present in dispersion, is rather low, so that the formation of continuous large area of monolayers flakes produced by UILPE has been never reported. More generally, the deposition of UILPE materials in thin homogeneous films has always represented one of the major challenges in this field, both because of the low concentrations and the large size polydispersity of the nanosheets. Moreover, the electrical performance of UILPE materials is modest.[283-284]

For the UILPE of graphite into graphene, the use of molecules that non-covalently interact with graphene has been largely explored to overcome some of these issues. In particular, as discussed in chapter 2.1, molecule-assisted LPE approach involves the use of *ad-hoc* molecular systems for

[2] Large part of the work presented within this chapter have been published: T. Leydecker, M. Eredia, F. Liscio, S. Milita, G. Melinte, O. Ersen, M. Sommer, A. Ciesielski, P. Samorì, Graphene exfoliation in the presence of semiconducting polymers for improved film homogeneity and electrical performances, Carbon, 2018, 130, 495–502.

Dr. T. Leydecker and M. Eredia contributed equally to this work.

enhancing the performance of ultrasound-induced LPE process. These molecules act as stabilizing agents and allow to obtain higher concentrations of graphene in dispersion.As the unique purpose of the molecule-assisted exfoliation is the one of enhancing the exfoliation, often, molecules chosen by design were expected not to affect the structure and quality of graphene, being non-functional small molecules like alkanes.

Inspired by the success of molecule-assisted LPE, we opted to exfoliate graphite in the presence of functional molecules that can both act as stabilizer agents and provide functionality to graphene and to the final multicomponent system. We decided to use organic semiconductors (OSCs) for exfoliating graphite, with the final aim to explore the use of graphene as active material for application in electronics.

In this chapter we report on a novel approach of ultrasound-induced liquid-phase exfoliation of graphite powder, that involves the use of π-conjugated polymers, i.e. poly(3-hexylthiophene) (P3HT) or poly[4-(4,4-dihexadecyl-4H-cyclopenta[1,2-b:5,4-b']dithiophen-2-yl)-alt-[1,2,5]thiadiazolo-[3,4-c]pyridine] (PCDTPT). This strategy allowed to produce hybrid systems graphene/semiconducting polymer in a one-step procedure. The polymers, acting as stabilizing agents of graphene flakes, have enabled the exfoliation and the production of homogeneous bi-component dispersions. The presence of the polymer has improved the uniformity of deposition and has allowed the formation by spin-coating of thin films which were used to fabricate Field-Effect Transistors (FETs). Therefore, there are two primary objectives of this study: i) to investigate the effect of *ad hoc* polymers on the exfoliation of graphite by ultrasonication, ii) to explore the potential of the proposed composites graphene/semiconducting polymer as active material in FETs.

After an introduction that lay out the research background, this chapter is divided in two main sections. A section for materials and methods (section 6.2) describes the procedures used for producing few-layer graphene (FLG) by ultrasound-induced LPE in the presence and the absence (control experiments) of the two chosen semiconducting polymers (section 6.2.1); methods and techniques for film preparation (section 6.2.2) and their characterization (section 6.2.3 and 6.2.4) are reported as well. The last section reports the results of this research (section 6.3).

6.1 Introduction

The use of graphene as active material in electronic devices has been hindered by the lack of a bandgap. Yet, combining graphene with semiconducting polymers could allow to create new active layers for FETs with improved performances respect to traditional organic semiconductors (OSCs). Indeed, OSCs perform well but not flawlessly in terms of electrical performances, usually with a high I_{on}/I_{off} but modest mobility. On the other hand, they have a different set of advantages, of which graphene could benefit greatly. Their physical properties can be tuned *via* chemical functionalization,[285-286] they are compatible with low-cost solution processing techniques[287-288] and can be deposited under advantageous conditions (low temperature and ambient pressure), thereby they are suitable for up-scalable processes even on flexible supports.[289] Because of these reasons, several attempts of combining these two types of materials have been reported in the literature.[209, 290-296] Typically, they are based on multi-step procedures relying on the subsequent deposition of graphene and the polymeric semiconductor, exploiting different deposition techniques like spin-coating, ink-jet printing or thermal evaporation.[71, 293-294] In particular, Torrisi and co-workers fabricated the active channel of a transistor by successive printing of graphene ink and poly[5,5′-bis(3-dodecyl-2-thienyl)-2,2′-bithiophene (PQT-12), reaching high electrical performances (mobility of 100 $cm^2V^{-1}s^{-1}$).[71] These

approaches relied on the thermal annealing of the graphene film prior to the deposition of the OSC to remove the high boiling point solvent used for graphene exfoliation, and for fine-tuning of the graphene ionization energy before the OSC deposition by thermal annealing in air. Thus, this process of production is quite cumbersome, but, more importantly, the active channel consists of two separate layers, as graphene layer and polymer layer are deposited one on top of each other. Consequently, structural and electronic interactions between graphene and OSC can be limited due to the face-to-face geometry of their interface.

Aiming at achieving a greater electronic cross-talk between the two components, graphene and OSCs can be blended prior deposition in form of films.[209, 295-296] Recently, for example, it has been demonstrated that UILPE graphene can be co-deposited with a polymeric semiconductor and used in thin-film transistors in order to boost the ambipolar character of the polymer.[209] However, blending graphene with polymers can result in phase segregation between the two components[209] that promote graphene random aggregation,[290] and can lead to the lost in crystallinity of the semiconductor matrix.[291] As a consequence, the deposition of the blend can be poorly controlled.[292] An interesting alternative approach consists in exploiting the exfoliation of graphite in the presence of OSCs in order to promote the homogeneous blending of graphene and polymer. OSCs could, indeed, assist the exfoliation of graphite into graphene, as commonly demonstrated *via* molecule-assisted liquid–phase exfoliation, and act as a dispersion stabilizing agent (DSAs) [83, 297] to stabilize the graphene sheets within the polymer matrix.

Although working with polymers allows to tune viscosity and concentration of the exfoliation medium, playing a role on the dispersion of layered crystals, their use to assist the liquid-phase exfoliation has not been extensively explored. The reasons are multiple, like the complexity of the system, or the low quality of the exfoliation that has been attributed to the bulky polymer that do not slip between the graphitic layers as well as small molecules.[80] Moreover, certainly, the difficulty to get completely rid of the polymer once the material is exfoliated has limited the use of this process for the exfoliation of 2DMs. In our strategy, instead, polymer present in dispersion will not need to be removed after the exfoliation, but rather it will be beneficial for charge transport properties of the final hybrid material.

For achieving optimal performances, the polymer should be chosen in view of its structure, to be able to interact with graphitic basal planes, capacity to transport charges and energetic levels close to the work function of the graphene, i.e. around 5.0 eV.[209]

Here we demonstrate that the addition of the two *p*-type semiconductors, i.e. P3HT and PCDTPT, during the process of ultrasound-induced LPE of graphite in 1,2-orthodichlorobenzene (*o*-DCB) results in the improved exfoliation towards the formation of a few-layer graphene (FLG) and allows to obtain homogeneous polymer/graphene hybrid systems. Moreover, the electrical characterization of graphene/PCDTPT hybrids, when integrated as active layer in bottom-contact bottom-gate FETs, revealed a 30-fold increase of the field-effect mobility if compared to pristine polymer samples.

This result can be attributed to the unique combination of properties of few-layer graphene sheets and semiconducting polymers that has allowed to improve the charge-transport in the channel of the field-effect transistor.

Such findings represent a step forward towards the optimization of graphene exfoliation and processing into electronic devices. Furthermore, this work represents a new opportunity for improving the efficiency of existing technologies, like organic-based field-effect transistors, through the use of graphene.

6.2 Materials and methods

The experiments of UILPE have been carried out by using graphite synthetic flakes, purchased by Sigma-Aldrich (Product No. 332461), as starting material for the production of graphene, together with two polymers, P3HT and PCDTPT. P3HT was synthetized in the group of M. Sommer at the "Institut für Makromolekulare Chemie" in Freiburg. Molecular weights, polydispersity and monomer weights of the two polymers are reported in **Table 6. 1**.

Table 6. 1. Molecular weights, polydispersity and monomer weight of the polymers P(NDI2OD-T2), P3HT and PCDTPT.

Material	Molecular weight (kDa)	Polydispersity	Monomer weight (Da)
P(NDI2OD-T2)	17	1.8	989.5
P3HT	2.1	1.26	166.3
PCDTPT	79	2.5	1520.5

1,2-dichlorobenzene (o-DCB) anhydrous was employed as solvent for the exfoliation process and for solubilizing pure polymers as well. Criteria for selecting the solvent are discussed in detail in section 6.3.

6.2.1 Experiments of ultrasound-induced liquid-phase exfoliation

The exfoliation of graphite in the presence of polymers was carried out by adding a polymer solution (5 mg ml^{-1} in 1,2-dichlorobenzene (o-DCB) to graphite powder at a concentration of 50 mg ml^{-1}. The dispersions were prepared in nitrogen atmosphere and exposed to ultrasounds (frequency of 5 Hz, power of 50 W) for 6 hours by means of a Cup-Horn sonicator (Qsonica: model #431C2). The sonicator was equipped with a recirculating chiller to keep the temperature of the bath constant at 45°C during all the experiment.

Control experiments were prepared by sonication of graphite in pure solvent (o-DCB) in the same operative conditions and keeping the same % w/V. The resulting graphene dispersions were not undergone centrifugation, as it is common practice, but they were used without purification, as done for graphene produced in the presence of polymers.

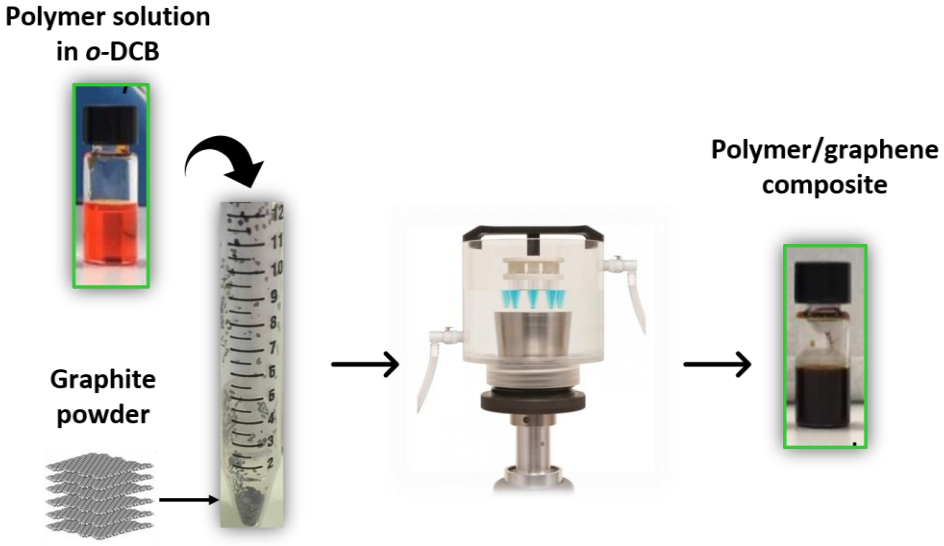

Figure 6. 1 Schematic description of the process of graphite UILPE in the presence of polymers. The two insets in green report the photographs of the polymer solution and the final composite polymer/graphene.

6.2.2 Film fabrication

Bottom-contact bottom-gate configuration transistors were purchased from IPMS Fraunhofer Institute. They consisted of on n++-Si substrates with 230 nm of thermally grown SiO_2 as the gate dielectric (15 nF capacitance) and pre-patterned pairs of gold electrodes with interdigitated geometry as the source and drain. All solutions, composites and devices were prepared and measured under inert atmosphere (N_2 filled glovebox) to avoid oxidative doping of the materials and ensure reproducibility of the experiments. In order to evaluate the impact of graphene on the performance of OSC polymers/graphene composites, a series of control experiments were designed. In particular, control samples, i.e. mono-component films consisting of neat polymer (either P3HT or PCDTPT) and graphene exfoliated in the absence of polymers, were prepared by spin-coating 150 μL solutions/dispersions in o-DCB at the concentration of 5 mg ml^{-1} and 50 mg ml^{-1}, respectively. All the solutions were prepared using 1,2-dicholorobenzene as solvent. The samples were all fabricated by spin-coating at the same conditions of deposition: spin rate of 2500 rpm (acceleration 4000 rpm/s).

6.2.3 Morphological and structural characterization

Graphene, polymer and hybrid graphene/polymer films were characterized by optical microscopy (OM), using an Olympus BX51 optical microscope, and by Atomic Force Microscopy (AFM) with Veeco Dimension 3100 atomic force microscope operating on a Nanoscope IV control unit under ambient condition. Topographic AFM imaging was performed by operating in tapping-mode. AFM images were used to determine the roughness of such films.

Graphene exfoliated with and without polymers have been deposited by drop-casting on TEM grids and characterized by High-Resolution Transmission Electron Microscopy (HR-TEM) in the group of Prof. O. Ersen at the "Institut de Physique et Chimie des Matériaux de Strasbourg (IPCMS)".

Structural characterization has been performed by Dr. F. Liscio in the group of S. Milita (Istituto per la Microelettronica e Microsistemi (IMM) – CNR, Bologna), whom are greatly acknowledged for the deep and supportive structural investigation.

All the thin films were characterized by specular scans using a SmartLab-Rigaku diffractometer equipped with a rotating anode (Cu Kα, λ = 1.54180 Å), followed by a parabolic mirror to collimate the incident beam, and a series of variable slits (placed before and after the sample position). Reflectivity oscillation were fitted until q_z=0.2$Å^{-1}$, making use of a single-layer model on top of the substrate within the Parratt formalism. Thickness and surface roughness of the films were extracted, together with density values. The vertical size of the crystallites was evaluated from the peak width using the Scherrer-formula.

The 2D-GIWAXS (Grazing-incidence wide-angle X-ray scattering) images were recorded at the XRD1 beamline of the Elettra synchrotron facility at Trieste (Italy) using a monochromatic beam with a wavelength of 1 Å. The incident angle of the X-ray beam, αi, was chosen 0.05°, 0.1° and 0.12°, in order to probe the crystal structure at different penetration depth (~10 nm, ~30, >30 nm). The diffraction patterns were recorded using a 2D camera (Pilatus detector) placed normal to the incident beam direction.

6.2.4 Electrical characterization

Devices fabrication and their electrical characterization were performed in our lab. (Nanochemistry laboratory) by Dr. Tim Leydecker, whom I greatly acknowledge.

The electrical performances of the graphene/polymer composites, as well as of the correspondent blank experiments, were studied as thin active films, deposited by spin-coating, in the channel of a bottom-contact bottom-gate FET (channel length L = 20 μm), supported on SiO_2 (detailed description of the film preparation is reported in Section 6.2.2). OFET properties were evaluated under negative gate bias. Experimental data were analysed using the standard field-effect transistor equations. The field-effect mobility was determined in the linear regime from the slope of I_{GS} versus V_{GS} plots.

The ionization energy value of graphene was measured by a Photoelectron Spectrometer, AC-2, by RKI Instruments working at ambient conditions. The analyzed films were realized following the same experimental procedure as employed in the realization of FET devices in order to ensure full consistency with the films that were electrically characterized.

6.3 Results

In this work we have focused our attention on two *p*-type organic semiconducting polymers, P3HT and PCDTPT, whose chemical structures are portrayed in **Figure 6. 2**.

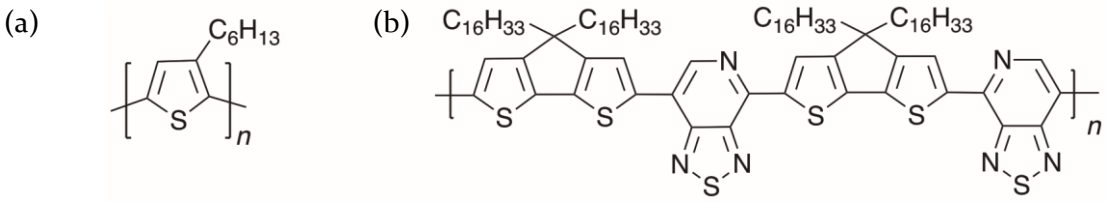

Figure 6. 2. Chemical structure of the two chosen *p*-type polymeric semiconductors: (a) P3HT and (b) PCDTPT.

The choice of these polymers was firstly driven from their HOMO levels, 4.96 eV and 5.16 eV for P3HT and PCDTPT respectively (see **Table 6. 2**), being close to the work function of graphene, that is 4.94 eV (**Figure 6. 3**) as determined by ambient UV photoelectron spectroscopy (See section 6.2.4). In this way, we wanted to ensure a good energy matching between the two materials, promoting the charge transport within the film.

Table 6. 2. HOMO and LUMO energy levels of the conjugated polymers P3HT and PCDTPT.

Material	HOMO [eV]	LUMO [eV]	Band gap [eV]
P3HT[298]	-4.96	-3.04	1.92
PCDTPT[299]	-5.16	-3.70	1.46

All reported values for polymers were obtained from cyclic voltammetry in the cited works.

Known that alkanes possess high affinity for the basal plane of graphene,[83] we have chosen two polymers with alkyl chains, but that arrange themselves differently in the solid state. P3HT, that possesses alkyl side chains and high molecular planarity, is known to form crystalline domains that are responsible for high charge carrier mobilities,[300] so that it is considered a prototypical p-type polymer semiconductor. On the other hand, PCDTPT, due to its limited planarity, is prone to form amorphous structures both at the nano- and meso-scale. Therefore, we suppose that, for regioregular P3HT, the polymer-polymer interaction/stacking into crystalline lamellae, caused by the strong π- π stacking between adjacent core moieties and interdigitation of hexyl side chains belonging to neighbouring molecules, is favoured over the interaction polymer-graphene flakes. On the other hand, amorphous structure of PCDTPT and its rigid backbone may be the key for achieving intimate interconnection between polymer and graphene. Moreover, the longer alkyl chains in PCDTPT, compared to P3HT, may result in a higher affinity for the basal plane of graphite/graphene.[83, 301]

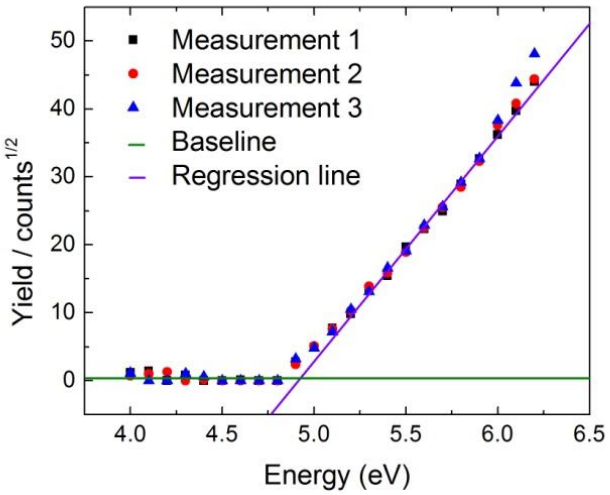

Figure 6. 3. Ambient photoelectron spectrometer measurements. Measurements 1, 2 and 3 represent different spots of the film in which the measurements were performed. The measured ionization energy is around 4.94 eV for every sample.

The exfoliation of graphite flakes in the presence of P3HT or PCDTPT was carried out by ultrasound-induced liquid-phase exfoliation[15] in 1,2-orthodichlorobenzene (*o*-DCB). Mixing of the polymers (5 mg ml^{-1}) and graphite (50 mg ml^{-1}) were sonicated for 6 hours using a Cup-Horn sonicator at a frequency of 5 Hz (power of 50 W). The choice of the solvent is based on its surface tension of 36.6 mJ m^{-2}, [302] that makes it a good candidate for the graphite exfoliation.[303] Moreover, it is a good solvent for both P3HT[304] and PCDTPT.[305]

Known that the UILPE is generally a low-yield process of exfoliation, where a large part of the product is un-exfoliated material that fast precipitate at the bottom of the vial, we have chosen the initial graphite concentration accordingly. It is indeed known that a higher initial concentration of starting material will also give a higher concentration of exfoliated nanosheets.[17, 66] Therefore, we have decided to use a high relative amount of graphite to ensure the formation of high graphene-content films and to maximize the impact of graphene in the electrical performances of the hybrid film. The exfoliation was performed in a cup-horn sonicator because such apparatus offers a more homogeneous ultrasound exposure and, unlike the conventional ultrasonic baths, allows operating at low frequency, thereby avoiding the extensive damaging of the materials during the exfoliation process.

The exfoliation of graphite flakes in the presence of polymers has enabled the production of homogeneous bi-component dispersions (see inset in **Figure 6. 1**) which, owing to the good solution processability of the polymers, were deposited in form of film. The films were prepared by spin-coating as this technique allows to have control over the thickness of the film and obtaining thin homogeneous films, contrary to other techniques like dip-coating, spray-coating or ink-jet printing. The electrical characteristics of the composites polymer/graphene were studied through bottom-contact bottom-gate FETs based on the hybrid film as thin active layer. In order to assess the impact of graphene on the performance of OSC polymers a series of control experiments have been performed. In particular, control samples, i.e. mono-component films consisting of neat polymer (either P3HT or PCDTPT) and graphene (exfoliated in the absence of polymers) were prepared and characterized in the same fashion of the composites (see sections 6.2.1 for a detailed description of samples preparation and characterization).

It is necessary to specify that in this work the term "graphene" will be employed in its broadest sense to refer to the control samples based on exfoliated graphite in absence of polymer. In parallel, more appropriate terms like multiple layer graphene (MLG) or few layer graphene (FLG), will be used when specifically describing the material produced in this work.

Figure 6. 4a-f displays the morphology of these films as investigated by OM and AFM, while the obtained values of field-effect mobilities, I_{on}/I_{off} ratios and Root-Mean-Square Roughness (R_{RMS}) for such films are reported in **Table 6. 3**.

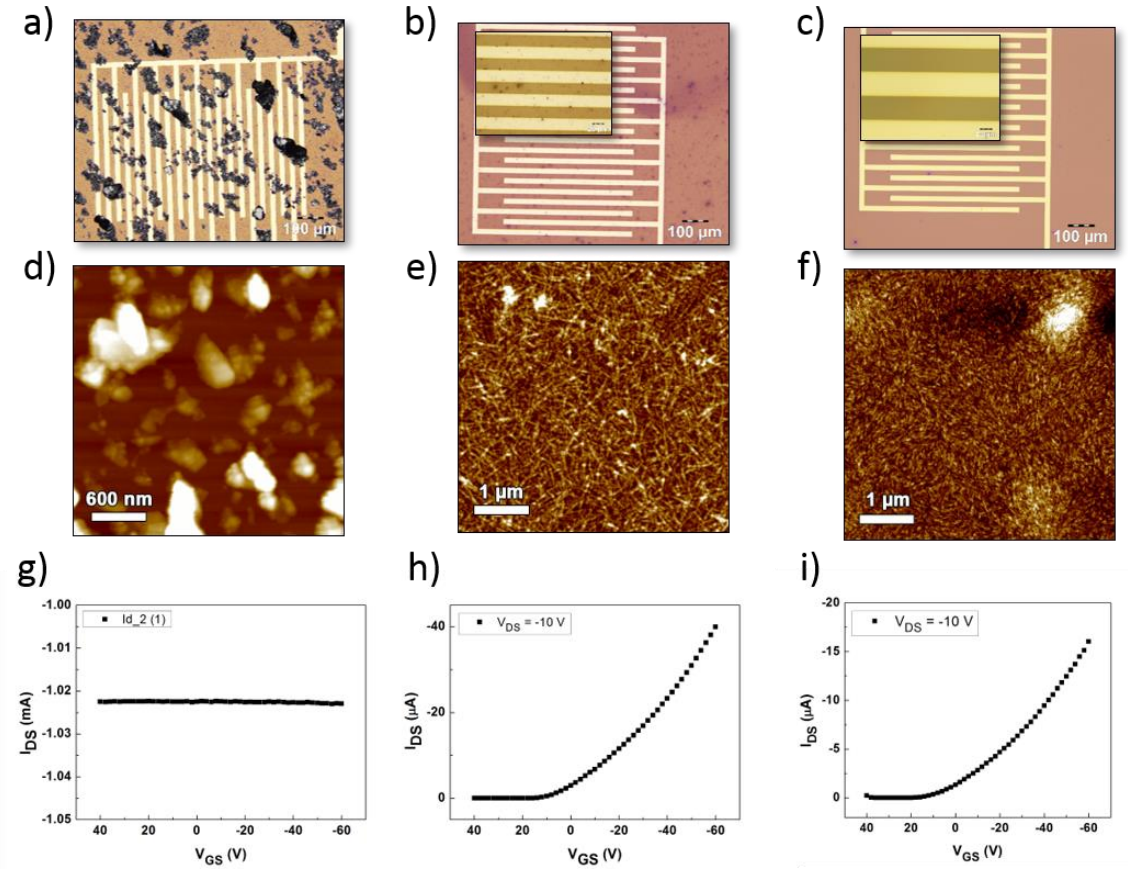

Figure 6. 4. OM, topographical AFM and transfer curves of films produced from (a,d,g) dispersions of neat graphene exfoliated in 1,2-dichlorobenzene, (b,e,h) solutions of pure P3HT [L = 20 µm, VDS = -0.1 V], and (c,f,i) solutions of pure PCDTPT. Z-scales: (d) 72 nm; (e) 48 nm; (f) 8 nm.

Optical and AFM characterization have revealed a poor graphite exfoliation as evidenced by the presence of aggregates of multi-layer graphene (MLG) and large un-exfoliated graphitic particles that can reach tens of μm in lateral size (**Figure 6. 4**a). Such outcome can be in part ascribed to the mild exfoliation conditions employed for graphite exfoliation, according to the parameters used for not damaging the polymer during composites preparation. Moreover, it should be noted that, similarly to polymer/graphene composites, control samples based on graphene were not further purified to separate thin sheets from thicker ones. Typically, indeed, dispersions of single component 2DMs produced through ultrasound-induced LPE are never used directly (see chapter 2, section 2.2.1), but only after separation of the exfoliated flakes from the un-exfoliated material and upon size selection processes, e.g. by ultracentrifugation.[170] Nevertheless, in this work, single or multiple steps of centrifugation were avoided to prevent the occurrence of phase separation between the two components in the case of polymer/graphene composites which have been produced by one step UILPE process. The presence of big aggregates and inhomogeneous deposition of graphene samples can be probably attributed also to other factors, including the high loading of starting material (graphite powder at a concentration of 50 mg ml^{-1}) still coupled with a missed purification step, the employed deposition method, i.e. spin-coating, and the modest interaction of the material with the SiO_2 substrate. On the contrary, both polymeric films appear smooth and homogeneous with a roughness of R_{RMS} = 1-6 nm, as determined on AFM images sized 5×5 μm^2 (**Figure 6. 4**b,c,e,f and **Table 6. 3**).

Table 6. 3. Summary of the electrical performances and Root-Mean-Square Roughness (R_{RMS}) of the pristine and hybrid films.

Material	Filter pore size	μ / $cm^2V^{-1}s^{-1}$	I_{on}/I_{off}	R_{RMS} / nm
Graphene	/	/	1	14.5
P3HT	/	1×10^{-2}	10^5	5.87
PCDTPT	/	4.2×10^{-3}	10^6	1.05
Graphene:P3HT	/	/	1	13.4
Graphene:P3HT	5 μm	1×10^{-2}	10^5	11.2
Graphene:P3HT	0.45 μm	3×10^{-3}	10^6	1.3
Graphene:PCDTPT	/	1.2×10^{-1}	1.4	11.8
Graphene:PCDTPT	5 μm	8×10^{-2}	30	43.2
Graphene:PCDTPT	0.45 μm	5×10^{-3}	10^6	12.8

All reported values were obtained from the transfer curves presented in **Figure 6. 4**, **Figure 6. 5** and **Figure 6. 8**.

Figure 6. 4g-i report the electrical characterization performed on each type of mono-component film. Graphene sample exhibited electrical characteristics that lack of a semiconducting behavior. Such a

result can be ascribed to the presence of the graphite aggregates larger than the inter-electrodic channel as depicted in **Figure 6. 4**a. On the other hand, neat films of P3HT and PCDTPT revealed a semiconducting behavior when spin-coated on a SiO_2 surface. In particular, the bottom-contact bottom-gate transistors exhibited p-type field-effect mobility around 10^{-2} and 4×10^{-3} $cm^2V^{-1}s^{-1}$ for P3HT and PCDTPT respectively and I_{on}/I_{off} exceeding 10^4 for both of them.

Turning now to the hybrid materials, their dispersions, prepared as explained in section 6.2.1, were spin-coated without additional purification steps. In addition, to remove large unexfoliated particles or aggregates, while avoiding phase segregation, the dispersions were simply filtered with polytetrafluoroethylene filters with pore sizes of either 5 μm or 0.45 μm. 5 μm filter were used in order to keep in the dispersion only particles with a size just slightly smaller than the FETs channel length (20 μm). The 0.45 μm filter was selected to retain in the dispersion only the smallest graphene flakes.

AFM height images of the films and transfer curves of the FETs are shown in **Figure 6. 5** and in **Figure 6. 8**. Similarly, also the dispersions of neat graphene, i.e. exfoliated in the absence of the polymers, have been filtered with 5 μm and 0.45 μm and characterized by optical microscopy, AFM (**Figure 6. 6**) and by exploring their electrical properties.

Interestingly, OM and AFM characterization showed that when the material is produced in the presence of P3HT (**Figure 6. 5**a,d), compared to the neat graphene sample (**Figure 6. 4**a,d), present a reduced number of large un-exfoliated particles that indicate a clear improvement of the exfoliation. Together with fragmented graphitic particles, AFM imaging (**Figure 6. 5**d) shows, indeed, the existence of flat and well-defined few-layered graphene flakes which offer a good coverage of the substrate thanks to the unifying presence of the polymer. However, the resulting films based on unfiltered graphene/P3HT system featured electrical characteristics which are similar to those of unfiltered graphene samples, i.e. they do not exhibit any semiconducting behavior (**Figure 6. 5**g). OM and AFM images confirm the assumption that graphene aggregates and un-exfoliated particles are large enough to bridge the electrodes, also in this case (**Figure 6. 5**a). Nevertheless, a slight improvement in the homogeneity of the film is observed (R_{RMS} (graphene) = 14.5 nm; R_{RMS} (graphene:P3HT) = 13.4 nm, as determined on AFM images sized 3×3 μm^2), indicating that the bi-component approach leads to a slightly more favorable deposition compared to the case of neat graphene.

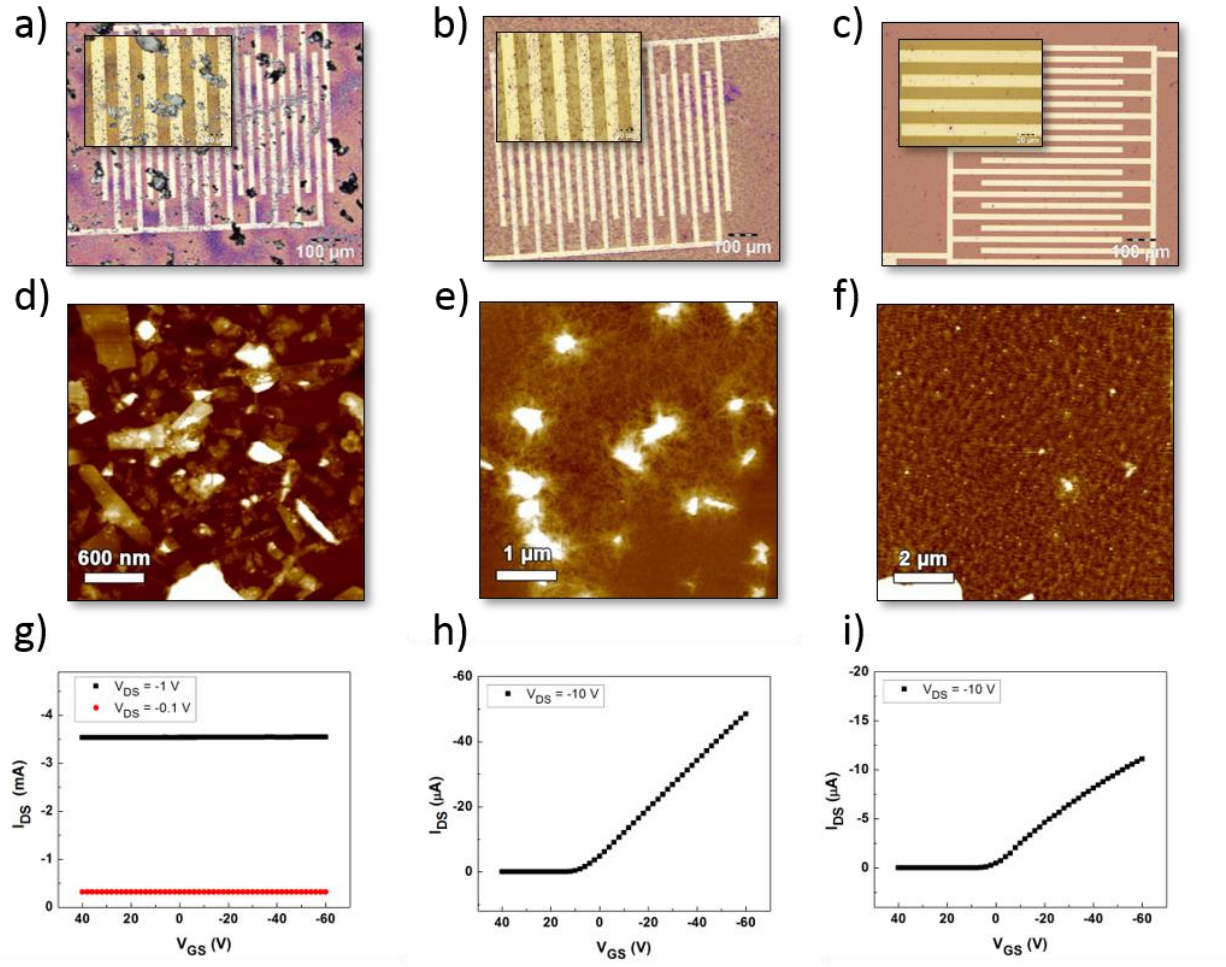

Figure 6. 5 OM, topographical AFM and transfer curves of films produced from dispersions of graphene exfoliated in the presence of P3HT. (a,d,g) pristine solution, as well as after filtering using a pore-sized filter: (b,e,h) 5 µm, and (c,f,i) 0.45 µm. Z-scales: (d) 55 nm, (e) 78 nm, (f) 20 nm.

Upon filtering through a 5 µm membrane, a very homogeneous film including a great amount of µm-sized multi-layer graphene flakes located all over the sample (**Figure 6. 5**b,e) was observed, in contrast with a barely covered substrate obtained after filtration of the neat graphene sample. In this last case, where graphene particles are wide apart from each other (**Figure 6. 6** a,b) it was found indeed that such films do not exhibit (semi-)conducting characteristics, due to the absence of a continuous percolation path for the charges to move from the source to the drain electrode. These results provide evidence for the difficulty of processing UILPE graphene solutions into homogeneous thin films.

Although, homogeneous film P3HT/graphene were obtained after 5 µm filtration, AFM height images evidenced the absence of thin flakes while most of the graphitic particles are smaller than 1 µm. Consequently, the electrical performances of such films are not modified compared to a pristine P3HT films and mobility of 0.01 $cm^2V^{-1}s^{-1}$ with I_{on}/I_{off} of 10^5 are measured. Considering I_{on}/I_{off} close to 1 and the high off-current observed previously in the graphitic material (**Figure 6. 4**g), the recovery of the electrical performances of P3HT (high I_{on}/I_{off}, low off-current, **Figure 6. 4**h and **Figure 6. 5**h), indicates the absence of a continuous pathway of graphitic material in the channel of the transistor. When the dispersion P3HT/graphene was filtered using a 0.45 µm filter, a very homogeneous film was produced (**Figure 6. 5**c,f) but lower field-effect mobilities were measured (**Figure 6. 5**i; $\mu = 3 \times 10^{-3}$ $cm^2V^{-1}s^{-1}$, I_{on}/I_{off} over 10^5).

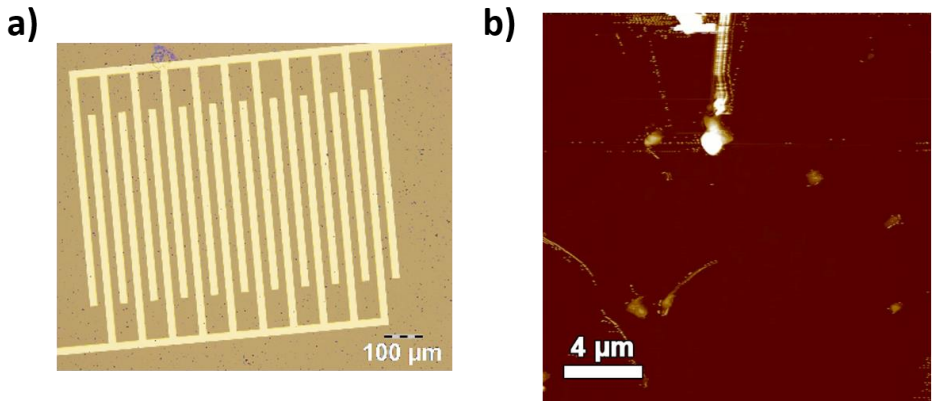

Figure 6. 6. OM (a) and AFM (b) images of graphene exfoliated in *o*-DCB, in absence of organic semiconductors, deposited on SiO_2 after filtering the dispersion through a filter with pores of 5 µm. The imaging of the sample upon filtration with 0.45 µm is not reported here as the substrate result naked. Z-scales: (b) 87.8 nm.

To interpret such results and obtain further in-depth information on our systems, neat P3HT films and P3HT/graphene films, as prepared and after filtration, were characterized by X-ray diffraction in specular and grazing incidence geometries. These measurements revealed that both the solution filtering and the graphite introduction affect the morphology and the polymer aggregation inside the film, i.e. the crystalline order and orientation. The specular scans are reported in **Figure 6. 7**a; morphological parameters of the films (see**Table 6. 4**) were extracted from the reflectivity (XRR) oscillations, observed in the region below q=0.2 $Å^{-1}$. The surface roughness drastically increases when P3HT is blended with graphene flakes (except for the blend obtained filtering by 0.45 µm pores), so that oscillations are damped, and the numerical value cannot be extracted as observed by AFM images.

In line with previous reports, P3HT aggregates in edge-on configuration on SiO_2 surface, as indicated by the presence of the lamellar peak (100) at q = 0.37 $Å^{-1}$ in the specular scan (**Figure 6. 7**), with spacing of 1.7 nm. Interestingly, this peak is clearly observed only for the un-filtered P3HT. The vertical crystalline size extracted from the peak width matches with the film thickness, pointing that P3HT is well-stacked through the film. This is confirmed by the invariance of the reflection when the film is probed at different penetration depths (**Figure A I 1** and **Figure A I 2**).

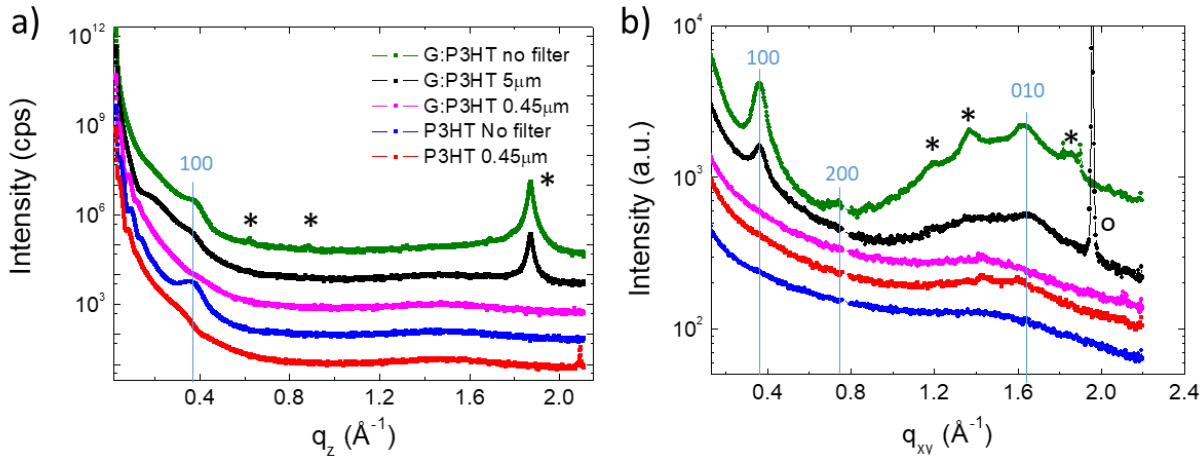

Figure 6. 7. (a) Specular scans, and (b) in-plane integrated intensities of GIWAXS images (**Figure A I 1**) of the P3HT and graphene:P3HT spin-coated films, shifted for clarity. Bragg peaks coming from graphene solution and substrate are labelled by stars and open circles, respectively.

The observation of multiple diffraction orders, i.e. (100), (200) and (300) reflections along the out-of-plane direction in the 2D GIWAXS images (**Figure A I 1** and **Figure A I 2**), points out the high crystalline order typical for this polymer. The introduction of graphene in the blend affects the orientation of the polymer aggregation. Indeed, for un-filtered and 5 μm filtered solution, the lamellar peaks appear along the in-plane direction and decrease along the out-of-plane direction, indicating the addition of P3HT in face-on orientation (likely lying on graphene's surface).

Despite a change in morphology and in the orientation of the polymer aggregation, no change in electrical performances is observed (mobility of 0.01 $cm^2V^{-1}s^{-1}$ and I_{on}/I_{off} over 10^3 in both cases, **Table 6. 3**) with respect to pristine P3HT. This could be due to the low number of graphitic particles upon filtering (**Figure 6. 5**e). When using a 0.45 μm-size filter the polymer appears being amorphous, as proven by the almost disappearance of lamellar peaks (**Figure 6. 7**, **Figure A I 1**,**Figure A I 3**), thereby explaining the lowering of the field-effect mobility.

Table 6. 4. Parameters calculated from XRR and Bragg peaks fitting for P3HT/graphene composites

Sample	Thickness (nm)	Density (g cm^{-3})	Roughness (nm)	Spacing (nm)	Vertical coherence of lamellar stacking (nm)
P3HT No filter	12.25 ± 0.07	0.99 ± 0.01	1.60 ± 0.05	1.687 ± 0.005	14.15 ± 0.08
P3HT Filter 0.45 μm	13.55 ± 0.09	1.03 ± 0.01	2.13 ± 0.06	-	-
Graphene:P3HT No filter	-	-	-	1.686 ± 0.006	10.08 ± 0.09
Graphene:P3HT Filter 5 μm	-	-	-	-	-
Graphene:P3HT Filter 0.45 μm	14.07 ± 0.06	1.18 ± 0.03	1.96 ± 0.05	-	-

Surprisingly, a different behavior is observed when graphite exfoliation is exfoliated in the presence of PCDTPT. PCDTPT/graphene composites and the respective films were prepared and characterized following the same procedures described for P3HT case. OM and AFM images as well as transfer curves are presented in **Figure 6. 8**. The presence of PCDTPT during the exfoliation of graphite determine the formation of homogeneous PCDTPT/graphene films as evidenced by both optical and AFM characterization. These films contains a relatively high concentration of exfoliated graphene flakes and they do not feature any large un-exfoliated particles or aggregates (**Figure 6. 8**a,d). Consequently, unlike previous cases of pure graphene (**Figure 6. 4**g) and hybrid graphene/P3HT (**Figure 6. 5**g), for graphene/PCDTPT hybrids the transfer curves do not feature high I_{DS} current unaffected by V_{GS} (**Figure 6. 8**g).

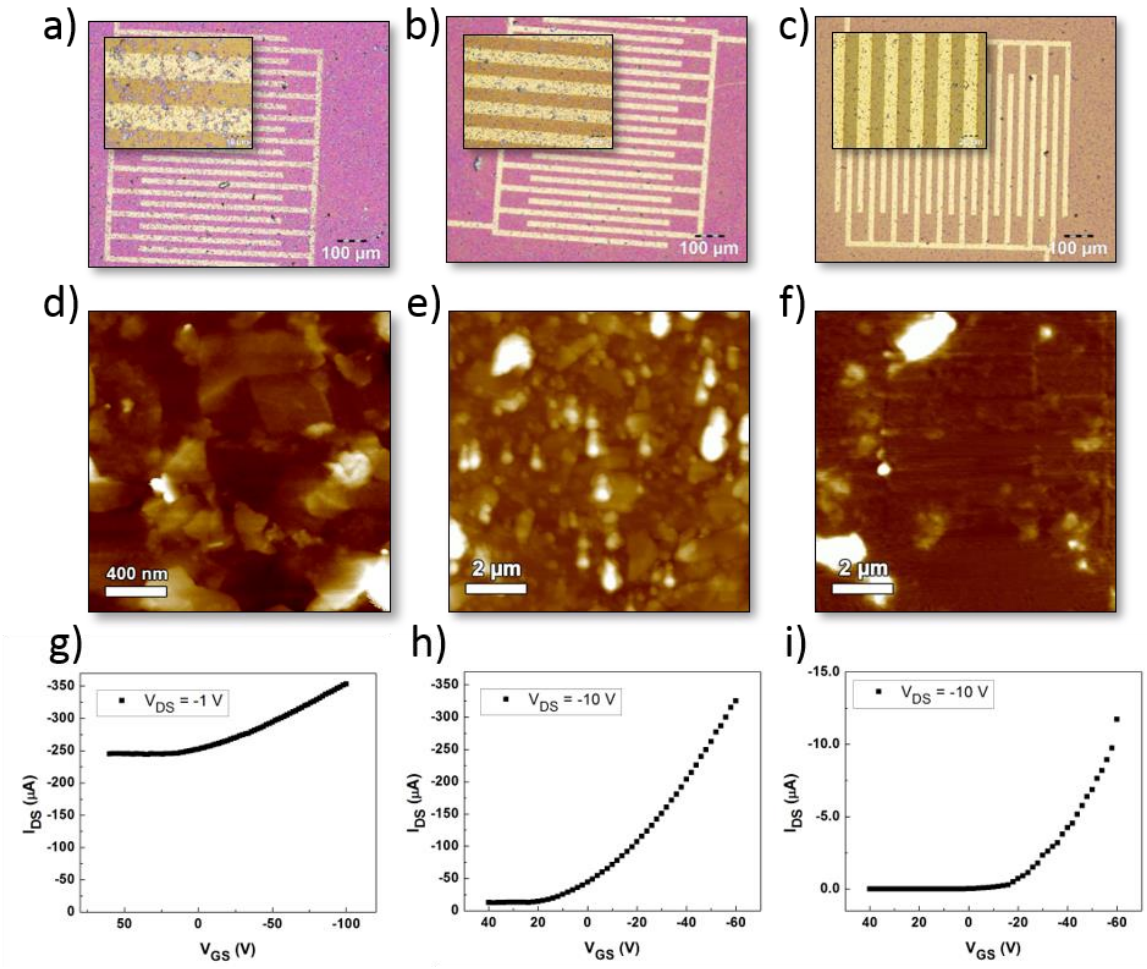

Figure 6. 8. OM, topographical AFM and transfer curves of films produced from dispersions of graphene exfoliated in the presence of PCDTPT. (a,d,g) pristine solution, as well as after filtering using a pore size of (b,e,h) 5 µm, and (c,f,i) 0.45 µm. Z-scales: (d) 86 nm; (e) 358 nm, (f) 77 nm.

These results are particularly remarkable since they indicate that PCDTPT promotes the exfoliation of graphite, forming a well-intermixed bi-component material that can be processed into homogeneous films. Unfortunately, the determination of the efficiency of the two processes, e.g. exfoliation in the presence of P3HT and PCDTPT, is hindered by the presence of the polymer and the high polydispersity of the samples, this latest accentuated by a missed proper flakes selection process. The presence of the polymer, that it is difficult to completely remove, precludes indeed the possibility to perform a statistical study of flakes thickness, for example, by means of AFM, that would allow to quantitatively discriminate the two samples in terms of yield of thin layers. Alternatively, the samples have been characterized by HR-TEM but this analysis didn't show any differences among the samples due to their highly polydispersity (**Figure 6. 9**). However, a further proof of a more efficient exfoliation is given by the roughness of the film - R_{RMS} (graphene:PCDTPT) = 11.8 nm - that is significantly lower compared to pristine graphene film - R_{RMS} (graphene) = 14.5 nm - and graphene:P3HT- R_{RMS}= 13.4 nm - as determined on 3×3 µm^2 and 2×2 µm^2 AFM images.

This difference in the quality of the exfoliation, as evidenced by OM and AFM imaging, can be ascribed to the different molecular structures of the two polymers. PCDTPT is indeed a more rigid polymer compared to P3HT, featuring also longer alkyl chains, that could explain its higher affinity for graphene.

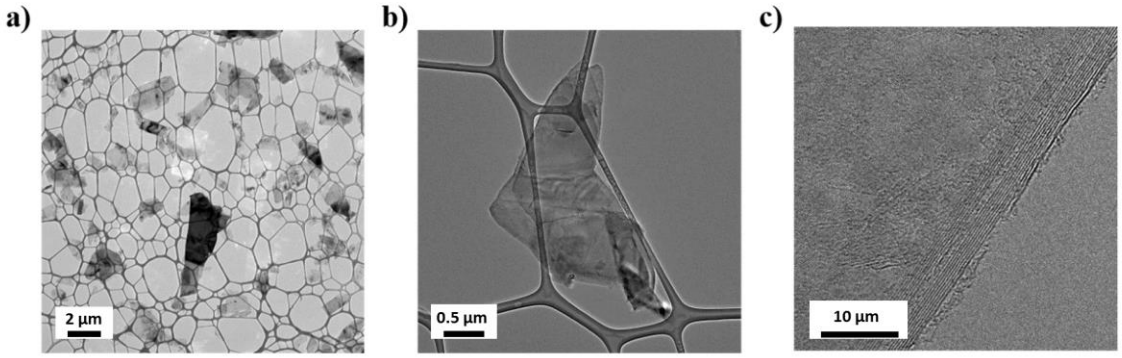

Figure 6. 9. Transmission electron microscopy analysis of graphene prepared by Ultrasounds-Induced Liquid-Phase Exfoliation of graphite powder in the presence or absence of conjugated polymers (P3HT, PCDTPT). a) TEM image of graphene nanosheets produced in *o*-DCB in absence of polymer; b) TEM image of an individual graphitic flake after exfoliation in the presence of P3HT; c) HR-TEM image of the edge of a multilayer graphene sheet produced in the presence of PCDTPT.

Furthermore, the recorded transfer curves did not display the typical behavior of films containing big graphitic particles bridging the electrodes. On the contrary, the resulting transfer curve (**Figure 6. 8**g) is an addition of current issued from graphitic material and the tested polymer, implying that both materials play an important role in the charge carrier transport between the source and drain electrodes. The measured field-effect mobility of the hybrid films exceeded 0.1 $cm^2V^{-1}s^{-1}$, being 30-fold greater than pure PCDTPT films.

The structural characterization of these films, e.g. neat PCDTPT films and graphene/PCDTPT films as prepared and after filtration, by means of X-ray diffraction in specular and grazing incidence geometries, allowed to discover that the hybrid PCDTPT/graphene film is composed of two different populations of aggregates: one with edge-on configuration on silicon oxide and the other face-on on graphene surfaces. Indeed, the analysis of the pure PCDTPT film showed typical features, e.g. (100) and (010) reflections (the latter coming from the π-π stacking periodicity) appearing along the out-of-plane and in-plane directions, respectively (**Figure A I 7**,**Figure A I 8**), revealing that the neat PCDTPT polymer aggregates with edge-on orientation. On the other side, with the introduction of graphene, the (100) and (200) lamellar peaks along the specular direction (**Figure 6. 10**, **Figure A I 7**, **Figure A I 9**, **Figure A I 10**) broadens, whereas they appear narrower along the in-plane direction, indicating the interaction between PDCTPT and graphene surface induces the polymer to self-organize in a face-on configuration.

This explains the electrical performance of such hybrids. In fact, while the I_{on} is mostly, yet not exclusively, dependent on the layer of semiconductor at the interface with the dielectric, the I_{off} is mostly dependent on the bulk of the semiconducting film. Therefore, the observed transfer curve is a combination of charge transport at the interface (PCDTPT aggregated in edge-on configuration, high I_{on}/I_{off}, low current) and charge transport in the bulk (PCDTPT aggregated in face-on configuration on graphene, high I_{on} and I_{off} currents).

While in P3HT/graphene hybrid, FLG was removed upon filtration (**Figure 6. 5**e), films produced from the filtered PCDTPT/graphene system still contained some FLG, demonstrating a stronger interaction of graphene with the polymer (**Figure 6. 8**e), that is further proved by similar roughness measured for all the film, except for the non-filtered one, where the high roughness is due to the presence of thick

sheets (**Table 6. 5**) Moreover, the absence of Bragg reflections on both specular scan and GIWAXS images (**Figure 6. 10**, **Figure A I 7, Figure A I 9**) after filtration of neat PCDTPT, combined with the fact that the film thickness does not change when the sample is prepared from filtered solution (**Table 6. 5**).suggests that small aggregates are already formed in solution and successively transferred to the substrate surface. It could be that the filter removes the aggregates (e.g. resulting from the self-aggregation of the longest polymers) and consequently the polymer self-organizes in amorphous phase once deposited on the surface.

AFM images showed a lower concentration of graphene particles after filtering of the solution using a 5 µm pore size filter. Consequently, the slight reduction in the mobility that is accompanied by a large decrease of the conductivity can be explained with the reduced amount of graphitic material within the film (**Figure 6. 8**e). On the other hand, filtration with 0.45 µm membranes lead to the presence of very few small graphene aggregates within a layer of PCDTPT that does not seem to play any role, so that the mobilities of such film result comparable to pure PCDTPT films.

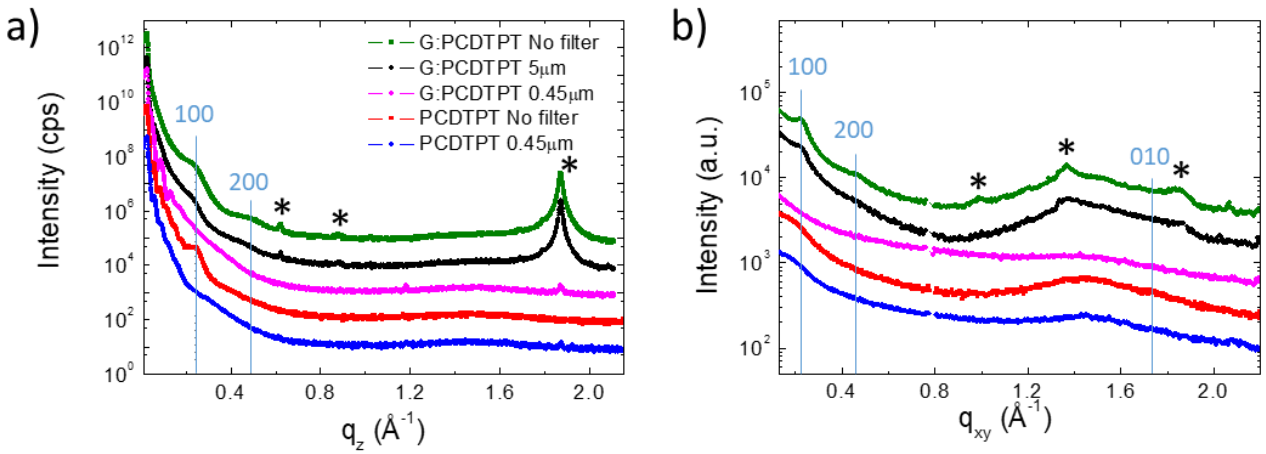

Figure 6. 10. (a)Specular scans and (b) in-plane integrated intensities of GIWAXS images (**Figure A I 7**) of the PCDTPT and graphene:PCDTPT spin-coated films, shifted for clarity. Bragg peaks coming from graphene solution are labelled by stars.

Table 6. 5 Parameters calculated from XRR and Bragg peaks fitting for PDCTPT/graphene composites

Sample	**Thickness (nm)**	**Density (g/cm^3)**	**Roughness (nm)**	**Spacing (nm)**	**Vertical coherence of lamellar stacking (nm)**
PDCTPT No filter	22.21 ± 0.10	0.80 ± 0.03	1.54 ± 0.09	2.60± 0.01	13.2± 0.2
PDCTPT Filter 0.45 µm	20.4 ± 0.1	0.58 ± 0.04	1.6 ± 0.1	-	-
Graphene:PDCTPT No filter	-	-	-	~2.6	< 10
Graphene:PDCTPT Filter 5 µm	7.6 ± 0.2	0.67 ± 0.04	1.8 ± 0.1	~2.6	-
Graphene:PDCTPT Filter 0.45 µm	13.91 ± 0.03	0.96 ± 0.02	1.39 ± 0.02	-	-

6.4 Conclusions

The purpose of the present study is merging 2DMs with molecular systems to explore the possibility of modulating and/or improving 2DMs performances. In particular, in this work, graphene has been combined with organic semiconductors with the final aim of introducing the hybrid system graphene/OSCs as active material in electronics.

A novel one-step procedure has been developed to produce graphene *via* ultrasound-induced liquid-phase exfoliation directly within a suitably selected polymer matrix that is employed as exfoliation medium. Such approach turned out to be ideal for obtaining homogeneous bi-component graphene/polymer hybrid systems. Indeed, even if the exfoliation was performed in very mild conditions, strong interactions between graphitic material and the organic semiconductors have determined an improved exfoliation of the material compared to the exfoliation performed in *o*-DCB. As a consequence, the exfoliated material is homogeneously intermixed with the polymer, without meet with phase segregation. However, this study has shown that the selection of an adequate polymer is the key parameter for achieving a higher quality of the material, as proved by an improved exfoliation when graphene is produced in the presence of PCDTP, rather than P3HT.

This strategy of merging graphene with *ah-hoc* macromolecular systems during the production phase has allowed of improving graphene processing as well. In particular, when graphene is produced in the presence of PCDTPT, it can be processed in uniform large area thin films simply by spin-coating. In these films graphene flakes homogeneously cover the whole substrate, while being embedded in the polymer matrix. In this way, it is overcome the general issue of obtaining non-uniform random depositions of graphene that generally are limited to small areas, and which are common when

attempting to produce thin films. GIWAXS data provided further evidence that FLG exfoliated in the presence of PCDTPT exhibits to good coverage once spin-coated, with homogeneous polymer aggregation along the film thickness. As a result of the homogeneous intermixing of the two components, higher electrical performance can be achieved as proved by a 30-fold improvement of the mobility when PCDTPT is combined with graphene and introduced as thin active layer in field-effect transistors. These performances were obtained from unfiltered solutions, highlighting the role of aggregation at the solution stage of fabrication. On the other hand, the study of filtered dispersions demonstrated that it is possible to modulate the electrical performances of hybrid systems to achieve the desired trade-off between mobility and Ion/Ioff ratio, thereby giving proof of the high versatility of the developed approach. Furthermore, investigation of the differences in aggregation between bulk and semiconductor/dielectric interface lead to better understanding of the electrical characteristics measured in hybrid graphene/polymer films.

One source of weakness of this study was the use of mild experimental conditions. Further studies could be performed to assess the effect of a more powerful sonication on the considered system, aiming to achieve a better exfoliation, that although highly improved respect to the process in absence of the polymer, remain still poor, as evidenced by the presence of thick graphene sheets. Moreover, if necessary, an alternative purification procedure may be designed to maximize the number of thin graphene layers playing an active role on the hybrid systems. Despite its exploratory nature, this study is a gateway to optimization of graphene exfoliation and its deposition, and to the improvement of the performance of active layers in FETs, as it highlights the importance of combining 2DMs with adequate molecular systems for improving exfoliation and deposition of 2D systems, as well as for obtain new hybrid systems with improved electrical performance respect to the single components.

CHAPTER 7.

GENERAL CONCLUSION AND OUTLOOK

This PhD thesis has been focussed on the production of 2DMs (e.g. graphene and MoS_2) by exfoliation in liquid media and explored their potential applications in the electronics field. Particular attention was paid to the ultrasound-induced and electrochemical exfoliation processes, which are respectively the most established methods of 2DMs' exfoliation in liquid media and the most promising for their mass production. In each chapter, the morphology and structure of produced materials have been characterized. Field-effect transistors (FETs) and resistors were fabricated to reveal the electrical performances of individual sheets or films, highlighting their potential use in various fields including electronics and sensing.

Since electrochemical exfoliation (EE) approach is just emerging in the community, the knowledge on involved mechanisms and properties of the electrochemically exfoliated materials are still limited. In the first experimental chapter of this thesis, we aimed at shedding light on structure and properties of graphene and MoS_2 produced by means of electrochemical approach, in view of outlining their potential applications. To this purpose, a comprehensive structural characterization of the materials was combined with the study of their electrical characteristics.

By means of X-ray photoelectron spectroscopy, we have demonstrated the versatility of the electrochemical approach with respect to other liquid-phase exfoliation methods. We showed indeed that, *via* electrochemical exfoliation, it is possible to produce graphene with different content of oxygen functionalities depending on the employed parameters. Although, in anodic conditions, the oxidation of the exfoliated material is unavoidable, we proved that electrochemical exfoliation can yield to the mass production of a material that largely differs in its structure and properties from graphene oxide. Furthermore, if necessary, a few-seconds microwave treatment can be employed. Upon such post-treatment, a large part of oxygen functionalities can be successfully removed, while keeping unaltered the properties of the material. Such findings, supported by a combination of structural and electrical characterization performed both at single flake level and on film, allowed to conclude that the electrical performances of electrochemically exfoliated graphene (EEG) – which exhibits field-effect mobilities of 1-10 $cm^2V^{-1}s^{-1}$ – are hindered by the presence of structural defects in EEG basal plane, rather than by the content of oxygen. For the first time, in this work nanoscopic mechanical defects were revealed though morphological characterization of the flake's surface by AFM, combined with structural information obtained by Raman spectroscopy ($I_D/I_G \sim 1.5$). Their formation has been attributed to the rather invasive nature of the process of exfoliation, which requires further optimization for yielding high-quality graphene. To allow the use of EEG material on large scale, we developed a very effective method for the production of large area thin films which exhibit very similar electrical characteristics to single flakes, demonstrating hence that the electrochemical approach, in combination with proper deposition methods, provides the opportunity for introducing graphene in low-cost flexible (opto-) electronic devices. Furthermore, the emergence of the *n*-conductivity in EEG upon thermal annealing, reported here for the first time, lead to an ambipolar transport which may be of interest for the development of logic circuits.

To explore the versatility of the electrochemical approach towards the production of other 2DMs, while avoiding their oxidation, we have developed an alternative strategy for the exfoliation of MoS_2 which exploits the cathodic intercalation of positive ions. By using an electrolyte based on DMSO-solvated lithium-ions, we proved the facile exfoliation of a MoS_2 crystal in 1 to 3 layers nanosheets, featuring a higher amount of 2H-phase (~60%) compared to existing approaches, and with the further advantage of operating in ambient conditions. We succeeded in improving the electronic properties of FETs based on single flake EEMoS_2 through a combination of vacuum annealing and defect healing with short linear thiolated molecules, reaching μFE values up to 2×10^{-2} cm^2 V^{-1} s^{-1} and $I_{on}/I_{off} \approx 100$. Such findings, combined with XPS characterization, suggested that the electrochemical approach can induces in MoS_2 the formation of sulfur vacancies. The electrochemical approach can be considered hence an effective exfoliation method and, at the same time, a simple and low-cost method for defect-engineering of pristine MoS_2 - compared to commonly used approaches such as ions bombardment, electron irradiation, thermal annealing, plasma treatments, *etc*. The presence of sulfur vacancies is considered a source of improved chemical reactivity of the material compared to pristine MoS_2. This aspect could be conveniently exploited, for example, in the field of sensors.

The introduction of 2DMs in the field of gas sensors can consent the miniaturization of sensing devices and could, in principle, even improve the sensitivity of such devices owing to their high surface area available for the absorption of environmental species. In the second experimental chapter (chapter 5) we preliminary explored the use of MoS_2 nanosheets as sensor of humidity, by producing the material *via* ultrasonication. Chemiresistors based on homogeneous MoS_2 thin films showed unprecedented sensitivity towards humidity, over 3 orders of magnitude higher than previous reports. Our devices exhibit a 7 orders of magnitude current change with relativity humidity varying from 0% to 80% RH. Their response to humid air is fully reversible and fast (~100 ms). Such high sensitivity was attributed to the reduced particle sizes (~50 nm), but could be also ascribed to other parameters, including the high homogeneity of the film within the channel as well as the thickness of the film. These results highlight the potential of liquid-phase exfoliated MoS_2 as humidity sensor and demonstrate the feasibility of large area sensing devices based on 2DMs.

With the aim of finding the keystone for modulating the physico-chemical properties of 2DMs, in chapter 6, we developed a strategy for successfully merging 2DMs with molecular systems, exploiting the liquid-phase exfoliation approach. By performing the ultrasonic exfoliation of graphite flakes directly within a semiconducting polymer matrix, e.g. P3HT and PCDTPT, homogeneous graphene/polymer composites were deposited in form of thin films (8-15 nm) for fabrication of field-effect transistors. However, the choice of the polymer is crucial for having a strong interaction between the two components. A clear enhancement both of the graphite exfoliation and electrical performance of the final devices was observed in the case of PCDTPT composites, as demonstrated by a 30-fold improvement of the mobility measured for PCDTPT/graphene hybrid system compared to the pure polymer. We demonstrated hence that the liquid-phase exfoliation method can be successfully employed for "bridging" graphene with molecular systems leading to remarkable advantages such the better-quality 2D ink processing, as well as, the formation of new multicomponent systems for electronics that feature superior field-effect mobility compared to the bare organic semiconductor thanks to the presence of graphene.

In conclusion, although some limitations need to be overcome to improve the quality of the exfoliated materials and fully benefitting of the extraordinary properties of 2DMs, liquid-phase exfoliation approaches offer a good trade-off between quality and quantity of produced material. This aspect, together with improved methods of processing from liquid-phase makes possible many of the foreseen application for graphene and other 2DMs.

Depending on the employed exfoliation method, the produced material can be more or less defective which is a critical factor for their introduction in devices in view of the chosen application. Owing to this versatility, liquid-phase exfoliation approaches consent to cover a wide spectrum of applications. Electrochemical exfoliation succeeds, for instance, in producing large and atomically thin sheets ideal for low-cost flexible and transparent electronic devices. Moreover, at the same time, the gram-scale production of porous materials is offering great opportunities for energy related applications. On the other hand, ultrasonication approach results convenient for the production of composites as well as permit of obtaining high preforming materials for gas sensing. Further optimization of LPE methods in eco-friendly solvents will be the subject of future efforts in order to meet industrial demand and safety regulations.

So far, a great attention has been given to the methods of exfoliation investigating on the effects of various operative conditions with the principal objective of achieving high efficiency of the processes (high yields of exfoliation in short time). Yet, the development of new systems based on 2DMs requires a detailed understanding of the properties of these new materials, supported by a morphological and electrical investigation of the materials, as reported in this work. This thesis aims to stimulate other work in this direction for a deep awareness of 2DMs and their potential. The processing of inks is a key parameter for the operation of devices, as well. On the basis of the findings achieved in this work, it appears clear that large area 2DMs is possible even using very simple methods, paving the way towards the simplification of deposition approaches and the integration of homogeneous and controlled film in working devices.

Since the formation of structural defects is recognized as a bottleneck of the electrical performances in electrochemically exfoliated 2DMs, a still open challenge regards the comprehension of the mechanism of electrochemical exfoliation for the purpose of optimizing the process. Future studies, for example, should focus on the choice of electrolytes that promote an efficient exfoliation under conditions at which the formation of structural defects is not favored. On the other hand, the identification of structural defects in electrochemically exfoliated graphene opens the route to many different potential applications (e.g. selectively porous membranes for gases, salts or biomolecules).

Moreover, demonstrating that it is possible to gain control over the functional groups in EEG, in the next future this aspect could be exploited to modulate the material's properties and generating multicomponent systems through controlled chemical functionalization. The devolvement of strategies for the reliable functionalization of EEG would allow the chemical tunability of its properties for various application in electronics and composites, as well as could lead to the realization of selective and cost-effective sensors toward different analytes.

Similarly, one of the main challenges for the next future is to gain control over vacancies in MoS_2. Defects introduced during the exfoliation process could enhance the reactivity of MoS_2 towards environmental species, thereby allowing its application in the field of gas sensing. This work aims hence to stimulate further work in this direction in order to lay out the future fate of electrochemically exfoliated materials. The effect of these defects on the sensing properties of MoS_2 could be investigated, in comparison with our findings on sulfur vacancies-free MoS_2 produced by sonication. Moreover, our approach could allow to demonstrate the feasibility of a controlled functionalization of MoS_2 at the sulfur vacancies that, so far, has been studied on single flake devices or MoS_2 produced by sonication, which don't contain significant amount of vacancies. The functionalization with *ad-hoc* molecules could be exploited for different purposes as, for example, for improving sensitivity and selectivity of MoS_2-based devices towards a specific analyte, paving the way to the introduction of

2DMs in the field of sensors, or to modulating its properties for applications in various fields of electronics.

These strategies could involve a two-step process consisting in the control of defects during the exfoliation process and the subsequent modification of the material through functionalization in correspondence of such defects.

More interestingly, in the next future, LPE approaches could become not only methods of exfoliation but also strategies for tuning the properties of 2DMs and producing multifunctional systems which can be applied in various fields in function of the conferred functionality. This will be possible exploiting both the ultrasonication approach, in the wake of our work on graphene/polymer composites, and electrochemically driving the functionalization/absorption of molecular systems on the material's surface during the electrochemical exfoliation. That would allow the simultaneous exfoliation and functionalization of the material in one-step process, towards the formation of homogeneous functional systems.

Overall, this work shows that the production and processing of 2DMs in liquid media open up several opportunities for introducing 2D in several fields of applications, including electronics. In particular, inks based on 2DMs can be explored for printing on flexible supports to be introduced in low-cost flexible electronic devices, that would revolutionize the market in the next years. LPE inks could be integrated into wearable products or transparent surfaces which can, for instance, find application as low-cost sensors for measuring vital signs or to sensing environmental conditions, opening the door for lightweight and smart devices These innovative products will be made possible only by combining the extraordinary properties available in 2DMs with scalable and cost-effective production methods like LPEs.

APPENDIX I

Structural characterization

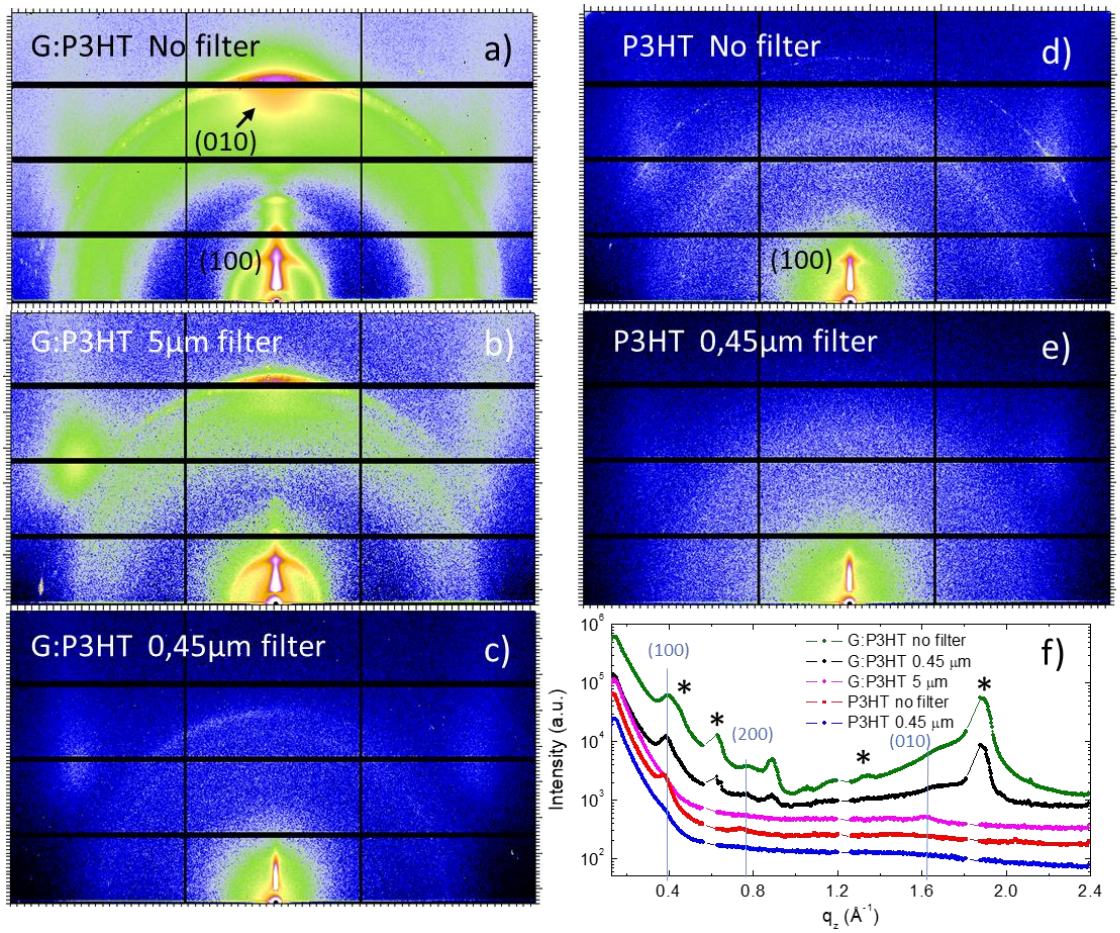

Figure A I 1. (a-e) GIWAXS images collected at the incident angle α_i =0.1° and (f) their out-of-plane integrated intensities collected for the P3HT and graphene:P3HT spin-coated films. Bragg peaks coming from graphene solution are labelled by stars.

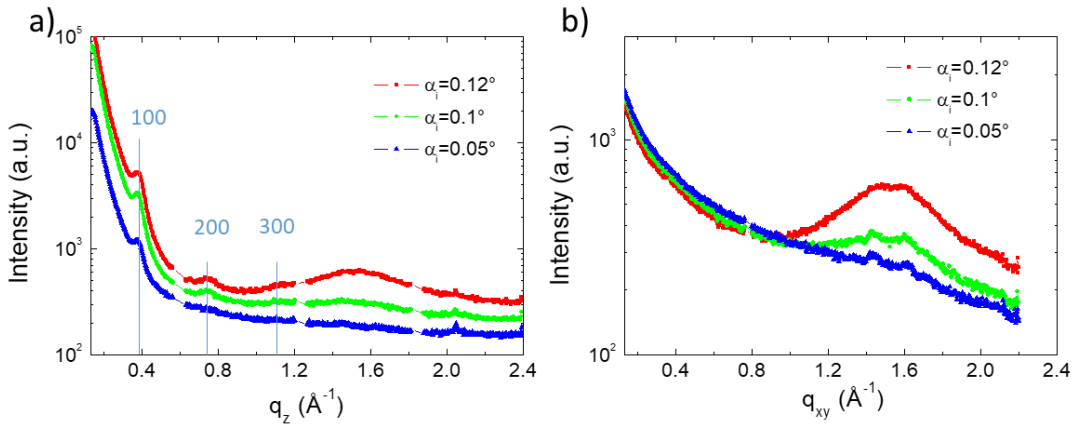

Figure A I 2. (a) Out-of-plane and (b) in-plane integrated intensities of GIWAXS images collected at different incidence angles for the no-filtered P3HT spin-coated film.

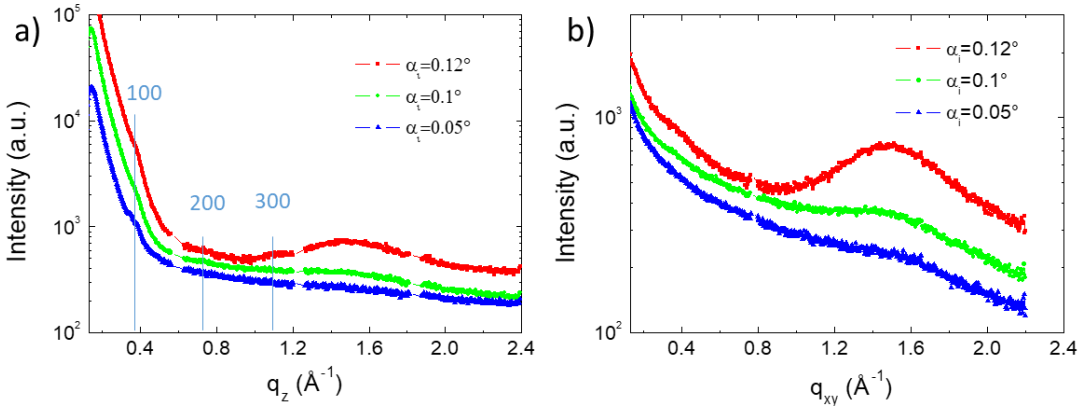

Figure A I 3. (a) Out-of-plane and (b) in-plane integrated intensities of GIWAXS images collected at different incidence angles for the 0.45 µm-filter P3HT spin-coated film.

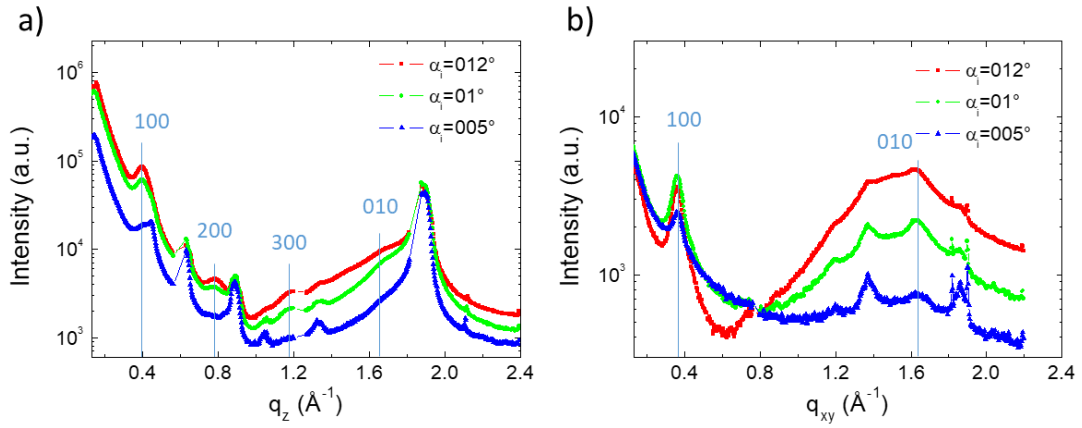

Figure A I 4. (a) Out-of-plane and (b) in-plane integrated intensities of GIWAXS images collected at different incidence angles for the no-filter graphene:P3HT spin-coated film.

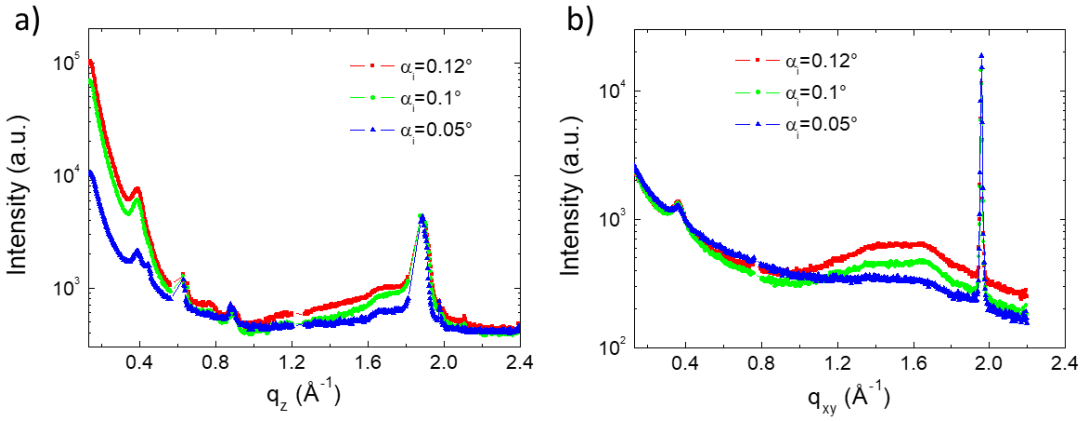

Figure A I 5. (a) Out-of-plane and (b) in-plane integrated intensities of GIWAXS images collected at different incidence angles for the 5µm-filter graphene:P3HT spin-coated film.

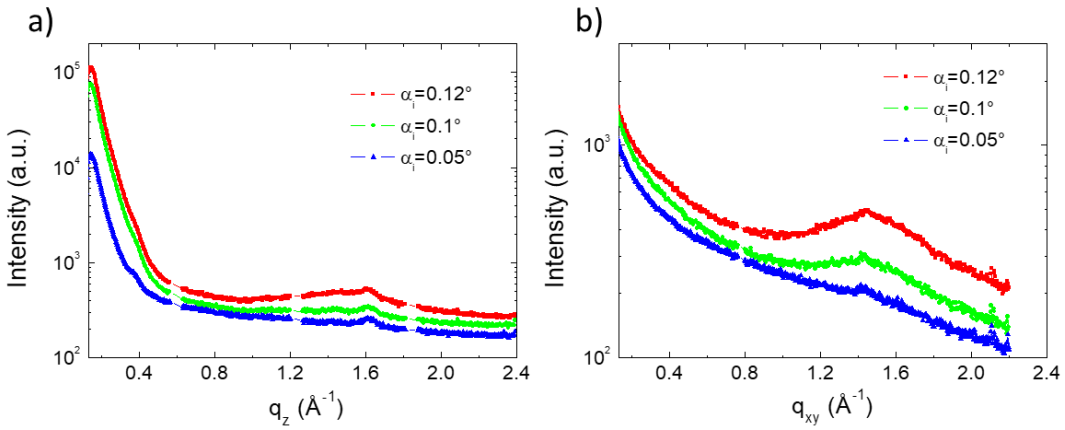

Figure A I 6. (a) Out-of-plane and (b) in-plane integrated intensities of GIWAXS images collected at different incidence angles for the 0.45 µm-filter graphene:P3HT spin-coated film.

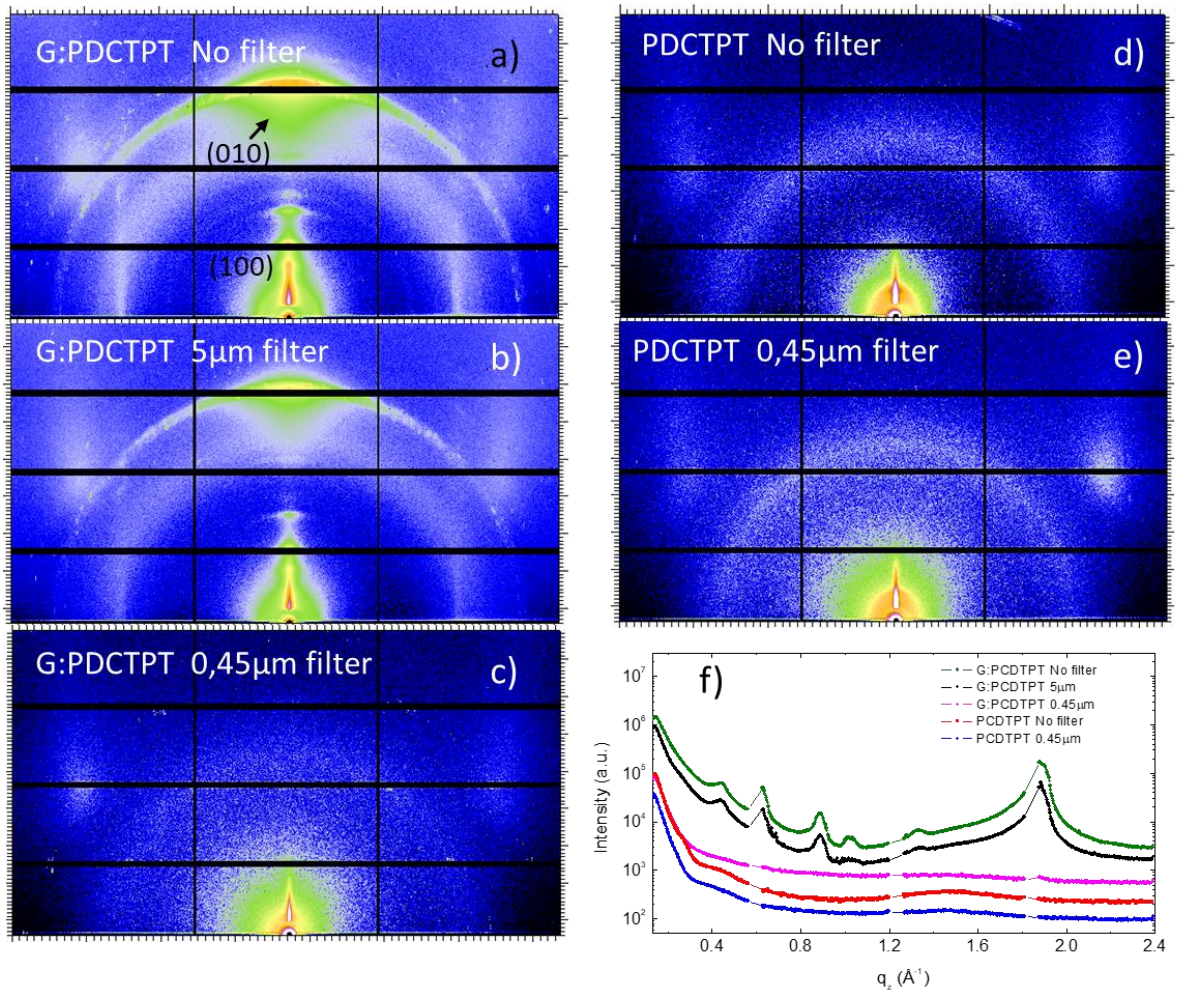

Figure A I 7. (a-e) GIWAXS images and (f) their out-of-plane integrated intensities collected with α_i=0.1° for the PCDTPT and graphene:PCDTPT spin-coated films.

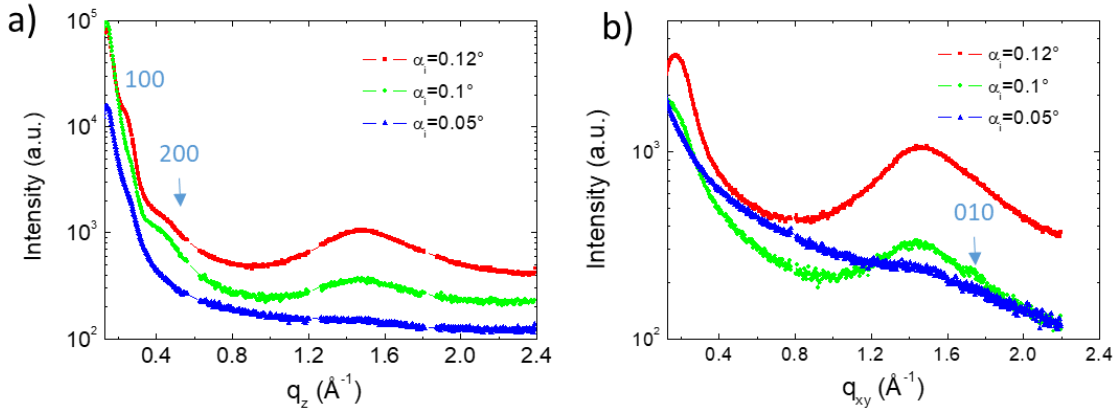

Figure A I 8. (a) Out-of-plane and (b) in-plane integrated intensities of GIWAXS images collected at different incidence angles for the no-filtered PCDTPT spin-coated film.

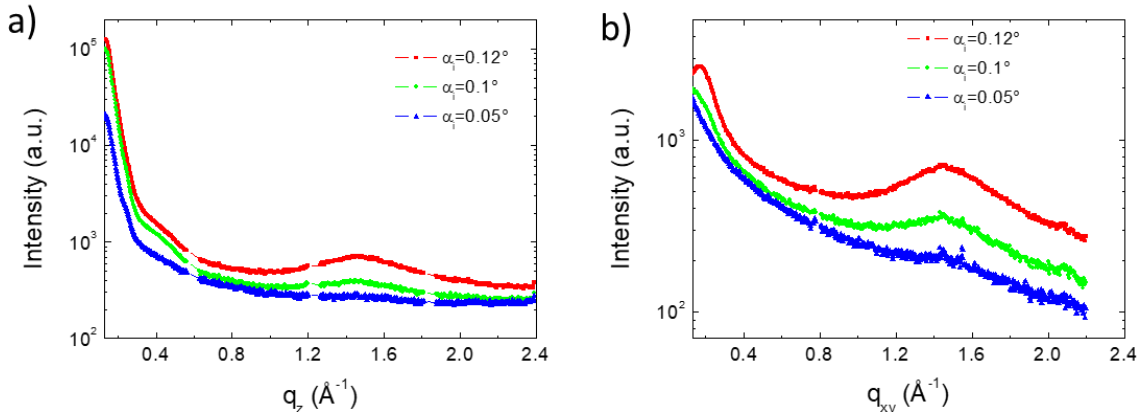

Figure A I 9. (a) Out-of-plane and (b) in-plane integrated intensities of GIWAXS images collected at different incidence angles for the PCDTPT spin-coated film from the solution filtered by 0.45 µm millipore.

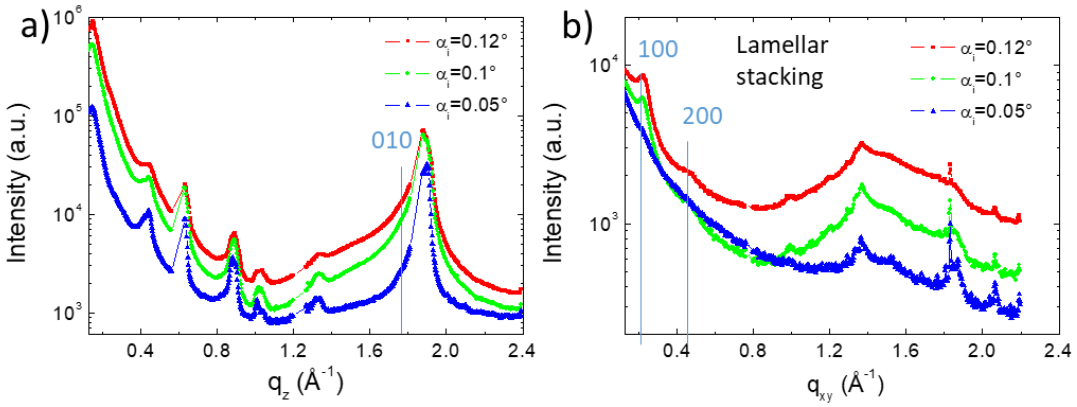

Figure A I 10. (a) Out-of-plane and (b) in-plane integrated intensities of GIWAXS images collected at different incidence angles for the graphene:PCDTPT spin-coated film.

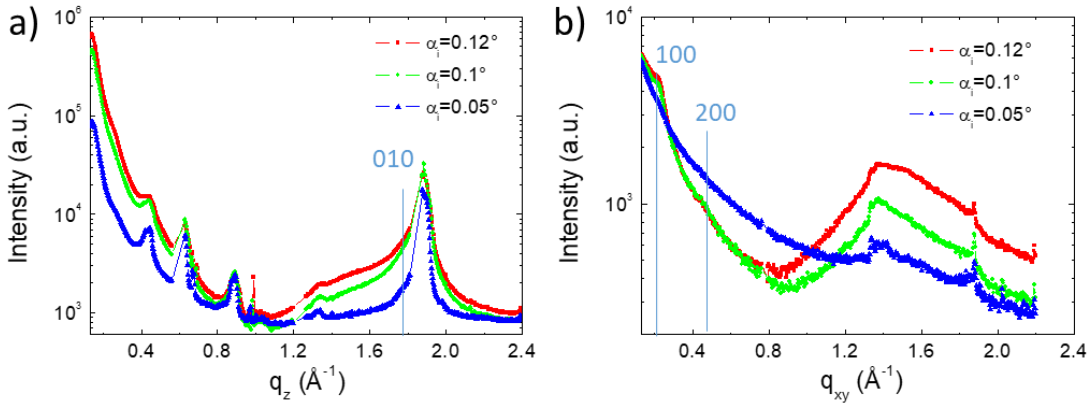

Figure A I 11. (a) Out-of-plane and (b) in-plane integrated intensities of GIWAXS images collected at different incidence angles for the graphene:PCDTPT spin-coated film from the solution filtered by the 5 µm millipore.

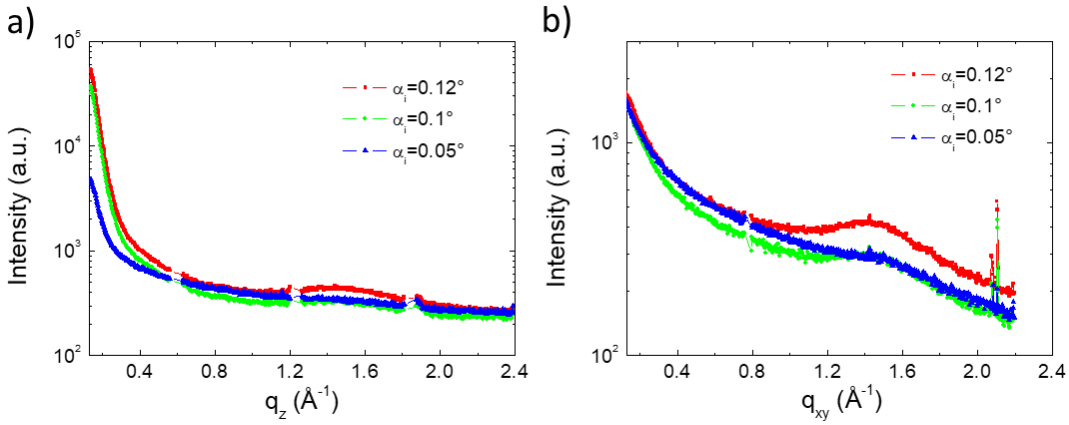

Figure A I 12. (a) Out-of-plane and (b) in-plane integrated intensities of GIWAXS images collected at different incidence angles for the graphene:PCDTPT spin-coated film from the solution filtered by the 0.45 µm millipore.

REFERENCES

(1) Cao, X. Y.; Halder, A.; Tang, Y. Y.; Hou, C. Y.; Wang, H. Z.; Duus, J. O.; Chi, Q. J. Engineering two-dimensional layered nanomaterials for wearable biomedical sensors and power devices. *Mat Chem Front* **2018**, *2*, 1944-1986.

(2) Chhowalla, M.; Jena, D.; Zhang, H. Two-dimensional semiconductors for transistors. *Nat Rev Mater* **2016**, *1*.

(3) Fiori, G.; Bonaccorso, F.; Iannaccone, G.; Palacios, T.; Neumaier, D.; Seabaugh, A.; Banerjee, S. K.; Colombo, L. Electronics based on two-dimensional materials. *Nat Nanotechnol* **2014**, *9*, 768-779.

(4) Koppens, F. H. L.; Mueller, T.; Avouris, P.; Ferrari, A. C.; Vitiello, M. S.; Polini, M. Photodetectors based on graphene, other two-dimensional materials and hybrid systems. *Nat Nanotechnol* **2014**, *9*, 780-793.

(5) Fowler, J. D.; Allen, M. J.; Tung, V. C.; Yang, Y.; Kaner, R. B.; Weiller, B. H. Practical Chemical Sensors from Chemically Derived Graphene. *ACS Nano* **2009**, *3*, 301-306.

(6) Dan, Y. P.; Lu, Y.; Kybert, N. J.; Luo, Z. T.; Johnson, A. T. C. Intrinsic Response of Graphene Vapor Sensors. *Nano Lett* **2009**, *9*, 1472-1475.

(7) Wu, Q.; Xu, Y. X.; Yao, Z. Y.; Liu, A. R.; Shi, G. Q. Supercapacitors Based on Flexible Graphene/Polyaniline Nanofiber Composite Films. *ACS Nano* **2010**, *4*, 1963-1970.

(8) Bernardi, M.; Palummo, M.; Grossman, J. C. Extraordinary Sunlight Absorption and One Nanometer Thick Photovoltaics Using Two-Dimensional Monolayer Materials. *Nano Lett* **2013**, *13*, 3664-3670.

(9) Wang, X.; Zhi, L. J.; Mullen, K. Transparent, conductive graphene electrodes for dye-sensitized solar cells. *Nano Lett* **2008**, *8*, 323-327.

(10) Lin, Z.; McCreary, A.; Briggs, N.; Subramanian, S.; Zhang, K. H.; Sun, Y. F.; Li, X. F.; Borys, N. J.; Yuan, H. T.; Fullerton-Shirey, S. K.; Chernikov, A.; Zhao, H.; McDonnell, S.; Lindenberg, A. M.; Xiao, K.; LeRoy, B. J.; Drndic, M.; Hwang, J. C. M.; Park, J.; Chhowalla, M.; Schaak, R. E.; Javey, A.; Hersam, M. C.; Robinson, J.; Terrones, M. 2D materials advances: from large scale synthesis and controlled heterostructures to improved characterization techniques, defects and applications. *2d Mater* **2016**, *3*.

(11) Novoselov, K. S.; Geim, A. K.; Morozov, S. V.; Jiang, D.; Zhang, Y.; Dubonos, S. V.; Grigorieva, I. V.; Firsov, A. A. Electric field effect in atomically thin carbon films. *Science* **2004**, *306*, 666-669.

(12) Jariwala, D.; Marks, T. J.; Hersam, M. C. Mixed-dimensional van der Waals heterostructures. *Nat Mater* **2017**, *16*, 170-181.

(13) Lin, L.; Deng, B.; Sun, J. Y.; Peng, H. L.; Liu, Z. F. Bridging the Gap between Reality and Ideal in Chemical Vapor Deposition Growth of Graphene. *Chem Rev* **2018**, *118*, 9281-9343.

(14) Coleman, J. N.; Lotya, M.; O'Neill, A.; Bergin, S. D.; King, P. J.; Khan, U.; Young, K.; Gaucher, A.; De, S.; Smith, R. J.; Shvets, I. V.; Arora, S. K.; Stanton, G.; Kim, H. Y.; Lee, K.; Kim, G. T.; Duesberg, G. S.; Hallam, T.; Boland, J. J.; Wang, J. J.; Donegan, J. F.; Grunlan, J. C.; Moriarty, G.; Shmeliov, A.; Nicholls, R. J.; Perkins, J. M.; Grieveson, E. M.; Theuwissen, K.; McComb, D. W.; Nellist, P. D.; Nicolosi, V. Two-Dimensional Nanosheets Produced by Liquid Exfoliation of Layered Materials. *Science* **2011**, *331*, 568-571.

(15) eHernandez, Y.; Nicolosi, V.; Lotya, M.; Blighe, F. M.; Sun, Z. Y.; De, S.; McGovern, I. T.; Holland, B.; Byrne, M.; Gun'ko, Y. K.; Boland, J. J.; Niraj, P.; Duesberg, G.; Krishnamurthy, S.; Goodhue, R.; Hutchison, J.; Scardaci, V.; Ferrari, A. C.; Coleman, J. N. High-yield production of graphene by liquid-phase exfoliation of graphite. *Nat Nanotechnol* **2008**, *3*, 563-568.

(16) Ciesielski, A.; Samori, P. Supramolecular Approaches to Graphene: From Self-Assembly to Molecule-Assisted Liquid-Phase Exfoliation. *Advanced Materials* **2016**, *28*, 6030-6051.
(17) Paton, K. R.; Varrla, E.; Backes, C.; Smith, R. J.; Khan, U.; O'Neill, A.; Boland, C.; Lotya, M.; Istrate, O. M.; King, P.; Higgins, T.; Barwich, S.; May, P.; Puczkarski, P.; Ahmed, I.; Moebius, M.; Pettersson, H.; Long, E.; Coelho, J.; O'Brien, S. E.; McGuire, E. K.; Sanchez, B. M.; Duesberg, G. S.; McEvoy, N.; Pennycook, T. J.; Downing, C.; Crossley, A.; Nicolosi, V.; Coleman, J. N. Scalable production of large quantities of defect-free few-layer graphene by shear exfoliation in liquids. *Nat Mater* **2014**, *13*, 624-630.
(18) Karagiannidis, P. G.; Hodge, S. A.; Lombardi, L.; Tomarchio, F.; Decorde, N.; Milana, S.; Goykhman, I.; Su, Y.; Mesite, S. V.; Johnstone, D. N.; Leary, R. K.; Midgley, P. A.; Pugno, N. M.; Torrisi, F.; Ferrari, A. C. Microfluidization of Graphite and Formulation of Graphene-Based Conductive Inks. *ACS nano* **2017**, *11*, 2742-2755.
(19) Knieke, C.; Berger, A.; Voigt, M.; Taylor, R. N. K.; Rohrl, J.; Peukert, W. Scalable production of graphene sheets by mechanical delamination. *Carbon* **2010**, *48*, 3196-3204.
(20) Bonaccorso, F.; Lombardo, A.; Hasan, T.; Sun, Z. P.; Colombo, L.; Ferrari, A. C. Production and processing of graphene and 2d crystals. *Mater Today* **2012**, *15*, 564-589.
(21) Yang, S.; Ricciardulli, A. G.; Liu, S.; Dong, R.; Lohe, M. R.; Becker, A.; Squillaci, M. A.; Samori, P.; Mullen, K.; Feng, X. Ultrafast Delamination of Graphite into High-Quality Graphene Using Alternating Currents. *Angew Chem Int Edit* **2017**, *56*, 6669-6675.
(22) Ejigu, A.; Kinloch, I. A.; Prestat, E.; Dryfe, R. A. W. A simple electrochemical route to metallic phase trilayer MoS2: evaluation as electrocatalysts and supercapacitors. *Journal of Materials Chemistry A* **2017**, *5*, 11316-11330.
(23) Li, H.; Yin, Z. Y.; He, Q. Y.; Li, H.; Huang, X.; Lu, G.; Fam, D. W. H.; Tok, A. I. Y.; Zhang, Q.; Zhang, H. Fabrication of Single- and Multilayer MoS2 Film-Based Field-Effect Transistors for Sensing NO at Room Temperature. *Small* **2012**, *8*, 63-67.
(24) Mosciatti, T.; Haar, S.; Liscio, F.; Ciesielski, A.; Orgiu, E.; Samori, P. A Multifunctional Polymer-Graphene Thin-Film Transistor with Tunable Transport Regimes. *ACS Nano* **2015**, *9*, 2357-2367.
(25) Hernandez, Y.; Nicolosi, V.; Lotya, M.; Blighe, F. M.; Sun, Z. Y.; De, S.; McGovern, I. T.; Holland, B.; Byrne, M.; Gun'ko, Y. K.; Boland, J. J.; Niraj, P.; Duesberg, G.; Krishnamurthy, S.; Goodhue, R.; Hutchison, J.; Scardaci, V.; Ferrari, A. C.; Coleman, J. N. High-yield production of graphene by liquid-phase exfoliation of graphite. *Nat Nanotechnol* **2008**, *3*, 563-568.
(26) Abdelkader, A. M.; Cooper, A. J.; Dryfe, R. A. W.; Kinloch, I. A. How to get between the sheets: a review of recent works on the electrochemical exfoliation of graphene materials from bulk graphite. *Nanoscale* **2015**, *7*, 6944-6956.
(27) Parvez, K.; Wu, Z. S.; Li, R. J.; Liu, X. J.; Graf, R.; Feng, X. L.; Mullen, K. Exfoliation of Graphite into Graphene in Aqueous Solutions of Inorganic Salts. *J. Am. Chem. Soc.* **2014**, *136*, 6083-6091.
(28) Su, C. Y.; Lu, A. Y.; Xu, Y. P.; Chen, F. R.; Khlobystov, A. N.; Li, L. J. High-Quality Thin Graphene Films from Fast Electrochemical Exfoliation. *ACS Nano* **2011**, *5*, 2332-2339.
(29) Nicolosi, V.; Chhowalla, M.; Kanatzidis, M. G.; Strano, M. S.; Coleman, J. N. Liquid Exfoliation of Layered Materials. *Science* **2013**, *340*, 1420-+.
(30) Balandin, A. A.; Ghosh, S.; Bao, W. Z.; Calizo, I.; Teweldebrhan, D.; Miao, F.; Lau, C. N. Superior thermal conductivity of single-layer graphene. *Nano Lett* **2008**, *8*, 902-907.
(31) Nair, R. R.; Blake, P.; Grigorenko, A. N.; Novoselov, K. S.; Booth, T. J.; Stauber, T.; Peres, N. M. R.; Geim, A. K. Fine structure constant defines visual transparency of graphene. *Science* **2008**, *320*, 1308-1308.
(32) Lee, C.; Wei, X. D.; Kysar, J. W.; Hone, J. Measurement of the elastic properties and intrinsic strength of monolayer graphene. *Science* **2008**, *321*, 385-388.
(33) Radisavljevic, B.; Radenovic, A.; Brivio, J.; Giacometti, V.; Kis, A. Single-layer MoS2 transistors. *Nat Nanotechnol* **2011**, *6*, 147-150.

(34) Xia, F. N.; Wang, H.; Jia, Y. C. Rediscovering black phosphorus as an anisotropic layered material for optoelectronics and electronics. *Nat Commun* **2014**, *5*.
(35) Kubota, Y.; Watanabe, K.; Tsuda, O.; Taniguchi, T. Deep ultraviolet light-emitting hexagonal boron nitride synthesized at atmospheric pressure. *Science* **2007**, *317*, 932-934.
(36) Zhang, Y.; Zhang, L. Y.; Zhou, C. W. Review of Chemical Vapor Deposition of Graphene and Related Applications. *Accounts Chem Res* **2013**, *46*, 2329-2339.
(37) Bonaccorso, F.; Sun, Z.; Hasan, T.; Ferrari, A. C. Graphene photonics and optoelectronics. *Nat Photonics* **2010**, *4*, 611-622.
(38) Li, H. A.; Li, Y.; Aljarb, A.; Shi, Y. M.; Li, L. J. Epitaxial Growth of Two-Dimensional Layered Transition-Metal Dichalcogenides: Growth Mechanism, Controllability, and Scalability. *Chem Rev* **2018**, *118*, 6134-6150.
(39) Tetlow, H.; de Boer, J. P.; Ford, I. J.; Vvedensky, D. D.; Coraux, J.; Kantorovich, L. Growth of epitaxial graphene: Theory and experiment. *Phys Rep* **2014**, *542*, 195-295.
(40) Stengl, V.; Henych, J.; Slusna, M.; Ecorchard, P. Ultrasound exfoliation of inorganic analogues of graphene. *Nanoscale Res Lett* **2014**, *9*.
(41) Varrla, E.; Backes, C.; Paton, K. R.; Harvey, A.; Gholamvand, Z.; McCauley, J.; Coleman, J. N. Large-Scale Production of Size-Controlled MoS2 Nanosheets by Shear Exfoliation. *Chem Mater* **2015**, *27*, 1129-1139.
(42) Leon, V.; Quintana, M.; Herrero, M. A.; Fierro, J. L. G.; de la Hoz, A.; Prato, M.; Vazquez, E. Few-layer graphenes from ball-milling of graphite with melamine. *Chem Commun* **2011**, *47*, 10936-10938.
(43) Frindt, R. F. Single Crystals of MoS2 Several Molecular Layers Thick. *Journal of Applied Physics* **1966**, *37*, 1928-1929.
(44) Joensen, R. F. F., and S. Roy Morrison Single-layer MoS_2. *Mater. Res. Bull* **1986;**, *21*, 457–61.
(45) Lu, X. K.; Yu, M. F.; Huang, H.; Ruoff, R. S. Tailoring graphite with the goal of achieving single sheets. *Nanotechnology* **1999**, *10*, 269-272.
(46) Chhowalla, M.; Shin, H. S.; Eda, G.; Li, L. J.; Loh, K. P.; Zhang, H. The chemistry of two-dimensional layered transition metal dichalcogenide nanosheets. *Nature Chemistry* **2013**, *5*, 263-275.
(47) Wilson, J. A.; Yoffe, A. D. The transition metal dichalcogenides discussion and interpretation of the observed optical, electrical and structural properties. *Advances in Physics* **1969**, *18*, 193-335.
(48) Zhou, J. D.; Lin, J. H.; Huang, X. W.; Zhou, Y.; Chen, Y.; Xia, J.; Wang, H.; Xie, Y.; Yu, H. M.; Lei, J. C.; Wu, D.; Liu, F. C.; Fu, Q. D.; Zeng, Q. S.; Hsu, C. H.; Yang, C. L.; Lu, L.; Yu, T.; Shen, Z. X.; Lin, H.; Yakobson, B. I.; Liu, Q.; Suenaga, K.; Liu, G. T.; Liu, Z. A library of atomically thin metal chalcogenides. *Nature* **2018**, *556*, 355-+.
(49) Lu, G. Y.; Wu, T. R.; Yuan, Q. H.; Wang, H. S.; Wang, H. M.; Ding, F.; Xie, X. M.; Jiang, M. H. Synthesis of large single-crystal hexagonal boron nitride grains on Cu-Ni alloy. *Nat Commun* **2015**, *6*.
(50) Golias, E.; Krivenkov, M.; Varykhalov, A.; Sanchez-Barriga, J.; Rader, O. Band Renormalization of Blue Phosphorus on Au(111). *Nano Lett* **2018**, *18*, 6672-6678.
(51) Naguib, M.; Mochalin, V. N.; Barsoum, M. W.; Gogotsi, Y. 25th Anniversary Article: MXenes: A New Family of Two-Dimensional Materials. *Advanced Materials* **2014**, *26*, 992-1005.
(52) Chen, S. S.; Wu, Q. Z.; Mishra, C.; Kang, J. Y.; Zhang, H. J.; Cho, K. J.; Cai, W. W.; Balandin, A. A.; Ruoff, R. S. Thermal conductivity of isotopically modified graphene. *Nat Mater* **2012**, *11*, 203-207.
(53) Stankovich, S.; Dikin, D. A.; Dommett, G. H. B.; Kohlhaas, K. M.; Zimney, E. J.; Stach, E. A.; Piner, R. D.; Nguyen, S. T.; Ruoff, R. S. Graphene-based composite materials. *Nature* **2006**, *442*, 282-286.
(54) Wilson, M. Electrons in atomically thin carbon sheets behave like massless particles. *Phys Today* **2006**, *59*, 21-23.

(55) Geim, A. K.; Novoselov, K. S. The rise of graphene. *Nat Mater* **2007**, *6*, 183-191.
(56) Wang, Q. H.; Kalantar-Zadeh, K.; Kis, A.; Coleman, J. N.; Strano, M. S. Electronics and optoelectronics of two-dimensional transition metal dichalcogenides. *Nat Nanotechnol* **2012**, *7*, 699-712.
(57) Py, M. A.; Haering, R. R. Structural Destabilization Induced by Lithium Intercalation in Mos2 and Related-Compounds. *Can J Phys* **1983**, *61*, 76-84.
(58) Ganal, P.; Olberding, W.; Butz, T.; Ouvrard, G. Soft Chemistry Induced Host Metal Coordination Change from Octahedral to Trigonal Prismatic in 1t-Tas2. *Solid State Ionics* **1993**, *59*, 313-319.
(59) Yang, J. F.; Parakash, B.; Hardell, J.; Fang, Q. F. Tribological properties of transition metal di-chalcogenide based lubricant coatings. *Front Mater Sci* **2012**, *6*, 116-127.
(60) Bertolazzi, S.; Gobbi, M.; Zhao, Y. D.; Backes, C.; Samori, P. Molecular chemistry approaches for tuning the properties of two-dimensional transition metal dichalcogenides. *Chem Soc Rev* **2018**, *47*, 6845-6888.
(61) Splendiani, A.; Sun, L.; Zhang, Y. B.; Li, T. S.; Kim, J.; Chim, C. Y.; Galli, G.; Wang, F. Emerging Photoluminescence in Monolayer MoS2. *Nano Lett* **2010**, *10*, 1271-1275.
(62) Mak, K. F.; Lee, C.; Hone, J.; Shan, J.; Heinz, T. F. Atomically Thin MoS2: A New Direct-Gap Semiconductor. *Phys Rev Lett* **2010**, *105*.
(63) The crystal structure of molybdenite. *J. Am. Chem. Soc.* **1923**, *45*, 1466-1471.
(64) Chen, L.; Hernandez, Y.; Feng, X. L.; Mullen, K. From Nanographene and Graphene Nanoribbons to Graphene Sheets: Chemical Synthesis. *Angew Chem Int Edit* **2012**, *51*, 7640-7654.
(65) Narita, A.; Feng, X. L.; Hernandez, Y.; Jensen, S. A.; Bonn, M.; Yang, H. F.; Verzhbitskiy, I. A.; Casiraghi, C.; Hansen, M. R.; Koch, A. H. R.; Fytas, G.; Ivasenko, O.; Li, B.; Mali, K. S.; Balandina, T.; Mahesh, S.; De Feyter, S.; Mullen, K. Synthesis of structurally well-defined and liquid-phase-processable graphene nanoribbons. *Nature Chemistry* **2014**, *6*, 126-132.
(66) Backes, C.; Higgins, T. M.; Kelly, A.; Boland, C.; Harvey, A.; Hanlon, D.; Coleman, J. N. Guidelines for Exfoliation, Characterization and Processing of Layered Materials Produced by Liquid Exfoliation. *Chem Mater* **2017**, *29*, 243-255.
(67) Eda, G.; Unalan, H. E.; Rupesinghe, N.; Amaratunga, G. A. J.; Chhowalla, M. Field emission from graphene based composite thin films. *Appl Phys Lett* **2008**, *93*.
(68) Kymakis, E.; Stratakis, E.; Stylianakis, M. M.; Koudoumas, E.; Fotakis, C. Spin coated graphene films as the transparent electrode in organic photovoltaic devices. *Thin Solid Films* **2011**, *520*, 1238-1241.
(69) Blake, P.; Brimicombe, P. D.; Nair, R. R.; Booth, T. J.; Jiang, D.; Schedin, F.; Ponomarenko, L. A.; Morozov, S. V.; Gleeson, H. F.; Hill, E. W.; Geim, A. K.; Novoselov, K. S. Graphene-based liquid crystal device. *Nano Lett* **2008**, *8*, 1704-1708.
(70) Cataldi, P.; Bayer, I. S.; Bonaccorso, F.; Pellegrini, V.; Athanassiou, A.; Cingolani, R. Foldable Conductive Cellulose Fiber Networks Modified by Graphene Nanoplatelet-Bio-Based Composites. *Adv Electron Mater* **2015**, *1*.
(71) Torrisi, F.; Hasan, T.; Wu, W. P.; Sun, Z. P.; Lombardo, A.; Kulmala, T. S.; Hsieh, G. W.; Jung, S. J.; Bonaccorso, F.; Paul, P. J.; Chu, D. P.; Ferrari, A. C. Inkjet-Printed Graphene Electronics. *ACS Nano* **2012**, *6*, 2992-3006.
(72) Li, J. T.; Ye, F.; Vaziri, S.; Muhammed, M.; Lemme, M. C.; Ostling, M. Efficient Inkjet Printing of Graphene. *Advanced Materials* **2013**, *25*, 3985-3992.
(73) Bunch, J. S.; Yaish, Y.; Brink, M.; Bolotin, K.; McEuen, P. L. Coulomb oscillations and Hall effect in quasi-2D graphite quantum dots. *Nano Lett* **2005**, *5*, 287-290.
(74) Zhi, C. Y.; Bando, Y.; Tang, C. C.; Kuwahara, H.; Golberg, D. Large-Scale Fabrication of Boron Nitride Nanosheets and Their Utilization in Polymeric Composites with Improved Thermal and Mechanical Properties. *Advanced Materials* **2009**, *21*, 2889-+.

(75) Bang, G. S.; Nam, K. W.; Kim, J. Y.; Shin, J.; Choi, J. W.; Choi, S. Y. Effective Liquid-Phase Exfoliation and Sodium Ion Battery Application of MoS2 Nanosheets. *Acs Appl Mater Inter* **2014**, *6*, 7084-7089.
(76) Harvey, A.; He, X. Y.; Godwin, I. J.; Backes, C.; McAteer, D.; Berner, N. C.; McEvoy, N.; Ferguson, A.; Shmeliov, A.; Lyons, M. E. G.; Nicolosi, V.; Duesberg, G. S.; Donegan, J. F.; Coleman, J. N. Production of Ni(OH)(2) nanosheets by liquid phase exfoliation: from optical properties to electrochemical applications. *Journal of Materials Chemistry A* **2016**, *4*, 11046-11059.
(77) Naguib, M.; Mashtalir, O.; Carle, J.; Presser, V.; Lu, J.; Hultman, L.; Gogotsi, Y.; Barsoum, M. W. Two-Dimensional Transition Metal Carbides. *ACS Nano* **2012**, *6*, 1322-1331.
(78) Yi, M.; Shen, Z. G. A review on mechanical exfoliation for the scalable production of graphene. *Journal of Materials Chemistry A* **2015**, *3*, 11700-11715.
(79) Bracamonte, M. V.; Lacconi, G. I.; Urreta, S. E.; Torres, L. E. F. F. On the Nature of Defects in Liquid-Phase Exfoliated Graphene. *J Phys Chem C* **2014**, *118*, 15455-15459.
(80) Bonaccorso, F.; Bartolotta, A.; Coleman, J. N.; Backes, C. 2D-Crystal-Based Functional Inks. *Advanced Materials* **2016**, *28*, 6136-6166.
(81) Zhang, X. Y.; Coleman, A. C.; Katsonis, N.; Browne, W. R.; van Wees, B. J.; Feringa, B. L. Dispersion of graphene in ethanol using a simple solvent exchange method. *Chem Commun* **2010**, *46*, 7539-7541.
(82) Tang, Z. H.; Wei, Q. Y.; Guo, B. C. A generic solvent exchange method to disperse MoS2 in organic solvents to ease the solution process. *Chem Commun* **2014**, *50*, 3934-3937.
(83) Ciesielski, A.; Samori, P. Graphene via sonication assisted liquid-phase exfoliation. *Chem Soc Rev* **2014**, *43*, 381-398.
(84) Capasso, A.; Castillo, A. E. D.; Sun, H.; Ansaldo, A.; Pellegrini, V.; Bonaccorso, F. Ink-jet printing of graphene for flexible electronics: An environmentally-friendly approach. *Solid State Commun* **2015**, *224*, 53-63.
(85) Coleman, J. N. Liquid Exfoliation of Defect-Free Graphene. *Accounts Chem Res* **2013**, *46*, 14-22.
(86) O'Neill, A.; Khan, U.; Coleman, J. N. Preparation of High Concentration Dispersions of Exfoliated MoS2 with Increased Flake Size. *Chem Mater* **2012**, *24*, 2414-2421.
(87) Paria, S.; Khilar, K. C. A review on experimental studies of surfactant adsorption at the hydrophilic solid-water interface. *Adv Colloid Interfac* **2004**, *110*, 75-95.
(88) Lotya, M.; Hernandez, Y.; King, P. J.; Smith, R. J.; Nicolosi, V.; Karlsson, L. S.; Blighe, F. M.; De, S.; Wang, Z. M.; McGovern, I. T.; Duesberg, G. S.; Coleman, J. N. Liquid Phase Production of Graphene by Exfoliation of Graphite in Surfactant/Water Solutions. *J. Am. Chem. Soc.* **2009**, *131*, 3611-3620.
(89) Bao, W. Z.; Cai, X. H.; Kim, D.; Sridhara, K.; Fuhrer, M. S. High mobility ambipolar MoS2 field-effect transistors: Substrate and dielectric effects. *Appl Phys Lett* **2013**, *102*.
(90) Wang, G. X.; Wang, B.; Park, J.; Wang, Y.; Sun, B.; Yao, J. Highly efficient and large-scale synthesis of graphene by electrolytic exfoliation. *Carbon* **2009**, *47*, 3242-3246.
(91) Li, P.; Bae, S. H.; Zan, Q. Y.; Kim, N. H.; Lee, J. H. One-step process for the exfoliation and surface modification of graphene by electrochemical method. *Adv Mater Res-Switz* **2010**, *123-125*, 743-+.
(92) Parvez, K.; Li, R. J.; Puniredd, S. R.; Hernandez, Y.; Hinkel, F.; Wang, S. H.; Feng, X. L.; Mullen, K. Electrochemically Exfoliated Graphene as Solution-Processable, Highly Conductive Electrodes for Organic Electronics. *ACS Nano* **2013**, *7*, 3598-3606.
(93) Rao, K. S.; Sentilnathan, J.; Cho, H. W.; Wu, J. J.; Yoshimura, M. Soft Processing of Graphene Nanosheets by Glycine-Bisulfate Ionic-Complex-Assisted Electrochemical Exfoliation of Graphite for Reduction Catalysis. *Adv Funct Mater* **2015**, *25*, 298-305.

(94) Zeng, F. W.; Sun, Z. H.; Sang, X. G.; Diamond, D.; Lau, K. T.; Liu, X. X.; Su, D. S. In Situ One-Step Electrochemical Preparation of Graphene Oxide Nanosheet-Modified Electrodes for Biosensors. *Chemsuschem* **2011**, *4*, 1587-1591.
(95) Ambrosi, A.; Pumera, M. Electrochemically Exfoliated Graphene and Graphene Oxide for Energy Storage and Electrochemistry Applications. *Chem-Eur J* **2016**, *22*, 153-159.
(96) Liu, N.; Kim, P.; Kim, J. H.; Ye, J. H.; Kim, S.; Lee, C. J. Large-Area Atomically Thin MoS2 Nanosheets Prepared Using Electrochemical Exfoliation. *ACS Nano* **2014**, *8*, 6902-6910.
(97) Anwar, M. A.; Zainal, A. K.; Kurniawan, T.; Asmara, Y. P.; Harun, W. S. W.; Priyadonko, G.; Saptaji, K. Electrochemical Exfoliation of Pencil Graphite Core by Salt Electrolyte. *IOP Conference Series: Materials Science and Engineering* **2019**, *469*, 012105.
(98) Hossain, S. T.; Wang, R. G. Electrochemical Exfoliation of Graphite: Effect of Temperature and Hydrogen Peroxide Addition. *Electrochim Acta* **2016**, *216*, 253-260.
(99) Lin, Z. Y.; Liu, Y.; Halim, U.; Ding, M. N.; Liu, Y. Y.; Wang, Y. L.; Jia, C. C.; Chen, P.; Duan, X. D.; Wang, C.; Song, F.; Li, M. F.; Wan, C. Z.; Huang, Y.; Duan, X. F. Solution-processable 2D semiconductors for high-performance large-area electronics. *Nature* **2018**, *562*, 254-+.
(100) Munuera, J. M.; Paredes, J. I.; Villar-Rodil, S.; Ayan-Varela, M.; Pagan, A.; Aznar-Cervantes, S. D.; Cenis, J. L.; Martinez-Alonso, A.; Tascon, J. M. D. High quality, low oxygen content and biocompatible graphene nanosheets obtained by anodic exfoliation of different graphite types. *Carbon* **2015**, *94*, 729-739.
(101) Achee, T. C.; Sun, W. M.; Hope, J. T.; Quitzau, S. G.; Sweeney, C. B.; Shah, S. A.; Habib, T.; Green, M. J. High-yield scalable graphene nanosheet production from compressed graphite using electrochemical exfoliation. *Sci Rep-Uk* **2018**, *8*.
(102) Ambrosi, A.; Pumera, M. Exfoliation of layered materials using electrochemistry. *Chem Soc Rev* **2018**, *47*, 7213-7224.
(103) Yang, Y. C.; Hou, H. S.; Zou, G. Q.; Shi, W.; Shuai, H. L.; Li, J. Y.; Ji, X. B. Electrochemical exfoliation of graphene-like two-dimensional nanomaterials. *Nanoscale* **2019**, *11*, 16-33.
(104) Cooper, A. J.; Wilson, N. R.; Kinloch, I. A.; Dryfe, R. A. W. Single stage electrochemical exfoliation method for the production of few-layer graphene via intercalation of tetraalkylammonium cations. *Carbon* **2014**, *66*, 340-350.
(105) Rao, K. S.; Senthilnathan, J.; Liu, Y. F.; Yoshimura, M. Role of Peroxide Ions in Formation of Graphene Nanosheets by Electrochemical Exfoliation of Graphite. *Sci Rep-Uk* **2014**, *4*.
(106) Kumar, M. K. P.; Shanthini, S.; Srivastava, C. Electrochemical exfoliation of graphite for producing graphene using saccharin. *Rsc Advances* **2015**, *5*, 53865-53869.
(107) Parveen, N.; Ansari, M. O.; Cho, M. H. Simple route for gram synthesis of less defective few layered graphene and its electrochemical performance (vol 5, pg 44920, 2015). *Rsc Advances* **2016**, *6*, 17384-17385.
(108) Kuila, T.; Khanra, P.; Kim, N. H.; Lim, J. K.; Lee, J. H. Effects of sodium hydroxide on the yield and electrochemical performance of sulfonated poly(ether-ether-ketone) functionalized graphene. *Journal of Materials Chemistry A* **2013**, *1*, 9294-9302.
(109) Sahoo, S. K.; Mallik, A. Simple, Fast and Cost-Effective Electrochemical Synthesis of Few Layer Graphene Nanosheets. *Nano* **2015**, *10*.
(110) Coros, M.; Pogacean, F.; Rosu, M. C.; Socaci, C.; Borodi, G.; Magerusan, L.; Biris, A. R.; Pruneanu, S. Simple and cost-effective synthesis of graphene by electrochemical exfoliation of graphite rods. *Rsc Advances* **2016**, *6*, 2651-2661.
(111) Gurzeda, B.; Florczak, P.; Kempinski, M.; Peplinska, B.; Krawczyk, P.; Jurga, S. Synthesis of graphite oxide by electrochemical oxidation in aqueous perchloric acid. *Carbon* **2016**, *100*, 540-545.
(112) Munuera, J. M.; Paredes, J. I.; Villar-Rodil, S.; Ayan-Varela, M.; Martinez-Alonso, A.; Tascon, J. M. D. Electrolytic exfoliation of graphite in water with multifunctional electrolytes: en route towards high quality, oxide-free graphene flakes. *Nanoscale* **2016**, *8*, 2982-2998.

(113) Yang, S.; Bruller, S.; Wu, Z. S.; Liu, Z. Y.; Parvez, K.; Dong, R. H.; Richard, F.; Samori, P.; Feng, X. L.; Mullen, K. Organic Radical-Assisted Electrochemical Exfoliation for the Scalable Production of High-Quality Graphene. *J. Am. Chem. Soc.* **2015**, *137*, 13927-13932.
(114) Chen, C. H.; Yang, S. W.; Chuang, M. C.; Woon, W. Y.; Su, C. Y. Towards the continuous production of high crystallinity graphene via electrochemical exfoliation with molecular in situ encapsulation. *Nanoscale* **2015**, *7*, 15362-15373.
(115) Munuera, J. M.; Paredes, J. I.; Enterria, M.; Pagan, A.; Villar-Rodil, S.; Pereira, M. F. R.; Martins, J. I.; Figueiredo, J. L.; Cenis, J. L.; Martinez-Alonso, A.; Tascon, J. M. D. Electrochemical Exfoliation of Graphite in Aqueous Sodium Halide Electrolytes toward Low Oxygen Content Graphene for Energy and Environmental Applications. *Acs Appl Mater Inter* **2017**, *9*, 24085-24099.
(116) You, X.; Liu, N.; Lee, C. J.; Pak, J. J. An electrochemical route to MoS2 nanosheets for device applications. *Mater Lett* **2014**, *121*, 31-35.
(117) Ambrosi, A.; Sofer, Z.; Luxa, J.; Pumera, M. Exfoliation of Layered Topological Insulators Bi2Se3 and Bi2Te3 via Electrochemistry. *ACS Nano* **2016**, *10*, 11442-11448.
(118) Abdelkader, A. M.; Kinloch, I. A.; Dryfe, R. A. W. Continuous Electrochemical Exfoliation of Micrometer-Sized Graphene Using Synergistic Ion Intercalations and Organic Solvents. *Acs Appl Mater Inter* **2014**, *6*, 1632-1639.
(119) Zeng, Z. Y.; Yin, Z. Y.; Huang, X.; Li, H.; He, Q. Y.; Lu, G.; Boey, F.; Zhang, H. Single-Layer Semiconducting Nanosheets: High-Yield Preparation and Device Fabrication. *Angew Chem Int Edit* **2011**, *50*, 11093-11097.
(120) Zeng, Z.; Yin, Z.; Huang, X.; Li, H.; He, Q.; Lu, G.; Boey, F.; Zhang, H. Single-layer semiconducting nanosheets: high-yield preparation and device fabrication. *Angewandte Chemie* **2011**, *50*, 11093-7.
(121) Xia, Z. Y.; Giambastiani, G.; Christodoulou, C.; Nardi, M. V.; Koch, N.; Treossi, E.; Bellani, V.; Pezzini, S.; Corticelli, F.; Morandi, V.; Zanelli, A.; Palermo, V. Synergic Exfoliation of Graphene with Organic Molecules and Inorganic Ions for the Electrochemical Production of Flexible Electrodes. *Chempluschem* **2014**, *79*, 439-446.
(122) Kappera, R.; Voiry, D.; Yalcin, S. E.; Branch, B.; Gupta, G.; Mohite, A. D.; Chhowalla, M. Phase-engineered low-resistance contacts for ultrathin MoS2 transistors (vol 13, pg 1128, 2014). *Nat Mater* **2014**, *13*.
(123) Eda, G.; Yamaguchi, H.; Voiry, D.; Fujita, T.; Chen, M. W.; Chhowalla, M. Photoluminescence from Chemically Exfoliated MoS2. *Nano Lett* **2011**, *11*, 5111-5116.
(124) Lin, Z. Y.; Liu, Y.; Halim, U.; Ding, M. N.; Liu, Y. Y.; Wang, Y. L.; Jia, C. C.; Chen, P.; Duan, X. D.; Wang, C.; Song, F.; Li, M. F.; Wan, C. Z.; Huang, Y.; Duan, X. F. Solution-processable 2D semiconductors for high-performance large-area electronics. *Nature* **2018**, *562*, 254-258.
(125) Li, F. W.; Xue, M. Q.; Zhang, X. L.; Chen, L.; Knowles, G. P.; MacFarlane, D. R.; Zhang, J. Advanced Composite 2D Energy Materials by Simultaneous Anodic and Cathodic Exfoliation. *Adv Energy Mater* **2018**, *8*.
(126) Hamberg, I.; Granqvist, C. G. Evaporated Sn-Doped In2o3 Films - Basic Optical-Properties and Applications to Energy-Efficient Windows. *Journal of Applied Physics* **1986**, *60*, R123-R159.
(127) Minami, T. Transparent conducting oxide semiconductors for transparent electrodes. *Semicond Sci Tech* **2005**, *20*, S35-S44.
(128) Granqvist, C. G. Transparent conductors as solar energy materials: A panoramic review. *Sol Energ Mat Sol C* **2007**, *91*, 1529-1598.
(129) Geng, J. X.; Jung, H. Porphyrin Functionalized Graphene Sheets in Aqueous Suspensions: From the Preparation of Graphene Sheets to Highly Conductive Graphene Films. *J Phys Chem C* **2010**, *114*, 8227-8234.
(130) Kholmanov, I. N.; Domingues, S. H.; Chou, H.; Wang, X. H.; Tan, C.; Kim, J. Y.; Li, H. F.; Piner, R.; Zarbin, A. J. G.; Ruoff, R. S. Reduced Graphene Oxide/Copper Nanowire Hybrid Films as High-Performance Transparent Electrodes. *ACS Nano* **2013**, *7*, 1811-1816.

(131) Ricciardulli, A. G.; Yang, S.; Feng, X. L.; Blom, P. W. M. Solution-Processable High-Quality Graphene for Organic Solar Cells. *Acs Appl Mater Inter* **2017**, *9*, 25412-25417.
(132) Hu, L. H.; Wu, F. Y.; Lin, C. T.; Khlobystov, A. N.; Li, L. J. Graphene-modified LiFePO4 cathode for lithium ion battery beyond theoretical capacity. *Nat Commun* **2013**, *4*.
(133) Liu, R. L.; Wan, L.; Liu, S. Q.; Pan, L. X.; Wu, D. Q.; Zhao, D. Y. An Interface-Induced Co-Assembly Approach Towards Ordered Mesoporous Carbon/Graphene Aerogel for High-Performance Supercapacitors. *Adv Funct Mater* **2015**, *25*, 526-533.
(134) Li, X. M.; Yang, T. T.; Yang, Y.; Zhu, J.; Li, L.; Alam, F. E.; Li, X.; Wang, K. L.; Cheng, H. Y.; Lin, C. T.; Fang, Y.; Zhu, H. W. Large-Area Ultrathin Graphene Films by Single-Step Marangoni Self-Assembly for Highly Sensitive Strain Sensing Application. *Adv Funct Mater* **2016**, *26*, 1322-1329.
(135) Li, L.; Li, X. M.; Du, M. D.; Guo, Y. C.; Li, Y. C.; Li, H. B.; Yang, Y.; Alam, F. E.; Lin, C. T.; Fang, Y. Solid-Phase Coalescence of Electrochemically Exfoliated Graphene Flakes into a Continuous Film on Copper. *Chem Mater* **2016**, *28*, 3360-3366.
(136) Finn, D. J.; Lotya, M.; Cunningham, G.; Smith, R. J.; McCloskey, D.; Donegan, J. F.; Coleman, J. N. Inkjet deposition of liquid-exfoliated graphene and MoS2 nanosheets for printed device applications. *J Mater Chem C* **2014**, *2*, 925-932.
(137) Anichini, C.; Czepa, W.; Pakulski, D.; Aliprandi, A.; Ciesielski, A.; Samori, P. Chemical sensing with 2D materials. *Chem Soc Rev* **2018**, *47*, 4860-4908.
(138) Benameur, M. M.; Radisavljevic, B.; Heron, J. S.; Sahoo, S.; Berger, H.; Kis, A. Visibility of dichalcogenide nanolayers. *Nanotechnology* **2011**, *22*.
(139) Blake, P.; Hill, E. W.; Castro Neto, A. H.; Novoselov, K. S.; Jiang, D.; Yang, R.; Booth, T. J.; Geim, A. K. Making graphene visible. *Appl Phys Lett* **2007**, *91*.
(140) Li, H.; Wu, J. M. T.; Huang, X.; Lu, G.; Yang, J.; Lu, X.; Zhang, Q. H.; Zhang, H. Rapid and Reliable Thickness Identification of Two-Dimensional Nanosheets Using Optical Microscopy. *ACS Nano* **2013**, *7*, 10344-10353.
(141) Ciesielski, A.; Haar, S.; El Gemayel, M.; Yang, H. F.; Clough, J.; Melinte, G.; Gobbi, M.; Orgiu, E.; Nardi, M. V.; Ligorio, G.; Palermo, V.; Koch, N.; Ersen, O.; Casiraghi, C.; Samori, P. Harnessing the Liquid-Phase Exfoliation of Graphene Using Aliphatic Compounds: A Supramolecular Approach. *Angew Chem Int Edit* **2014**, *53*, 10355-10361.
(142) Sim, D. M.; Kim, M.; Yim, S.; Choi, M. J.; Choi, J.; Yoo, S.; Jung, Y. S. Controlled Doping of Vacancy-Containing Few-Layer MoS2 via Highly Stable Thiol-Based Molecular Chemisorption. *ACS Nano* **2015**, *9*, 12115-12123.
(143) Backes, C.; Smith, R. J.; McEvoy, N.; Berner, N. C.; McCloskey, D.; Nerl, H. C.; O'Neill, A.; King, P. J.; Higgins, T.; Hanlon, D.; Scheuschner, N.; Maultzsch, J.; Houben, L.; Duesberg, G. S.; Donegan, J. F.; Nicolosi, V.; Coleman, J. N. Edge and confinement effects allow in situ measurement of size and thickness of liquid-exfoliated nanosheets. *Nat Commun* **2014**, *5*.
(144) Cummins, D. R.; Martinez, U.; Sherehiy, A.; Kappera, R.; Martinez-Garcia, A.; Schulze, R. K.; Jasinski, J.; Zhang, J.; Gupta, R. K.; Lou, J.; Chhowalla, M.; Sumanasekera, G.; Mohite, A. D.; Sunkara, M. K.; Gupta, G. Efficient hydrogen evolution in transition metal dichalcogenides via a simple one-step hydrazine reaction. *Nat Commun* **2016**, *7*.
(145) Tan, S. J. R.; Abdelwahab, I.; Ding, Z. J.; Zhao, X. X.; Yang, T. S.; Loke, G. Z. J.; Lin, H.; Verzhbitskiy, I.; Poh, S. M.; Xu, H.; Nai, C. T.; Zhou, W.; Eda, G.; Jia, B. H.; Loh, K. P. Chemical Stabilization of 1T ' Phase Transition Metal Dichalcogenides with Giant Optical Kerr Nonlinearity. *J. Am. Chem. Soc.* **2017**, *139*, 2504-2511.
(146) Ferrari, A. C.; Basko, D. M. Raman spectroscopy as a versatile tool for studying the properties of graphene. *Nat Nanotechnol* **2013**, *8*, 235-246.
(147) Ferrari, A. C.; Meyer, J. C.; Scardaci, V.; Casiraghi, C.; Lazzeri, M.; Mauri, F.; Piscanec, S.; Jiang, D.; Novoselov, K. S.; Roth, S.; Geim, A. K. Raman spectrum of graphene and graphene layers. *Phys Rev Lett* **2006**, *97*.

(148) Ferrari, A. C.; Robertson, J. Interpretation of Raman spectra of disordered and amorphous carbon. *Phys Rev B* **2000**, *61*, 14095-14107.
(149) Gupta, A.; Chen, G.; Joshi, P.; Tadigadapa, S.; Eklund, P. C. Raman scattering from high-frequency phonons in supported n-graphene layer films. *Nano Lett* **2006**, *6*, 2667-2673.
(150) Ferrari, A. C. M., J. C.; Scardaci, V. ; Casiraghi,C.; Lazzeri,M. Mauri,F.; Piscanec,S.; Jiang, D. The Raman Fingerprint of Graphene. *Phys. Rev. Lett.* **2006**, 187401-187404.
(151) Backes, C.; Paton, K. R.; Hanlon, D.; Yuan, S.; Katsnelson, M. I.; Houston, J.; Smith, R. J.; McCloskey, D.; Donegan, J. F.; Coleman, J. N. Spectroscopic metrics allow in situ measurement of mean size and thickness of liquid-exfoliated few-layer graphene nanosheets. *Nanoscale* **2016**, *8*, 4311-4323.
(152) Ricciardella, F.; Vollebregt, S.; Polichetti, T.; Miscuglio, M.; Alfano, B.; Miglietta, M. L.; Massera, E.; Di Francia, G.; Sarro, P. M. Effects of graphene defects on gas sensing properties towards NO2 detection. *Nanoscale* **2017**, *9*, 6085-6093.
(153) Mercado, E.; Goodyear, A.; Moffat, J.; Cooke, M.; Sundaram, R. S. A Raman metrology approach to quality control of 2D MoS2 film fabrication. *J Phys D Appl Phys* **2017**, *50*.
(154) Li, H.; Zhang, Q.; Yap, C. C. R.; Tay, B. K.; Edwin, T. H. T.; Olivier, A.; Baillargeat, D. From Bulk to Monolayer MoS2: Evolution of Raman Scattering. *Adv Funct Mater* **2012**, *22*, 1385-1390.
(155) Lee, C.; Yan, H.; Brus, L. E.; Heinz, T. F.; Hone, J.; Ryu, S. Anomalous Lattice Vibrations of Single- and Few-Layer MoS2. *ACS Nano* **2010**, *4*, 2695-2700.
(156) Calandra, M. Chemically exfoliated single-layer MoS2: Stability, lattice dynamics, and catalytic adsorption from first principles. *Phys Rev B* **2013**, *88*.
(157) Bohr, J. Adhesive tape exfoliation: Why it works for graphene. *Epl-Europhys Lett* **2015**, *109*.
(158) Zhao, Y. D.; Qiao, J. S.; Yu, Z. H.; Yu, P.; Xu, K.; Lau, S. P.; Zhou, W.; Liu, Z.; Wang, X. R.; Ji, W.; Chai, Y. High-Electron- Mobility and Air-Stable 2D Layered PtSe2 FETs. *Adv Mater* **2017**, *29*.
(159) Cai, X. K.; Luo, Y. T.; Liu, B.; Cheng, H. M. Preparation of 2D material dispersions and their applications. *Chem Soc Rev* **2018**, *47*, 6224-6266.
(160) Liu, L.; Shen, Z. G.; Yi, M.; Zhang, X. J.; Ma, S. L. A green, rapid and size-controlled production of high-quality graphene sheets by hydrodynamic forces. *Rsc Advances* **2014**, *4*, 36464-36470.
(161) Yi, M.; Shen, Z. G. Fluid dynamics: an emerging route for the scalable production of graphene in the last five years. *Rsc Advances* **2016**, *6*, 72525-72536.
(162) Coleman, J. N. Liquid Exfoliation of Defect-Free Graphene. *Acc. Chem. Res.* **2013**, *46*, 14-22.
(163) Ambrosi, A.; Pumera, M. Electrochemically Exfoliated Graphene and Graphene Oxide for Energy Storage and Electrochemistry Applications. *Chem. Eur. J.* **2016**, *22*, 153-159.
(164) Sevilla, M.; Ferrero, G. A.; Fuertes, A. B. Aqueous Dispersions of Graphene from Electrochemically Exfoliated Graphite. *Chem.Eur. J.* **2016**, *22*, 17351-17358.
(165) Liu, J. L.; Yang, H. P.; Zhen, S. G.; Poh, C. K.; Chaurasia, A.; Luo, J. S.; Wu, X. Y.; Yeow, E. K. L.; Sahoo, N. G.; Lin, J. Y.; Shen, Z. X. A Green Approach to the Synthesis of High-Quality Graphene Oxide Flakes *via* Electrochemical Exfoliation of Pencil Core. *RSC Adv.* **2013**, *3*, 11745-11750.
(166) Abdelkader, A. M.; Kinloch, I. A.; Dryfe, R. A. W. High-Yield Electro-Oxidative Preparation of Graphene Oxide. *Chem. Commun.* **2014**, *50*, 8402-8404.
(167) Liu, J. L.; Yang, H. P.; Zhen, S. G.; Poh, C. K.; Chaurasia, A.; Luo, J. S.; Wu, X. Y.; Yeow, E. K. L.; Sahoo, N. G.; Lin, J. Y.; Shen, Z. X. A green approach to the synthesis of high-quality graphene oxide flakes via electrochemical exfoliation of pencil core. *Rsc Advances* **2013**, *3*, 11745-11750.
(168) Cao, J. Y.; He, P.; Mohammed, M. A.; Zhao, X.; Young, R. J.; Derby, B.; Kinloch, I. A.; Dryfe, R. A. W. Two-Step Electrochemical Intercalation and Oxidation of Graphite for the Mass Production of Graphene Oxide. *J. Am. Chem. Soc.* **2017**, *139*, 17446-17456.
(169) Ciesielski, A.; Samorì, P. Supramolecular Approaches to Graphene: From Self-Assembly to Molecule-Assisted Liquid-Phase Exfoliation. *Adv. Mater.* **2016**, *28*, 6030-6051.
(170) Bonaccorso, F.; Lombardo, A.; Hasan, T.; Sun, Z. P.; Colombo, L.; Ferrari, A. C. Production and Processing of Graphene and 2d Crystals. *Mater. Today* **2012**, *15*, 564-589.

(171) Parvez, K.; Wu, Z. S.; Li, R. J.; Liu, X. J.; Graf, R.; Feng, X. L.; Müllen, K. Exfoliation of Graphite into Graphene in Aqueous Solutions of Inorganic Salts. *J. Am. Chem. Soc.* **2014**, *136*, 6083-6091.
(172) Kholmanov, I. N.; Magnuson, C. W.; Aliev, A. E.; Li, H. F.; Zhang, B.; Suk, J. W.; Zhang, L. L.; Peng, E.; Mousavi, S. H.; Khanikaev, A. B.; Piner, R.; Shvets, G.; Ruoff, R. S. Improved Electrical Conductivity of Graphene Films Integrated with Metal Nanowires. *Nano Lett.* **2012**, *12*, 5679-5683.
(173) Mayorov, A. S.; Gorbachev, R. V.; Morozov, S. V.; Britnell, L.; Jalil, R.; Ponomarenko, L. A.; Blake, P.; Novoselov, K. S.; Watanabe, K.; Taniguchi, T.; Geim, A. K. Micrometer-Scale Ballistic Transport in Encapsulated Graphene at Room Temperature. *Nano Lett.* **2011**, *11*, 2396-2399.
(174) Yu, P.; Tian, Z. M.; Lowe, S. E.; Song, J. C.; Ma, Z. R.; Wang, X.; Han, Z. J.; Bao, Q. L.; Simon, G. P.; Li, D.; Zhong, Y. L. Mechanically-Assisted Electrochemical Production of Graphene Oxide. *Chem. Mater.* **2016**, *28*, 8429-8438.
(175) Hsieh, C. T.; Hsueh, J. H. Electrochemical Exfoliation of Graphene Sheets from a Natural Graphite flask in the presence of sulfate ions at different temperatures. *RSC Adv.* **2016**, *6*, 96015-96015.
(176) Ejigu, A.; Kinloch, I. A.; Prestat, E.; Dryfe, R. A. W. A simple electrochemical route to metallic phase trilayer MoS_2: evaluation as electrocatalysts and supercapacitors. *J. Mater. Chem. A* **2017**, *5*, 11316-11330.
(177) Ejigu, A.; Miller, B.; Kinloch, I. A.; Dryfe, R. A. W. Optimisation of electrolytic solvents for simultaneous electrochemical exfoliation and functionalisation of graphene with metal nanostructures. *Carbon* **2018**, *128*, 257-266.
(178) Novoselov, K. S.; Jiang, D.; Schedin, F.; Booth, T. J.; Khotkevich, V. V.; Morozov, S. V.; Geim, A. K. Two-Dimensional Atomic Crystals. *Proc. Natl. Acad. Sci. USA* **2005**, *102*, 10451-10453.
(179) Valles, C.; Drummond, C.; Saadaoui, H.; Furtado, C. A.; He, M.; Roubeau, O.; Ortolani, L.; Monthioux, M.; Penicaud, A. Solutions of Negatively Charged Graphene Sheets and Ribbons. *J. Am. Chem. Soc.* **2008**, *130*, 15802-15804.
(180) Paton, K. R.; Varrla, E.; Backes, C.; Smith, R. J.; Khan, U.; O'Neill, A.; Boland, C.; Lotya, M.; Istrate, O. M.; King, P.; Higgins, T.; Barwich, S.; May, P.; Puczkarski, P.; Ahmed, I.; Moebius, M.; Pettersson, H.; Long, E.; Coelho, J.; O'Brien, S. E.; McGuire, E. K.; Sanchez, B. M.; Duesberg, G. S.; McEvoy, N.; Pennycook, T. J.; Downing, C.; Crossley, A.; Nicolosi, V.; Coleman, J. N. Scalable production of large quantities of defect-free few-layer graphene by shear exfoliation in liquids. *Nature Materials* **2014**, *13*, 624.
(181) Zhou, M.; Tian, T.; Li, X. F.; Sun, X. D.; Zhang, J.; Cui, P.; Tang, J.; Qin, L. C. Production of Graphene by Liquid-Phase Exfoliation of Intercalated Graphite. *Int J Electrochem Sc* **2014**, *9*, 810-820.
(182) Hasan, T.; Torrisi, F.; Sun, Z.; Popa, D.; Nicolosi, V.; Privitera, G.; Bonaccorso, F.; Ferrari, A. C. Solution-phase exfoliation of graphite for ultrafast photonics. *Phys Status Solidi B* **2010**, *247*, 2953-2957.
(183) Briggs, D.; Riviere, J. C. *Practical Surface Analysis: By Auger and X-ray Photoelectron Spectroscopy*. Wiley New York: Chichester, 1983.
(184) Hsiao, M. C.; Liao, S. H.; Yen, M. Y.; Teng, C. C.; Lee, S. H.; Pu, N. W.; Wang, C. A.; Sung, Y.; Ger, M. D.; Ma, C. C. M.; Hsiao, M. H. Preparation and Properties of a Graphene Reinforced Nanocomposite Conducting Plate. *J. Mater. Chem.* **2010**, *20*, 8496-8505.
(185) Park, S.; An, J. H.; Piner, R. D.; Jung, I.; Yang, D. X.; Velamakanni, A.; Nguyen, S. T.; Ruoff, R. S. Aqueous Suspension and Characterization of Chemically Modified Graphene Sheets. *Chem. Mater.* **2008**, *20*, 6592-6594.
(186) Kovtun, A.; Jones, D.; Dell'Elce, S.; Treossi, E.; Liscio, A.; Palermo, V. Accurate chemical analysis of oxygenated graphene-based materials using X-ray photoelectron spectroscopy. *Carbon* **2019**, *143*, 268-275.

(187) Ganguly, A.; Sharma, S.; Papakonstantinou, P.; Hamilton, J. Probing the Thermal Deoxygenation of Graphene Oxide Using High-Resolution In Situ X-ray-Based Spectroscopies. *J. Phys. Chem. C* **2011**, *115*, 17009-17019.
(188) Ferrari, A. C.; Robertson, J. Interpretation of Raman Spectra of Disordered and Amorphous Carbon. *Phys. Rev. B* **2000**, *61*, 14095-14107.
(189) Cancado, L. G.; Jorio, A.; Ferreira, E. H. M.; Stavale, F.; Achete, C. A.; Capaz, R. B.; Moutinho, M. V. O.; Lombardo, A.; Kulmala, T. S.; Ferrari, A. C. Quantifying Defects in Graphene *via* Raman Spectroscopy at Different Excitation Energies. *Nano Lett.* **2011**, *11*, 3190-3196.
(190) Eckmann, A.; Felten, A.; Mishchenko, A.; Britnell, L.; Krupke, R.; Novoselov, K. S.; Casiraghi, C. Probing the Nature of Defects in Graphene by Raman Spectroscopy. *Nano Lett.* **2012**, *12*, 3925-3930.
(191) Annett, J.; Cross, G. L. W. Self-Assembly of Graphene Ribbons by Spontaneous Self-Tearing and Peeling from a Substrate. *Nature* **2016**, *535*, 271-275.
(192) Lherbier, A.; Dubois, S. M. M.; Declerck, X.; Niquet, Y. M.; Roche, S.; Charlier, J. C. Transport Properties of Graphene Containing Structural Defects. *Phys. Rev. B, PRB* **2012**, *86*.
(193) Voiry, D.; Yang, J.; Kupferberg, J.; Fullon, R.; Lee, C.; Jeong, H. Y.; Shin, H. S.; Chhowalla, M. High-Quality Graphene *via* Microwave Reduction of Solution-Exfoliated Graphene Oxide. *Science* **2016**, *353*, 1413-1416.
(194) Dreyer, D. R.; Park, S.; Bielawski, C. W.; Ruoff, R. S. The Chemistry of Graphene Oxide. *Chem. Soc. Rev.* **2010**, *39*, 228-240.
(195) Larciprete, R.; Fabris, S.; Sun, T.; Lacovig, P.; Baraldi, A.; Lizzit, S. Dual Path Mechanism in the Thermal Reduction of Graphene Oxide. *J. Am. Chem. Soc.* **2011**, *133*, 17315-17321.
(196) Liu, L.; Tan, C. L.; Chai, J. W.; Wu, S. X.; Radko, A.; Zhang, H.; Mandler, D. Electrochemically "Writing" Graphene from Graphene Oxide. *Small* **2014**, *10*, 3555-3559.
(197) Chen, J.; Shepherd, R. L.; Razal, J. M.; Huang, X.; Zhang, W. M.; Zhao, J.; Harris, A. T.; Wang, S.; Minett, A. I.; Zhang, H. Scalable Solid-Template Reduction for Designed Reduced Graphene Oxide Architectures. *ACS Appl. Mater. Interfaces* **2013**, *5*, 7676-7681.
(198) Bagri, A.; Mattevi, C.; Acik, M.; Chabal, Y. J.; Chhowalla, M.; Shenoy, V. B. Structural Evolution during the Reduction of Chemically Derived Graphene Oxide. *Nat. Chem.* **2010**, *2*, 581-587.
(199) Becerril, H. A.; Mao, J.; Liu, Z.; Stoltenberg, R. M.; Bao, Z.; Chen, Y. Evaluation of Solution-Processed Reduced Graphene Oxide Films as Transparent Conductors. *ACS Nano* **2008**, *2*, 463-470.
(200) Wang, S.; Ang, P. K.; Wang, Z. Q.; Tang, A. L. L.; Thong, J. T. L.; Loh, K. P. High Mobility, Printable, and Solution-Processed Graphene Electronics. *Nano Lett.* **2010**, *10*, 92-98.
(201) Mayorov, A. S.; Gorbachev, R. V.; Morozov, S. V.; Britnell, L.; Jalil, R.; Ponomarenko, L. A.; Blake, P.; Novoselov, K. S.; Watanabe, K.; Taniguchi, T.; Geim, A. K. Micrometer-Scale Ballistic Transport in Encapsulated Graphene at Room Temperature. *Nano Lett* **2011**, *11*, 2396-2399.
(202) Bae, S.; Kim, H.; Lee, Y.; Xu, X. F.; Park, J. S.; Zheng, Y.; Balakrishnan, J.; Lei, T.; Kim, H. R.; Song, Y. I.; Kim, Y. J.; Kim, K. S.; Ozyilmaz, B.; Ahn, J. H.; Hong, B. H.; Iijima, S. Roll-to-roll production of 30-inch graphene films for transparent electrodes. *Nat. Nanotechnol.* **2010**, *5*, 574-578.
(203) Yu, Q. K.; Jauregui, L. A.; Wu, W.; Colby, R.; Tian, J. F.; Su, Z. H.; Cao, H. L.; Liu, Z. H.; Pandey, D.; Wei, D. G.; Chung, T. F.; Peng, P.; Guisinger, N. P.; Stach, E. A.; Bao, J. M.; Pei, S. S.; Chen, Y. P. Control and characterization of individual grains and grain boundaries in graphene grown by chemical vapour deposition. *Nat Mater* **2011**, *10*, 443-449.
(204) Li, X. S.; Magnuson, C. W.; Venugopal, A.; Tromp, R. M.; Hannon, J. B.; Vogel, E. M.; Colombo, L.; Ruoff, R. S. Large-Area Graphene Single Crystals Grown by Low-Pressure Chemical Vapor Deposition of Methane on Copper. *J Am Chem Soc* **2011**, *133*, 2816-2819.
(205) Petrone, N.; Dean, C. R.; Meric, I.; van der Zande, A. M.; Huang, P. Y.; Wang, L.; Muller, D.; Shepard, K. L.; Hone, J. Chemical Vapor Deposition-Derived Graphene with Electrical Performance of Exfoliated Graphene. *Nano Lett* **2012**, *12*, 2751-2756.

(206) Emtsev, K. V.; Bostwick, A.; Horn, K.; Jobst, J.; Kellogg, G. L.; Ley, L.; McChesney, J. L.; Ohta, T.; Reshanov, S. A.; Rohrl, J.; Rotenberg, E.; Schmid, A. K.; Waldmann, D.; Weber, H. B.; Seyller, T. Towards wafer-size graphene layers by atmospheric pressure graphitization of silicon carbide. *Nat Mater* **2009**, *8*, 203-207.
(207) Ciesielski, A.; Haar, S.; El Gemayel, M.; Yang, H.; Clough, J.; Melinte, G.; Gobbi, M.; Orgiu, E.; Nardi, M. V.; Ligorio, G.; Palermo, V.; Koch, N.; Ersen, O.; Casiraghi, C.; Samorì, P. Harnessing the Liquid-Phase Exfoliation of Graphene Using Aliphatic Compounds: A Supramolecular Approach. *Angew. Chem. Int. Ed.* **2014**, *53*, 10355-10361.
(208) Novoselov, K. S.; Jiang, D.; Schedin, F.; Booth, T. J.; Khotkevich, V. V.; Morozov, S. V.; Geim, A. K. Two-dimensional atomic crystals. *Proc. Natl. Acad. Sci. U.S.A.* **2005**, *102*, 10451-10453.
(209) El Gemayel, M.; Haar, S.; Liscio, F.; Schlierf, A.; Melinte, G.; Milita, S.; Ersen, O.; Ciesielski, A.; Palermo, V.; Samori, P. Leveraging the Ambipolar Transport in Polymeric Field-Effect Transistors via Blending with Liquid-Phase Exfoliated Graphene. *Adv. Mater.* **2014**, *26*, 4814-+.
(210) Eda, G.; Yamaguchi, H.; Voiry, D.; Fujita, T.; Chen, M.; Chhowalla, M. Photoluminescence from chemically exfoliated MoS_2. *Nano Lett.* **2011**, *11*, 5111-5116.
(211) Coleman, J. N.; Lotya, M.; O'Neill, A.; Bergin, S. D.; King, P. J.; Khan, U.; Young, K.; Gaucher, A.; De, S.; Smith, R. J. Two-dimensional nanosheets produced by liquid exfoliation of layered materials. *Science* **2011**, *331*, 568-571.
(212) Fan, X.; Xu, P.; Zhou, D.; Sun, Y.; Li, Y. C.; Nguyen, M. A. T.; Terrones, M.; Mallouk, T. E. Fast and efficient preparation of exfoliated 2H MoS_2 nanosheets by sonication-assisted lithium intercalation and infrared laser-induced 1T to 2H phase reversion. *Nano Lett.* **2015**, *15*, 5956-5960.
(213) Qi, Y.; Wang, N.; Xu, Q.; Li, H.; Zhou, P.; Lu, X.; Zhao, G. A green route to fabricate MoS_2 nanosheets in water–ethanol–CO_2. *Chem. Commun.* **2015**, *51*, 6726-6729.
(214) Zeng, Z.; Yin, Z.; Huang, X.; Li, H.; He, Q.; Lu, G.; Boey, F.; Zhang, H. Single-layer semiconducting nanosheets: high-yield preparation and device fabrication. *Angew. Chem. Int. Ed.* **2011**, *50*, 11093-11097.
(215) You, X.; Liu, N.; Lee, C. J.; Pak, J. J. An electrochemical route to MoS_2 nanosheets for device applications. *Mater. Lett.* **2014**, *121*, 31-35.
(216) Chhowalla, M.; Amaratunga, G. A. J. Thin films of fullerene-like MoS_2 nanoparticles with ultra-low friction and wear. *Nature* **2000**, *407*, 164-167.
(217) Fleischauer, P. D.; Bauer, R. Chemical and structural effects on the lubrication properties of sputtered MoS_2 films. *Tribol. Trans.* **1988**, *31*, 239-250.
(218) Yang, D.; Sandoval, S. J.; Divigalpitiya, W. M. R.; Irwin, J. C.; Frindt, R. F. Structure of single-molecular-layer MoS_2. *Phys. Rev. B* **1991**, *43*, 12053-12056.
(219) Acerce, M.; Voiry, D.; Chhowalla, M. Metallic 1T phase MoS_2 nanosheets as supercapacitor electrode materials. *Nat. Nanotechnol.* **2015**, *10*, 313-318.
(220) Kim, J.; Kim, J. S.; Kim, T.; Choi, H.; Lee, J.; Ji, H. J.; Lim, S. C. Phase conversion of chemically exfoliated molybdenum disulfide. *Curr. Appl. Phys.* **2017**, *17*, 60-65.
(221) Xu, D. Y.; Zhu, Y. Z.; Liu, J. P.; Li, Y.; Peng, W. C.; Zhang, G. L.; Zhang, F. B.; Fan, X. B. Microwave-assisted 1T to 2H phase reversion of MoS_2 in solution: a fast route to processable dispersions of 2H-MoS_2 nanosheets and nanocomposites. *Nanotechnology* **2016**, *27*, 385604.
(222) Chng, E. L. K.; Sofer, Z.; Pumera, M. MoS_2 exhibits stronger toxicity with increased exfoliation. *Nanoscale* **2014**, *6*, 14412-14418.
(223) Lukowski, M. A.; Daniel, A. S.; Meng, F.; Forticaux, A.; Li, L.; Jin, S. Enhanced hydrogen evolution catalysis from chemically exfoliated metallic MoS_2 nanosheets. *J. Am. Chem. Soc.* **2013**, *135*, 10274-10277.
(224) Ambrosi, A.; Sofer, Z.; Pumera, M. Lithium intercalation compound dramatically influences the electrochemical properties of exfoliated MoS_2. *Small* **2015**, *11*, 605-612.

(225) El Garah, M.; Bertolazzi, S.; Ippolito, S.; Eredia, M.; Janica, I.; Melinte, G.; Ersen, O.; Marletta, G.; Ciesielski, A.; Samorì, P. MoS2 nanosheets via electrochemical lithium-ion intercalation under ambient conditions. *FlatChem* **2018**, *9*, 33-39.
(226) Jiang, L.; Zhang, S.; Kulinich, S. A.; Song, X.; Zhu, J.; Wang, X.; Zeng, H. Optimizing hybridization of 1T and 2H phases in MoS_2 monolayers to improve capacitances of supercapacitors. *Mater. Res. Lett.* **2015**, *3*, 177-183.
(227) Cummins, D. R.; Martinez, U.; Sherehiy, A.; Kappera, R.; Martinez-Garcia, A.; Schulze, R. K.; Jasinski, J.; Zhang, J.; Gupta, R. K.; Lou, J. Efficient hydrogen evolution in transition metal dichalcogenides via a simple one-step hydrazine reaction. *Nat. Commun.* **2016**, *7*, 11857.
(228) Knirsch, K. C.; Berner, N. C.; Nerl, H. C.; Cucinotta, C. S.; Gholamvand, Z.; McEvoy, N.; Wang, Z.; Abramovic, I.; Vecera, P.; Halik, M. Basal-plane functionalization of chemically exfoliated molybdenum disulfide by diazonium salts. *ACS Nano* **2015**, *9*, 6018-6030.
(229) Papageorgopoulos, C. A.; Jaegermann, W. Li intercalation across and along the van der Waals surfaces of MoS_2 (0001). *Surf. Sci.* **1995**, *338*, 83-93.
(230) Voiry, D.; Mohite, A.; Chhowalla, M. Phase engineering of transition metal dichalcogenides. *Chem. Soc. Rev.* **2015**, *44*, 2702-2712.
(231) Westphal, E.; Pliego Jr, J. R. Absolute solvation free energy of Li^+ and Na^+ ions in dimethyl sulfoxide solution: a theoretical ab initio and cluster-continuum model study. *J. Chem. Phys.* **2005**, *123*, 074508.
(232) Bertolazzi, S.; Bonacchi, S.; Nan, G. J.; Pershin, A.; Beljonne, D.; Samori, P. Engineering Chemically Active Defects in Monolayer MoS2 Transistors via Ion-Beam Irradiation and Their Healing via Vapor Deposition of Alkanethiols. *Advanced Materials* **2017**, *29*.
(233) Mignuzzi, S.; Pollard, A. J.; Bonini, N.; Brennan, B.; Gilmore, I. S.; Pimenta, M. A.; Richards, D.; Roy, D. Effect of disorder on Raman scattering of single-layer MoS_2. *Phys. Rev. B* **2015**, *91*, 195411.
(234) Bertolazzi, S.; Bonacchi, S.; Nan, G.; Pershin, A.; Beljonne, D.; Samorì, P. Engineering chemically active defects in monolayer MoS_2 transistors via ion-beam irradiation and their healing via vapor deposition of alkanethiols. *Adv. Mater.* **2017**, *29*, 1606760.
(235) Kelly, A. G.; Hallam, T.; Backes, C.; Harvey, A.; Esmaeily, A. S.; Godwin, I.; Coelho, J.; Nicolosi, V.; Lauth, J.; Kulkarni, A.; Kinge, S.; Siebbeles, L. D. A.; Duesberg, G. S.; Coleman, J. N. All-printed thin-film transistors from networks of liquid-exfoliated nanosheets. *Science* **2017**, *356*, 69-72.
(236) Knirsch, K. C.; Berner, N. C.; Nerl, H. C.; Cucinotta, C. S.; Gholamvand, Z.; McEvoy, N.; Wang, Z. X.; Abramovic, I.; Vecera, P.; Halik, M.; Sanvito, S.; Duesberg, G. S.; Nicolosi, V.; Hauke, F.; Hirsch, A.; Colernan, J. N.; Backes, C. Basal-plane functionalization of chemically exfoliated molybdenum disulfide by diazonium salts. *ACS Nano* **2015**, *9*, 6018-6030.
(237) Li, S. L.; Tsukagoshi, K.; Orgiu, E.; Samorì, P. Charge transport and mobility engineering in two-dimensional transition metal chalcogenide semiconductors. *Chem. Soc. Rev.* **2016**, *45*, 118-151.
(238) {Radisavljevic, R., B.; Radenovic, A.; Brivio, J.; Giacometti, V.; Kis, A. Single-layer MoS_2 transistors. *Nat. Nanotechnol.* **2011**, *6*, 147-150.
(239) Radisavljevic, B.; Kis, A. Measurement of mobility in dual-gated MoS_2 transistors. *Nat. Nanotechnol.* **2013**, *8*, 147-148.
(240) Radisavljevic, B.; Kis, A. Mobility engineering and a metal-insulator transition in monolayer MoS_2. *Nature Materials* **2013**, *12*, 815-820.
(241) Fuhrer, M. S.; Hone, J. Measurement of mobility in dual-gated MoS_2 transistors. *Nature Nanotechnology* **2013**, *8*, 146.
(242) Cho, S. Y.; Kim, S. J.; Lee, Y.; Kim, J. S.; Jung, W. B.; Yoo, H. W.; Kim, J.; Jung, H. T. Highly Enhanced Gas Adsorption Properties in Vertically Aligned MoS2 Layers. *ACS Nano* **2015**, *9*, 9314-9321.

(243) Makarova, M.; Okawa, Y.; Aono, M. Selective Adsorption of Thiol Molecules at Sulfur Vacancies on MoS2(0001), Followed by Vacancy Repair via S-C Dissociation. *J Phys Chem C* **2012**, *116*, 22411-22416.
(244) Kim, J. S.; Yoo, H. W.; Choi, H. O.; Jung, H. T. Tunable Volatile Organic Compounds Sensor by Using Thiolated Ligand Conjugation on MoS2. *Nano Lett* **2014**, *14*, 5941-5947.
(245) Jeong, M.; Kim, S.; Ju, S. Y. Preparation and characterization of a covalent edge-functionalized lipoic acid-MoS2 conjugate. *Rsc Advances* **2016**, *6*, 36248-36255.
(246) Tsai, C.; Li, H.; Park, S.; Park, J.; Han, H. S.; Norskov, J. K.; Zheng, X. L.; Abild-Pedersen, F. Electrochemical generation of sulfur vacancies in the basal plane of MoS2 for hydrogen evolution. *Nat Commun* **2017**, *8*.
(247) Caron, A.; Redon, N.; Thevenet, F.; Hanoune, B.; Coddeville, P. Performances and limitations of electronic gas sensors to investigate an indoor air quality event. *Build Environ* **2016**, *107*, 19-28.
(248) Khan, Y.; Ostfeld, A. E.; Lochner, C. M.; Pierre, A.; Arias, A. C. Monitoring of Vital Signs with Flexible and Wearable Medical Devices. *Advanced Materials* **2016**, *28*, 4373-4395.
(249) Carmona, E. N.; Sberveglieri, V.; Ponzoni, A.; Galstyan, V.; Zappa, D.; Pulvirenti, A.; Comini, E. Detection of food and skin pathogen microbiota by means of an electronic nose based on metal oxide chemiresistors. *Sensor Actuat B-Chem* **2017**, *238*, 1224-1230.
(250) Efremenko, Y.; Mirsky, V. M. Virtual sensor array consisting of a single sensor element with variable affinity: An application for analysis of fish freshness. *Sensor Actuat B-Chem* **2017**, *241*, 652-657.
(251) Zhou, W.; Zou, X. L.; Najmaei, S.; Liu, Z.; Shi, Y. M.; Kong, J.; Lou, J.; Ajayan, P. M.; Yakobson, B. I.; Idrobo, J. C. Intrinsic Structural Defects in Monolayer Molybdenum Disulfide. *Nano Lett* **2013**, *13*, 2615-2622.
(252) Komsa, H. P.; Krasheninnikov, A. V. Native defects in bulk and monolayer MoS2 from first principles. *Phys Rev B* **2015**, *91*.
(253) Noh, J. Y.; Kim, H.; Kim, Y. S. Stability and electronic structures of native defects in single-layer MoS2. *Phys Rev B* **2014**, *89*.
(254) Chianelli, R. R.; Ruppert, A. F.; Behal, S. K.; Kear, B. H.; Wold, A.; Kershaw, R. The Reactivity of Mos2 Single-Crystal Edge Planes. *J Catal* **1985**, *92*, 56-63.
(255) Gonzalez, C.; Biel, B.; Dappe, Y. J. Theoretical characterisation of point defects on a MoS2 monolayer by scanning tunnelling microscopy. *Nanotechnology* **2016**, *27*.
(256) Laursen, A. B.; Kegnaes, S.; Dahl, S.; Chorkendorff, I. Molybdenum sulfides-efficient and viable materials for electro - and photoelectrocatalytic hydrogen evolution. *Energ Environ Sci* **2012**, *5*, 5577-5591.
(257) Hinnemann, B. G. M., P.; Bonde, B.; Jørgensen, K.P.; Nielsen, J.H; Horch,S.; Chorkendorff,Ib. and Nørskov, J. K. Biomimetic Hydrogen Evolution: MoS2 Nanoparticles as Catalyst for Hydrogen Evolution. *J. Am. Chem. Soc.* **2005**, 5308-5309.
(258) Bollinger, M. V.; Lauritsen, J. V.; Jacobsen, K. W.; Norskov, J. K.; Helveg, S.; Besenbacher, F. One-dimensional metallic edge states in MoS2. *Phys Rev Lett* **2001**, *87*.
(259) Wang, T. Y.; Gao, D. L.; Zhuo, J. Q.; Zhu, Z. W.; Papakonstantinou, P.; Li, Y.; Li, M. X. Size-Dependent Enhancement of Electrocatalytic Oxygen-Reduction and Hydrogen-Evolution Performance of MoS2 Particles. *Chem-Eur J* **2013**, *19*, 11939-11948.
(260) Xie, J. F.; Zhang, J. J.; Li, S.; Grote, F.; Zhang, X. D.; Zhang, H.; Wang, R. X.; Lei, Y.; Pan, B. C.; Xie, Y. Controllable Disorder Engineering in Oxygen-Incorporated MoS2 Ultrathin Nanosheets for Efficient Hydrogen Evolution (vol 135, pg 17881, 2013). *J. Am. Chem. Soc.* **2014**, *136*, 1680-1680.
(261) Chung, D. Y.; Park, S. K.; Chung, Y. H.; Yu, S. H.; Lim, D. H.; Jung, N.; Ham, H. C.; Park, H. Y.; Piao, Y.; Yoo, S. J.; Sung, Y. E. Edge-exposed MoS2 nano-assembled structures as efficient electrocatalysts for hydrogen evolution reaction. *Nanoscale* **2014**, *6*, 2131-2136.

(262) Benson, J.; Li, M. X.; Wang, S. B.; Wang, P.; Papakonstantinou, P. Electrocatalytic Hydrogen Evolution Reaction on Edges of a Few Layer Molybdenum Disulfide Nanodots. *Acs Appl Mater Inter* **2015**, *7*, 14113-14122.
(263) Gonzalez, C.; Biel, B.; Dappe, Y. J. Adsorption of small inorganic molecules on a defective MoS2 monolayer. *Phys Chem Chem Phys* **2017**, *19*, 9485-9499.
(264) Yu, N. N.; Wang, L.; Li, M.; Sun, X. T.; Hou, T. J.; Li, Y. Y. Molybdenum disulfide as a highly efficient adsorbent for non-polar gases. *Phys Chem Chem Phys* **2015**, *17*, 11700-11704.
(265) Zeng, Y. M.; Lin, S. W.; Gu, D. D.; Li, X. G. Two-Dimensional Nanomaterials for Gas Sensing Applications: The Role of Theoretical Calculations. *Nanomaterials-Basel* **2018**, *8*.
(266) Kim, Y. H.; Kim, K. Y.; Choi, Y. R.; Shim, Y. S.; Jeon, J. M.; Lee, J. H.; Kim, S. Y.; Han, S.; Jang, H. W. Ultrasensitive reversible oxygen sensing by using liquid-exfoliated MoS2 nanoparticles. *Journal of Materials Chemistry A* **2016**, *4*, 6070-6076.
(267) Late, D. J.; Huang, Y. K.; Liu, B.; Acharya, J.; Shirodkar, S. N.; Luo, J. J.; Yan, A. M.; Charles, D.; Waghmare, U. V.; Dravid, V. P.; Rao, C. N. R. Sensing Behavior of Atomically Thin-Layered MoS2 Transistors. *ACS Nano* **2013**, *7*, 4879-4891.
(268) Chen, X.; Berner, N. C.; Backes, C.; Duesberg, G. S.; McDonald, A. R. Functionalization of Two-Dimensional MoS2: On the Reaction Between MoS2 and Organic Thiols. *Angew Chem Int Edit* **2016**, *55*, 5803-5808.
(269) Yao, Y. G.; Tolentino, L.; Yang, Z. Z.; Song, X. J.; Zhang, W.; Chen, Y. S.; Wong, C. P. High-Concentration Aqueous Dispersions of MoS2. *Adv Funct Mater* **2013**, *23*, 3577-3583.
(270) Sim, D. M.; Han, H. J.; Yim, S.; Choi, M. J.; Jeon, J.; Jung, Y. S. Long-Term Stable 2H-MoS2 Dispersion: Critical Role of Solvent for Simultaneous Phase Restoration and Surface Functionalization of Liquid-Exfoliated MoS2. *Acs Omega* **2017**, *2*, 4678-4687.
(271) Fan, X. B.; Xu, P. T.; Li, Y. C.; Zhou, D. K.; Sun, Y. F.; Nguyen, M. A. T.; Terrones, M.; Mallouk, T. E. Controlled Exfoliation of MoS2 Crystals into Trilayer Nanosheets. *J. Am. Chem. Soc.* **2016**, *138*, 5143-5149.
(272) Jaramillo, T. F.; Jorgensen, K. P.; Bonde, J.; Nielsen, J. H.; Horch, S.; Chorkendorff, I. Identification of active edge sites for electrochemical H-2 evolution from MoS2 nanocatalysts. *Science* **2007**, *317*, 100-102.
(273) Li, H.; Lu, G.; Wang, Y. L.; Yin, Z. Y.; Cong, C. X.; He, Q. Y.; Wang, L.; Ding, F.; Yu, T.; Zhang, H. Mechanical Exfoliation and Characterization of Single- and Few-Layer Nanosheets of WSe2, TaS2, and TaSe2. *Small* **2013**, *9*, 1974-1981.
(274) Xie, J. F.; Zhang, H.; Li, S.; Wang, R. X.; Sun, X.; Zhou, M.; Zhou, J. F.; Lou, X. W.; Xie, Y. Defect-Rich MoS2 Ultrathin Nanosheets with Additional Active Edge Sites for Enhanced Electrocatalytic Hydrogen Evolution. *Advanced Materials* **2013**, *25*, 5807-+.
(275) Yuan, H.; Liu, X. H.; Ma, L. M.; Gong, P. W.; Yang, Z. G.; Wang, H. G.; Wang, J. Q.; Yang, S. R. High efficiency shear exfoliation for producing high-quality, few-layered MoS2 nanosheets in a green ethanol/water system. *Rsc Advances* **2016**, *6*, 82763-82773.
(276) Smith, R. J.; King, P. J.; Lotya, M.; Wirtz, C.; Khan, U.; De, S.; O'Neill, A.; Duesberg, G. S.; Grunlan, J. C.; Moriarty, G.; Chen, J.; Wang, J. Z.; Minett, A. I.; Nicolosi, V.; Coleman, J. N. Large-Scale Exfoliation of Inorganic Layered Compounds in Aqueous Surfactant Solutions. *Advanced Materials* **2011**, *23*, 3944-+.
(277) Backes, C.; Berner, N. C.; Chen, X.; Lafargue, P.; LaPlace, P.; Freeley, M.; Duesberg, G. S.; Coleman, J. N.; McDonald, A. R. Functionalization of Liquid-Exfoliated Two-Dimensional 2H-MoS2. *Angew Chem Int Edit* **2015**, *54*, 2638-2642.
(278) Lukowski, M. A.; Daniel, A. S.; Meng, F.; Forticaux, A.; Li, L. S.; Jin, S. Enhanced Hydrogen Evolution Catalysis from Chemically Exfoliated Metallic MoS2 Nanosheets. *J. Am. Chem. Soc.* **2013**, *135*, 10274-10277.
(279) Voiry, D.; Salehi, M.; Silva, R.; Fujita, T.; Chen, M. W.; Asefa, T.; Shenoy, V. B.; Eda, G.; Chhowalla, M. Conducting MoS2 Nanosheets as Catalysts for Hydrogen Evolution Reaction. *Nano Lett* **2013**, *13*, 6222-6227.

(280) McAteer, D.; Gholamvand, Z.; McEvoy, N.; Harvey, A.; O'Malley, E.; Duesberg, G. S.; Coleman, J. N. Thickness Dependence and Percolation Scaling of Hydrogen Production Rate in MoS2 Nanosheet and Nanosheet-Carbon Nanotube Composite Catalytic Electrodes. *ACS Nano* **2016**, *10*, 672-683.
(281) Santosh, K. C.; Longo, R. C.; Wallace, R. M.; Cho, K. Surface oxidation energetics and kinetics on MoS2 monolayer. *Journal of Applied Physics* **2015**, *117*.
(282) Cai, M. Z.; Thorpe, D.; Adamson, D. H.; Schniepp, H. C. Methods of graphite exfoliation. *J Mater Chem* **2012**, *22*, 24992-25002.
(283) Boyd, D. A.; Lin, W. H.; Hsu, C. C.; Teague, M. L.; Chen, C. C.; Lo, Y. Y.; Chan, W. Y.; Su, W. B.; Cheng, T. C.; Chang, C. S.; Wu, C. I.; Yeh, N. C. Single-step deposition of high-mobility graphene at reduced temperatures. *Nat. Commun.* **2015**, *6*.
(284) Schwierz, F. Graphene transistors. *Nat. Nanotechnol.* **2010**, *5*, 487-496.
(285) Mei, Y. C.; Loth, M. A.; Payne, M.; Zhang, W. M.; Smith, J.; Day, C. S.; Parkin, S. R.; Heeney, M.; McCulloch, I.; Anthopoulos, T. D.; Anthony, J. E.; Jurchescu, O. D. High Mobility Field-Effect Transistors with Versatile Processing from a Small-Molecule Organic Semiconductor. *Adv. Mater.* **2013**, *25*, 4352-4357.
(286) Nouchi, R.; Kubozono, Y. Anomalous hysteresis in organic field-effect transistors with SAM-modified electrodes: Structural switching of SAMs by electric field. *Org. Electron.* **2010**, *11*, 1025-1030.
(287) Yan, H.; Chen, Z. H.; Zheng, Y.; Newman, C.; Quinn, J. R.; Dotz, F.; Kastler, M.; Facchetti, A. A high-mobility electron-transporting polymer for printed transistors. *Nature* **2009**, *457*, 679-U1.
(288) Forrest, S. R. Exciton formation statistics under electrical injection in organic semiconductor thin films. *J. Lumin.* **2004**, *110*, 378-383.
(289) Arias, A. C.; MacKenzie, J. D.; McCulloch, I.; Rivnay, J.; Salleo, A. Materials and Applications for Large Area Electronics: Solution-Based Approaches. *Chem. Rev.* **2010**, *110*, 3-24.
(290) Basu, S.; Adriyanto, F.; Wang, Y. H. Blending effect of 6,13-bis (triisopropylsilylethynyl) pentacene-graphene composite layers for flexible thin film transistors with a polymer gate dielectric. *Nanotechnology* **2014**, *25*.
(291) Huang, J.; Hines, D. R.; Jung, B. J.; Bronsgeest, M. S.; Tunnell, A.; Ballarotto, V.; Katz, H. E.; Fuhrer, M. S.; Williams, E. D.; Cumings, J. Polymeric semiconductor/graphene hybrid field-effect transistors. *Org. Electron.* **2011**, *12*, 1471-1476.
(292) Kumari, A.; Singh, I.; Prasad, N.; Dixit, S. K.; Rao, P. K.; Bhatnagar, P. K.; Mathur, P. C.; Bhatia, C. S.; Nagpal, S. Improving the efficiency of a poly(3-hexylthiophene)-CuInS2 photovoltaic device by incorporating graphene nanopowder. *J. Nanophotonics* **2014**, *8*, 083092.
(293) Mosciatti, T.; Haar, S.; Liscio, F.; Ciesielski, A.; Orgiu, E.; Samorì, P. A Multifunctional Polymer-Graphene Thin-Film Transistor with Tunable Transport Regimes. *Acs Nano* **2015**, *9*, 2357-2367.
(294) Ha, T. J.; Akinwande, D.; Dodabalapur, A. Hybrid graphene/organic semiconductor field-effect transistors. *Appl. Phys. Lett.* **2012**, *101*.
(295) Huang, X.; Qi, X. Y.; Boey, F.; Zhang, H. Graphene-based composites. *Chem. Soc. Rev.* **2012**, *41*, 666-686.
(296) Bkakri, R.; Kusmartseva, O. E.; Kusmartsev, F. V.; Song, M.; Bouazizi, A. Degree of phase separation effects on the charge transfer properties of P3HT:Graphene nanocomposites. *J. Lumin.* **2015**, *161*, 264-270.
(297) Li, D.; Muller, M. B.; Gilje, S.; Kaner, R. B.; Wallace, G. G. Processable aqueous dispersions of graphene nanosheets. *Nat. Nanotechnol.* **2008**, *3*, 101-105.
(298) Orgiu, E.; Crivillers, N.; Rotzler, J.; Mayor, M.; Samori, P. Tuning the charge injection of P3HT-based organic thin-film transistors through electrode functionalization with oligophenylene SAMs. *J Mater Chem* **2010**, *20*, 10798-10800.

(299) Ying, L.; Hsu, B. B. Y.; Zhan, H. M.; Welch, G. C.; Zalar, P.; Perez, L. A.; Kramer, E. J.; Nguyen, T. Q.; Heeger, A. J.; Wong, W. Y.; Bazan, G. C. Regioregular Pyridal[2,1,3]thiadiazole pi-Conjugated Copolymers. *J. Am. Chem. Soc.* **2011**, *133*, 18538-18541.
(300) Kurta, R. P.; Grodd, L.; Mikayelyan, E.; Gorobtsov, O. Y.; Zaluzhnyy, I. A.; Fratoddi, I.; Venditti, I.; Russo, M. V.; Sprung, M.; Vartanyants, I. A.; Grigorian, S. Local structure of semicrystalline P3HT films probed by nanofocused coherent X-rays. *Phys. Chem. Chem. Phys.* **2015**, *17*, 7404-7410.
(301) Rabe, J. P.; Buchholz, S. Commensurability and Mobility in 2-Dimensional Molecular-Patterns on Graphite. *Science* **1991**, *253*, 424-427.
(302) Hamilton, C. E.; Lomeda, J. R.; Sun, Z. Z.; Tour, J. M.; Barron, A. R. High-Yield Organic Dispersions of Unfunctionalized Graphene. *Nano Lett.* **2009**, *9*, 3460-3462.
(303) Haar, S.; Ciesielski, A.; Clough, J.; Yang, H. F.; Mazzaro, R.; Richard, F.; Conti, S.; Merstorf, N.; Cecchini, M.; Morandi, V.; Casiraghi, C.; Samorì, P. A Supramolecular Strategy to Leverage the Liquid-Phase Exfoliation of Graphene in the Presence of Surfactants: Unraveling the Role of the Length of Fatty Acids. *Small* **2015**, *11*, 1691-1702.
(304) Na, J. Y.; Kang, B.; Sin, D. H.; Cho, K.; Park, Y. D. Understanding Solidification of Polythiophene Thin Films during Spin-Coating: Effects of Spin-Coating Time and Processing Additives. *Sci Rep-Uk* **2015**, *5*.
(305) Luo, H. W.; Yu, C. M.; Liu, Z. T.; Zhang, G. X.; Geng, H.; Yi, Y. P.; Broch, K.; Hu, Y. Y.; Sadhanala, A.; Jiang, L.; Qi, P. L.; Cai, Z. X.; Sirringhaus, H.; Zhang, D. Q. Remarkable enhancement of charge carrier mobility of conjugated polymer field-effect transistors upon incorporating an ionic additive. *Sci Adv* **2016**, *2*.

LIST OF ABBREVIATIONS

2DM	Two-dimensional material
AFM	Atomic force microscopy
BP	Black phosphorus
CB	Conduction band
CNP	Charge neutrality point
CVD	Chemical vapor deposition
DI	Deionized water
DMF	Dimethlyformamide
DMSO	Dimethyl sulfoxide
DSA	Dispersion stabilizing agent
EE	Electrochemical exfoliation
EEG	Electrochemically exfoliated graphene
EEMoS_2	Electrochemically exfoliated MoS_2
E_g	Energy gap
FET	Field-effect transistor
FL	Few-layer
FLG	Few-layer graphene
GIWAXS	Grazing-incidence wide-angle X-ray scattering
GO	Graphene oxide
h-BN	Hexagonal boron nitride
HF	Hydrogen fluoride
HR-TEM	High-resolution transmission electron microscopy
IPA	Isopropyl alcohol
LPE	Liquid-phase exfoliation
ME	Mechanical exfoliation
MLG	Multiple layer graphene
MoS_2	Molybdenum disulfide
MW	Microwave
NMP	N-methyl-2-pyrrolidone
OFET	Organic field-effect transistor
OSC	Organic semiconductor
P3HT	Poly(3-hexylthiophene)
PCDTPT	Poly[4-(4,4-dihexadecyl-4H-cyclopenta[1,2-b:5,4-b']dithiophen-2-yl)-alt-[1,2,5]thiadiazolo-[3,4-c]pyridine]
r-GO	Reduced graphene oxide
R_{RMS}	Root-mean-square roughness
SE	Shear exfoliation
SL	Single-layer
SLG	Single-layer graphene
TMC	Transition metal carbide

TMDs	Transition metal dichalcogenides
UILPE	Ultrasound-induced liquid-phase exfoliation
UV-O_3	Ultraviolet-ozone
VB	Valence band
V_{ds}	Drain-source voltage
vdW	van der Waals
V_g	Gate voltage
XPS	X-ray photoelectron spectroscopy
XRR	X-Ray reflectivity

STATEMENT OF WORK

The experiments and data reported in this thesis have been carried out and collected by myself except for those listed below:

Chapter 4: HR-TEM measurements were performed by Georgian Melinte in the group of Prof. Ovidiu Ersen (IPCMS, Strasbourg, France). Fabrication of devices and electrical measurements on EEG and EEMoS_2 were performed with Simone Bertolazzi and Tim Leydecker, post-doc in Nanochemistry lab. Experiments of MoS_2 sulfur-vacancy healing with butanethiol have been performed by Stefano Ippolito (Nanochemistry lab., Strasbourg, France).

Chapter 5: Electrical characterization measurements on MoS_2-based sensors and data analysis were carried out by Marc-Antoine Stoeckel, PhD in Nanochemistry lab.

Chapter 6: The synthesis of P3HT polymer was performed in the group of Prof. Michael Sommer (Institut für Makromolekulare Chemie, Freiburg, Germany). Ambient photoelectron spectrometer measurements and electrical measurements on graphene/polymer films were performed by Tim Leydecker. XRD and 2D-GIWAXS measurements and analysis were performed by Dr. Fabiola Liscio in the group of S. Milita (Istituto per la Microelettronica e Microsistemi (IMM) – CNR, Bologna). HR-TEM images were recorded by Georgian Melinte.

The projects reported in this manuscript were designed with Prof. Paolo Samorì and Dr. Artur Ciesielski. The interns under my supervision helped with some of the experiments.

AKNOWLEDGEMENTS

I express my deepest gratitude to many people I have met during this new and exciting experience that is the PhD.

First, I wish to thank my advisor, Prof. Paolo Samorì, for accepting me being part of his great multicultural and multidisciplinary research group, and for his supervision to my work. Working under his guidance was a great chance for me, for knowing the international research world and challenge myself on many different and cutting edge scientific topics. I am grateful for his trust and the freedom he gave me to follow my scientific interests. I highly appreciated him for being always forthcoming and for his great humanity that will inspire me for forever.

What shall I say about my co-advisor Artur Ciesielski? He is an example to follow. He is a master on our research field, he is sensitive and he was always present, ready to encourage me and give me good advices.

I will be always grateful to both of them because, besides being always present and collaborative, they enriched me both professionally and personally.

I am also thankful to Prof. Artur Stefankiewicz, Prof. Mario Ruben and Prof. Mateo-Alonso Aurelio for accepting to be part of my PhD jury and for the time they have dedicated to this thesis.

A special thank go to my colleagues in the Nanochemistry Group who shared with me special moments and who made easier and pleasant these years in lab.

It was an enormous pleasure to take part of the International Research Training Group (IRTG) Soft Matter Science network coordinated by Prof. Günter Reiter and Prof. Jörg Baschnagel who gave me the opportunity to periodically discuss my findings with a big interdisciplinary group of brilliant colleagues during many events, including motivating summer schools and workshop.

I dedicate this thesis to my family, to my old friends and to all the beautiful people I met during these years. Thank you.

PUBLICATIONS

- “Graphene via Molecule-Assisted Ultrasound-Induced Liquid-Phase Exfoliation: A Supramolecular Approach”, M. Eredia, A. Ciesielski, P. Samorì in Muellen, K. and Feng, X. editors, Chemistry of Carbon Nanostructures, Chapter 6, **2016**, pages 173-193, De Gruyter.

- "Morphology and Electronic Properties of Electrochemically Exfoliated Graphene", M. Eredia, S. Bertolazzi, T. Leydecker, M. El Garah, I. Janica, G. Melinte, O. Ersen, A. Ciesielski, P. Samorì, *J. Phys. Chem. Lett.*, 8, **2017**, 3347–3355.

- "Asymmetric Injection in Organic Transistors via Direct SAM Functionalization of Source and Drain Electrodes", T. Mosciatti, P. Greco, T. Leydecker, M. Eredia, F. Biscarini, P. Samorì, *ACS Omega*, 2, **2017**, 3502–3508.

- "Hybrid Copper-Nanowire–Reduced-Graphene-Oxide Coatings: A “Green Solution” Toward Highly Transparent, Highly Conductive, and Flexible Electrodes for (Opto)Electronics", A. Aliprandi, T. Moreira, C. Anichini, M.-A. Stoeckel, M. Eredia, U. Sassi, M. Bruna, C. Pinheiro, C. A. T. Laia, S. Bonacchi, P. Samorì, *Adv. Mater.*, 29, **2017**, 1703225.

- "Graphene exfoliation in the presence of semiconducting polymers for improved film homogeneity and electrical performances", T. Leydecker, M. Eredia, F. Liscio, S. Milita, G. Melinte, O. Ersen, M. Sommer, A. Ciesielski, P. Samorì, *Carbon*, 130, **2018**, 495–502.

- "MoS2 nanosheets via electrochemical lithium-ion intercalation under ambient conditions", M. El Garah, S. Bertolazzi, S. Ippolito, M. Eredia, I. Janica, G. Melinte, O. Ersen, G. Marletta, A. Ciesielski, P. Samorì, *FlatChem*, 9, **2018**, 33–39.

- "Thermal insulation with 2D materials: liquid phase exfoliated vermiculite functional nanosheets", Janica, S. Del Buffa, A. Mikołajczak, M. Eredia, D. Pakulski, A. Ciesielski, P. Samorì, *Nanoscale*, 10, **2018**, 23182–23190.

- "Persian waxing of graphite: towards green large-scale production of graphene", A. Aliprandi, M. Eredia, C. Anichini, W. Baaziz, O. Ersen, A. Ciesielski, P. Samorì, *Chem. Commun.*, **2019**, in press (DOI: 10.1039/C9CC01822K).

CONFERENCES PRESENTATIONS

- “A Supramolecular Strategy to Leverage the Liquid-Phase Exfoliation of Graphene in the Presence of Surfactants: Unravelling the Role of the Length of Fatty Acids”, S. Haar, M. Eredia, M. El Gemayel, F. Richard, M. Gobbi, E. Orgiu, M. V. Nardi, G. Ligorio, N. Koch, S. Conti, N. Merstorf, M. Cecchini, G. Melinte, O. Ersen, R. Mazzaro, V. Morandi, J. Clough, H. Yang, C. Casiraghi, A. Ciesielski, P. Samorì, 13th European Conference on Molecular Electronics (ECME), Strasbourg (France), 1-5 September 2015. Poster presentation.

- “Graphene via electrochemical exfoliation: towards application in electronics”, M. Eredia, S. Bertolazzi, A. Ciesielski and P. Samorì, Graphene 2016, Genova (Italy), 19-22 April 2016. Poster presentation.

- "Morphology and electronic properties of electrochemically exfoliated graphene", M. Eredia, S. Bertolazzi, T. Leydecker, M. El Garah, I. Janica, G. Melinte, O. Ersen, A. Ciesielski and P. Samorì, 1st European Conference on Chemistry of Two-Dimensional Materials (Chem2DMat), Strasbourg (France), 22-26 August 2017. Poster presentation.

- "Morphology and electronic properties of electrochemically exfoliated graphene", M. Eredia, S. Bertolazzi, T. Leydecker, M. El Garah, I. Janica, G. Melinte, O. Ersen, A. Ciesielski and P. Samorì, Flatlands, Lausanne (Switzerland), 29 August- 1 September 2017. Poster presentation.

- "An in-depth study on the electronic properties of electrochemically exfoliated graphene". M. Eredia, S. Bertolazzi, T. Leydecker, A. Ciesielski and P. Samorì, Graphene Week 2017, Athens (Greece), 25-29 September 2017. Poster presentation.

- "Materials innovation for the global circular economy and sustainable society", M. Eredia, VI World Materials Summit (e-MRS), Strasbourg, 18-21 November 2017. Poster presentation.

Matilde EREDIA

2D materials: exfoliation in liquid-phase and electronics applications

Résumé

Cette thèse est consacrée à la production de matériaux 2D en phase liquide, en utilisant des approches pouvant permettre la production en masse de graphène et de matériaux apparentés. Notre objectif est de surmonter certains problèmes critiques pour le traitement et l'utilisation pratique des encres à base de matériaux 2D et de fournir une compréhension approfondie de la relation structure-propriétés dans ces matériaux, constituant des étapes obligatoires pour leurs applications futures. Cette thèse porte principalement sur l'UILPE et l'exfoliation électrochimique du graphène et du disulfure de molybdène (MoS_2), qui ont été choisis comme matériaux prototypes à 2 dimensions. Les approches synthétiques sont combinées à une caractérisation physico-chimique des matériaux produits, à l'aide de techniques telles que l'AFM, la microscopie électronique, la spectroscopie XPS et Raman, ainsi qu'à une caractérisation électrique. Des applications dans le domaine de la détection et de l'électronique ont été explorées et ont permis de démontrer que des approches d'exfoliation en phase liquide pouvaient être utilisées pour obtenir un contrôle précis des propriétés des matériaux 2D ouvrant la voie à leur intégration en tant que matériaux actifs dans de nouveaux dispositifs multifonctionnels.

Résumé en anglais

This thesis is devoted to the production in liquid-phase of two-dimensional materials, by using approaches that may enable mass production of graphene and related materials. We aim to overcome some issues that are critical for the processing and practical use of 2D materials-inks and to provide a deep understanding of the structure-properties relationship in such materials being mandatory steps toward their future applications. This thesis mainly focuses on ultrasound-induced liquid-phase exfoliation and electrochemical exfoliation of graphene and molybdenum disulfide, which have been chosen as prototypical 2D materials. The synthetic approaches have been combined with a multiscale physico-chemical and electrical characterization of the produced materials, by employing techniques such as AFM, XPS and Raman spectroscopy. Applications in the field of sensing and electronics have been explored and allowed to demonstrate that liquid-phase exfoliation approaches can be conveniently employed to achieve a fine control on the properties of 2D materials paving the way to their integration as active materials in novel multifunctional devices.

Keywords: Two-dimensional materials, liquid-phase exfoliation, electrochemical exfoliation, solution process, thin films, graphene composites, physico-chemical characterization.